Impact of Connection Type on Performance of

Non-Seismic Concentrically Braced Frames

Ryan Ballard

A thesis

submitted in partial fulfillment of the

requirements for the degree of

Master of Science in Civil Engineering

University of Washington

2015

Committee:

Jeffrey W. Berman

Charles W. Roeder

Dawn E. Lehman

Program Authorized to Offer Degree

Civil and Environmental Engineering

University of Washington

Abstract

Impact of Connection Type on Performance of
Non-Seismic Concentrically Braced Frames

Ryan M. Ballard

Chair of Supervisory Committee:
Dr. Jeffrey W. Berman
Department of Civil and Environmental Engineering

Concentrically braced frame (CBF) structural systems resist lateral loads using braces framed diagonally between frame work points defined at the intersection of beam, column, and brace centerlines. In the past few decades, research on CBFs has primarily focused on improving seismic detailing requirements for new construction. Braced frames designed prior to 1988, termed non-seismic concentrically braced frames (NCBFs), had much less stringent design requirements the consequences of which include high variability in the beam-to-connection detail, an inability to develop the yield capacity of the brace, and unknown controlling failure modes. Evaluation and retrofit of existing NCBF systems can be challenging in part due to the lack of experimental research evaluating the variety of connection details and deficiencies present in existing NCBF infrastructure.

As part of a large NSF supported effort to provide guidance on the seismic evaluation and retrofit of NCBFs, five NCBF frames focusing on bolted beam-to-column connections were designed and tested at the University of Washington Structural Research Laboratory. The results are compared to the results of nine previous NCBF tests using measured response parameters and observed performance. It was found that the brace type along with the continuity, flexibility, and deficiencies of the connection could dramatically impact the deformation capacity, failure mode, and yielding hierarchy observed in an NCBF. Backbone curves developed for all fourteen experiments provide modeling parameters to be used in the development of modified procedures for evaluation and retrofit of braced frames.

Acknowledgements

First I would like to thank my advisors Jeff Berman, Charles Roeder, and Dawn Lehman for bringing me onto the project and providing funding for this research. Writing this master's thesis I believe is one of my greatest accomplishments to date. I am incredibly thankful that they gave me an opportunity to not only make an impact on the engineering community, but also to develop my skills as an engineer. Although difficult at times, I learned a lot from their guidance and support.

Thank you to the other students that were on my research project. Dan Sloat and Molly Johnson taught me everything I needed to know to start my experimental research in the lab. They were always of great assistance even as they were finishing their thesis. Andy Sen was an invaluable reference that always seemed to know the answer to my questions. I greatly appreciate his support and friendship as I went through the hurdles of writing a master's thesis. I would also like to thank Marsha Swatosh whose positive attitude and optimism helped to fuel me through tough meetings and long days.

Thank you to Anthony Gasca who was an invaluable asset throughout this research project. He was an incredibly hard working and dedicated lab assistant that not only helped me to assemble, instrument and test all five braced frames but also pulled together an entire appendix for this thesis. I would also like to thank the lab technician, Vince C., for providing necessary support and knowledge in the lab as well as Doug L. for his good quality welds and entertaining company.

Thank you to my fellow Wisconsinite, namesake, structural engineer, graduate student, co-worker and friend Ryan Ganey. Ryan represents one of many of the incredible individuals I had the pleasure of getting to know over the past two years, and I'm sure our friendship sure will continue well past our graduation.

Most of all I would like to thank my fiancée, Taylor Hoffman, for her unwavering support as I pursued my master's degree through the hardships of a long-distance relationship and the demands of the program.

Table of Contents

Table of Figures

Table of Tables

Chapter 1: Introduction

1.1 Behavior of Concentrically Braced Frames

Concentrically braced frames (CBFs) are stiff, strong lateral force resisting systems that feature steel braces aligned with the intersections of the beam, column, and brace centerlines that occur in the corner connections or the center of the beam. Over the last several decades, CBFs have been popular throughout the United States to resist lateral forces from wind and earthquake because they are relatively inexpensive to construct.

Special concentrically braced frames (SCBFs) are a modern form of CBF construction used in regions of high seismicity. The components of SCBFs (connections, beams, and columns) are designed for the expected capacity of the braces to ensure that the braces can buckle and yield prior to the connection or frame members reaching any limit states. This philosophy along with other detailing requirements work to promote system ductility and to control the failure mode.

The design requirements for SCBFs have evolved over the last several decades thanks to a significant amount of research. However, only limited research has been done on existing CBFs that do not meet these requirements. CBFs designed prior to 1988, termed non-seismic concentrically braced frames (NCBFs) were designed prior to the introduction of capacity based design and could exhibit poor performance relative to an SCBF in the event of an earthquake as shown in Figure 1-1. The prediction of NCBF performance is difficult due to the wide variety of connection types and system configurations that stem from the lack of detailing requirements.

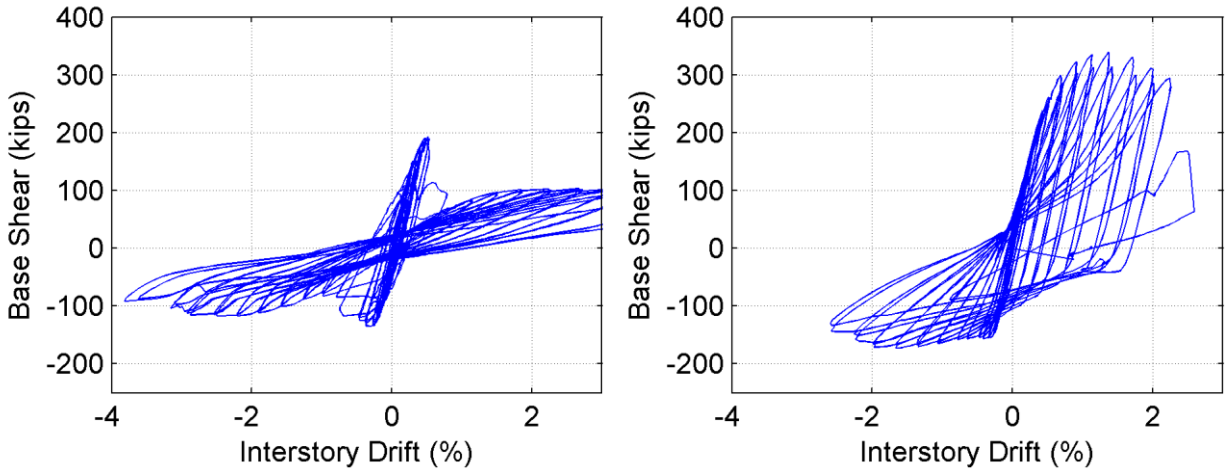

a. Example NCBF (Hsiao et. all 2012) b. Example SCBF (Herman 2007)

Figure 1-1: Example of SCBF and NCBF Performance

1.2 Research Program

The engineering community recognizes that many of the existing structures on the west coast having NCBFs do not meet modern SCBF seismic design requirements and may be in need of retrofit. Evaluation and retrofit of existing braced frames is guided by ASCE 41 (2013). However, little experimental evidence on NCBF behavior was available in the early 1990's when the ASCE 41 provisions were first developed.

In an NSF funded collaborative effort to understand the seismic performance of NCBFs and to establish economical retrofit strategies for these systems, a series of experiments at the University of Washington (UW), the University of California, Berkeley, and the National Center for Research on Earthquake Engineering (NCREE) in Taipei Taiwan were developed as shown in Figure 1-2. These tests were designed to represent existing infrastructure identified in an infrastructure review conducted by Sloat (2014) and evaluate both NCBF component and system levels behaviors.

(a) UW, courtesy of Molly Johnson (b) Berkeley, courtesy of Jiun-Wei Lai (c) NCREE

Figure 1-2: Experimental Setup at Various NCBF Testing Locations (Sen 2014)

1.3 Research Objectives

The research presented in this thesis builds off of tests by Sloat (2014) and Johnson (2014) at UW SRL. These tests were based off of an infrastructure review and looked at a subset of connection details and deficiencies common to NCBF infrastructure. The research objectives for this particular thesis are outlined below.

- Conduct experiments on additional braced frame specimens at the UW SRL with a focus on connection type and brace retrofit options including:
    - Bolted end plate connections;
    - Integrated gusset-shear plate connections;
    - Retrofit with buckling restrained braces.

- Compare the performance of NCBF tests to date to draw conclusions about the impact of connection type, and brace type on the performance of NCBFs.

- Determine the yielding hierarchy and failure modes in NCBFs with bolted end plate and integrated gusset shear plate connections and correlate that hierarchy to calculated deficiencies.

- Develop backbone curves for all UW NCBF experiments and provide recommendations for the modification and improvement of current evaluation and retrofit procedures in ASCE 41.

- Provide recommendations for future experimental and analytical work to provide a more complete picture of NCBF performance.

1.4 Report Overview

This report is divided into nine chapters and represents the work done to achieve the research objectives. Chapter 2 provides an in depth review of the project background including a review of braced frame design approaches used in the last several decades, a summary of an infrastructure review conducted by Sloat (2014), and a summary of all NCBF tests conducted by Sloat (2014) and Johnson (2014). This information provides context for the development the five NCBF experiments presented in this thesis. Design of the experimental specimens is described in Chapter 3.

Chapter 4 describes the experimental setup used to test the specimens designed in Chapter 3 and provides general instrumentation layout for each experiment. Chapter 5 contains all of the experimental observations and categorizes observed damage into performance states. The performance states in chapter 5 are used to develop performance state summary tables that highlight the progression of damage at increasing levels of drift and are also used throughout individual test narratives.

Chapter 6 analyzes the test data collected for each experiment and is used to support conclusions about individual specimen performance. Chapter 7 compares the performance and response of the five tested specimens with other NCBF specimens with similar characteristics and draws conclusions about the impact of brace and connection on frame ductility. Chapter 8 looks at all of the NCBF tests prior to June 2015 and tabulates backbone parameters relevant for ASCE 41 retrofit. The backbone curves are used to compare specimens with similar deficiencies and failure modes to guide the recommendations for future work. Chapter 9 summarizes the findings of this research project and presents overall conclusions and recommendations for future work.

Appendix A contains detailed instrumentation plans for each experiment. Appendix B contains connection specific design expressions and force distributions used to evaluate each connection. Appendix C contains a detailed report about the material coupon testing done for all NCBF tests to date.

Appendix D contains supplemental data analysis plots that provide additional information about the performance of each specimen beyond what is presented in the main body of the document. Appendix E contains background information on BRB testing as well as BRB details, design, and past experimental research.

Chapter 2: Project Background

2.1 Introduction

This chapter discusses the evolution of braced frame design and details previous NCBF research conducted at UW to provide context and motivation for the research presented in this thesis. Section 2.2 reviews the design approaches currently employed in practice for the design and retrofit of braced frame structures and compares them to the design requirements for braced frames designed prior to 1988. Section 2.3 introduces a demand capacity ratio (DCR) evaluation used to assess existing infrastructure and summarizes findings from an infrastructure review conducted by Sloat (2014). Section 2.4 summarizes the findings of 9 past NCBF experiments conducted by Hsiao et. all (2012), Sloat (2014), and Johnson (2014). Each summary contains the goal of each experiment along with the connection detail, connection DCRs, and a summary of the performance including a base shear vs. drift hysteresis, yield hierarchy, and photos of observed damage. These summaries serve as reference for Chapters 7 and 8 which compare the performance of the past NCBF experiments with the tests presented in this thesis.

2.2 Review of Past and Present Design Approaches

2.2.1 Current AISC SCBF Design Requirements

Seismic design of steel structures is guided by AISC 341 (2010), Seismic Provisions for Structural Steel Buildings. AISC 341 provides numerous detailing requirements for SCBFs. These requirements were developed over decades of observation of damage incurred by earthquakes and numerous laboratory tests of braced frames. Table 2-1 summarizes some of the requirements for SCBF construction and the rationale behind each requirement.

Table 2-1: Detailing Requirements for SCBF Components

	Requirement	Reason
Brace Slenderness	KL/r < 200	Tension only bracing expressly prohibited. Slender braces that meet required compactness limits tolerate relatively large inelastic post-buckling deformation. However, extremely slender braces have much smaller compressive resistance than tensile resistance, and they sustain large dynamic loads on impact from load reversal.
Brace Compactness	Seismically Compact	Delay brace fracture from severe local buckling and high strain concentrations at the brace plastic hinge.
Framing Member Compactness	Seismically Compact	Beams and columns may develop significant flexural demands at large drifts. These demands are neglected in design but compactness requirements ensure that the framing members can develop stable plastic hinges.
Brace End Rotation	Required[1]	Reduce the strain concentration on gusset plates and gusset plate welds induced by brace buckling and connection rotation.
Brace Connection Design	Design for Expected Brace Capacity	The brace must be able to buckle and yield to develop adequate system ductility. Connection and framing elements not designed to develop the expected brace force could significantly limit the ductility of the overall system.
Framing Member Design		
Welds	Must be Demand Critical Welds	Reduce risk of brittle weld fractures and facilitate stable crack propagation in weld filler metal.

1 – Can do fixed ends if the connections are designed for the plastic moment capacity of the brace.

As shown in Table 2-1, the brace connection must be designed for the expected capacity of the brace. Specific limit states for the brace connection are shown in Table 2-2 and are based on equations from the steel design manual (AISC 2010) and the Balanced Design Procedure (BDP) (Roeder et. all 2011). Variables for each of the design equations are shown in Table 2-3. Demands on each component are based on one of two equilibrium approaches depending on the connection type and are described in more detail in Section 2.3.2.

Table 2-2: Limit States and Corresponding Resistance Expressions for AISC and BDP approaches (Roeder et. all 2011)

Limit state	AISC design		Balanced design	
	Resistance (φR_n)	ϕ	Resistance (βR_n)	β
Whitmore yielding	$\phi F_y B_w t_p$	0.90	$\beta R_y F_y B_w t_p$	1.0
Brace net section fracture	$\phi U(R_{tb}F_{ub}A_{nb} + F_{up}A_{gp})$	0.75	$\beta U(R_{tb}F_{ub}A_{nb} + F_{up}A_{gp})$	0.95
Brace to gusset weld	$\phi(0.6)F_{EXX}N_w L_c(.707)w_2$	0.75	Same as AISC	0.75
Brace to gusset base metal	$\phi(0.6)F_u N_s L_c t_f$	0.75	Same as AISC	0.75
Block shear	$\phi\{(0.6F_u A_{nv} + U_{bs}F_u A_{nt}) \le (0.6F_y A_{gv} + U_{bs}F_u A_{nt})\}$	0.75	$\beta\{(0.6F_u A_{nv} + U_{bs}F_u A_{nt})\}$	0.85
Whitmore fracture	$\phi F_u B_w t_p$	0.75	$\beta F_u B_w t_p$	0.85
Gusset plate buckling	$\phi B_w t_p F_{cr}$	0.90	$\beta B_w t_p F_{cr}$	0.90
Interface welds	$\phi(0.6)F_{EXX}[1 + 0.5(\sin\gamma)^{1.5}]2\ L_w(.707)w_1 \ge UFM$	0.75	$2(1.5)\beta(0.6)F_{EXX}(.707)w_1 \ge R_y F_y t_p$	0.75

Table 2-3: Variable Definitions for Limit State Equations

$\emptyset$	AISC design procedure resistance factor
β	BDP design procedure resistance factor
F_y	Yield capacity of the gusset plate
F_u	Ultimate capacity of the gusset plate
F_{ub}	Ultimate capacity of the brace
F_{up}	Ultimate capacity of net section reinforcement
F_{cr}	Critical buckling capacity of gusset plate
F_{EXX}	Ultimate strength of the weld filler metal.
R_y	Ratio of nominal and expected yield capacity gusset plate
R_{tb}	Ratio of nominal and expected ultimate capacity of brace

B_w	Whitmore width
t_p	Thickness of the gusset plate
U	Shear Lag Factor
A_{nb}	Net tension area of the brace
A_{gp}	Gross area of the net section reinforcement plates
N_w	Number of welds
L_c	Length of the splice weld connection
w_2	Thickness of the beam-to-gusset plate weld
N_s	Number of shear planes of shear yielding surface
t_f	Thickness of base metal connecting brace-gusset

A_{nv}	Net shear area of the gusset plate block shear pathway
U_{bs}	Stress uniformity factor
A_{nt}	Net tension area of the gusset plate block shear pathway
A_{gv}	Gross tension area of the gusset plate block shear pathway
γ	Angle of resultant stress on gusset plate weld group
L_w	Length of gusset plate weld group
w_1	Thickness of single gusset plate fillet weld
UFM	Uniform Force Method demands on gusset plate interface welds

The BDP was developed as an alternate approach to AISC braced frame design and promotes a yielding hierarchy in braced frame connections to achieve higher levels of overall frame ductility while at the same time limiting undesirable failure modes. The primary differences between the AISC and BDP approaches include the substitution of balance factors for resistance factors, the use of expected gusset plate and brace material properties instead of nominal material properties, and a different approach to gusset plate interface weld design that requires the capacity of the weld be larger than the expected capacity of the gusset plate.

2.2.2 Braced Frame Design Prior to 1988

The SCBF design requirements in use today have evolved over the past 25 years. Prior to that there were few requirements. Table 2-4 shows the design requirement of braced frames designed prior to 1988 compared to the design requirements of SCBFs. As shown, many of the detailing requirements were not considered prior to 1988, and many braced frames in existing infrastructure could be vulnerable in the event of an earthquake due to the lack of these requirements.

Table 2-4: Differences in NCBF and SCBF detailing requirements (Sloat 2014)

Component	Pre-1988 Braced Frames	SCBFs
Brace Slenderness	No Limit	KL/r <200
Brace Compactness	No Limit	Seismically Compact
Framing Member Compactness	No Limit	Seismically Compact
Brace End Rotation Clearance	No Limit	Required
Brace Connection Design	Design for Seismic Loads	Design for Expected Brace Capacity
Framing Member Design	Design for Seismic Loads	Design for Expected Brace Capacity

Since braced frames designed prior to 1988 were only designed for the seismic loads, connections and frame members may reach failure mode limit states prior to brace buckling or yielding which usually occur at less than 0.5% drift range. Controlling failure limit states in these braced frames are often unknown due to the lack of detailing requirements and high variability in connection type and connection deficiencies. All of this makes it difficult to predict the behavior or failure mode of any given braced frame designed prior to 1988 and can in some cases require extensive retrofit strategies to address the uncertainties.

2.2.3 ASCE 41 Braced Frame Evaluation and Retrofit

ASCE41 (2013) is the U.S. standard for seismic evaluation and retrofit of existing structures. There are three tiers of building evaluation described in ASCE41 ranging from general screening, to full system analysis. The evaluation tier chosen by the engineer is based on the level of component/ systematic deficiencies of the structure and the client's individual preferences. For each tier, ASCE 41 describes defines how to evaluate building conditions and proposed retrofits for a variety of structural systems including concentrically braced frame structures. ASCE 41 evaluation is performance-based, i.e., the owner and structural engineer must define desired building seismic performance for different seismic hazard levels.

The purpose of the tier 1 evaluation is to quickly identify any potential deficiencies in a building using a prescribed checklist, and enable the engineer/ client to determine the best course of action. For a braced frame structure the checklist is selected based on the level of seismicity in the area, the level of performance required (immediate occupancy or life safety), and the rigidity of the diaphragms among other things.

In order for a building to be successfully retrofitted in tier 2 analysis, all of the checklist items marked as non-compliant or unknown during tier 1 analysis must be addressed. Additionally the building must meet a base shear calculation where the lateral capacity of each frame component is multiplied by an "m-factor" and compared with the computed earthquake demands. The "m-factor" is based on a primary deformation-controlled component. All other components (termed force-controlled) of the frame must be designed to meet the demands of the deformation controlled elements. For braced frames:

> *"Axial tension and compression in braces shall be considered deformation controlled. Actions on beams and columns with axial load that exceeds 10% of the axial strength shall be considered force or deformation controlled as determined for fully restrained frame columns in section 9.4.2.4. Compression, tension shear, and bending actions on brace connection, including gusset plates bolts, welds, and other connectors shall be considered force controlled, unless connections are explicitly modeled, and experimental evidence suggests that stable, desirable ductility can be achieved in a particular connection element." (ASCE 2014 section 9.5.2.4)*

This means that if a connection element cannot develop the brace capacity if must be retrofitted for the building to meet ASCE 41 requirements. For braces the "m-factors" are based on the slenderness of the brace, the type of brace, loading direction (tension or compression), and are subject to a number of reduction factors for consideration such as brace compactness. Figure 2-1 shows the m-factors for steel braces.

	m-factors for linear procedures				
		Primary		Secondary	
Component/ Action	IO	LS	CP	LS	CP
Braces in Compression (except EBF braces)					
a. Slender $\frac{Kl}{r} \geq 4.2\sqrt{\frac{E}{F_y}}$					
1. W, I, 2L in-plane	1.25	6	8	7	9
2. 2L out-of-plane 2C out-of-plane	1.25	5	7	6	8
3. HSS, pipes, tubes, L	1.25	5	7	6	8
b. Stocky $\frac{Kl}{r} \leq 2.1\sqrt{\frac{E}{F_y}}$					
1. W, I, 2L in-plane	1.25	5	7	6	8
2. 2L out-of-plane 2C out-of-plane	1.25	4	6	5	7
3. HSS, pipes, tubes, L	1.25	4	6	5	7
Interpolate for Intermediate					
Braces in Tension (except EBF braces)					
1. 2L, HSS, L braces	1.25	4	5.6	5.6	7
2. Other	1.25	5	7	8	10
4. Buckling Restrained Braces	2.3	5.6	7.5	7.5	10

multiply m by 0.8 for deficient connections (DCR >1.0)

multiply m by 0.5 for non-compact braces (stocky braces)

multiply by 0.5 for stiches that do not meet requirements

Figure 2-1: Acceptance Criteria for Linear Procedures (Table 9-4 ASCE 41 2014)

Tier 3 systematic evaluation requires extensive data collection from a building and a comprehensive nonlinear analysis of the entire structure to demonstrate a specified level of performance. Tier 3 analysis may be done if the building system is complicated, has severe irregularities, or significant cost savings can be achieved through a tier 3 analysis. For steel structures, component behaviors are defined by backbone curves and their associated modeling parameters. A generalized force-deformation backbone curve for steel components is shown in Figure 2-2. The values Q and Q_y are generalized component loads and expected strengths while θ and Δ represent the rotations and displacements of the component. The parameters a, b, and c and the points A, B, C, D, and E define the capacities that the component can achieve at a given level of deformation.

The modeling parameters for braced frames are shown in Figure 2-3 along with associated reduction factors. The modeling parameters are generally based on frames that have been detailed for regions of high seismicity and are applied to the models of the brace.

Modeling of braced frame connections is left to the engineer's judgment, while modeling of the framing components is based on the non-linear modeling of the members from the moment frame section.

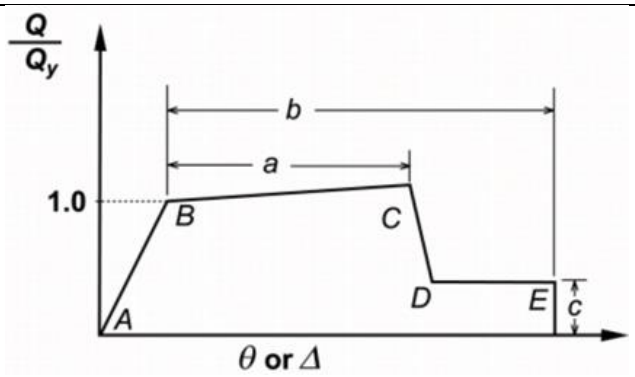

Q/Q_y	Normalized Capacity
θ or Δ	Component Deformation
A	Origin
B	Yield Capacity
C	Ultimate Capacity
D	Residual Capacity
E	Complete Failure
a	Inelastic Deformation Capacity
b	Inelastic Deformation Capacity
c	Residual Strength Ratio

Figure 2-2: Generalized Force-Deformation Relation for Steel Elements or Components (Fig. 9-1 ASCE 2014)

	Modeling Parameters			Acceptance Criteria		
	Plastic Deformation		Residual	Plastic Deformation		
Component/ Action	a	b	c	IO	LS	CP
Braces in Compression (except EBF braces)						
a. Slender $\frac{Kl}{r} \geq 4.2\sqrt{\frac{E}{F_y}}$						
1. W, I, 2L in-plane	$0.5\Delta_c$	$0.5\Delta_c$	0.3	$0.5\Delta_c$	$8\Delta_c$	$10\Delta_c$
2. 2L out-of-plane 2C out-of-plane	$0.5\Delta_c$	$0.5\Delta_c$	0.3	$0.5\Delta_c$	$7\Delta_c$	$9\Delta_c$
3. HSS, pipes, tubes, L	$0.5\Delta_c$	$0.5\Delta_c$	0.3	$0.5\Delta_c$	$7\Delta_c$	$9\Delta_c$
4. Single angle	$0.5\Delta_c$	$0.5\Delta_c$	0.3	$0.5\Delta_c$	$9\Delta_c$	$12\Delta_c$
b. Stocky $\frac{Kl}{r} \leq 2.1\sqrt{\frac{E}{F_y}}$						
1. W, I, 2L in-plane	$1\Delta_c$	5	0.5	$0.5\Delta_c$	$7\Delta_c$	$8\Delta_c$
2. 2L out-of-plane 2C out-of-plane	$1\Delta_c$	4	0.5	$0.5\Delta_c$	$6\Delta_c$	$7\Delta_c$
3. HSS, pipes, tubes, L	$1\Delta_c$	4	0.5	$0.5\Delta_c$	$6\Delta_c$	$7\Delta_c$
c. intermediate	Linear interpolation between the values for slender and stocky braces (after application of all applicable modifiers) shall be used.					
Braces in Tension (except EBF braces)						
1. W	$10\Delta_T$	$13\Delta_T$	0.6	$0.5\Delta_T$	$10\Delta_T$	$13\Delta_T$
2. L	$9\Delta_T$	$12\Delta_T$	0.6	$0.5\Delta_T$	$9\Delta_T$	$12\Delta_T$
3. HSS	$9\Delta_T$	$11\Delta_T$	0.6	$0.5\Delta_T$	$8\Delta_T$	$11\Delta_T$
4. Pipe	$8\Delta_T$	$9\Delta_T$	0.6	$0.5\Delta_T$	$7\Delta_T$	$9\Delta_T$
5. Single Angle	$10\Delta_T$	$11\Delta_T$	0.6	$0.5\Delta_T$	$8\Delta_T$	$10\Delta_T$
Beams, columns in tension (except EBF beams, columns)	$5\Delta_T$	$7\Delta_T$	1	$0.5\Delta_T$	$6\Delta_T$	$7\Delta_T$
Buckling Restrained Braces	$13.3\Delta_y$	$13.3\Delta_y$	1	$3.0\Delta_y$	$10\Delta_y$	$13.3\Delta_y$

Δc is the axial deformation at expected buckling load, Δt is the yield deformation
multiply m by 0.8 for deficient connections (DCR >1.0)
multiply m by 0.5 for non-compact braces (stocky braces)
multiply by 0.5 for stiches that do not meet requirements

Figure 2-3: Modeling Parameters and Acceptance Criteria for Braces (Table 9-7, ASCE 41 2014)

2.3 Evaluation of Exiting Infrastructure

2.3.1 Infrastructure Review

Sloat (2014) conducted an infrastructure review of 12 CBF buildings designed prior to 1988 to better understand existing infrastructure in regions of high seismicity. Building information including the type of building, number of stories, brace configuration, and connection type was identified from existing structural drawings provided by various companies and building authorities.

General classifications of the buildings from the infrastructure review are shown in Table 2-5. Overall there was a wide variety of building types, brace configurations, and connection types amongst the example structures. The most prevalent brace type was HSS (70% of building used) while the most prevalent configuration was Chevron bracing (also known as inverted-V) used in 70% of the buildings. Brace connection types varied from building to building and a total of eight unique connection configurations were identified as shown in Figure 2-4.

Table 2-5: Existing Infrastructure Survey - Building type, Brace Configuration, and Connection Type (Sloat 2014)

Building	Date	State	Building Use	Number of Stories	Brace Type	Brace Configuration	Connection Type
83CA3A	Oct-83	CA	Corporate HQ	3	HSS, W	Single Diagonal, Chevron	(e) Integrated Gusset-Shear Plate
82TN4A	Nov-82	TN	Corporate HQ	3,5	HSS, Pipe	Single Diagonal, Chevron	(b) Bolted Continuous Shear Tab
88CA3A	Jan-88	CA	Research	2,3	HSS, Pipe	Single Diagonal, Chevron	(e) Integrated Gusset-Shear Plate
80CA4A	Sep-80	CA	Office	4	HSS, W	Chevron, Single Diagonal	(g) Gusset-to-Beam Only
80WA8A	Jun-80	WA	Hospital	8	Angles	X-Bracing, Single Diagonal	(e) Integrated Gusset-Shear Plate, (c) Bolted Split Shear Plate, (d) Bolted End Plate
86WA3A	Apr-86	WA	Hospital	3	HSS	Chevron, Single Diagonal	(a) Welded Continuous Shear Plate
88UT1A	Oct-88	UT	Retail	1	Angles	X-Bracing, Single Diagonal	(d) Bolted End Plate
83CA2A	May-83	CA	Office	2	HSS	Chevron, Single Diagonal	(e) Integrated Gusset-Shear Plate
74CA6A	Jul-74	CA	Hospital	6	W	X-Bracing, Single Diagonal	(f) Double Integrated Gusset-Shear Plate
82OR9A	Jun-82	OR	Hospital	9	W	Single Diagonal, Multi-Story X	(f) Double Integrated Gusset-Shear Plate
92WA2A	Feb-92	WA	School	2,3	HSS	Chevron	(a) Welded Continuous Shear Plate
86CA4A	Aug-86	CA	Office	4	HSS	Chevron	(h) Bolted Split Double Angles

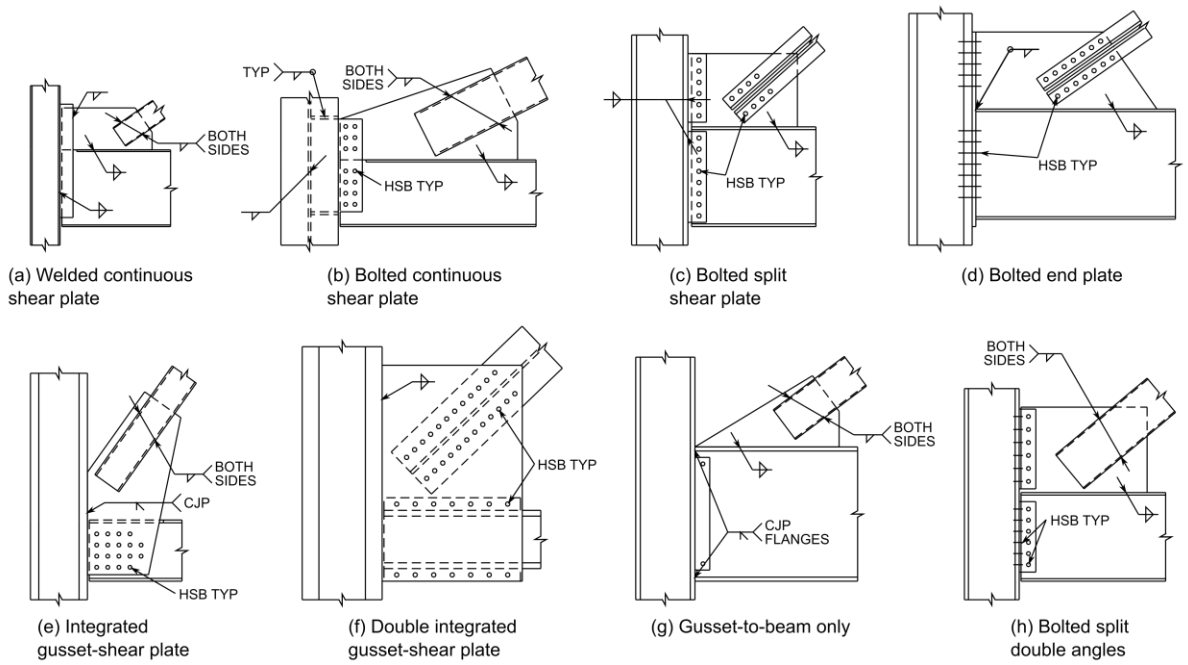

Figure 2-4: Connection Types Identified in the Infrastructure Review

After identifying and classifying the buildings Sloat (2014) conducted a demand to capacity ratio evaluation on a subset of connections from each building. The demand capacity ratio was similar to the procedure presented in Section 2.3.2 and was used to guide the design of nine experiments evaluating the bolted and welded shear plate connections presented in Section 2.4.

Common deficiencies found in the evaluation include brace net section fracture, brace splice weld fracture, Whitmore Yielding, and beam-to-gusset plate weld fracture. These frames were also typically detailed with non-compact braces, inadequate brace end rotation clearance, and non-ductile welds. System level deficiencies such as weak beams and vertical discontinuities were also observed but are not within the scope of this thesis.

2.3.2 Demand to Capacity Ratio Evaluation

Demand to capacity ratio evaluation is used to determine the level of deficiency in a connection for specific yielding mechanism and failure mode limit states. When the demand on a specific connection component is greater than its associated capacity, that component is considered to be deficient. To consistently calculate the capacities and demands on the various connections identified in the infrastructure review several assumptions (listed below) are made. The limit state equations used to estimate the capacity of braced frame connection components are presented in Sections 2.2.1.

1. Demands on the connection are based upon the expected brace capacity in tension and compression, because yielding and buckling of the brace are the primary yield mechanisms in CBFs. The expected brace capacity in tension is calculated using measured material strengths (documented in Appendix C). Compression capacity of the brace is calculated assuming a K of 1.0 and L_b measured from brace end to brace end as done for SCBF connection details.

2. The distribution of the forces and moments through the connections are determined by equilibrium. The Uniform Force Method (UFM) is often used for this equilibrium evaluation. However, the connections studied in this research project are not always well suited to the UFM. In these cases, equilibrium at the interface between the connection element and the face of the column is considered as shown in Table 2-6. This method is termed the continuous vertical method (CVM) and is used for connections with a continuous element that extend over both the gusset and beam (e.g. bolted end plate). Application of the CVM for the connection types utilizing a continuous connection element at the column interface (listed in Table 2-6) are detailed in Appendix B.

3. The BDP is used as an alternative method to evaluate gusset plate interface welds where the gusset plate weld capacities are evaluated relative to tension yield strength of the gusset plates using the measured material properties of the gusset plate.

4. For the CVM, the horizontal component of the brace force is transferred to the beam while the vertical component of the brace force is transferred to the column for all evaluated connections. This is a good assumption for the specimens tested at UW because the actuator force is delivered to the connection and brace directly through the beam (see Section 4.2).

5. Flexural deformation and moments in the frame are neglected in the connection evaluation.

6. Resistance factors ($\emptyset$ factors for AISC and β factors for BDP) are set as 1.0 for all limit states to more accurately represent the actual capacities.

7. Where measured material properties are not available to compute demands or capacities, the expected material properties ($R_y F_y$) are used. This is necessary for the evaluation of reference

connections from the infrastructure review and provides a better comparison (as opposed to using nominal material strengths) to DCRs computed using measured material properties.

8. The DCR evaluation method for connection specific limit states is identified using an abbreviated code indicated in the pretenses after applicable limit states wherever DCRs are presented. The codes “BR-CVM” and “BR-UFM” mean that the limit state was evaluated considering the expected brace capacity using the force distribution calculated from the CVM and UFM respectively. The code “GP” is used for weld limit states and means the capacity of the weld was checked against the yield capacity of the gusset plate as done for the BDP. Any limit states without a code are considered to be directly in the line of the brace force and are not influenced by the assumed force distribution.

9. Welds evaluating using the BR-CVM or BR-UFM were assumed to have linear elastic stress distributions and were checked at the extreme edge of the weld group.

Table 2-6: Force Distribution on Connection Elements

Method	**Continuous Vertical Method (CVM)**	**Uniform Force Method (UFM)**
Example Free Body Diagram	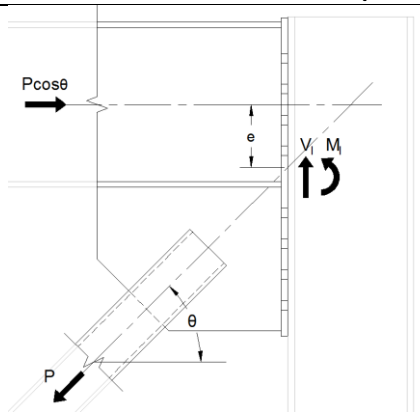	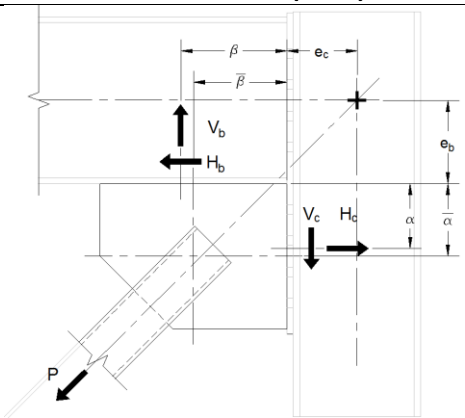
General Description	Consider equilibrium about a continuous vertical cut at the interface between the column and beam/gusset plate connection to determine shear, V_i $(P \sin\theta)$, and moment, $M_i(Pe\cos\theta)$, acting at the connection centroid.	Consider equilibrium about the gusset plate and distribute forces based on minimized eccentricities as described in part 13 of the AISC (2010) manual.
Applicable Connections[1]	Welded Continuous Shear Plate Bolted Continuous Shear Plate Bolted End Plate Integrated Gusset-Shear Plate	Split Bolted Shear Plate Bolted Split Double Angles

1- More specific force distributions for individual connection components for the continuous vertical method are shown in appendix B.

2.4 Previous NCBF Tests

2.4.1 Overview of Testing Program

A series of experiments were developed to evaluate common deficiencies and connection details found in the infrastructure review Sloat (2014). There were nine single bay tests that evaluated a variety NCBF connection configurations (Hsiao 2012, Sloat 2014, and Johnson 2014) as well as four two story tests (Sen 2014) that evaluated the weak beam found in many chevron CBFs.

Results from all 9 UW single bay tests are summarized in Table 2-7 through Table 2-15 in Section 2.4.4. Each summary contains a connection detail, connection DCRs, and an overview of the specimen performance including base shear vs. interstory drift hysteresis, yield hierarchy, failure mode, and photographs of important performance states. All of the UW tests were carried out using a similar setup to Johnson (2005) and Powell (2009). DCRs, force drift hysteresis, and connection details that are presented in this section are adapted from the original thesis to be consistent with the specimens tested in this thesis.

Sections 2.4.2 and 2.4.3 look specifically at the tests conducted by Sloat (2014) and Johnson (2014) and discuss the connection types tested as well as the conclusion made.

2.4.2 Welded Shear Plates - Sloat (2014)

Sloat (2014) designed and tested six experiments (Table 2-8 through Table 2-12) examining the performance of NCBFs with welded continuous shear plate details. Reference connections for the welded continuous shear plate are shown in Figure 2-5. Deficiencies for the reference connections included brace net section fracture, brace-gusset plate weld fracture, gusset plate Whitmore yielding, beam-to-gusset plate weld fracture, and shear tab to gusset plate/ beam weld fracture. The reference connections also had non-compact braces that did not meet current seismic compaction requirements.

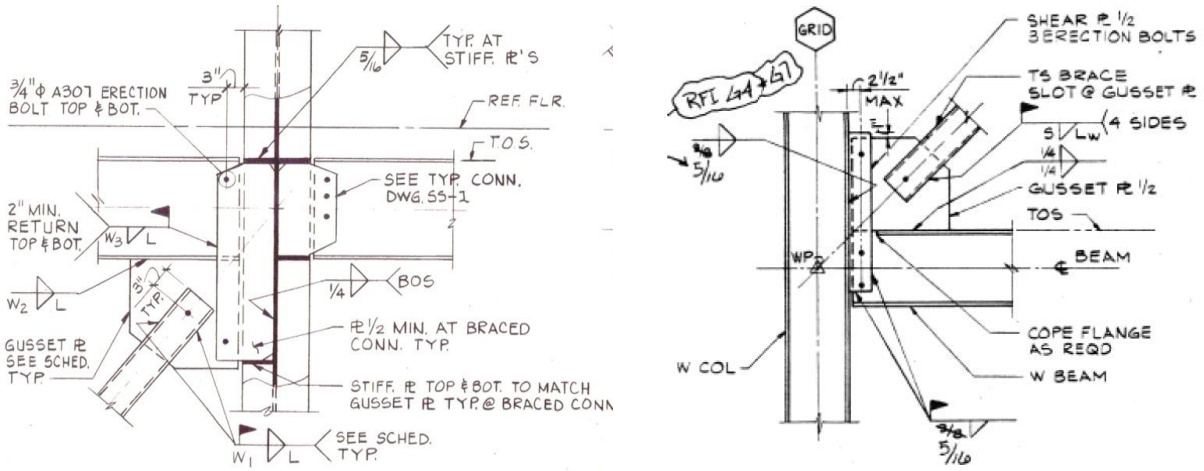

Figure 2-5: Reference Connections for Welded Shear Tab Sloat (2014)

After conducting a prototype test (NCBF1, Table 2-8) Sloat designed a few retrofit options to improve the inelastic deformation capacity of the original prototype connection detail. These retrofit options targeted specific deficiencies from the original prototype connection detail listed above.

The research conducted by Sloat (2014) had the following conclusions.

- The inelastic deformation capacity of a deficient NCBF connection can be greatly increased without addressing all of the deficient demand to capacity ratios.

- Severe brace local slenderness directly affects the inelastic deformation capacity of the system. Filling a non-compact section with concrete can increase the fracture life of a non-compact brace.

- Brace net section fracture, gusset plate Whitmore yielding, and shear yielding had little negative impact on the overall inelastic deformation capacity of the frame. This most likely occurred because the failure mode was ductile.

- The gusset plate-to-beam weld can be protected from deformation demands by an in plane buckling retrofit.

2.4.3 Bolted Shear Plates - Johnson (2014)

Johnson (2014) evaluated NCBF connections using split (2 tests, Table 2-14 and Table 2-15) and continuous bolted shear plates (1 test, Table 2-13). Reference connections for the test specimen design are shown in Figure 2-6. Deficiencies for the reference connection included brace net section, brace block shear, brace-to-gusset plate splice weld, column-to-gusset plate bolt shear, column-to-beam bolt shear and column-to-beam bolt bearing. Specimen Names from the original thesis (Johnson 2014) have been adapted to fit the naming convention used by Sloat (2014) and the experiments presented in this document.

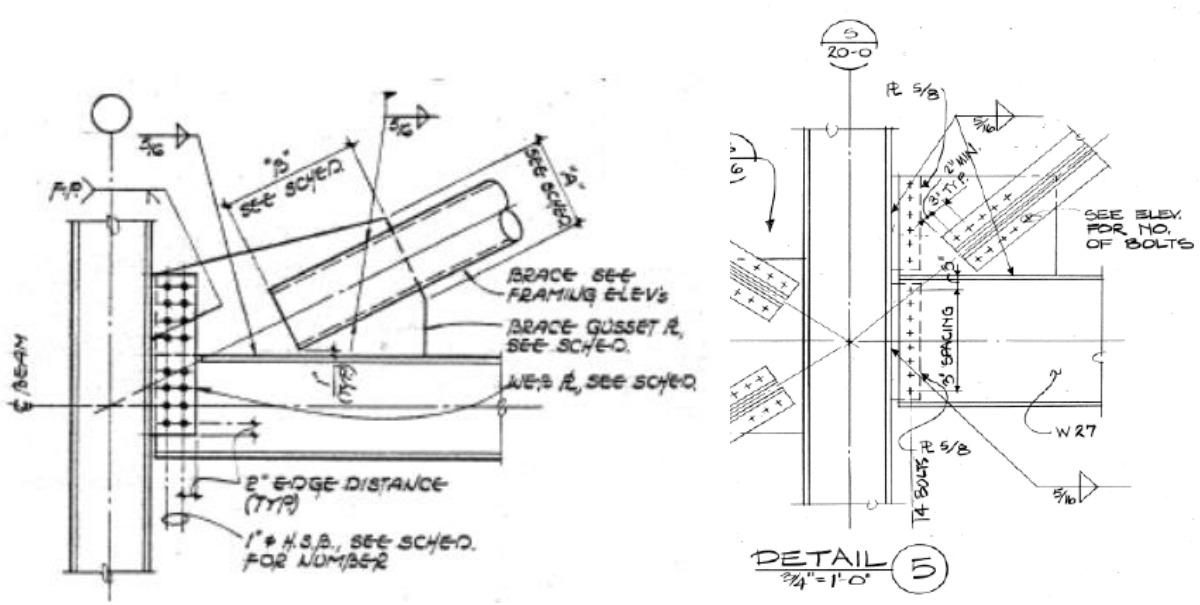

a. Bolted Continuous Shear Plate b. Bolted Split Shear Plate

Figure 2-6: Reference Connections for Bolted Shear Plate Design Johnson (2014)

The research conducted by Johnson (2014) had the following conclusions.

- Bolt shear does not appear to greatly reduce the inelastic deformation capacity of the connections provided that bolt hole elongation is allowed to develop.

- Bolt hole elongation greatly increases the inelastic deformation capacity of the frame and reduces demands on other components of the connection and the frame.

- The beam-to-gusset plate weld of NCBF connections can prematurely fracture if is not designed to develop the yield capacity of the gusset plate. This is especially true when there is out-of-plane deformation of the brace and gusset plate yielding.

- The bolted continuous shear plate performed better than the bolted split shear plate.

2.4.4 Previous NCBF Test Summaries

Table 2-7: NCBF0 Test Summary

Goal: Pilot NCBF test. Test a typical NCBF connection detail designed using braced frame design procedures from before 1988.

Connection Detail and DCRs

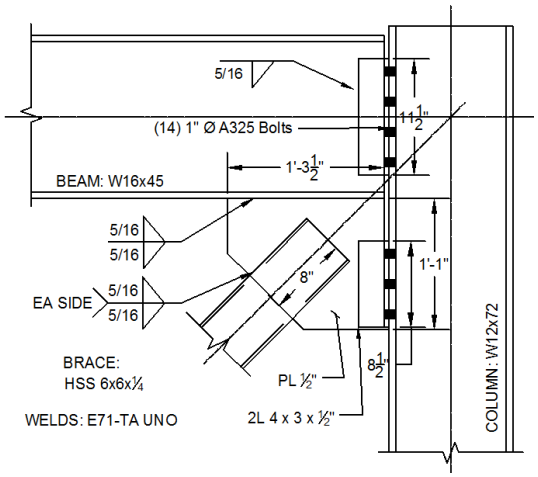

	Limit State	DCR
Yielding Mechanisms	Gusset Plate Whitmore Yielding	0.97
	Bolt Bearing Gusset Plate Angles (BR-UFM)	0.36
	Bolt Bearing Beam Web Angles (BR-UFM)	0.32
Failure Modes	Brace Net Section Fracture	**1.17**
	Brace Splice Fracture	**1.72**
	Brace Block Shear	0.95
	Gusset Plate Whitmore Fracture	0.75
	Gusset Plate Block Shear	0.73
	Gusset Plate-to-Beam Weld Fracture (GP)	**1.26**
	Gusset Plate-to-Beam Weld Fracture (BR-UFM)	0.62
	Bolt Rupture Gusset Plate Angles (BR-UFM)	**2.41**
	Bolt Rupture Beam Web Angles (BR-UFM)	**1.40**
Geometric Limits	Brace Compactness Ratio (b/t)/λhd	1.76
	Slenderness Ratio (KL/r)max	90

Specimen Performance Summary

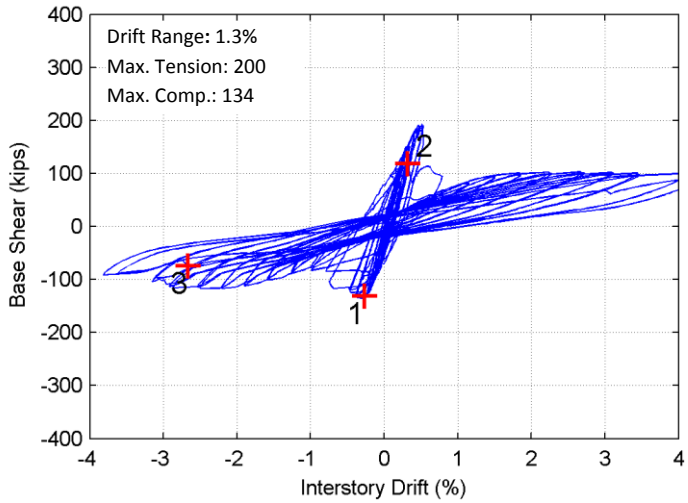

Yield Hierarchy: Brace → Bolted Angles

Failure Mode: Brace Splice Weld Fracture

1. Brace begins to buckle out-of-plane
2. Brace splice weld fractures.
3. Bolted angles connecting gusset plate and column fracture.

(2) Brace Splice Weld Fracture

(3) Bolted Angle Fracture

Table 2-8: NCBF1 Test Summary (Adapted from Sloat 2014)

Goal: Baseline evaluation of a typical welded continuous shear plate detail identified in the infrastructure review using a non-compact brace.

Connection Detail and DCRs

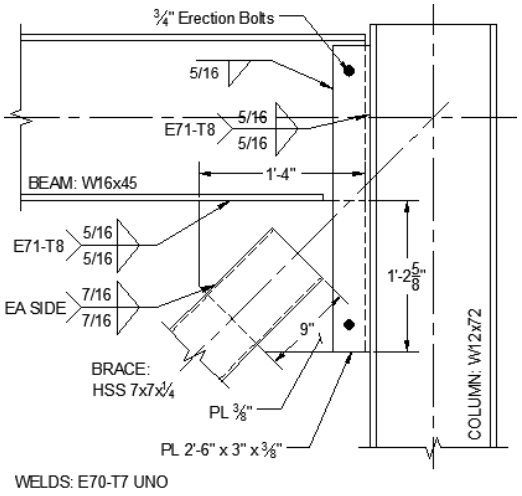

Type	Limit State	DCR
Yielding Mechanisms	Gusset Plate Whitmore Yielding	*1.21*
	Shear Plate Yielding	0.61
Failure Modes	Brace Net Section Fracture	**1.19**
	Brace Splice Fracture	0.85
	Brace Block Shear	1.00
	Gusset Plate Whitmore Fracture	0.87
	Gusset Plate Block Shear	**1.02**
	Beam-to-Gusset Plate Weld Fracture (GP)	0.67
	Beam-to-Gusset Plate Weld Fracture (BR-CVM)	0.65
	Shear Plate Weld Fracture (GP)	**1.35**
	Shear Plate Weld Fracture (BR-CVM)	**1.28**
Geometric Limits	Brace Compactness Ratio (b/t)/λhd	2.31
	Slenderness Ratio (KL/r)max	61

Specimen Performance Summary

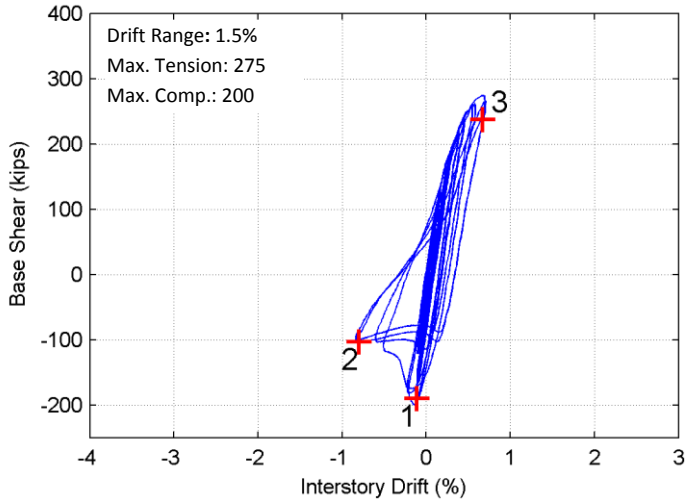

Yield Hierarchy: Yielding could not be observed during test.

Failure Mode: Brace Fracture

Damage Progression

1. Brace begins to buckle out-of-plane.
2. Brace begins hinging at mid-span.
3. Brace fractures.

(2) Brace Hinging

(3) Brace Fracture

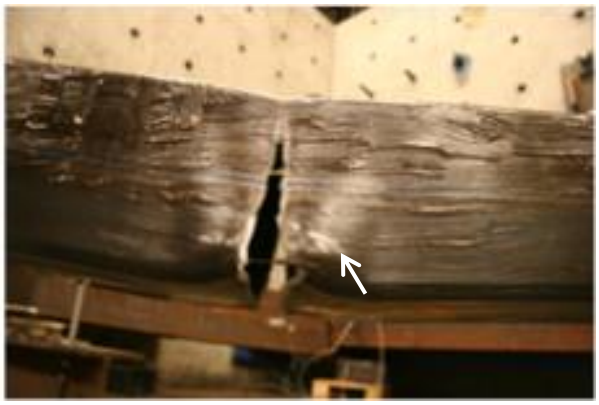

Table 2-9: NCBF1 –R2 Test Summary (Adapted from Sloat 2014)

Goal: Retrofit evaluation of welded continuous shear plate using highly ductile brace to increase system drift range.

Connection Detail and DCRs

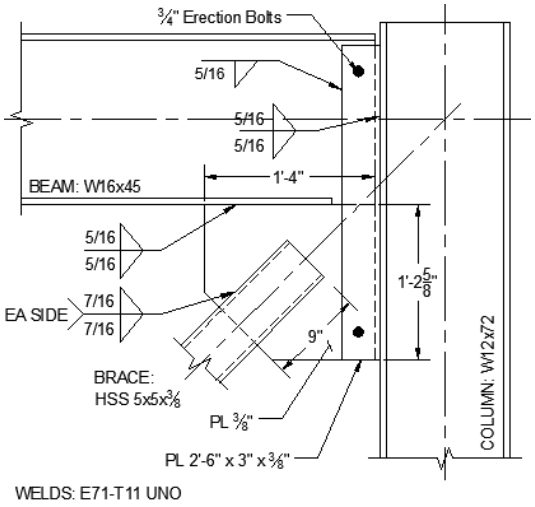

Type	Limit State	DCR
Yielding Mechanisms	Gusset Plate Whitmore Yielding	*1.32*
	Shear Plate Yielding	0.58
Failure Modes	Brace Net Section Fracture	**1.24**
	Brace Splice Fracture	0.82
	Brace Block Shear	0.67
	Gusset Plate Whitmore Fracture	0.94
	Gusset Plate Block Shear	**1.14**
	Beam-to-Gusset Plate Weld Fracture (GP)	0.67
	Beam-to-Gusset Plate Weld Fracture (BR-CVM)	0.63
	Shear Plate Weld Fracture (GP)	**1.35**
	Shear Plate Weld Fracture (BR-CVM)	**1.22**
Geometric Limits	Brace Compactness Ratio $(b/t)/\lambda_{hd}$	0.95
	Slenderness Ratio (KL/r)max	89

Specimen Performance Summary

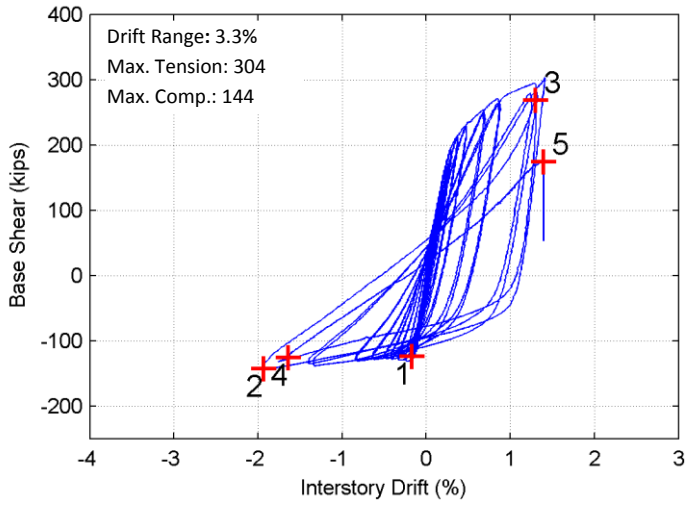

Yield Hierarchy: Connection (Gusset Plate) → Brace

Failure Mode: Shear plate weld fracture

Damage Progression

1. Brace begins to buckle out-of-plane.
2. Initial weld tearing observed at edge of beam-to-gusset plate and shear plate-to-gusset plate connections.
3. Moderate weld tearing in center of gusset plate-to-shear plate weld
4. Complete weld tearing of gusset plate to-shear plate weld
5. **Shear plate weld fracture**

(3) Weld Crack Initiation

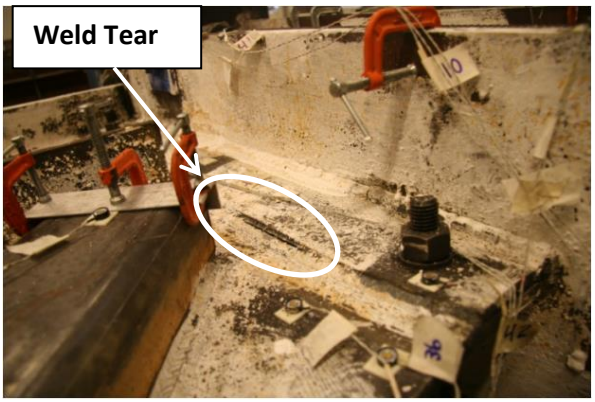

(5) Shear Plate Weld Fracture

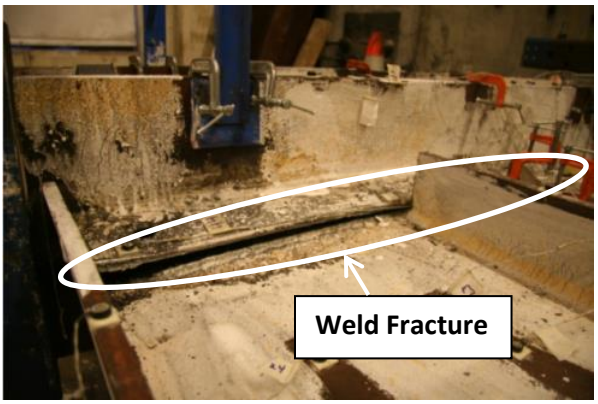

Table 2-10: NCBF1-R3 Test Summary (Adapted from Sloat 2014)

Goal: Retrofit evaluation of welded continuous shear plate using an in-plane buckling knife plate retrofit to reduce deformation demands on gusset plate and welds.

Connection Detail and DCRs

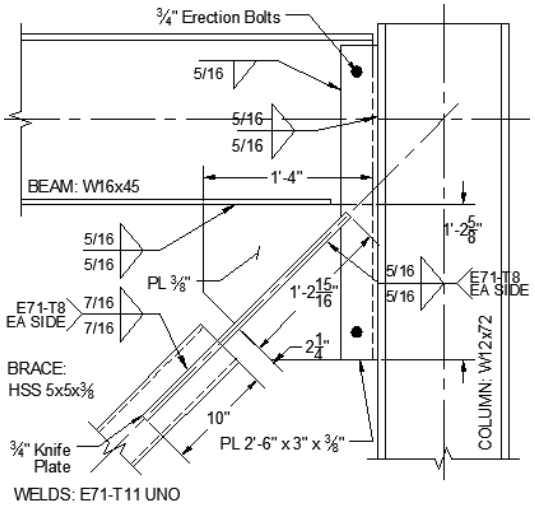

Type	Limit State	DCR
Yielding Mechanisms	Gusset Plate Whitmore Yielding	*1.05*
	Knife Plate Yielding	0.70
	Shear Plate Yielding	0.58
Failure Modes	Brace Net Section Fracture	**1.12**
	Brace Splice Fracture	0.49
	Brace Block Shear	0.40
	Gusset Plate Whitmore Fracture	0.77
	Gusset Plate Block Shear	**1.07**
	Beam-to-Gusset Plate Weld Fracture (GP)	0.67
	Beam-to-Gusset Plate Weld Fracture (BR-CVM)	0.63
	Shear Plate Weld Fracture (GP)	**1.35**
	Shear Plate Weld Fracture (BR-CVM)	**1.22**
Geometric Limits	Brace Compactness Ratio (b/t)/λhd	0.95
	Slenderness Ratio (KL/r)max	77

Specimen Performance Summary

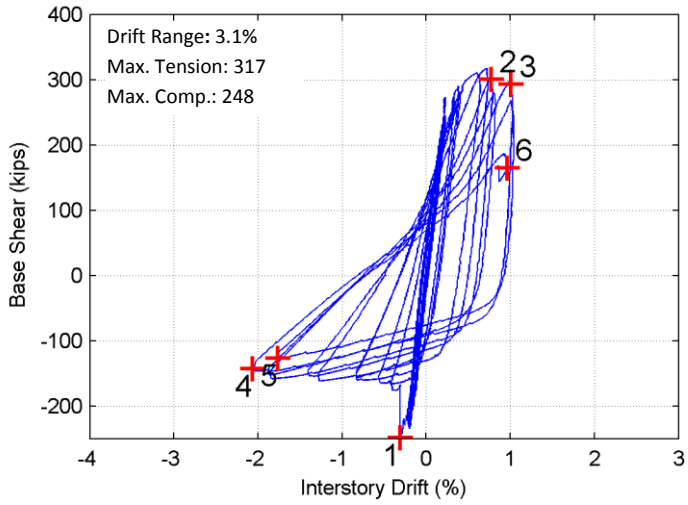

Yield Hierarchy: Connection (Shear Plate) → Brace

Failure Mode: Gusset Plate-to-Beam Weld Fracture → Shear Plate Weld Fracture

Damage Progression

1. Brace buckles in-plane.
2. Initial weld (<1/4") tearing in shear plate weld at end of knife plate.
3. Moderate weld tearing (4") in shear plate weld at end of knife plate.
4. Initial weld tearing (6") in beam-to-gusset plate
5. **Beam-to-gusset plate weld fracture.**
6. **Shear plate weld fracture**

Note: Originally this brace started buckling out-of-plane. A bearing support was put underneath the brace to force in-plane buckling

(3) Weld Crack Initiation

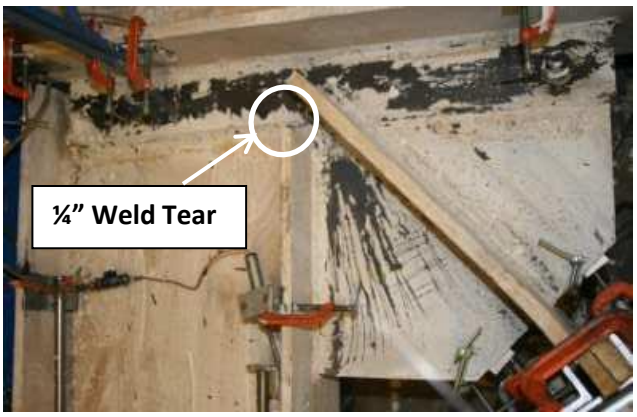

(6) NE Connection Damage at End of Test

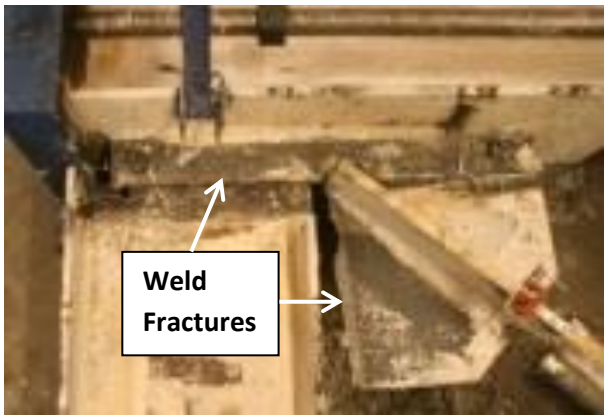

Table 2-11: NCBF1-R4 Test Summary (Adapted from Sloat 2014)

Goal: Retrofit evaluation of welded continuous shear plate using an in-plane buckling knife plate retrofit brace to reduce demands on gusset plate welds. Shorter knife plate to reduce local strains.

Connection Detail and DCRs

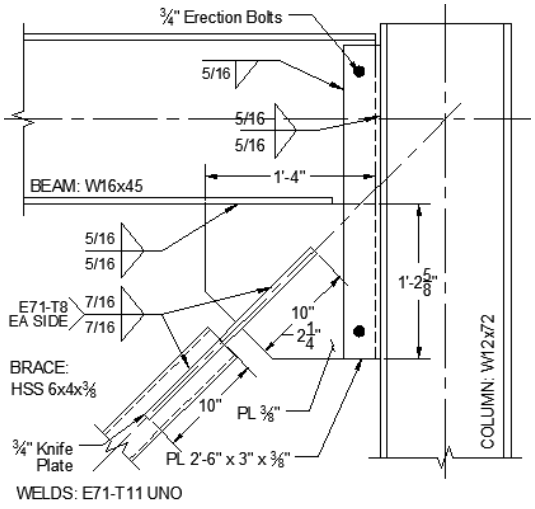

Type	Limit State	DCR
Yielding Mechanisms	Gusset Plate Whitmore Yielding	*1.53*
	Knife Plate Yielding	0.66
	Shear Plate Yielding	0.58
Failure Modes	Brace Net Section Fracture	**1.16**
	Brace Splice Fracture	0.69
	Brace Block Shear	0.57
	Gusset Plate Whitmore Fracture	**1.09**
	Gusset Plate Block Shear	**1.45**
	Beam-to-Gusset Plate Weld Fracture (GP)	0.67
	Beam-to-Gusset Plate Weld Fracture (BR-CVM)	0.59
	Shear Plate Weld Fracture (GP)	**1.35**
	Shear Plate Weld Fracture (BR-CVM)	**1.14**
Geometric Limits	Brace Compactness Ratio $(b/t)/\lambda_{hd}$	1.15
	Slenderness Ratio (KL/r)max	93

Specimen Performance Summary

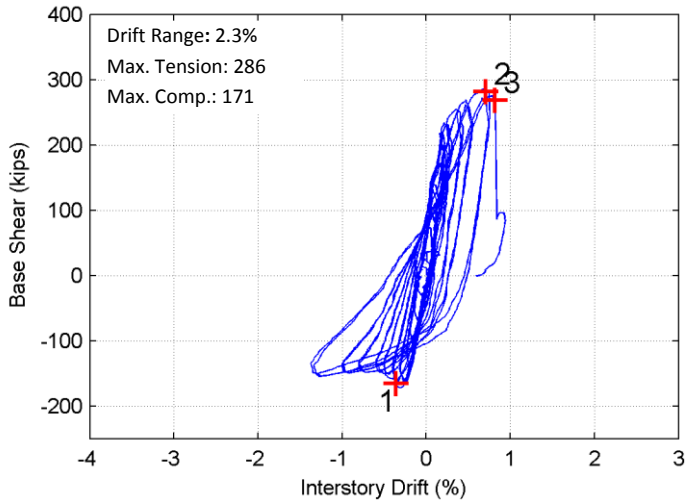

Yield Hierarchy: Connection **(**Gusset Plate) → Brace

Failure Mode: Shear Plate Weld Fracture

1. Brace begins to buckle in-plane.
2. Initial weld tearing at intersection of shear plate and gusset plate welds.
3. Shear plate weld fractures.

(2) Initial Weld Tearing

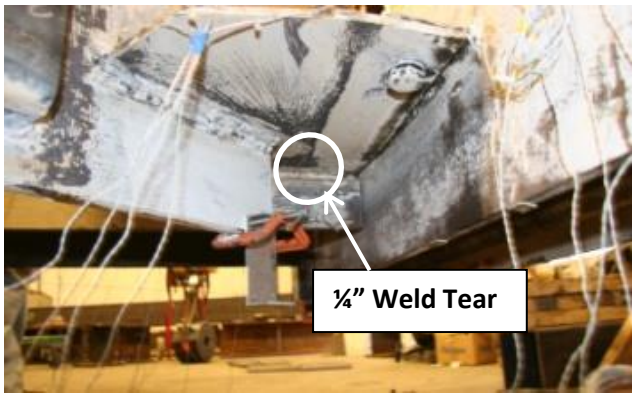

(3) Shear Plate Weld Fracture

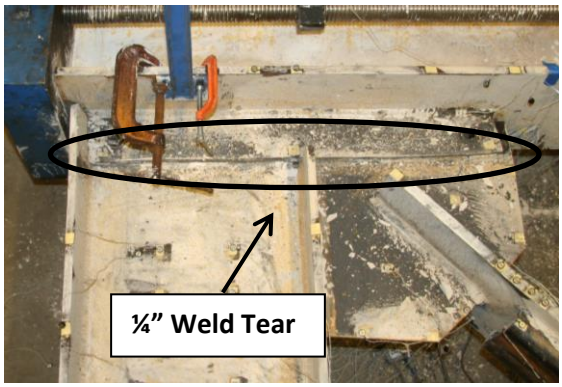

Table 2-12: NCBF1-R5 Test Summary (Adapted from Sloat 2014)

Goal: Retrofit evaluation of welded continuous shear plate using shear plate bolt reinforcement and concrete in-fill of non-compact brace to prolong brace live and protect vulnerable shear plate weld.

Connection Detail and DCRs

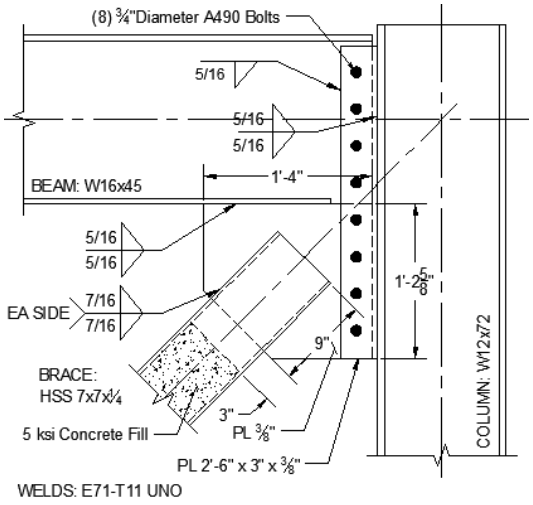

Type	Limit State	DCR
Yielding Mechanisms	Gusset Plate Whitmore Yielding	*1.21*
	Shear Plate Yielding	0.61
Failure Modes	Brace Net Section Fracture	**1.19**
	Brace Splice Fracture	0.85
	Brace Block Shear	1.00
	Gusset Plate Whitmore Fracture	0.87
	Gusset Plate Block Shear	**1.02**
	Beam-to-Gusset Plate Weld Fracture (GP)	0.67
	Beam-to-Gusset Plate Weld Fracture (BR-CVM)	0.65
	Shear Plate Weld Fracture (GP)	**1.35**
	Shear Plate Weld Fracture (BR-CVM)	**1.28**
Geometric Limits	**Brace Compactness Ratio (b/t)/λhd**	**2.31**
	Slenderness Ratio (KL/r)max	60.60

Specimen Performance Summary

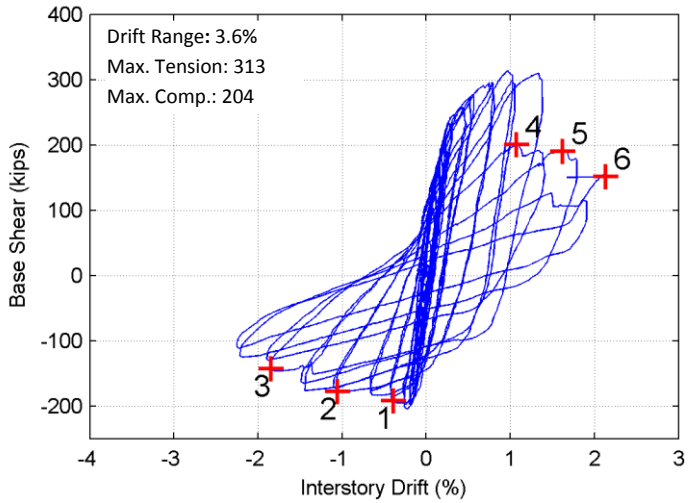

Yield Hierarchy: Connection (Gusset Plate) → Brace

Failure Mode: Beam-to-Gusset Plate Weld Fracture → Brace Fracture

1. Brace begins to buckle out-of-plane.
2. Initial weld tearing at edge of beam-to-gusset plate weld.
3. **Beam-to-gusset plate weld fractures**. Brace begins to hinge near mid-span.
4. Metal tearing in shear plate.
5. Brace tearing.
6. **Brace fracture.**

(4) Metal Tearing in Shear Plate

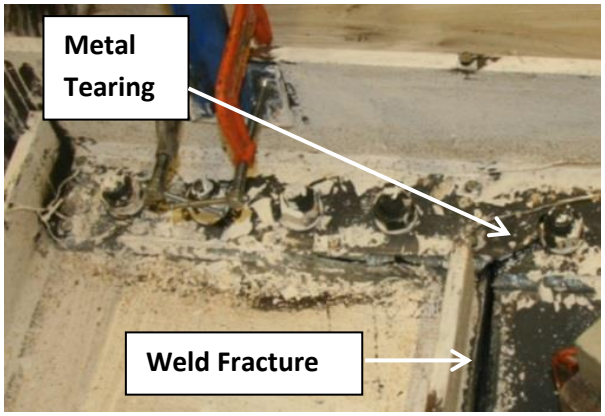

(6) Brace Fracture

Table 2-13: NCBF2 Test Summary (Adapted from Johnson 2014)

Goal: Baseline evaluation of bolted continuous shear plate connection identified in the infrastructure review.

Connection Detail and DCRs

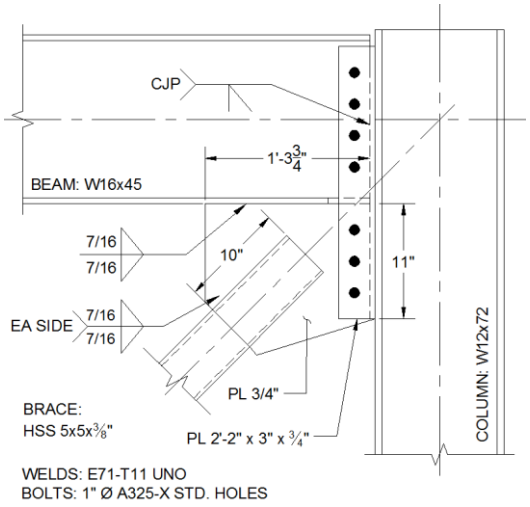

	Limit State	DCR
Yielding Mechanisms	Gusset Plate Whitmore Yielding	0.54
	Bolt Bearing Shear Plate (BR-CVM)	0.76
Failure Modes	Brace Net Section Fracture	**1.25**
	Brace Splice Fracture	0.73
	Brace Block Shear	0.68
	Gusset Plate Whitmore Fracture	0.38
	Gusset Plate Block Shear	0.35
	Gusset Plate-to-Beam Weld Fracture (GP)	**1.06**
	Gusset Plate-to-Beam Weld Fracture (BR-CVM)	0.76
	Bolt Rupture Shear Plate (BR-CVM)	**1.14**
Geometric Limits	Brace Compactness Ratio (b/t)/λhd	0.95
	Slenderness Ratio (KL/r)max	89.4

Specimen Performance Summary

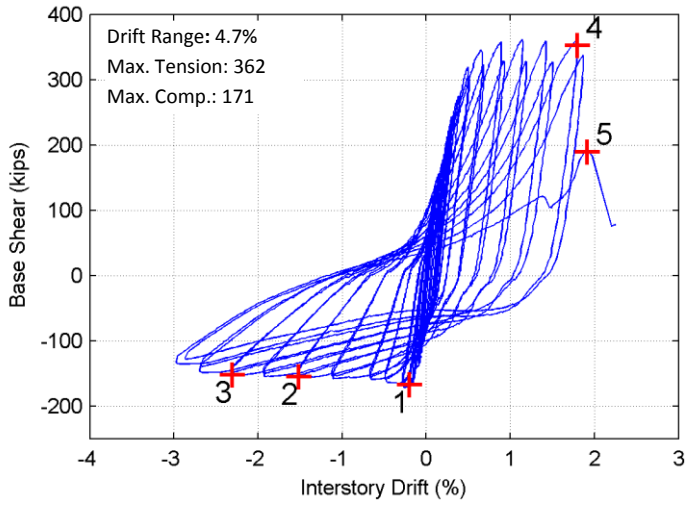

Yield Hierarchy: Brace → Connection (bolt hole elongation in beam web and bolt shear deformation in gusset plate)

Failure Mode: Brace fracture

1. Brace begins to buckle out-of-plane.
2. Initial weld tearing at edge of beam-to-gusset plate weld.
3. Brace begins to hinge at mid-span.
4. Brace begins tearing at hinge location.
5. **Brace fractures.**

(5) Brace Fracture

(5) NE Connection Damage at End of Test

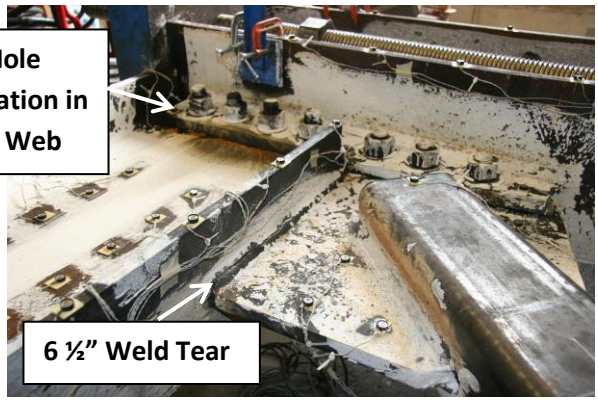

Table 2-14: NCBF3-1 Test Summary (Adapted from Johnson 2014)

Goal: Baseline evaluation of bolted split shear plate connection seen in the infrastructure review.

Connection Detail and DCRs

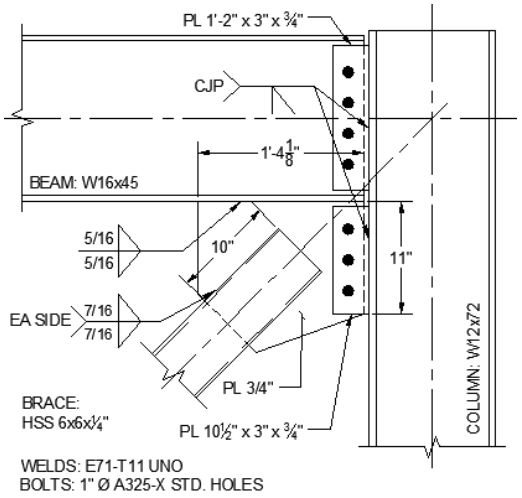

	Limit State	DCR
Yielding Mechanisms	Gusset Plate Whitmore Yielding	0.41
	Bolt Bearing Gusset Plate-Shear Plate (BR-UFM)	0.60
	Bolt Bearing Beam Web-Shear Plate (BR-UFM)	*1.17*
Failure Modes	Brace Net Section Fracture	**1.12**
	Brace Splice Fracture	0.59
	Brace Block Shear	0.76
	Gusset Plate Whitmore Fracture	0.29
	Gusset Plate Block Shear	0.27
	Gusset Plate Interface Weld Fracture (GP)	**1.62**
	Gusset Plate-to-Beam Weld Fracture (BR-UFM)	0.38
	Bolt Rupture Gusset Plate-Shear Plate (BR-UFM)	**1.04**
	Bolt Rupture Beam Web-Shear Plate (BR-UFM)	0.82
Geometric Limits	Brace Compactness Ratio (b/t)/λhd	1.72
	Slenderness Ratio (KL/r)max	71.50

Specimen Performance Summary

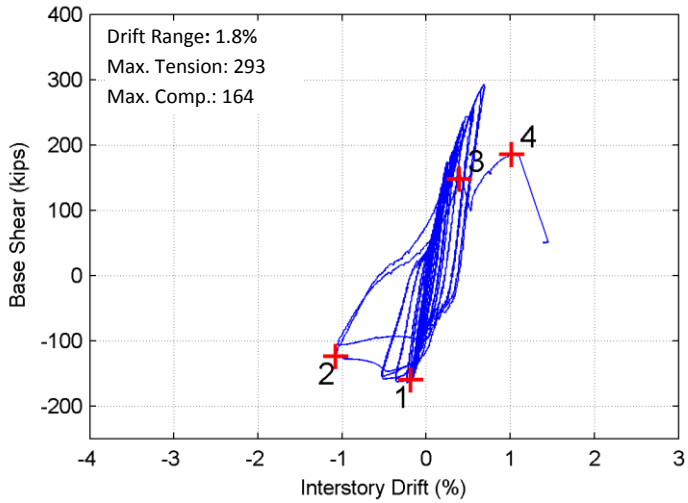

Yield Hierarchy: Brace → Connection (Gusset Plate)

Failure Mode: Gusset Plate-to-Beam Weld Fracture → Bolt Rupture in Gusset Plate-to-Shear Plate Connection

1. Brace begins to buckle out-of-plane.
2. Initial weld tearing at edge of beam-to-gusset plate weld.
3. **Beam-to-gusset plate weld fractures.**
4. **Bolt rupture in gusset plate-to-shear plate.**

(2) Initial Weld Tear in Beam-to-Gusset Plate Weld

(4) NE Connection Damage at End of Test

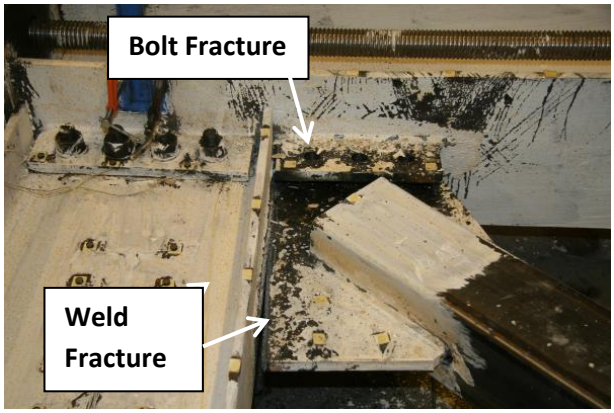

Table 2-15: NCBF3-2 Test Summary (Adapted from Johnson 2014)

Goal: Evaluate bolted split shear plate with a highly ductile brace and thinner gusset plate.

Connection Detail and DCRs

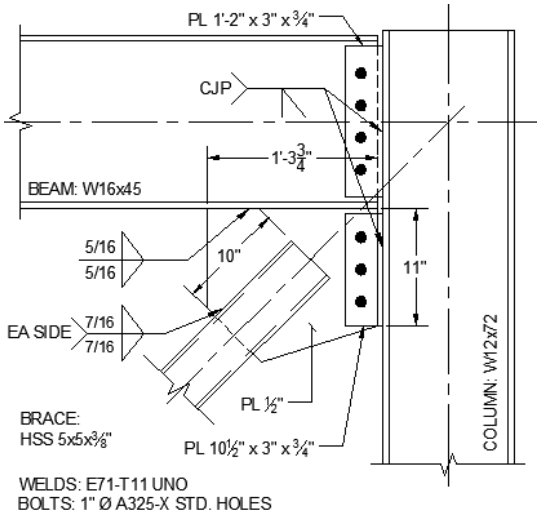

	Limit State (AISC-UFM)	DCR
Yielding Mechanisms	Gusset Plate Whitmore Yielding	0.72
	Bolt Bearing Gusset Plate-Shear Plate (BR-UFM)	0.88
	Bolt Bearing Beam Web-Shear Plate (BR-UFM)	*1.35*
Failure Modes	Brace Net Section Fracture	**1.21**
	Brace Splice Fracture	0.73
	Brace Block Shear	0.68
	Gusset Plate Whitmore Fracture	0.54
	Gusset Plate Block Shear	0.51
	Gusset Plate Interface Weld Fracture (GP)	**1.12**
	Gusset Plate-to-Beam Weld Fracture (BR-UFM)	0.64
	Bolt Rupture Gusset Plate-Shear Plate (BR-UFM)	**1.06**
	Bolt Rupture Beam Web-Shear Plate (BR-UFM)	0.94
Geometric Limits	Brace Compactness Ratio (b/t)/λhd	0.95
	Slenderness Ratio (KL/r)max	89.50

Specimen Performance Summary

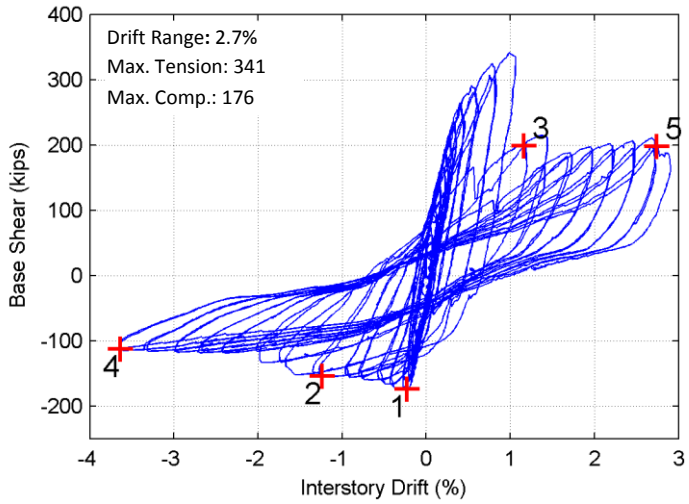

Yield Hierarchy: Brace → Connection (Bolt hole elongation in Gusset Plate)

Failure Mode: Beam-to-Gusset Plate Weld Fracture

1. Brace begins to buckle out-of-plane
2. Initial weld tearing at edge of beam-to-gusset plate weld.
3. **Beam-to-gusset plate weld fractures**
4. Brace begins hinging at mid-span
5. **Bolt ruptures in gusset plate-to-shear plate.**

(2) Beam-to-Gusset Plate Weld Fracture

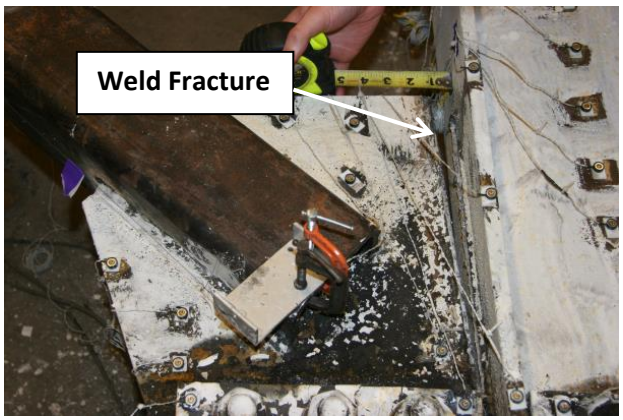

NE Connection Damage (6.2% Drift Range)

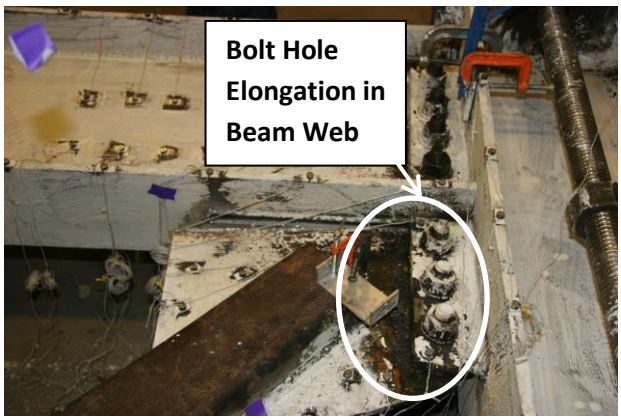

Chapter 3: Specimen Design

3.1 Introduction

This chapter documents the goals, the design methodology, and the connection details for five individual test specimens. The design of all five specimens is discussed individually in Sections 3.2 through 3.6. Specimen connection details were based on NCBF connection details identified during the infrastructure review (Section 2.3.1) including bolted end plate, integrated gusset-shear plate, and bolted continuous shear plate connections. DCR evaluation for reference connections and designed specimen connection details followed the procedures outlined in Section 2.3.2.

3.2 Specimen NCBF4-R1

The overall goal for the testing of Specimen NCBF4-R1 was to determine the deformation capacity of a single-bay frame using a bolted end plate connection that was similar to bolted end plate reference connections from the infrastructure review. This test provides a baseline evaluation of the bolted end plate connections and a comparison point to other baseline tests (Specimens NCBF1-R2, NCBF2, and NCBF3) conducted by Sloat (2014) and Johnson (2014).

Reference connections (shown in Figure 3-1) were selected from the infrastructure review to represent typical existing bolted end plate connections. Geometric details of the reference connections such as plate thicknesses and bolt details are shown in Table 3-1. The reference connections each use seismically compact angle braces bolted to the gusset plates. The angles are extended deep into the connection and provide minimal clearance for gusset plate out-of-plane deformation due to brace end rotation. Gusset plates and beam ends are connected to the end plate using all around fillet welds. The gross area of the brace for the Reference Connection 1, denoted BEP-Ref. 1 and shown in Figure 3-1a, is over three times as large as the brace in Reference Connection 2, denoted BEP-Ref. 2 and shown in Figure 3-1b. As such, the number of bolts, size of bolts, plate dimensions, and frame member sizes for the two reference connections are different and are documented in Table 3-1.

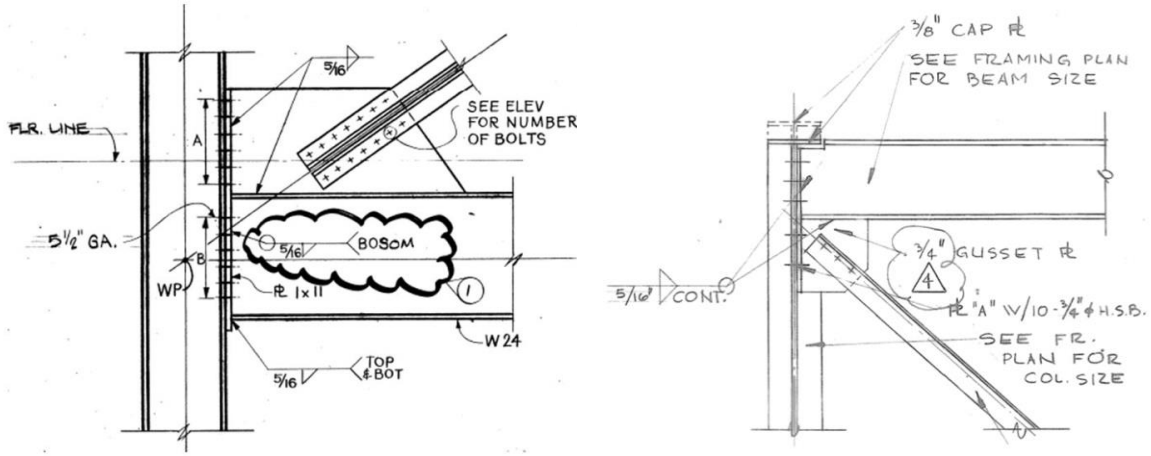

a. Reference Connection 1 (BEP-Ref. 1) b. Reference Connection 2 (BEP-Ref. 2)

Figure 3-1: Reference Connections for Bolted End Plate Connections

Table 3-1: Connection Geometry and Definition for Reference Bolted End Plate Connections

Connection Geometry	BEP-Ref. 1	BEP-Ref. 2	Scaled
Infrastructure Building Code (Sloat 2014)	80WA8A	88UT1A	NA
Brace Type	4L4x4x3/4	L6x4x3/4	4L3x3x3/8
Column Size	W14x257	W8x24	W12x72
Beam Size	W24x162	W16x31	W16x45
Brace Angle (deg)	33.7	38.7	45.0
Interface Weld Size	5/16"	5/16"	1/4"
Thickness of End Plate	1"	1/2"	5/8"
Thickness of Gusset Plate (in)	1"	3/4"	5/8"
Number of End Plate Bolts	24	10	16
Diameter of End Plate Bolts (in)	1-1/8"	3/4"	7/8"

To provide a better comparison between the reference bolted end plate connections a DCR evaluation was conducted. DCRs for the reference bolted end plate connections are shown in Table 3-2. Deficiencies for the reference connection are highlighted in the table and included brace net section fracture, bolt shear in the brace-to-gusset plate connection, beam-to-gusset plate weld fracture (using both the expected brace and expected gusset plate capacities).

Table 3-2: Demand Capacity Ratio for Reference Bolted End Plate Connections

	Limit State	BEP-Ref. 1	BEP-Ref. 2	NCBF4
Yielding Mechanisms	Gusset Plate Whitmore Yielding	0.83	0.81	0.76
	End Plate Bolt Bearing (BR-CVM)	0.14	0.47	0.18
Failure Modes	Brace Net Section Fracture	0.99	**1.14**	0.87
	Brace Splice Fracture	0.62	**1.10**	0.62
	Brace Block Shear	0.60	0.81	0.59
	Gusset Plate Whitmore Fracture	0.60	0.54	0.54
	Gusset Plate Block Shear	0.55	0.47	0.50
	Beam-to-Gusset Plate Weld Fracture (GP)	**1.98**	**1.26**	**1.54**
	Beam-to-Gusset Plate Weld Fracture (BR-CVM)	0.88	**2.02**	0.61
	Gusset Plate-to-End Plate Weld Fracture (BR-CVM)	0.98	0.41	0.69
	End Plate Bolt Shear (BR-CVM)	0.40	0.98	0.40
Geometric Limits	Brace Compactness Ratio $(b/t)/\lambda_{hd}$	0.42	0.63	0.52
	Slenderness Ratio $(KL/r)_{max}$	171	144	115

A representative bolted end plate connection, termed NCBF4 (shown in Figure 3-2), was designed to emulate the characteristics and deficiencies seen in the reference connections while satisfying the laboratory constraints. Associated connection details and DCRs for NCBF4 are shown alongside the reference connections in Table 3-1 and Table 3-2.

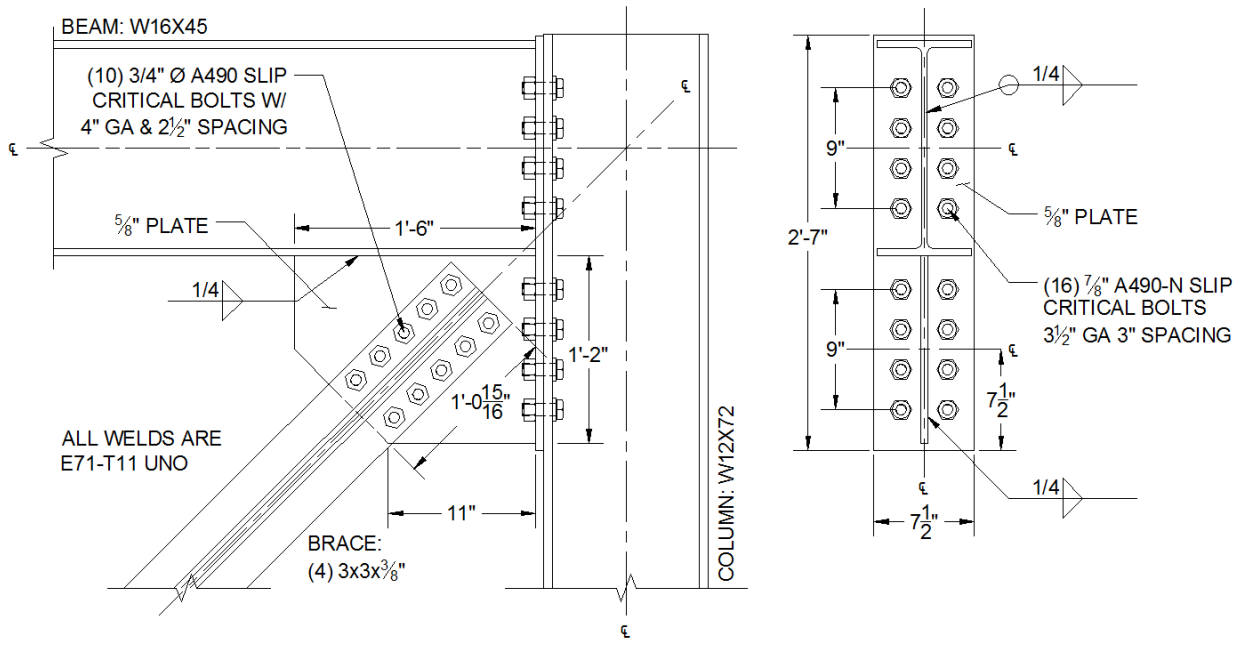

Figure 3-2: NCBF4 Connection Detail

Like the reference connections, NCBF4 uses seismically compact angles bolted to the gusset plate and extended deep into the gusset plate. A quadruple angle brace configuration is selected for NCBF4 (as seen in BEP-Ref. 1) as opposed to using one single angle brace (as seen in BEP-Ref. 2) because it is a more prevalent brace configuration in the infrastructure review. Each angle meets seismic compactness criteria and has an expected capacity within the loading capabilities of the actuator used in the experimental setup. Bolts connecting the brace-to-gusset plate and gusset plate thickness were selected such that NCBF4 would have similar DCRs to the reference connections for limit states related to the gusset plate and brace.

The selection of the bolt size, bolt type, and number of bolts in the end plates was done to match DCR values for the end plate bolt shear limit state seen in BEP-Ref. 1[1]. End plate thickness and bolt gauge/ spacing in the end plate were selected to match the potential for prying action in the end plate. The welds connecting the gusset plate to the beam and the end plate were sized based on bolt (GP and BR-CVM) weld design approaches.

Ideally a test of the scaled connection would be the best representation of the reference connections; however, quadruple angle bracing had not been tested in the SRL for several reasons including the inability to control the direction of buckling and the limited actuator capacity. Additionally, the initial tests for other connection configurations (Specimens NCBF1-R2, NCBF2, and NCBF3) tested by Sloat

[1] Since both reference connections had different DCRs for multiple limit states it was decided to base the design of the end plate for NCBF4 connection components based primarily on one reference connection. BEP-Ref. 1 was selected over BEP-Ref. 2 because of the similarities of column orientation and frame member size with the experimental setup.

(2014) and Johnson (2014) used a seismically compact 5x5x3/8" HSS section. To provide a better point of comparison, the first test specimen of the bolted end plate connection, Specimen NCBF4-R1, was a retrofit option where the angles were replaced by a highly ductile 5x5x3/8" HSS brace. The connection detail for Specimen NCBF4-R1 is shown in Figure 3-3.

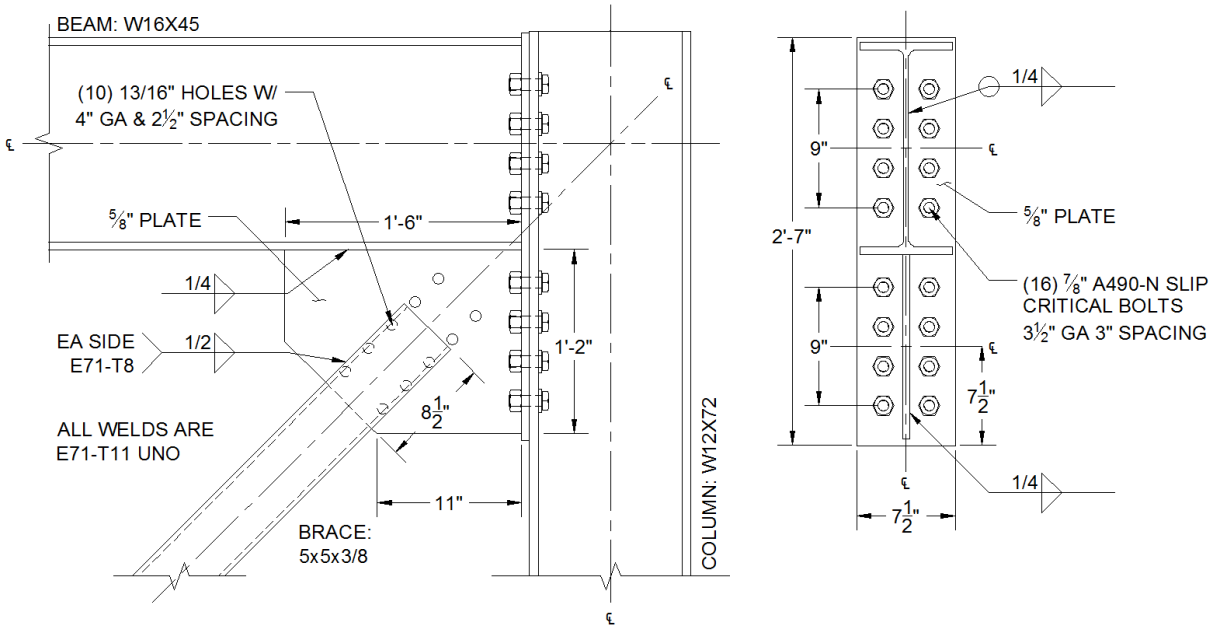

Figure 3-3: Connection Detail for NCBF4-R1

To make the retrofit more cost effective, the existing gusset plate was left in place. In practice, it would be much cheaper to remove the bolts from the angles than to cut/ grind out the gusset plate which would also require removal and replacement of bolts in the end plate. Since an existing gusset plate was simulated, bolt holes were drilled into the gusset plate to represent existing holes that would have been used for the quadruple angle brace connection. To reduce the out-of-plane deformation demands at the edge of the gusset plate a $3t_{gp}$ elliptical clearance was also provided. The seismically compact HSS brace was connected to the gusset plate with ductile welds sized to prevent splice weld fracture since some brace weld fractures were studied in other test specimens (e.g. Specimen NCBF0 – Powell 2009).

The DCRs for Specimen NCBF4-R1 are shown Table 3-3. In general the DCRs for Specimen NCBF4-R1 are similar to the scaled connection because the connection geometry is identical. Differences between the DCRs arise from a slight difference in the brace capacities, the brace-to-gusset plate connection detail, and material properties. Although Specimen NCBF4-R1 is shown as deficient for brace net section fracture (DCR = 1.20), this limit state has not been a large factor in past NCBF tests at the UW SRL with similar DCRs (i.e. Specimen NCBF2), and net section reinforcement was not provided.

Table 3-3: Demand Capacity Ratios for NCBF4-R1

	Limit State	NCBF4	NCBF4-R1
Yielding Mechanisms	Gusset Plate Whitmore Yielding	0.76	0.82
	End Plate Bolt Bearing (BR-CVM)	0.18	0.17
Failure Modes	Brace Net Section Fracture	0.87	**1.22**
	Brace Splice Fracture	0.62	0.76
	Brace Block Shear	0.59	0.77
	Gusset Plate Whitmore Fracture	0.54	0.60
	Gusset Plate Block Shear	0.50	0.59
	Beam-to-Gusset Plate Weld Fracture (GP)	**1.54**	**1.58**
	Beam-to-Gusset Plate Weld Fracture (BR-CVM)	0.61	0.63
	Gusset Plate-to-End Plate Weld Fracture (BR-CVM)	0.69	0.71
	End Plate Bolt Shear (BR-CVM)	0.40	0.41
Geometric Limits	Brace Compactness Ratio $(b/t)/\lambda_{hd}$	0.52	0.95
	Slenderness Ratio $(KL/r)_{max}$	115	88

3.3 Specimen NCBF4-R2

Specimen NCBF4-R2, shown in Figure 3-4, is a retrofit of NCBF4 connection detail developed in Section 3.2. The goal of Specimen NCBF4-R2 was to determine how much additional deformation the bolted end plate connection could accommodate provided that the beam-to-gusset plate weld was protected from high localized stress induced by out-of-plane deformation demands such as brace end rotation. To accomplish this, an in-plane buckling retrofit utilizing a knife plate and rectangular brace oriented about its weak axis was devised.

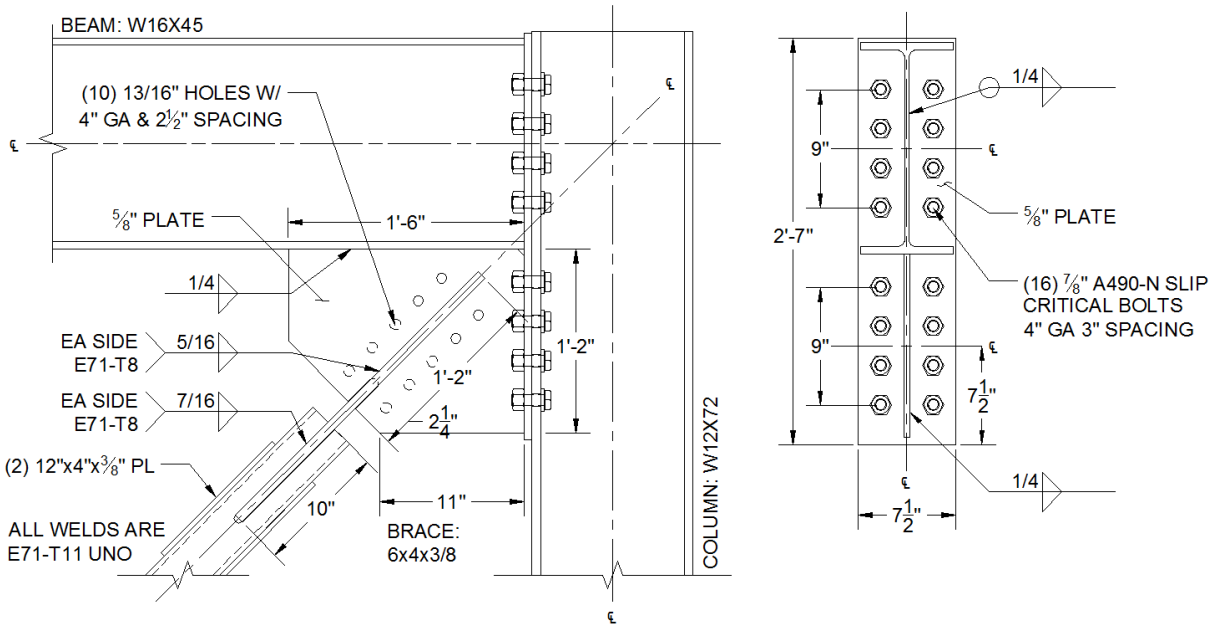

Figure 3-4: Connection Detail for NCBF4-R2

Ideally a knife plate in-plane buckling retrofit ensures in-plane brace buckling by providing gusset plate out-of-plane rotational restraint and reducing the critical buckling load for in-plane buckling. In theory this can be achieved for doubly symmetric cross sections such as a square HSS; however, previous tests designed to buckle in-plane using knife plate retrofits with square braces [NCBF1-R3 (Sloat 2014) and TNCBF1-R-HSS (Sen 2014)], developed out-of-plane brace buckling during testing. To ensure that in-plane buckling occurred in NCBF4-R2, a 6x4x3/8" rectangular brace oriented such that it would buckle about its weak axis in-plane was selected over a similar 5x5x3/8" square brace. Although the rectangular brace did not meet highly ductile compactness requirements per AISC 341 (2010), it still met overall seismic compactness requirements and was categorized in the lesser "moderately ductile" category, a consequence necessary to ensure in-plane buckling.

Like NCBF4-R1, the gusset plate of the scaled connection was left in place to reduce the overall cost of the retrofit. As such, the connection geometry for NCBF4-R2 is identical to both NCBF4-R1 and the scaled connection detail developed in Section 3.2. The DCR's for NCBF4-R2 and the representative scaled connection are shown in Table 3-4.

Table 3-4: Demand to Capacity Ratios for NCBF4-R2

	Limit State	Scaled	NCBF4-R2
Yielding Mechanisms	Gusset Plate Whitmore Yielding	0.76	0.82
	Knife Plate Yielding	NA	*1.12*
	End Plate Bolt Bearing (BR-CVM)	0.18	0.17
Failure Modes	Brace Net Section Fracture	0.87	NA
	Brace Splice Fracture	0.62	0.75
	Brace Block Shear	0.59	0.66
	Gusset Plate Whitmore Fracture	0.54	0.60
	Gusset Plate Block Shear	0.50	0.64
	Beam-to-Gusset Plate Weld Fracture (GP)	**1.54**	**1.58**
	Beam-to-Gusset Plate Weld Fracture (BR-CVM)	0.61	0.64
	Gusset Plate-to-End Plate Weld Fracture (BR-CVM)	0.69	0.72
	End Plate Bolt Shear (BR-CVM)	0.40	0.42
Geometric Limits	Brace Compactness Ratio $(b/t)/\lambda_{hd}$	0.52	1.21
	Slenderness Ratio $(KL/r)_{max}$	115	0.95

The knife plate cross-section, as shown in Figure 3-5, was sized to prevent gross tensile yielding when subject to the expected brace capacity to prevent failure modes from developing in the knife plate. The thickness of the knife plate and clear distance between the brace and gusset plate was selected as ¾" and three t_{kp} respectively per recommendation by (Tsai et al. 2013). The depth of the knife plate was also constrained to be less than the column flange width. All four corners of the knife plate were tapered to facilitate a better transfer of forces between the brace and the gusset plate (as opposed to a rectangular knife plate). Both the gusset plate and knife plate were slotted as shown in Figure 3-5 to prevent unnecessary stress concentrations from developing at the edge of the splice weld connecting the gusset plate and knife plate. The brace was slotted and welded to the knife plate. Brace-to-knife plate and knife plate-to-gusset plate splice weld were sized to prevent splice weld fracture from occurring. Net section reinforcement was also provided for the brace per AISC (2010).

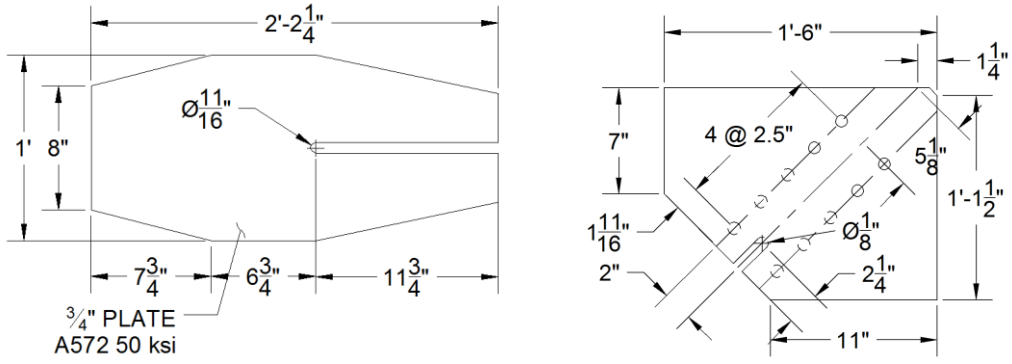

Figure 3-5: Shop Drawings for Knife Plate and Gusset Plate

As shown in Table 3-4 the primary calculated deficiencies for NCBF4-R2 is the beam-to-gusset plate weld fracture evaluated using the yield capacity of the gusset plate. For an out-of-plane buckling brace the gusset plate develops high localized stresses as it rotates out-of-plane to accommodate the buckling brace, but an in-plane buckling brace has the potential to avoid this. Since the gusset plate welds nominally satisfy strength requirements (BR-CVM) and the in-plane buckling is ensured, the beam-to-gusset plate weld fracture deficiency is considered to be addressed.

3.4 Specimen NCBF4-R3

Specimen NCBF4-R3, as shown in Figure 3-6, was a retrofit of the NCBF4 connection detail developed in Section 3.2. The goal of the retrofit was to test another brace option that could limit the deformation demands on the deficient gusset plate welds of an existing gusset plate. A BRB was selected as a viable retrofit for a bolted end plate connection because it places minimal out-of-plane deformation demands on the gusset plate, and could be used to replace deficient non-compact braces seen in the infrastructure review. A BRB retrofit option was designed to achieve a relatively high drift range for a braced frame similar to the BRBF connections tested by Christopulos (2005).

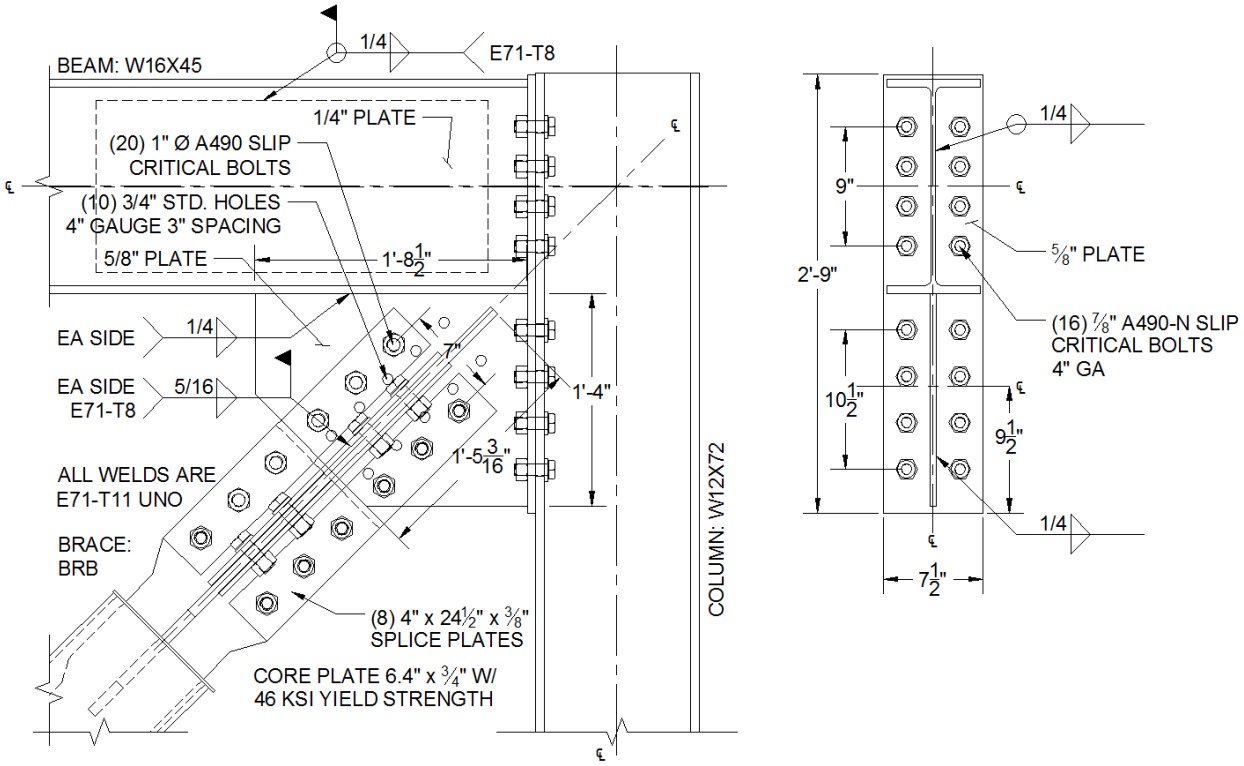

Figure 3-6: Connection Detail for NCBF4-R3

To use the available BRBs, the connection geometry required slight modifications from the representative connection design (NCBF4) to fit the BRB into the frame. Modifications to the representative connection included an increase in gusset plate edge dimensions, increase in end plate length, and modifications to the end plate bolt group connecting the gusset plate to the column. Per recommendations by Palmer et. all (2011), a beam web doubler was included to prevent deformation and damage to the beam web.

The DCRs for Specimen NCBF4-R3 are shown in Table 3-5. The DCRs for the BRB limit states (net section fracture, brace splice fracture, and block shear) are calculated in accordance with Section E.3 while DCRs for the bolted end plate connection limit states are in accordance with Section B.1. All of the DCR's (aside from beam-to-gusset plate weld fracture (GP)) are less than 1.0.

Table 3-5: Demand to Capacity Ratios for NCBF4-R3

	Limit State	NCBF4	NCBF4-R3
Yielding Mechanisms	Gusset Plate Whitmore Yielding	0.76	0.63
	Knife Plate Yielding	NA	NA
	End Plate Bolt Bearing (BR-CVM)	0.18	0.14
Failure Modes	Brace Net Section Fracture	0.87	0.56
	Brace Splice Fracture	0.62	0.33
	Brace Block Shear	0.59	0.36
	Gusset Plate Whitmore Fracture	0.54	0.43
	Gusset Plate Block Shear	0.50	0.44
	Beam-to-Gusset Plate Weld Fracture (GP)	**1.54**	**1.61**
	Beam-to-Gusset Plate Weld Fracture (BR-CVM)	0.61	0.52
	Gusset Plate-to-End Plate Weld Fracture (BR-CVM)	0.69	0.56
	End Plate Bolt Shear (BR-CVM)	0.40	0.38
Geometric Limits	Brace Compactness Ratio $(b/t)/\lambda_{hd}$	0.52	NA
	Slenderness Ratio $(KL/r)_{max}$	115	NA

3.5 Specimen NCBF5

The goal of developing and testing of Specimen NCBF 5 was to examine the performance of an NCBF with a connection detail representative of the integrated gusset-shear connections identified in the infrastructure review. This type of connection utilizes a single gusset plate that is welded to the column. Instead of connecting the beam directly to the column the beam is bolted to the gusset plate which serves as an integrated link between all of the framing components. Although this type of connection is relatively common from the infrastructure review (appears in three of the twelve buildings analyzed Sloat 2014), the geometry for the various integrated gusset-shear plate connections have significant variations including different brace types, bolt group configuration, column orientation, and brace angle. A total of four reference connections were used in the design of Specimen NCBF5. The reference connections for the integrated gusset-shear plate are shown in Figure 3-7 and Figure 3-8. The associated connection details are listed in Table 3-6.

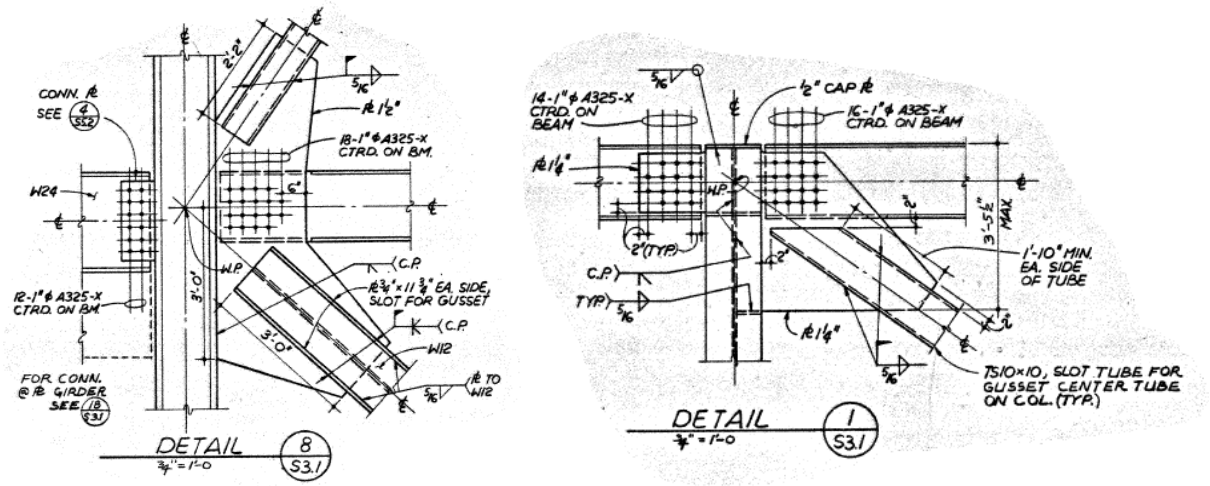

Figure 3-7: Reference Connections for Integrated Shear Plate (Building 1)

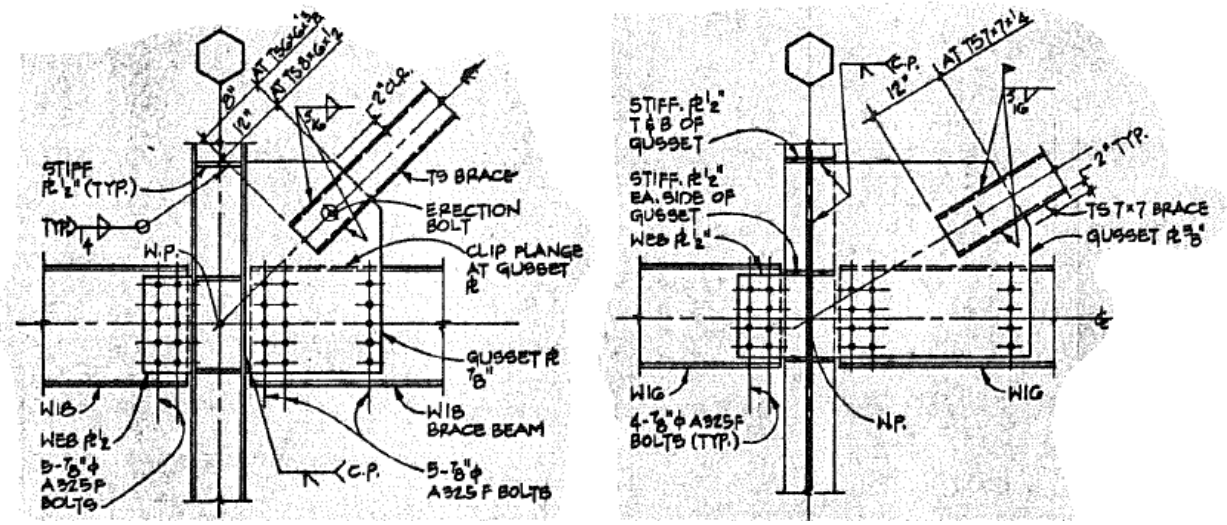

Figure 3-8: Reference Connections for Integrated Shear Plate (Building 2)

Table 3-6: Connection Geometry and Definitions for Integrated Gusset-Shear Plate Reference Connections

Connection Geometry Table	Building 1		Building 2		Specimen
	Ref. 1	Ref. 2	Ref. 3	Ref. 4	NCBF 5
Infrastructure Building Code (Sloat 2014)	83CA3A	83CA3A	88CA3A	88CA3A	NA
Brace Type	8x8x1/2	10x10x3/8	6x6x3/8	7x7x1/4	5x5x3/8
Column Size	W12x252	W12x170	W8x48	W8x48	W12x72
Column Orientation	Strong	Weak	Strong	Weak	Strong
Beam Size	W16x77	W16x77	W16x45	W16x45	W16x45
Brace Angle (degrees)	31.7	33.5	43.4	25.3	45.0
Thickness of Gusset Plate	1-1/2"	1-1/4"	7/8"	5/8"	7/8"
Number of Bolts in Beam Web	18	16	15	15	8
Bolt Type in Beam Web	A325-X	A325-X	A325-N	A325-N	A325-X
Diameter of Bolts in Beam Web	1"	1"	7/8"	7/8"	1"

The reference connections have a range of HSS braces with a variety of compactness ratios. The connections from Building 1 (Figure 3-7) have relativley strong columns and use a condensed bolt group pattern to connect the shear plate and the beam. The gusset plates are thicker than either of the framing member webs and are connected using CJP welds to the column. The connections from Building 2 (Figure 3-8) have much weaker columns than Building 1, and the bolt group is spread out. A DCR evaluation was conducted on all of the reference connections to identify other differences and comanalities between the reference connections. The DCRs for each of the reference connections are computed in accordance with Section 2.3.2 and Section B.2 and are shown in Table 3-7.

Table 3-7: Demand Capacity Ratios for Reference Connections and NCBF 5

NCBF5	Limit States	Building 1		Building 2		Specimen
		ISP-Ref. 1	ISP-Ref. 2	ISP-Ref. 3	ISP-Ref. 4	NCBF5
Yielding Mechanisms	Whitmore Yielding	0.52	0.52	0.79	0.71	0.70
	Base Metal Yielding Integrated Shear Tab	0.57	0.37	0.51	0.36	0.85
	Bolt Bearing in Beam-to Gusset Plate (BR-CVM)	0.64	0.58	0.47	0.48	0.55
Failure Modes	Brace Net Section Fracture	**1.09**	**1.10**	**1.29**	**1.15**	**1.15**
	Brace Splice Fracture	0.98	**1.04**	**1.64**	0.89	0.79
	Brace Block Shear	0.43	0.61	0.97	0.79	0.50
	Gusset Plate Whitmore Fracture	0.35	0.35	0.53	0.48	0.40
	Gusset Plate Block Shear	0.23	0.27	0.51	0.43	0.31
	Bolt Rupture in Beam-to-Gusset Plate (BR-CVM)	0.91	0.83	0.73	0.74	0.63
Geometric Limits	Brace Compactness Ratio $(b/t)/\lambda_{hd}$	1.22	2.20	1.22	2.31	0.95
	Slenderness Ratio $(KL/r)_{max}$	126	95	90	75	93

In general, the reference connections did not have many deficiencies. The main deficiencies include brace net section fracture and brace-to-gusset plate splice weld fracture. Brace net section fracture deficiencies have not been critical in past experiments (e.g. Specimen NCBF2 Table 2-13) and could be

easily retrofit with net section reinforcement plates. Brace splice weld fracture was seen in Specimen NCBF0 (Hsiao et. all 2012) and was not of interest in the design of Specimen NCBF5.

Although the reference connections did not have many calculated deficiencies identified in the DCR evaluation, it is important to consider the potential effects of additional frame forces that would have to be transferred through the beam-to-gusset plate bolt group. Due to uncertainty in the frame details and load transfer mechanism in the reference buildings, the frame forces were not directly computed; However, it was identified that the frame forces could potentially place demands on the bolts in excess of the bolt shear and/or bearing capacities since there was already a large component of horizontal force from the brace assumed to transfer across the bolt group. The beam web was also identified as a potential weak link in the connection due to its relatively thin thickness.

Specimen NCBF 5 was designed to represent the deficiencies and connection characteristics of the integrated gusset-shear plate reference connections discussed above. The connection detail for Specimen NCBF5 is shown in Figure 3-9. A summary of the connection details and the connection DCRs for Specimen NCBF5 are shown in Table 3-6 and Table 3-7 alongside the reference connections.

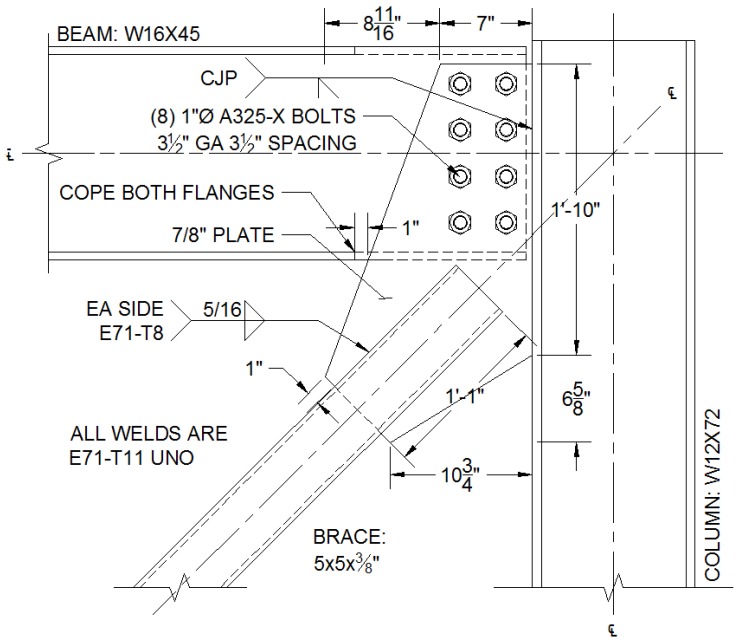

Figure 3-9: Connection Detail for Specimen NCBF5

A 5x5x3/8" HSS tube was selected for the bracing member so that comparisons could be drawn with other baseline connection tests (e.g. Specimen NCBF2 Johnson 2014) and to test the connection over the potential drift range of a highly ductile brace. A 13" long 5/16" fillet welds was found to match the brace net section demand to capacity ratio seen in the reference connections but was sized to prevent splice weld fracture. The gusset plate was then sized to have a DCR for Whitmore Yielding comparable to the four reference connections.

The bolt group for the reference connection uses a condensed pattern similar to the bolt patterns seen in the reference connections for Building 1. This pattern is used because it is assumed to be more prevalent in existing infrastructure than the spread bolt group seen in Building 2. The size and number of bolts in the beam-to-gusset plate connection was selected to match the bolt shear rupture limit state. The spacing of the bolts was selected to maximize the moment capacity of the bolt group.

Both flanges of the beam in Specimen NCBF5 were coped to better match the ratio between plastic moment capacity at the reduced beam section and the moment capacity of the bolt group. Moment capacity of the bolt group was calculated by assuming a constant horizontal force across the bolts and determining the eccentricity that it could be placed at. The calculations for the instantaneous center in this case do not directly indicate the capacity of the connection but rather serve as additional scaling checks.

3.6 Specimen NCBF2-R1

Specimen NCBF2-R1 was a retrofit connection of Specimen NCBF2 conducted by Johnson (2014). The connection detail, deficiencies, and performance for Specimen NCBF2 are described earlier in Section 2.4.4, but are reiterated here to provide context for the design of Specimen NCBF2-R1. Similar to the other tests, Specimen NCBF2 was designed based on a reference connection from the infrastructure review. The reference connection and geometric details for the connection are shown in Figure 3-10 and Table 3-8 respectively. The reference connection uses a continuous shear plate that is welded to the column and bolted to both the gusset plate and the beam web. Structural steel pipes are used to resist the lateral forces and are typically extended deep into the gusset plate connection. The gusset plate is over twice as thick as either the beam or column webs and the welds connecting the gusset plate to the beam are non-ductile.

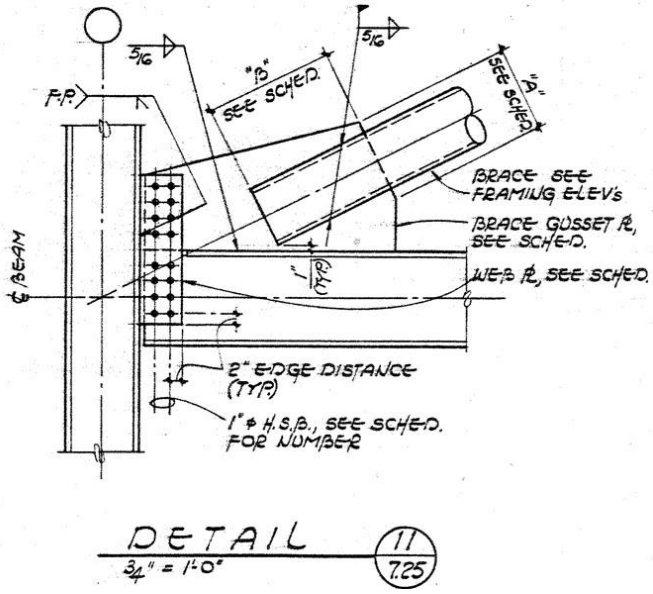

Figure 3-10: Reference Connection for Specimen NCBF2 (Johnson 2014)

Table 3-8: Connection Details for Continuous Shear Plate Connections

Connection Geometry	BCP - Ref 1.	NCBF2	NCBF2-R1
Infrastructure Building Code (Sloat 2014)	82TN4A	NA	NA
Brace Type	HSS12x12x1/2	HSS5x5x3/8	BRB
Column Size	W14x145	W12x72	W12x72
Beam Size	W18x50	W16x45	W16x45
Brace Angle (deg)	26.9	45.0	45.0
Beam-to-Gusset Plate Interface Weld Size	5/16"	5/16"	5/16"
Thickness of Shear Plate	3/4"	3/4"	3/4"
Thickness of Gusset Plate (in)	1-1/4"	3/4"	3/4"
Number of Shear Plate Bolts	16	7	7
Diameter of Shear Plate Bolts (in)	1"	1"	1"

A DCR evaluation was conducted on the connection using the assumed geometric details presented in Table 3-8 in accordance with Sections 2.3.2 and B.3. Calculated DCRs for the reference connection are shown in Table 3-9. Connection deficiencies include brace splice weld fracture, brace net section fracture, gusset plate-to-beam weld fracture (GP and BR-CVM), shear plate bolt fracture, and shear plate combined yielding The reference connection also utilizes a non-ductile pipe brace, welds that may not have met SCBF minimum demand critical toughness requirements, and limited rotation clearance for out-of-plane brace buckling.

Table 3-9: Demand Capacity Ratios for Continuous Bolted Shear Plates

	Limit State	Ref 1.	NCBF2	NCBF2-R1
Yielding Mechanisms	Gusset Plate Whitmore Yielding	0.89	0.54	0.82
	Shear Tab Plate Yielding (BR-CVM)	**1.11**	0.50	0.67
Failure Modes	Brace Net Section Fracture	**1.07**	**1.24**	0.73
	Brace Splice Fracture	**1.20**	0.73	0.33
	Brace Block Shear	0.42	0.68	0.36
	Gusset Plate Whitmore Fracture	0.61	0.38	0.44
	Gusset Plate Block Shear	0.31	0.35	0.33
	Gusset Plate Interface Weld Fracture (GP)	**2.10**	**1.16**	0.74
	Gusset Plate-to-Beam Weld Fracture (BR-CVM)	**1.02**	**1.25**	0.83
	Shear Tab Bolt Fracture (BR-CVM)	**1.08**	**1.14**	**1.05**
Geometric Limits	Brace Compactness Ratio $(b/t)/\lambda_{hd}$	1.07	0.95	NA
	Slenderness Ratio $(KL/r)_{max}$	58.82	89.41	NA

A detail of Specimen NCBF2 is shown in Figure 3-11. Specimen NCBF2 was designed by Johnson (2014) based on the reference connection geometry and DCRs. A number of the connection deficiencies described had previously been evaluated including brace compactness in Specimen NCBF1 and Whitmore yielding/ shear plate yielding in Specimen NCBF1-R2 (Sloat 2014). To avoid testing the same

deficiencies, the design of the representative connection focused on the bolt shear deficiency. The final design uses a single row of seven 1" diameter bolts connecting a ¾" shear plate with the beam web and gusset plate. The weld size connecting the beam-to-gusset plate was originally sized so that the AISC weld fracture limit state remained similar to the reference connection. The shear plate was increased in size and was detailed with a CJP weld. The brace was highly ductile HSS out-of-plane buckling brace that satisfied the seismically compact criteria defined by AISC 341 (2010)

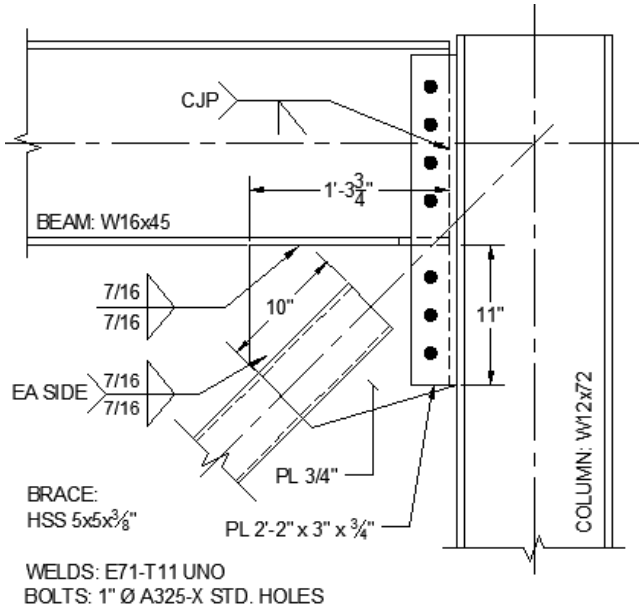

Figure 3-11: Connection Detail for NCBF2 (Johnson 2014)

Although having a bolt shear deficiency, limited clearance and non-ductile welds, Specimen NCBF2 was able to attain a drift range of 4.7% through several ductile mechanisms including brace buckling and bolt hole elongation (see Table 2-13). This specimen performed well with a highly ductile brace meeting seismic compactness criteria; however the reference connection originally had a non-compact brace. Other tests show that a non-compact brace suffers from premature brace fracture at the buckled region (Specimen NCBF1 Section 2.4.4). Possible retrofits of the deficient non-compact brace include a BRB or a concrete filled tube.

A BRB retrofit scheme (shown in Figure 3-12) was adopted to retrofit the deficient brace seen in the reference connection and to test the connection under increasing brace demands characteristic of BRBs as described in Appendix E. The connection detail for the BRB retrofit was nearly identical to Specimen NCBF2 except for slightly increased gusset plate dimensions and a beam web doubler. The beam web doubler was provided to reduce local yield damage of the beam web and provide a comparison point to the other BRB retrofit experiment, Specimen NCBF4-R3. The gusset plate dimensions and bolt hole locations in the gusset plate were adjusted slightly to accommodate the available BRB. The scaling procedure and rational for the gusset plate was also done for Specimen NCBF4-R3 and is described in more detail in Section 3.4. The DCRs for Specimen NCBF2-R1 are shown earlier in Table 3-9.

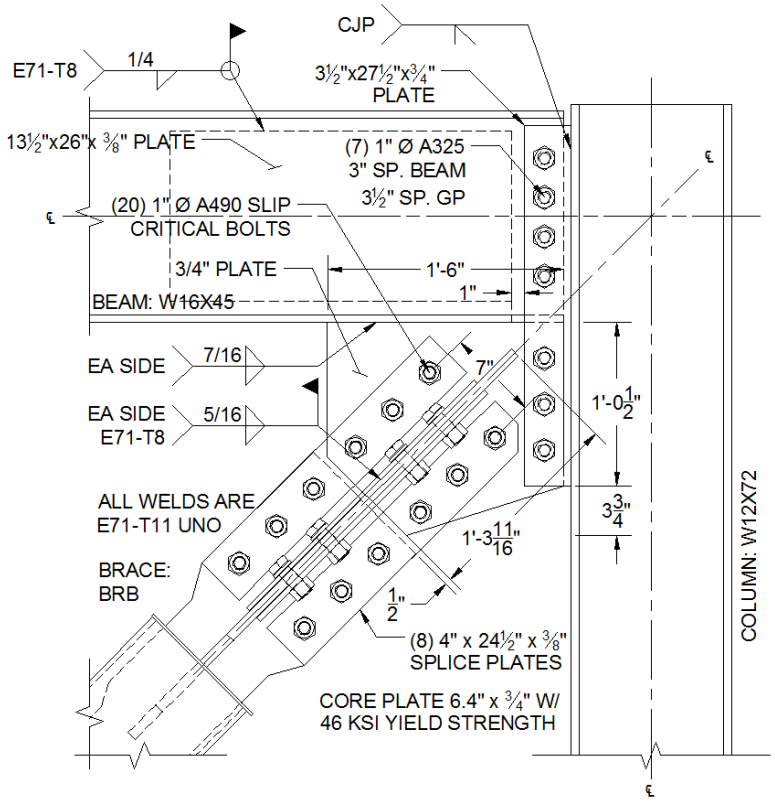

Figure 3-12: Connection Detail for Specimen NCBF2-R1

Chapter 4: Experimental Setup

4.1 Introduction

All tests conducted for the experimental program utilized the pre-existing experimental setup at the UW SRL originally established by Johnson (2005). This setup was designed to test braced frames in the horizontal plane (parallel to the ground) due to the low ceiling height of the SRL. A number of setup features were included to simulate the boundary conditions of an actual single bay braced frame while remaining within the limitations of the laboratory. The setup has had several modifications over its eight years of use to accommodate the different needs of over forty experiments. This chapter will provide an abbreviated overview of the experimental setup and call out important differences in the boundary conditions, instrumentation, fabrication techniques, and loading protocol utilized for the five NCBF tests conducted as part of this experimental program relative to previous tests.

The details of the experimental setup are well documented in previous master thesis (Johnson (2005), Powell (2009), and Sloat (2014)). For this reason, specific boundary conditions details/ descriptions have been omitted from the body of this chapter and can be found in those theses.

4.2 Overview of Boundary Conditions

A drawing of the experimental setup and associated boundary conditions is shown in Figure 4-1. A visual representation of the frame is also shown in Figure 4-2. Both figures show the same specimen connection detail introduced in (Section 3.6) (Specimen NCBF2-R1). A few new boundary conditions were added to the test setup as described in Section 4.3 and are boxed in Figure 4-1.

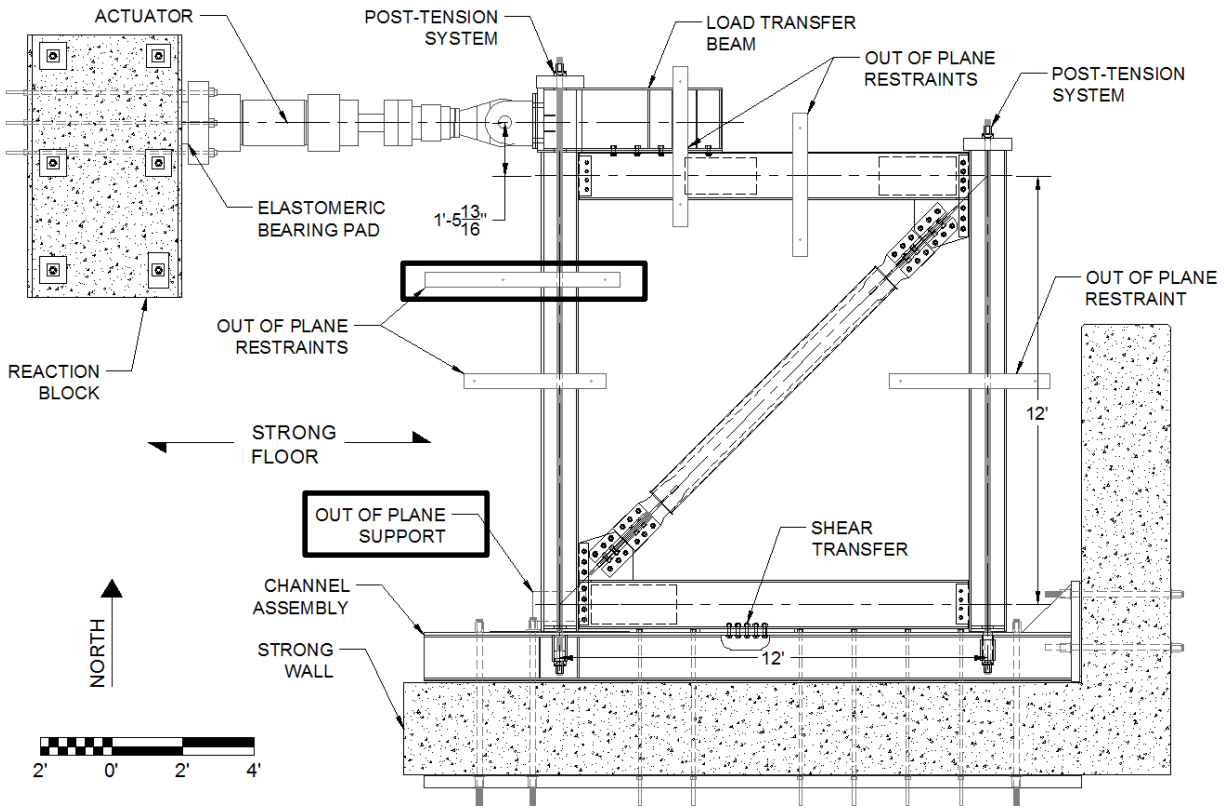

Figure 4-1: Drawing of Overall Test Setup

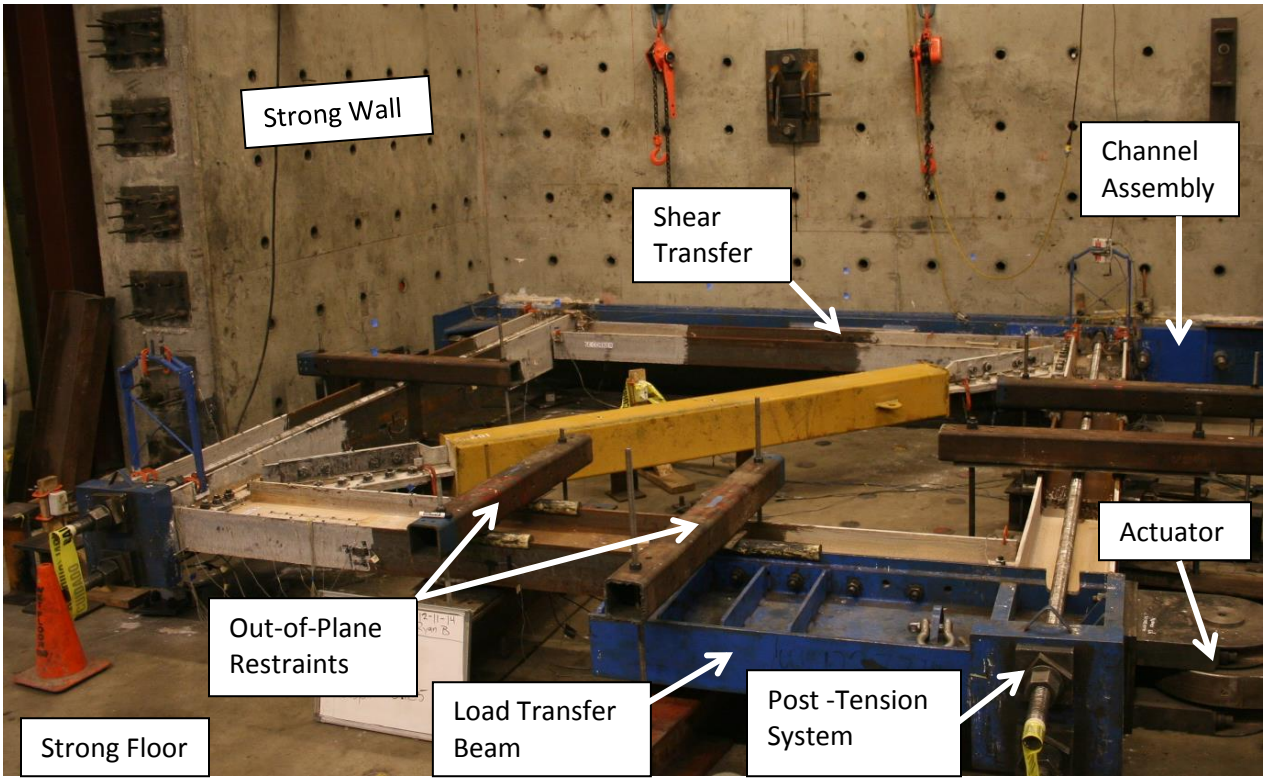

Figure 4-2: Picture of Experimental Setup (Specimen NCBF2-R1)

Lateral load is applied to the frame through a hydraulic actuator anchored to a reaction block. The actuator is attached to the frame through a load transfer beam. The load transfers from the actuator into the north beam and progresses through the brace, the columns, and the south beam. Most of the actuator load exits the system through the shear transfer connection in the middle of the south beam into the channel reaction assembly. Prior to each test, a vertical load of 450 kips is applied to each column by post tensioning four 1 ¾" high strength threaded tension rods anchored to the channel reaction assembly. All loads acting on the channel reaction assembly are transferred into the strong wall and eventually the strong floor. Several out-of-plane restraints are used to limit frame displacement and actuator distortion during loading. A web-doubler plate on the north beam and four column stiffeners at the column bases are installed to prevent local damage at their respective locations during loading. The entire setup lies approximately one foot above the strong floor, and if the frame were turned upright the north beam would represent the top floor of a single bay braced frame.

4.3 Boundary Conditions Modifications

During the testing of Specimen NCBF4-R2 two additional temporary out-of-plane restraints were installed on either end of the west column to realign the frame and correct actuator out-of-plane movement. The out-of-plane restraint on the north side of the west column had the same detail as the existing out-of-plane restraints (Powell 2009). The out-of-plane support on the south end of the west column prevented the out-of-plane displacement of the column towards the strong floor. The two temporary out-of-plane supports are shown in Figure 4-3.

Figure 4-3: New Out-of-Plane Supports

After the test it was determined that the issues that caused the frame to twist out-of-plane could occur again. Permanent out-of-plane restraints were built, installed, and were used in all subsequent tests: Specimens NCBF4-R3, NCBF5, and NCBF2-R1.

4.4 Fabrication

All of the braced frame test specimens were fabricated at the UW SRL. Frame components were fabricated and installed by students under the supervision of the lab technician. Material cuts were made using an acetylene torch and holes were drilled using either a stationary drill press or magnetic drill. Construction tolerance was 1/16 in.

All welds for the frame and connection were completed by a Washington Association of Building Official qualified welder. Welds were done using 5/64 in. self-shielded flux core wire. Fabshield 21b meeting AWS E71-T11 was used to simulate "existing" welds in older structures, since it does not have minimum toughness requirements as is common in older braced frame buildings. Coreshield 8 meeting AWS E71-T8 was used for all other welds. Results of Charpy V-Notch test results for each of the weld materials used is shown in Table 4-1.

Table 4-1: Charpy V-Notch Test Results on Weld Material (Johnson 2014)

Weld Material	Demand Critical Weld Material?	Average Toughness (ft-lbs)
E71-T8	Yes	81.8
E71-T11	No	20.0
E70-T7	No	27.7

Slip critical bolts were tightened using a hydraulic torque wrench. ASTM 959 direct tension indication (DTI) washers were used to indicate proper pre-tension in each of the bolts. Installation of pre-tension bolts was in accordance with the "Specification for Structural Joints Using High Strength Bolts" (RCSC 2009). Slip critical surfaces were prepared to meet class A surface criteria.

4.5 Instrumentation

This section describes the general instrumentation strategy and details the instrument types, installation/ calibration procedure, and the data acquisition systems utilized for the experimental program. Although the instrumentation plans for all the tests were similar, the exact instrumentation plans have slight variations. Dimensioned instrumentation drawings and complete instrument lists for each test are contained in Appendix A. The instrumentation plan for Specimen NCBF4-R2 will be used as an example for this section.

4.5.1 Potentiometers

Purpose

The potentiometers were arranged to capture important frame behaviors such as frame drift, brace elongation, and relative rotation of frame components. An abbreviated version of the potentiometer assignments is given in Table 4-2 and is followed by a more in depth discussion of the intended instrument purposes. Associated potentiometer layout is shown in Figure 4-4.

Table 4-2: Abbreviated Potentiometer Assignments and Locations

Groups	Channels	Purpose of Instrument	Type
Global Frame Behavior	1,2	Actuator Load and Displacement	Load Cell, LVDT
	33	Frame Lateral Displacement	P510
	36,37	Frame Diagonal Elongation	P510
	29-32	Out-of-Plane Displacement at Work Points	P510
Brace Behavior	35	Brace Elongation	P510
	34,38	Brace Mid-span Deflection	P510
Boundary Condition Slip	3-6	Reaction Block and Actuator Slip	D600
	7-9	Channel Assembly Uplift and Slip	D600
	14,24	Slip at Shear Release and Load Transfer Beam	D600
Frame Member Displacement and Deformation	10-12	West Column Uplift and Slip	D600
	15-17	East Column Uplift and Slip	D600
	18,19	Southeast Shear Tab Rotation	D600
	20,22	Northwest Shear Tab Rotation	D600
	25,26	West Column Plastic Hinge Rotation	D9600
	27,28	South Beam Plastic Hinge Rotation	D9600
Test Specific Channels	13,23	End Plate Slip/ NE	D600
	39-40	BRB core elongation	D9600
	41-44	NE/ SW Connection Relative Rotation	D600

Global Frame Behavior Potentiometers

- Channels 1 and 2 were used to measure actuator output values including the actuator force and actuator displacement. The actuator force was used directly in the construction of data analysis plots, while the actuator displacement was integral to the control of the MTS FlexTest system and was used for data filtering during the data post-processing phase of the project.

- Channel 33 was used to measure the frame lateral displacement at the edge of the east column. This measurement was smaller than the actuator displacement and the difference between the two represented some deformation of the frame and system losses such as slip at the boundary conditions of the test setup. Frame drift calculated from the frame lateral potentiometer did not account for the reduction in actual frame drift introduced by rigid body rotation of the frame and deformation of the post-tension rods.

- Channels 36 and 37 were used to measure the frame drift from frame diagonal elongation between the NE and SW work points of the frame. The potentiometers were attached to stands at a relatively large distance above the work points (~25" and 30" respectively) to provide clearance for out-of-plane brace buckling. Both potentiometers were necessary to correct for error introduced by rotation of the potentiometer mounts. Interstory drift determination using the two frame diagonal potentiometers are described in detail in Section 6.3.1. Frame drift from frame diagonal elongation was the most accurate estimation of frame drift because it was not influenced by losses at the boundary condition and it included the effects of connection displacements/deformations.

- Channels 29-32 were used to measure the out-of-plane displacement of the frame at the work points. They were used primarily to indicate the out-of-plane stability of the frame throughout the test.

Brace Behavior

- Channel 35 was used to measure the brace elongation throughout the test. This measurement was used to determine the relative contribution to overall frame drift coming from the brace and represented a portion of the frame diagonal measurement. This measurement was also helpful in determining the component performance of the brace.

- Channels 34 and 38 measured the mid-span deflection of the brace both in-plane and out-of-plane directions. This measurement was primarily used during testing to track the level of brace deformation at loading peaks and inform the testing group of the general level of brace ductility.

Boundary Condition Slip

All of the channels in the boundary condition slip section measured the displacement of the boundary conditions throughout the tests. The displacement of these elements were considered to be system losses and accounted for a portion of the difference between the frame lateral measurement (channel 33) and the actuator displacement (channel 2).

Frame Member Displacement and Deformation

- Column uplift and slip potentiometers (Channels 10-12, 15-17) were used to measure the relative displacement of the column flanges. These measurements were used to indicate the uplift condition at each of the column bases.

- Shear tab rotation was measured in the northwest and southeast corner to indicate the level of rotational ductility achieved by the bolted shear tabs.

Test Specific Channels

A few potentiometers were specific to each test setup. For the bolted end plate tests (Specimens NCBF4-R1, NCBF4-R2, and NCBF4-R3), two potentiometers were used to measure the relative slip between the end plates and the columns. For the BRB tests (Specimens NCBF4-R3 and NCBF2-R1), potentiometers were placed at either edge of the casing to measure the core plate elongation. In the last two tests (Specimens NCBF5 and NCBF2-R1), several potentiometers were used to measure the rotation of the NE and SW connection. This was done to monitor the level of ductility achieved by a bolt group that was expected to have high levels of bolt hole elongation.

Layout

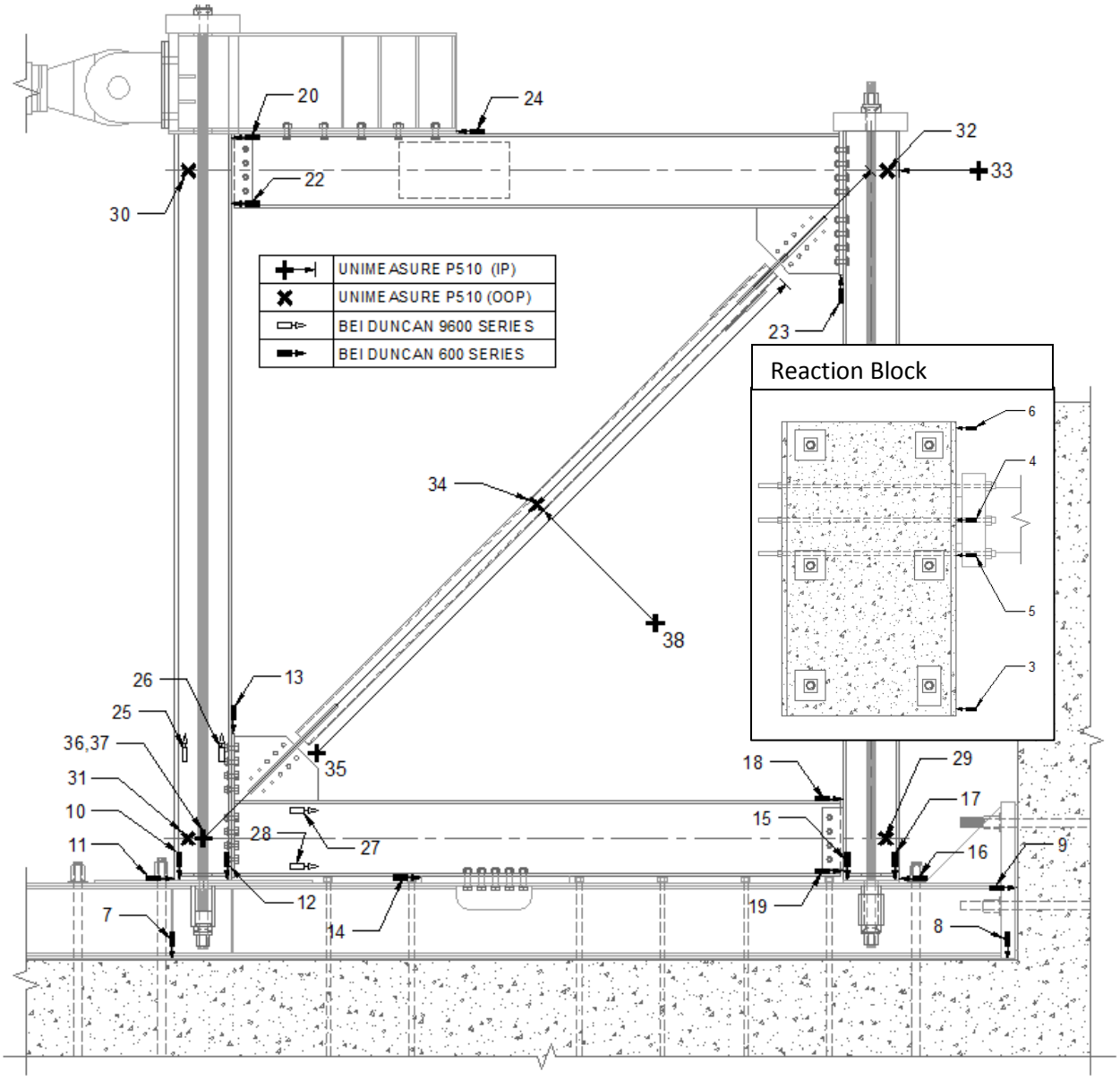

Figure 4-4: Typical Potentiometer Layout

System Details

There were three types of potentiometers used in each test setup to measure a wide range of possible global and relative displacement magnitudes. In general, UniMeasure P510 string potentiometers were used to measure large displacements (>3”), BEI Duncan 9600 potentiometers were used to measure moderate displacements (1” – 3”), and BEI Duncan 600 potentiometers were used to measure small displacements (<1”). The BEI Duncan Potentiometers came in a variety of gauge lengths and the appropriate gauge length for each measurement location was based on the expected displacement values of the instrument. All potentiometers were calibrated over the range of their expected displacements. The potentiometer type for each channel is listed in Table 4-2 and shown graphically in Figure 4-4.

4.5.2 Strain Gauges

Purpose

A typical strain gauge layout is shown in Figure 4-5. Pairs of strain gauges were used to measure the axial elongation and calculate the curvature of various locations along the framing members throughout the loading protocols. The data collected for the strain gauges is used to compute member forces in the frame and determine the relative contributions of the columns and braces in resisting the lateral load. Using a linear varying moment profile (constant shear) between strain gauge pairs, member shears for both columns and the north beam could be calculated. Brace forces were generally back calculated from the column shears and actuator load, but were also measured directly using a set of strain gauges on each face of the brace. Although only four strain gauges are needed to calculate member shear or brace force, a larger number of strain gauges were used on the columns (6) and braces (8) for redundancy in case of improper installation prior to testing or instrument failure during testing.

Layout

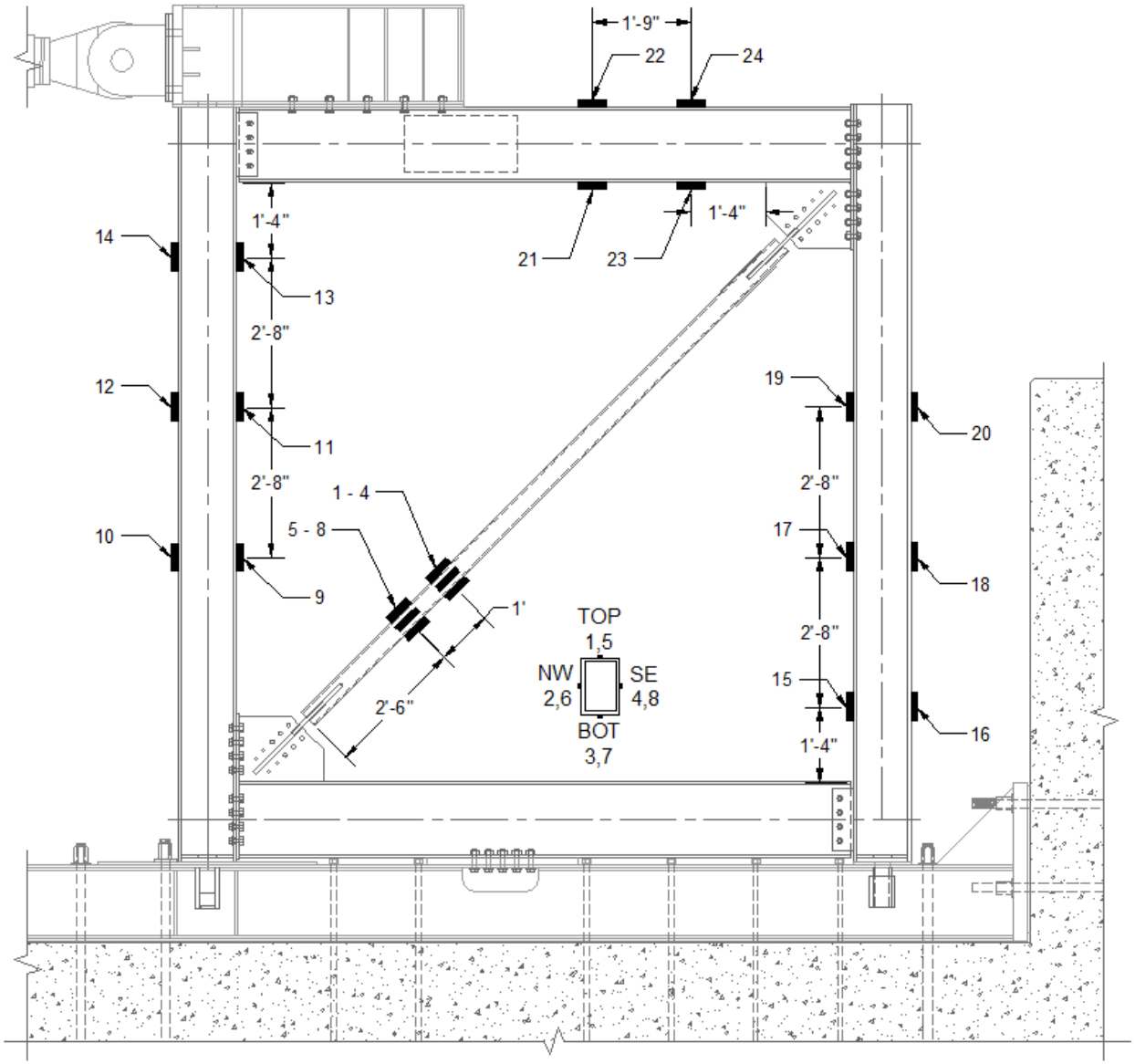

Figure 4-5: Typical Strain Gauge Layout

System Details

The strain gauges were aligned parallel to the member at the mid-depth of the flange and generally installed in regions not expected to have significant yielding. Tokyo Sokki Kenkyujo co., Ltd. FLA-6-11-5LT 3-wire uni-axial strain gauges were used in all of the tests. These strain gauges compensate for instrument temperature fluctuation and are considered to have a high reliability at elongation values up to ±2.0%. Surfaces preparation at strain gauge location included the removal of millscale using a belt sander and an alternating acid-base sandpaper treatment.

4.5.3 Northern Digital Inc. - OptoTrak LEDs

Purpose

The Northern Digital Inc. (NDI) OptoTrak system is used to measure absolute and relative displacements of the NE connection components and the brace during testing. Optotrak measurements were used to determine gusset plate rotation, brace out-of-plane displacement/deformation, relative slip of components, framing member rotations, among other deformations and movement. A typical layout of the LED markers is shown in Figure 4-6 and the associated purpose of each LED marker is presented in Table 4-3. Of the three types of instruments, the Optotrak LEDs had the greatest layout variation from test to test due to the differences in connection details. Exact location of the markers and their intended purpose are documented in Appendix A.

Table 4-3: Abbreviated Optotrak Marker Locations and Purpose

Channel	Location	Purpose
1-10	North Beam Flanges	Plastic Rotation of N Beam and Local Buckling of N Beam Flanges
11-22	North Beam Web	Web Buckling in N Beam
23-24, 30-31	East Column Flanges	Lateral Displacement of NE Work Point
25-29, 32-36	East Column Flanges	Plastic Rotation of E Column and Local Buckling of East Column Flanges
30-33, 37-39	End Plate and West Flange of East Column	Relative Displacement Between Column and End Plate
40-45	Gusset Plate	Gusset Plate Out-of-Plane Rotation
46-51	Top Edge of Knife Plate	Knife Plate In-Plane Rotation
52-56	Top flange of Brace	Brace Out-Of-Plane and In-Plane Displacement of Brace
57-58	Frame Diagonal Potentiometer Stand	Measure Rotation of Frame Diagonal Stands (Potentiometers 36 and 37)
59-60	Strong Floor	Stationary Reference Points on Strong Floor

Layout

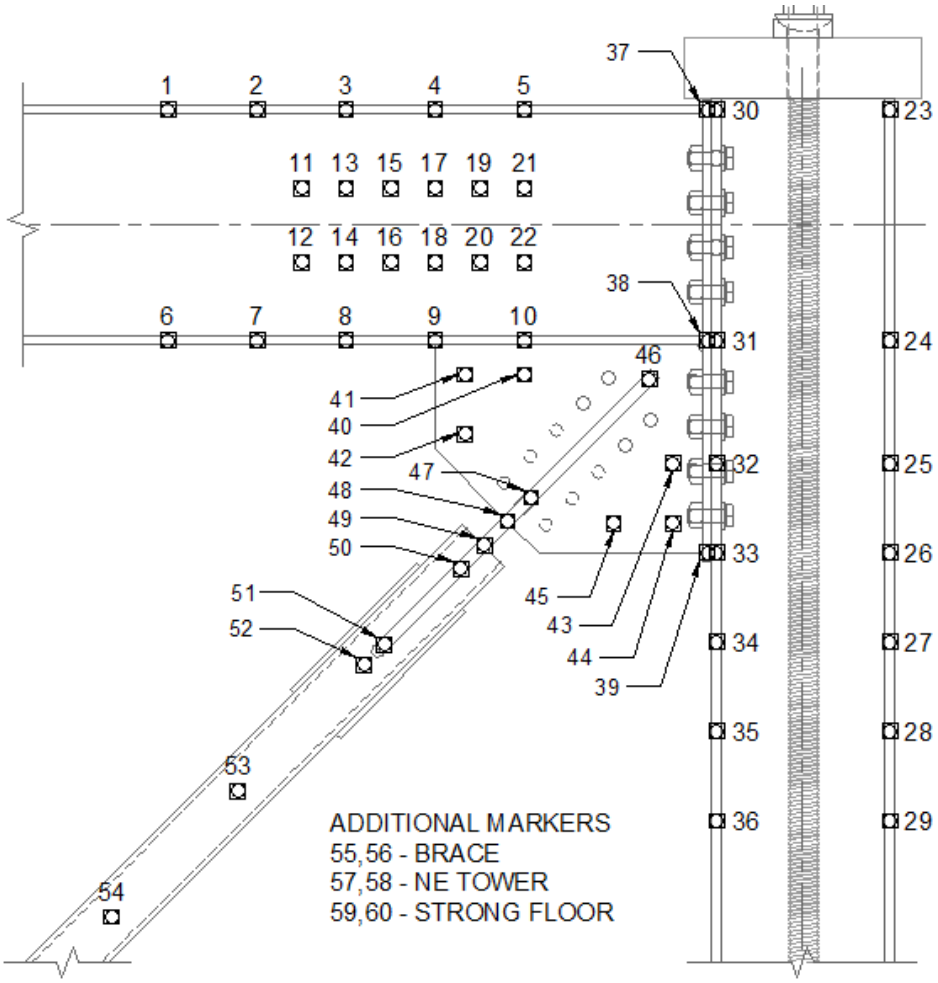

Figure 4-6: Typical OptoTrak LED Layout at NE corner

System Details

The NDI system tracks the location of LED markers in 3D space using a sensor that triangulates each marker's location with three infrared cameras. Each test uses two Optotrak sensors mounted to the strong wall and around 60 LED markers. Although the precision of the NDI system can be under 0.001 mm, several factors such as the distance between the sensor and markers can greatly reduce the precision. The registration software used to calibrate and align the sensors estimated that the precision of the Optotrak system was within an acceptable 0.3 mm for all of the tests. LED markers are attached to the frame using two sided tape. Millscale between the two-sided tape and base material was removed with a belt sander to enhance the bond between the frame and the LED markers.

4.6 Testing

4.6.1 Loading Protocol

The actuator was controlled using MTS FlexTest software and was run under displacement control. Three pre-programmed protocols were used for each test: elastic protocol, main protocol, and post-fracture protocol. The elastic protocol had three cycles at low target drift ranges (< 0.15% target drift) and was used at the start of each test to ensure instrument functionality. The main protocol had two cycles at each target drift. Each cycle consisted of a tension and a compression peak at the specified target drift. The main loading protocol and target drifts for each cycle are shown in Figure 4-7. The post-fracture protocol varies from test to test and was used to determine the post-fracture frame stiffness and capacity.

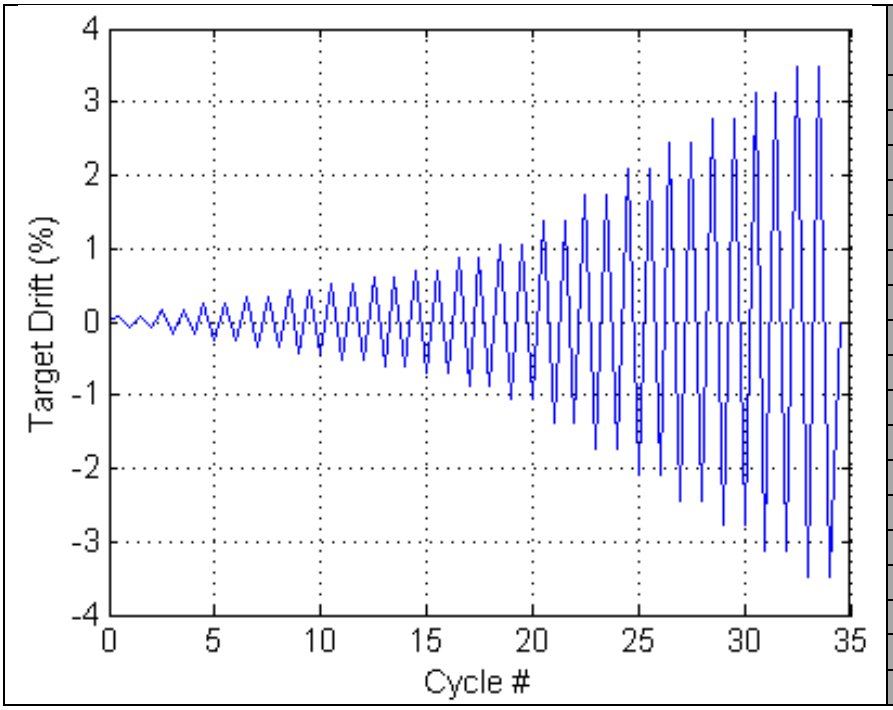

Cycle	Target	
	Disp. (in)	Drift (%)
1-2	± 0.125	± 0.087
3-4	± 0.250	± 0.174
5-6	± 0.375	± 0.260
7-8	± 0.500	± 0.347
9-10	± 0.625	± 0.434
11-12	± 0.750	± 0.521
13-14	± 0.875	± 0.608
15-16	± 1.000	± 0.694
17-18	± 1.250	± 0.868
19-20	± 1.500	± 1.042
21-22	± 2.000	± 1.389
23-24	± 2.500	± 1.736
25-26	± 3.000	± 2.083
27-28	± 3.500	± 2.431
29-30	± 4.000	± 2.778
31-32	± 4.500	± 3.125
33-34	± 5.000	± 3.472
END	0	0

Figure 4-7: Main Actuator Loading Protocol

The time to each compression and tension peak in the main protocol was specified to ensure pseudo static conditions in the frame and was calibrated based on the inter-story drift angle at the onset of first yielding or buckling in the frame θ_y. For the UW setup, the value of θ_y has previously been determined to occur at a target displacement of 0.625" (Kotulka 2007). The time to peak for each cycle is shown in Table 4-4. The main loading protocol was originally developed for the first UW braced frame tests by (Johnson 2005) and was based on recommendations from ATC-24 and the SAC Steel Project (1992).

Table 4-4: Main Loading Protocol Time to Peak

Inter-story drift angle	Time to Peak	Cycle #
$0 \leq \theta < \theta_y$	60 sec.	1-10
$\theta_y \leq \theta < 2\theta_y$	80 sec.	11-18
$2\theta_y \leq \theta < 4\theta_y$	120 sec.	19-24
$4\theta_y \leq \theta$	160 sec.	25-34

It is important to note that there is a substantial difference between the specified target drift and the actual applied drift. The difference between the two drift values comes from a number of sources. The most prominent sources of system loss were slip of the frame at the boundary conditions and deformation of the post tension rods. The applied drift history for each test is tabulated in each of the performance state tables contained in Chapter 5.

4.6.2 Visual Observations

To aid visual observations, each specimen was coated in a whitewash mixture consisting of a 4:1 volumetric ratio of water and Hydrostone. When yielding occurred in the steel members, the mill scale and whitewash flaked off, providing a sharp visual contrast that helped to identify yield patterns. This mixture is applied to all areas that damage was expected to occur during the tests.

At each displacement peak of the main loading protocol three photos were taken: one photo of the NE connection, one of the SW connection, and one of the overall frame. For the two connection photos, the cameras were positioned on stationary mounts above the respective work points while the overall camera was positioned on a tripod looking down on the frame from the northwest. If damage is suspected to occur during a cycle the loading protocol was manually paused for a longer period of time. Photos of observed damage were taken with a handheld camera while the onset and progression of damage was recorded in a test observations log. Test observations and photos are recorded in Chapter 5.

Chapter 5: Experimental Observations

5.1 Introduction

This chapter documents the observations during the testing of five NCBF and NCBF retrofit specimens using images of salient performance states. To aid in this discussion, definitive damage states are defined for each component (Section 5.2) including the brace, connection, and frame members. Sections 5.3 through Section 5.7 describe the observations for each test. Each test summary has the following: (1) the overall objective of the test, (2) a summary table of the demand to capacity ratio evaluation, and (3) a comprehensive summary of the frame performance including a table of drifts corresponding to performance states and a test narrative that refers to the performance states defined in Section 5.2.

5.2 Performance State Definitions

In performance-based design, it is critical to understand and be able to quantify the damage state(s) of a component and the system to quantify the need for repair or replacement. In addition, quantification of the occurrence of performance states facilitates comparison of the specimens.

This section summarizes the performance states for each component, including the braces (HSS or BRB), connection (categorized by type), and the framing elements (beams and columns). Both yield mechanisms and failure modes are identifies. For each type of performance state a numerical identifier is used to qualify the severity of the incurred damage: 1-initial, 2-moderate, 3-severe, and 4-failure. The failure modes are indicated by a unique acronym. Each category of component performance is provided in a table. The rows of the table provide increasingly severe performance states, which are both higher in number and darker in shading.

5.2.1 Brace Performance States

Two types of braces were used: buckling HSS tube braces and BRBs. Both types of brace are intended to be the primary ductile element. Their performance states are defined separately due to their unique behavior.

5.2.1.1 HSS Brace

The performance state definitions for HSS braces are shown in Table 5-1 and when appropriate indicated in parentheses. All performance states are defined for compression.

To accommodate deformation under compression loads an HSS brace will buckle about its weak axis as determined by the brace cross section and end connections. Initially, the brace buckled shape is approximately a sine wave (PS B1-B2). With larger out-of-plane deformations, local cupping forms at the mid-span of the brace (B3-BH) leading to tearing (B3-BT) and eventually fracture of the brace (B4-BF) during subsequent loading in tension.

Table 5-1: Brace Performance States (HSS)

Picture	Abb.	Performance State	Description
	B1	Initial Global Buckling	Brace mid-span deflection is visible but less than two times the brace depth.
	B2	Moderate Global Buckling	Brace mid-span deflection exceeds two times the brace depth.
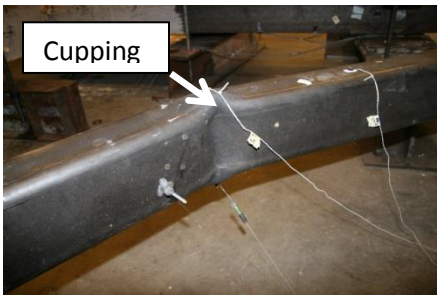	B3-BH	Initial Local Buckling (Brace Plastic Hinging)	Brace begins to buckle locally at brace mid-span.
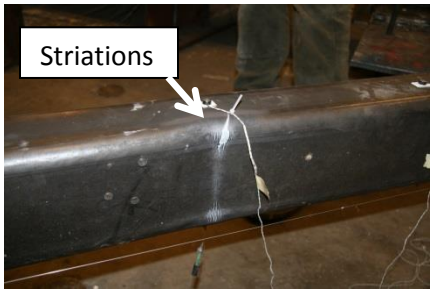	B3-BT	Brace Tearing	Striation lines begin to separate in plastic hinge region of brace.
	B4-BF	Brace Fracture	Brace fractures through entire section.

The brace out-of-plane deformation was measured using the Optotrak data (as described in 4.5.3). This measurement was used to distinguish between the B1 and B2 performance states.

5.2.1.2 Buckling Restrained Brace

Buckling restrained braces (BRBs) dissipate energy through compression and tensile yielding. Global and local buckling of the steel core plate is prevented by the surrounding concrete. A de-bonding material is used between the steel core plate and the concrete fill to limit interaction at the interface and allow for some Poisson expansion of the steel core. A complete detail of the BRBs used for the experimental program are provided in Appendix E.

BRB performance state definitions are shown in Table 5-2. Initial BRB performance states (PS B1-B3) are based on the overall inelastic deformation of the steel core plate (measurement described below Table 5-2). As the inelastic deformation of the core plate increases, two failure modes can develop in the BRB: out-of-plane hinging and core plate fracture. Out-of-plane hinging of the BRB typically results from a loss of connection stability culminating in plastic hinge of the steel core plate at the edge of the BRB casing (PS B4-BH). BRB core plate fracture was not observed in either of the two BRB retrofit specimens and is not shown in Table 5-2.

Table 5-2: Brace Performance States (BRB)

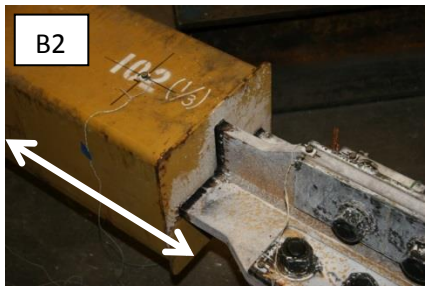	B1	Initial Core Plate Yielding	Initial yielding in BRB core plate
	B2[a]	Moderate Core Plate Yielding	BRB core plate elongation exceeds 1.5% drift range during cycle.
	B3[a]	Severe Core Plate Yielding	BRB core plate elongation exceeds 3.0% drift range during cycle.
	B4-BH	Out-of-plane hinging	Unstable plastic hinge develops at the edge of BRB casing.

Inelastic deformation of the core plate was measured using the relative displacement of the steel core plate and the edge of the BRB casing at each brace end. Since different levels of elongation were recorded for compression and tension cycles, the performance state thresholds were compared with the average elongation from successive tension and compression cycles.

5.2.2 Connection Performance States

Connection performance states are divided into overall yielding, weld damage, base material damage and bolt damage. Prying action is a performance state specific to the bolted end plate connections. The performance states for bolts are divided into levels based on the initial slip of the connections and the relative deformation of connected elements at the bolt holes.

5.2.2.1 Connection Yielding Performance State

Yielding performance states are defined as the percentage of area over which flaking of the whitewash has occurred; initial (PS Y1), moderate (PS Y2) and severe (PS Y3) states are shown in Table 5-3. Yielding performance states are defined for the gusset plates, end plates, and the shear plates. Although some yielding occurred in all of the named connection elements during the experimental program, the most prevalent source of yielding was the gusset plates, and therefore Table 5-3 provides an example for gusset plate yielding.

Table 5-3: Connection Yielding Performance States (NE gusset plate of Specimen NCBF4-R1)

Picture	Abb.	Performance State	Description
	Y1	Initial Yielding	First visible yield lines observed on connection element.
	Y2	Moderate Yielding	Whitewash is flaked off on >20% and <50% of planer area of connection element.
	Y3	Severe Yielding	Whitewash is flaked off on >50% of planer area of connection element.

5.2.2.2 Weld Performance States

The weld performance states are shown in Table 5-4. The performance states for weld damage are based on the length of weld tearing normalized by the initial length of the weld expressed as a percentage. Weld damage states are similar to the stages of crack propagation utilized in fracture mechanics. The initial (PS W1), moderate (PS W2), and severe weld tearing (PS W3) performance state thresholds are calibrated to represent the crack initiation phase, the stable crack propagation phase, and the unstable crack propagation phase, respectively. Severe weld tearing often leads to complete weld fracture (PS W4-WF).

Table 5-4: Weld Performance States (SW beam-gusset plate weld of Specimen NCBF4-R2)

Picture	Abb.	Performance State	Description
	W1	Initial Weld Tearing	First visible weld cracks are observed.
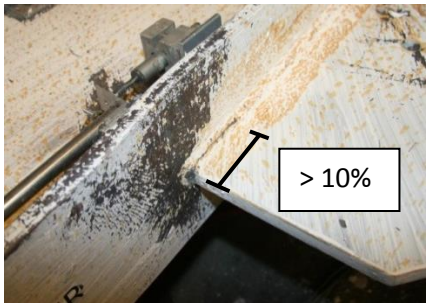	W2	Moderate Weld Tearing	Weld tear exceeds 10% of weld length.
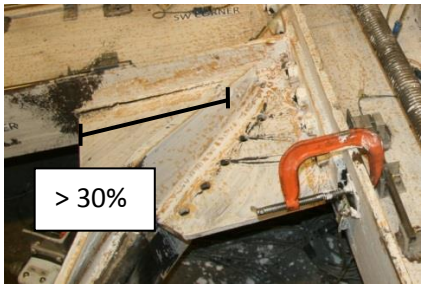	W3	Severe Weld Tearing	Weld tear exceeds 30% of weld length.
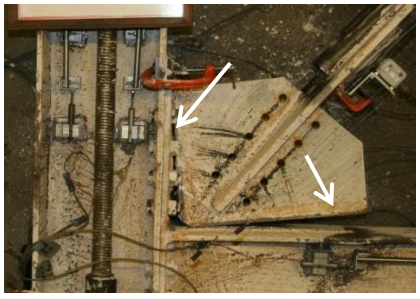	W4-WF	Weld Fracture	Weld fractures along entire length.

Critical welds such as the beam-to-gusset plate weld were checked every compressive cycle for signs of crack initiation. After crack initiation, the weld crack length was measured during all successive compression cycles. Once the weld reached performance state W3, it was measured during all successive tension and compression cycles. If the weld tear length was different between two sides of a connected element (i.e. the two sides of a gusset to beam weld), the maximum tear length was used.

5.2.2.3 End Plate Performance States

For the specimens with bolted end-plate connections, tension from the inner beam flange results in prying action of the end plates. The performance states for prying action are based on the separation distance between the end plate and the column flange when prying occurs and are illustrated in Table 5-5. Metal tearing indicates cracks in base metal and its application is also shown in Table 5-5.

Table 5-5: Bolted End Plate Performance States

Picture	Abb.	Performance State	Description
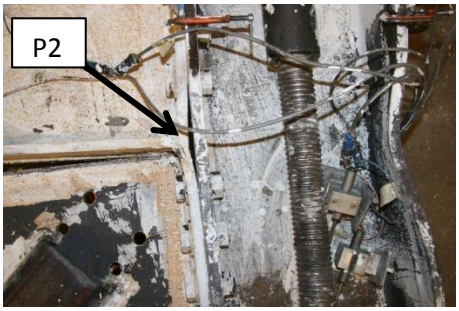	P1	Initial Prying	End plate and column begin separating at location between bolts
	P2	Moderate Prying	Separation exceeds half the end plate thickness.
	P3	Severe Prying	Separation exceeds the end plate thickness.
	P3-MT	Metal Tearing	Metal tearing observed in component.

5.2.2.4 Bolt Damage

Performance states for bolts are illustrated in Table 5-6. Performance States Bo1-Bo3 are based upon the relative movement of connection components which was measured using the Optotrak system.

Bolted connections transfer forces using friction at the connection interface (for slip-critical connections) and bolt bearing inside of the bolt holes. As forces in the connection become larger the frictional force is overcome, and bolt slip occurs (PS Bo1). After initial bolt slip, the connection forces are transferred through bolt bearing. Deformation in the bolted connection after initial slip (Performance states Bo2 and Bo3 in Table 5-6) resulted from the combination of bolt hole elongation, bolt shear deformation and rotation of the bolts inside of the bolt holes as illustrated in Figure 5-1. It was difficult to quantify the contribution from each of these sources, but overall deformation of ¼"at a bolt hole is assigned the severe deformation at the bolt hole performance state (Bo3).

Table 5-6: Bolt Performance States

Picture	Abb.	Performance State	Description
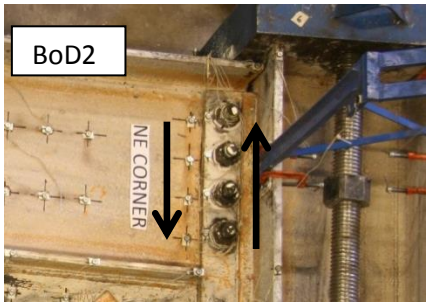	Bo1	Initial Bolt Slip	Bolt pretension is overcome and connection slip occurs.
	Bo2	Moderate Deformation at Bolt Hole	Overall deformation of bolt group exceeds 1/16"
	Bo3	Severe Deformation at Bolt Hole	Overall deformation of bolt group exceeds ¼"
	Bo4-BF	Bolt Fracture	Complete fracture of bolt occurs.

a. Bolt Hole Elongation

b. Bolt Shear Deformation

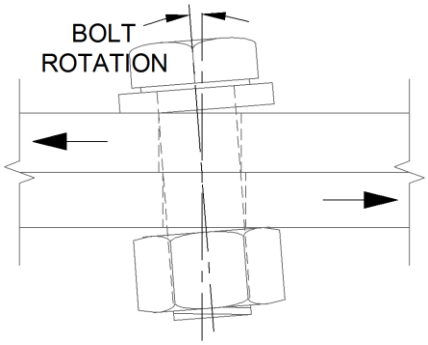

c. Bolt Rotation

Figure 5-1: Sources of Deformation at Bolt Hole

5.2.3 Frame Performance States

Damage in the frame is denoted with a two-part abbreviation, performance state followed by a location. Damage locations in the frame include the plastic hinge region (PH) in the column, the member web (W), the member inner flange (IF), and the member outer flange (OF). Performance states are listed in Table 5-7 while damage locations are shown in Figure 5-2. The location (NE connection, east column, etc.) of the damage is provided in the performance state tables and test narratives separately.

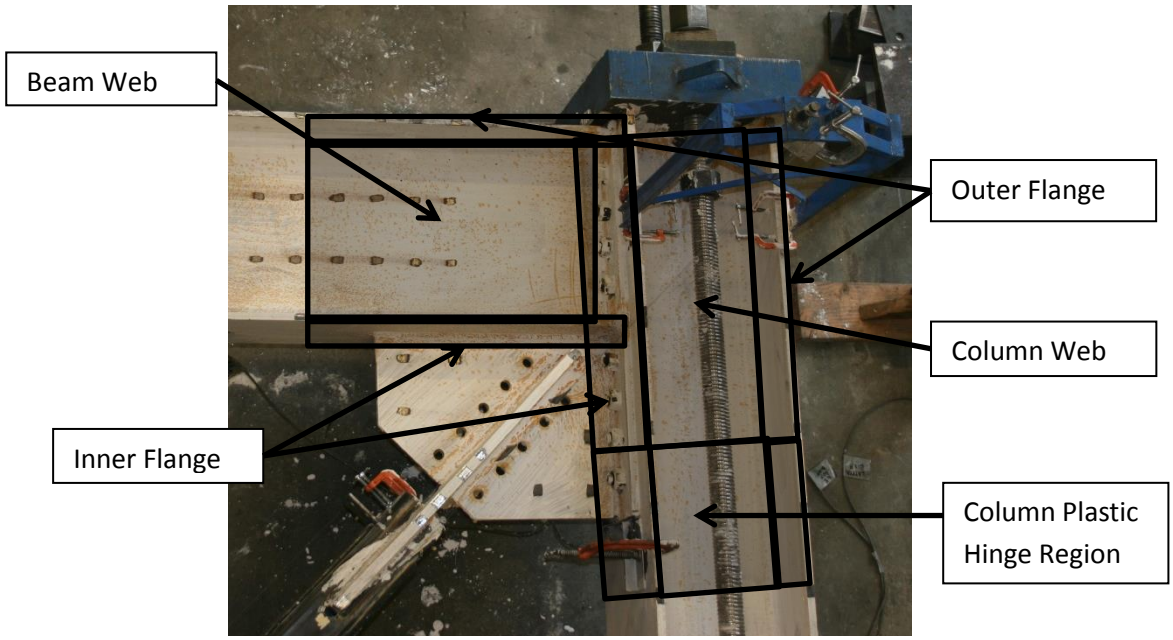

Figure 5-2: Frame Damage Locations

As shown in Figure 5-2, the plastic hinge region is assumed to extend half of the member depth in both directions away from the edge of the gusset plates. Note that damage past the plastic hinge location is correlated with damage at the plastic hinge location and is not explicitly documented. A plastic hinge denotation was not included for the beam as observations suggested the hinge region was contained

within the highlighted region in Figure 5-2. Note that the inner flange always refers to the flange closer to the gusset plate while outer flange refers to the flange further from the gusset plate.

Table 5-7: Frame Performance States

Picture	Abb.	Performance State	Description
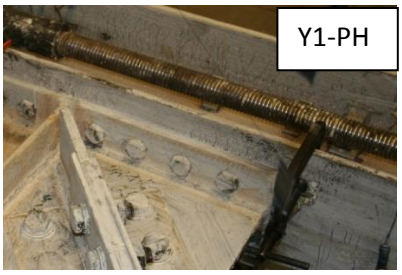	Y1	Initial yielding	First visible yield lines observed in specified frame location. (Example shown for plastic hinge location)
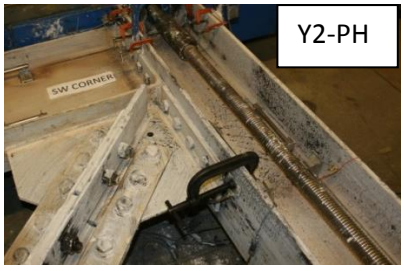	Y2	Moderate yielding	Whitewash is flaked off on >40% of specified frame location. (Example shown for plastic hinge location)
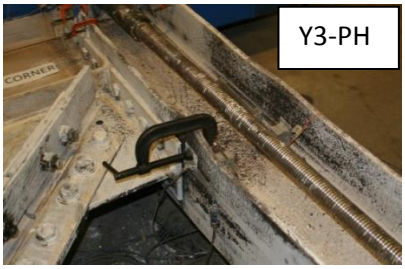	Y3	Severe yielding	Whitewash is flaked off on >80% of specified frame location. (Example shown for plastic hinge location)

Flange and Web Buckling

Performance states for flange and web buckling are similar to the HSS brace performance states and are illustrated in Table 5-8. The out-of-plane deformation of the flange or web is compared to the thickness of the element to determine the severity of the buckling. Initial local buckling is noted when the out-of-plane deformation became visible while moderate and severe local buckling are based on the magnitude of the out-of-plane deformation. Usually the out-of-plane local deformation is measured at the largest local buckle; however when the buckled shape is of a higher order the out-of-plane deformation is taken as the sum. Note that the upper flange in the photo showing performance state LB3 in Table 5-8 illustrates a higher order buckled shape.

Table 5-8: Local Buckling Damage States

Picture	Abb.	Performance State	Description
	LB1	Initial Local Buckling	OOP local deformation observed in flange and/or web.
	LB2	Moderate Local Buckling	OOP local deformation exceeds element thickness.
	LB3	Severe Local Buckling	OOP local deformation exceeds two times the element thickness.

5.3 Specimen NCBF4-R1 – Bolted End-Plate Connection, Out-of-Plane Buckling Brace

5.3.1 Overview

Specimen NCBF4-R1, as shown in Figure 5-3 and Figure 5-4, was designed to be a retrofit of a frame using quadruple angle bracing and bolted end plate connection at the gusset-beam-column connection and is discussed in detail in Section 3.2. The objective of the test was to determine the deformation capacity of a frame with bolted end plate connection representative of the bolted end plate connections identified in the infrastructure review (Section 2.3.1) and to provide a comparison point to other specimens tested by Sloat (2014) and Johnson (2014).

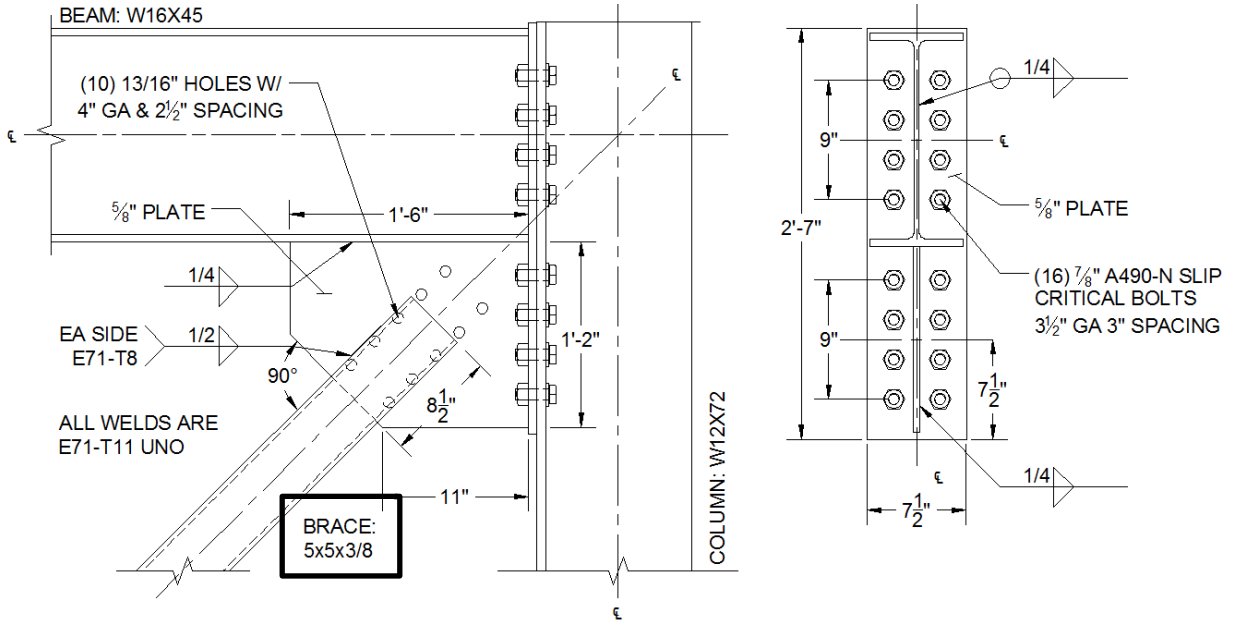

Figure 5-3: Specimen NCBF4-R1 Connection Detail

A seismically compact 5x5x3/8 HSS brace was used to replace bolted quadruple angles of the bolted end plate connection. The gusset plate remained intact. The holes in the gusset plate represent the bolt holes of an existing gusset plate used to connect the retrofitted quadruple angles. The connection utilized a bolted end plate that is connected to the column using sixteen 7/8” A490 bolts and was welded to the beam and gusset plate using ¼” fillet welds. All welds except for the brace-to-gusset welds were non-notch tough welds.

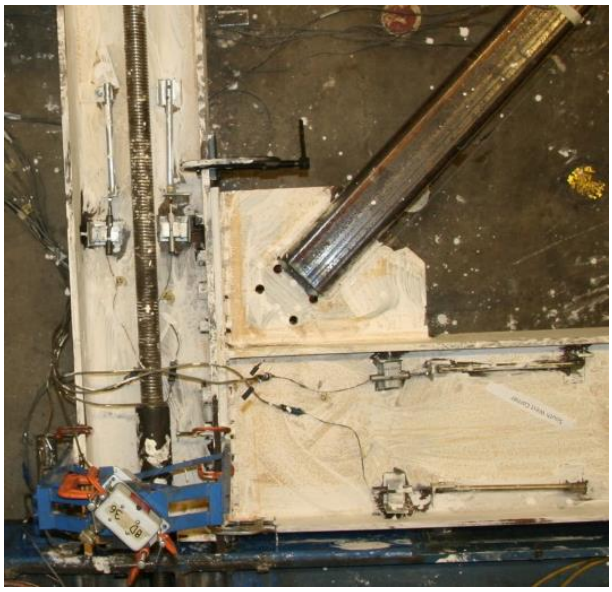

a. SW Connection

b. NE Connection

Figure 5-4: Specimen NCBF4-R1 Photos Prior to Testing

Table 5-9 shows the connection DCRs for specimen NCBF4-R1 as calculated in Section 3.2. The primary deficiencies of the connection are: fracture of the beam-to-gusset plate welds when evaluated with the BDP, limited gusset plate clearance, and non-ductile welds.

Table 5-9: Specimen NCBF4-R1 Demand Capacity Ratios

	Limit State	NCBF4-R1
Yielding Mechanisms	Gusset Plate Whitmore Yielding	0.82
	End Plate Bolt Bearing (BR-CVM)	0.17
Failure Modes	Brace Net Section Fracture	**1.22**
	Brace Splice Fracture	0.76
	Brace Block Shear	0.77
	Gusset Plate Whitmore Fracture	0.60
	Gusset Plate Block Shear	0.59
	Beam-to-Gusset Plate Weld Fracture (GP)	**1.58**
	Beam-to-Gusset Plate Weld Fracture (BR-CVM)	0.63
	Gusset Plate-to-End Plate Weld Fracture (BR-CVM)	0.71
	End Plate Bolt Shear (BR-CVM)	0.41
Geometric Limits	Brace Compactness Ratio $(b/t)/\lambda_{hd}$	0.95
	Slenderness Ratio $(KL/r)_{max}$	87.87

Although the welds did have adequate nominal capacity to develop the tensile yield strength of the brace (per AISC), they did not have enough strength to develop the yield capacity of the gusset plate (as evaluated with the BDP). DCRs for net section fracture was also above one; however, based on observations from previous tests (Sloat 2014 and Johnson 2014) this limit states was not expected to

limit the drift capacity of the frame. Shear yielding in the gusset plates, bolt bearing in end plate, bolt fracture in the end plate, weld fracture in the beam-to-column connection, Whitmore yielding, and prying action all had DCRs of less than 1.0.

Although not listed with the DCRs in Table 5-9, another potential yielding mechanism for Specimen NCBF4-R1 was yielding of the frame members. The bolted end plate connection is a deep connection that was considered to have the potential to develop significant restraint against relative rotation at the column interface and therefore develop large frame member moments.

5.3.2 Summary of Response and Performance

The frame achieved a drift range of 2.9%, as shown in Figure 5-5. The failure mode was beam-to-gusset plate weld fracture followed by gusset plate-to-end plate weld fracture of the NE corner connection. Table 5-10 shows the drift ranges when various performance states were observed. Damage to the frame included (1) severe yielding of both gusset plates (PS Y3), (2) moderate yielding in the columns (PS Y2-PH in W column & PS Y2-W in E column), (3) prying action in the NE end plate (PS P2), and (4) initial yielding in the N beam (PS Y1-IF).

Prying action of the end plate appeared to delay the unstable crack propagation characteristic of non-ductile welds by alleviating the amount of force being transferred through the beam-to-gusset plate weld. The framing members in this connection, particularly the columns, sustained more damage than what has been seen for frames that allow more rotation at the column interface. The bolts in the end plate connection did not sustain any observable damage, and slip did not occur in the end plate connection at any point during the test.

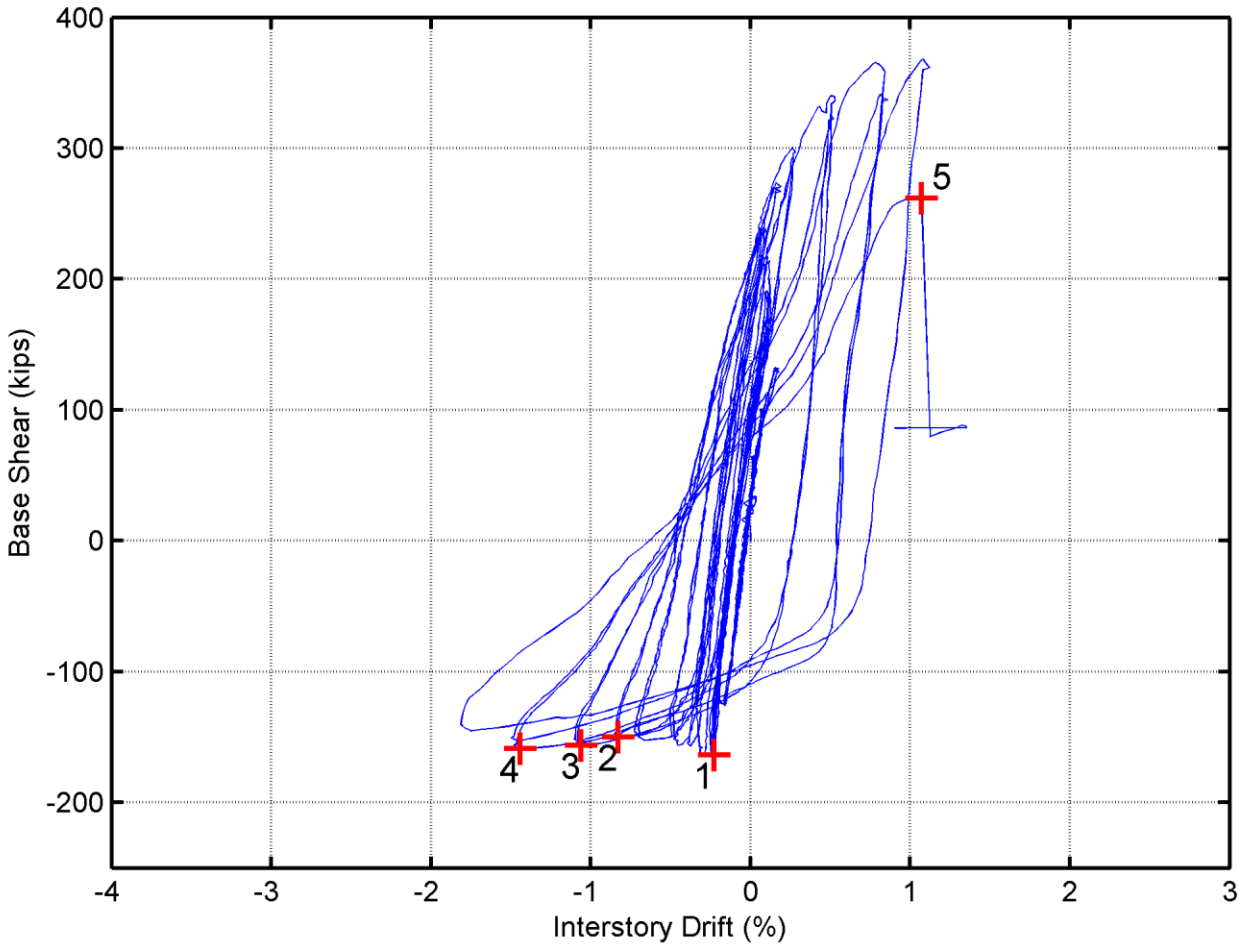

1. Brace begins to buckle visibly out-of-plane (PS B1).
2. Initial weld tearing (PS W1) observed in NE beam-to-gusset plate weld (2.5” long)
3. Severe weld tearing (PS W3) observed in NE beam-to-gusset plate weld (5.5” long)
4. Severe weld tearing (PS W3) observed in SW beam-to-gusset plate weld (5.5” long)
5. The NE beam-to-gusset plate and gusset plate-to-end plate welds fracture (PS W4-WF).

Figure 5-5: Specimen NCBF4-R1 Base Shear vs. Interstory Drift
(See Section 6.3.1 for details on generation of hysteresis.)

Table 5-10: Specimen NCBF4-R1 Performance State Summary Table

Cycle	Drift (%)			Brace	Northeast Connection									Southwest Connection								
	Range	Pos.	Neg.		East Column	North Beam	BR-GP Weld	GP	GP-Beam Weld	GP-EP Weld	Beam-EP Weld	EP	EP bolts	West Column	South Beam	BR-GP Weld	GP	GP-Beam weld	GP-EP Weld	Beam-EP Weld	EP	EP bolts
1	0.1	0.0	-0.1																			
2	0.1	0.0	-0.1																			
3	0.1	0.0	-0.1																			
4	0.1	0.0	-0.1																			
5	0.2	0.1	-0.1																			
6	0.2	0.1	-0.1																			
7	0.3	0.2	-0.2																			
8	0.4	0.2	-0.2																			
9	0.3	0.1	-0.2					Y1														
10	0.4	0.1	-0.2																			
11	0.4	0.1	-0.2	B1													Y1					
12	0.4	0.1	-0.3																			
13	0.4	0.1	-0.3																			
14	0.5	0.1	-0.4																			
15	0.6	0.1	-0.5																			
16	0.6	0.1	-0.5																			
17	0.9	0.2	-0.7					Y2														
18	0.9	0.2	-0.7																			
19	1.1	0.3	-0.8						W1,W2								Y2					
20	1.1	0.3	-0.8																			
21	1.6	0.5	-1.1						W3													
22	1.6	0.5	-1.1		Y1-PH	Y1-IF						Y1									Y1	
23	2.3	0.8	-1.5	B2										Y1-OF			Y3	W3				
24	2.4	0.9	-1.5									P1										
25	2.9	1.1	-1.8					Y3				P2		Y1-PH								
26	2.9	1.1	NA		Y2-W				W4-WF	W4-WF				Y2-PH								

5.3.3 Test Narrative

The frame performed elastically up to a drift range of 0.4%. At a drift range of 0.4%, initial yielding was observed in both gusset plates (PS Y1, Figure 5-6) as well as visible out-of-plane brace buckling (PS B1, Figure 5-7). Initial yield lines in the gusset plate appeared between the two existing holes nearest to the end of the brace and extended towards the gusset plate-to-end plate connection. Initial brace buckling corresponded to the peak strength of the frame in compression.

a. NE Corner **b. SW Corner**

Figure 5-6: Initial Yielding in Gusset Plates (PS-Y1, 0.4%)

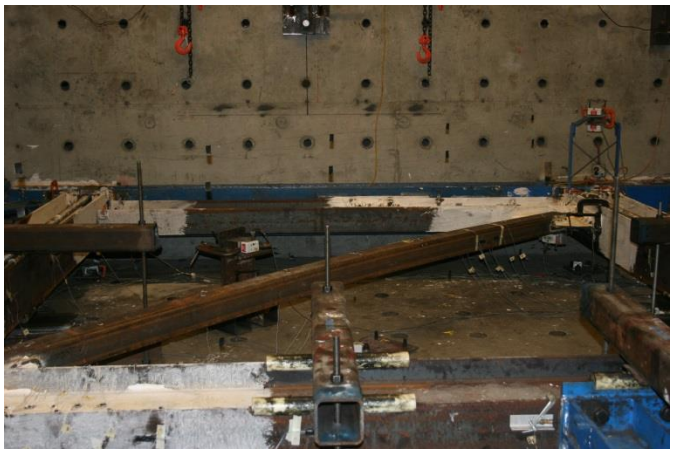

Figure 5-7: Initial Brace Buckling (PS-B1, 0.4%)

Each successive compression peak after initial buckling of the brace resulted in increasing out-of-plane deformation of the brace. The out-of-plane deformation of the brace resulted in out-of-plane rotation of the gusset plates. At 1.1% drift range, the out-of-plane rotation of the gusset plate caused cracking in the NE beam-gusset plate weld (PS W1, Figure 5-8), and the gusset plates had sustained a moderate level of yielding (PS Y2, Figure 5-9). The weld crack opened to a length of 2-3/4" (16% of the weld length) and was only contained within the bottom fillet weld. Yielding in the gusset plates was spread across the Whitmore section with concentrated yielding occurring between the two existing gusset plate holes.

Figure 5-8: Initial Weld Cracking in NE Beam-to-Gusset Plate Weld (PS W1, 1.1 %)

a. NE Corner Gusset Plate Yielding **b. SW Corner Gusset Plate Yielding**

Figure 5-9: Moderate Yielding in Gusset Plates (PS Y2, 1.1%)

By a drift range of 1.6%, the tear in the NE beam-to-gusset plate bottom fillet weld increased to a length of 5 ½" (31%) (PS-W3, Figure 5-10). While loading to the second tension peak at a 1.6% drift range, the weld crack propagated 3" into the top fillet (Figure 5-11); the first time that weld damage had propagated during a tension cycle. Initial frame damage was also observed at a drift range of 1.6%. Initial frame damage included initial yielding along the inside flange of the N beam (PS Y1-IF, Figure 5-12a), initial yielding in the plastic hinge region in the east column (PS Y1-PH, Figure 5-12b), and initial yielding in both end plates (PS Y1, Figure 5-13). Yield lines in the end plate originated from the bolt holes on the interior edge of the gusset plates and were likely in response to prying action induced by the gusset plate.

Figure 5-10: Severe Weld Tearing in NE Beam-to-Gusset Plate Weld (PS W3, 1.6%)

Figure 5-11: Weld Damage in NE Beam-to-Gusset Plate Upper Fillet Weld (1.6%)

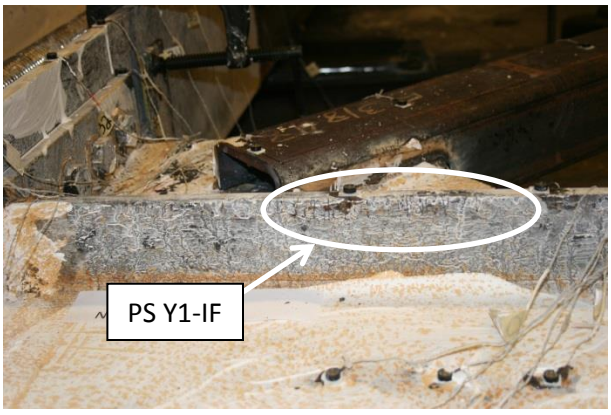

a. Inside Flange of N Beam

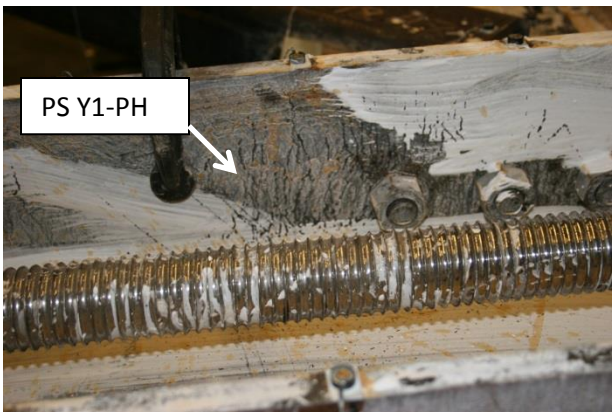

b. Inside Flange of E Column within PH region

Figure 5-12: Initial Yielding in NE Corner Frame Members (1.6%)

Figure 5-13: Initial Yielding in SW End Plate (PS Y1, 1.6%)

At a drift range of 2.3%, the brace out-of-plane deformation exceeded twice the brace depth (PS-B2, Figure 5-14). The weld cracking along the NE beam-to-gusset plate weld had propagated to 6 ¼" on the top and 7 ¾" on the bottom. A new tear also was observed in SW beam to GP weld. The weld tear was 2" on the top and 5 ½" on the bottom (PS W3, Figure 5-15). The NE beam-to-gusset plate weld tear continued to propagate in every successive tension and compressive cycles. Weld tear lengths throughout the test are documented in Table 5-11 near the end of this section.

Figure 5-14: Moderate Brace Global Buckling (PS B2, 2.3%)

Figure 5-15: Severe Weld Tear in SW Beam-to-Gusset Plate Weld (PS W3, 2.3%)

By a drift range of 2.9%, the NE beam-to-gusset plate weld tear was well over 50% of the weld length and the weld could no longer resist the out-of-plane deformation of the brace. The gusset plate began rotating about the end plate-to-gusset plate weld (Figure 5-16). Despite this severe out-of-plane deformation and the full brace compressive load, the beam-to-gusset plate weld remained intact for a few more cycles due to the additional ductility provided by prying action of the end plate. The prying action of the end plate had first become evident at a drift range of 2.4% but did not reach PS P2 until the cycle at 2.9% drift range (Figure 5-17). There was no prying action observed in the SW beam-to-gusset plate weld during the test.

a. NE Beam-to-Gusset Plate Weld Tear at 2.4% **b. NE Beam-to-Gusset Plate Weld Tear at 2.9%**

Figure 5-16: Out-of-Plane Displacement of NE Gusset Plate as a Result of Severe Weld Tearing

Figure 5-17: Prying Action of NE End Plate (PS P2, 2.9%)

Both gusset plates had also reached a severe yielding state at a drift range of 2.9% (PS Y3, Figure 5-18). Up until this point, yielding in the gusset plates during tensile loading occurred primarily along the Whitmore width while yielding in the compression cycles occurred primarily within an elliptical clearance as defined by Roeder et. all (2011).

a. NE Gusset Plate **b. SW Gusset Plate**

Figure 5-18: Severe Gusset Plate Yielding (PS Y3, 2.9%)

In the loading up to the tension peak of the 2nd cycle at 2.9% drift range, the NE beam-to-gusset plate weld tore the remaining length followed promptly by the fracture of the NE gusset plate-to-column weld (PS W4-WF, Figure 5-19). The fracture resulted in a large loss of lateral load capacity and marked the end of the test. Moderate yielding in the east column web (PS Y2-W, Figure 5-20a) and moderate yielding in the west column plastic hinge location (PS Y2-PH, Figure 5-20b) was also observed during this drift cycle.

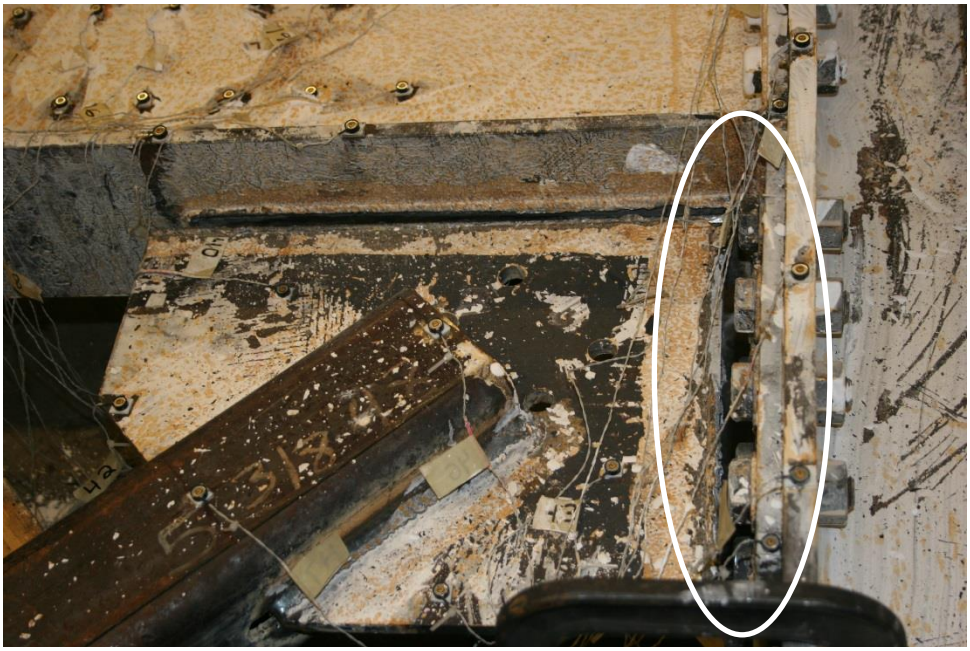

Figure 5-19: NE Gusset Plate-to-End Plate Weld Fracture (PS W4-WF, 2.9%)

a. SW Corner Outside Column Flange (Y2-PH)

b. NE Corner Column Web (Y2-W)

Figure 5-20: Column Damage at End of Test (2.9%)

Table 5-11: Specimen NCBF4-R1 Weld Tear Lengths

Cycle	Drift Range	NE Beam-to-Gusset Plate Weld Crack Length in Fillet Welds			SW Beam-to-Gusset Plate Weld Crack Length in Fillet Welds		
		Top	Bottom	Max	Top	Bottom	Max
+19	1.1%	0	0	0%	0	0	0%
-19	1.1%	0	2-1/2”	14%	0	0	0%
+20	1.1%	0	2-1/2”	14%	0	0	0%
-20	1.1%	0	3”	17%	0	0	0%
+21	1.6%	0	3”	17%	0	0	0%
-21	1.6%	0	5-1/2”	31%	0	0	0%
+22	1.6%	2-3/4”	5-1/2”	31%	0	0	0%
-22	1.6%	3-1/2”	5-1/2”	31%	0	0	0%
+23	2.3%	5”	5-1/2”	31%	0	0	0%
-23	2.3%	6-1/4”	7-3/4”	44%	2	5-1/2”	31%
+24	2.4%	8”	8”	46%	4-1/4”	5-1/2”	31%
-24	2.4%	9-1/4”	9-3/4”	56%	4-1/4”	5-1/2”	31%
+25	2.9%	10-1/2”	11”	63%	4-1/4”	5-1/2”	31%
-25	2.9%	15-1/2”	15-1/2”	89%	4-1/4”	5-1/2”	31%
+26	2.9%	17-1/2”	17-1/2”	100%	4-1/4”	5-1/2”	31%

5.4 Specimen NCBF4-R2: Bolted End Plate – In-Plane Buckling Brace

5.4.1 Overview

Specimen NCBF4-R2 was designed to simulate a retrofit of the scaled connection detail developed in Section 3.2. The connection detail for Specimen NCBF4-R2 is shown in Figure 5-21 and the connection before testing is shown in Figure 5-22. The connection was nominally identical to Specimen NCBF4-R1 (which was also designed as a retrofit of the same system) except that Specimen NCBF4-R2 utilized an in-plane buckling brace. The in-plane buckling brace was used to minimize the out-of-plane deformation demands placed on the gusset plate welds. To accommodate in-plane buckling, a knife plate was used to connect a HSS 6x4x3/8 brace that met the AISC requirements for a moderately ductile HSS brace to the existing gusset plate (note the holes in the gusset plate were there to simulate connection of the as-existing quad-angle brace). The design of Specimen NCBF4-R2 is discussed in more detail in Section 3.3.

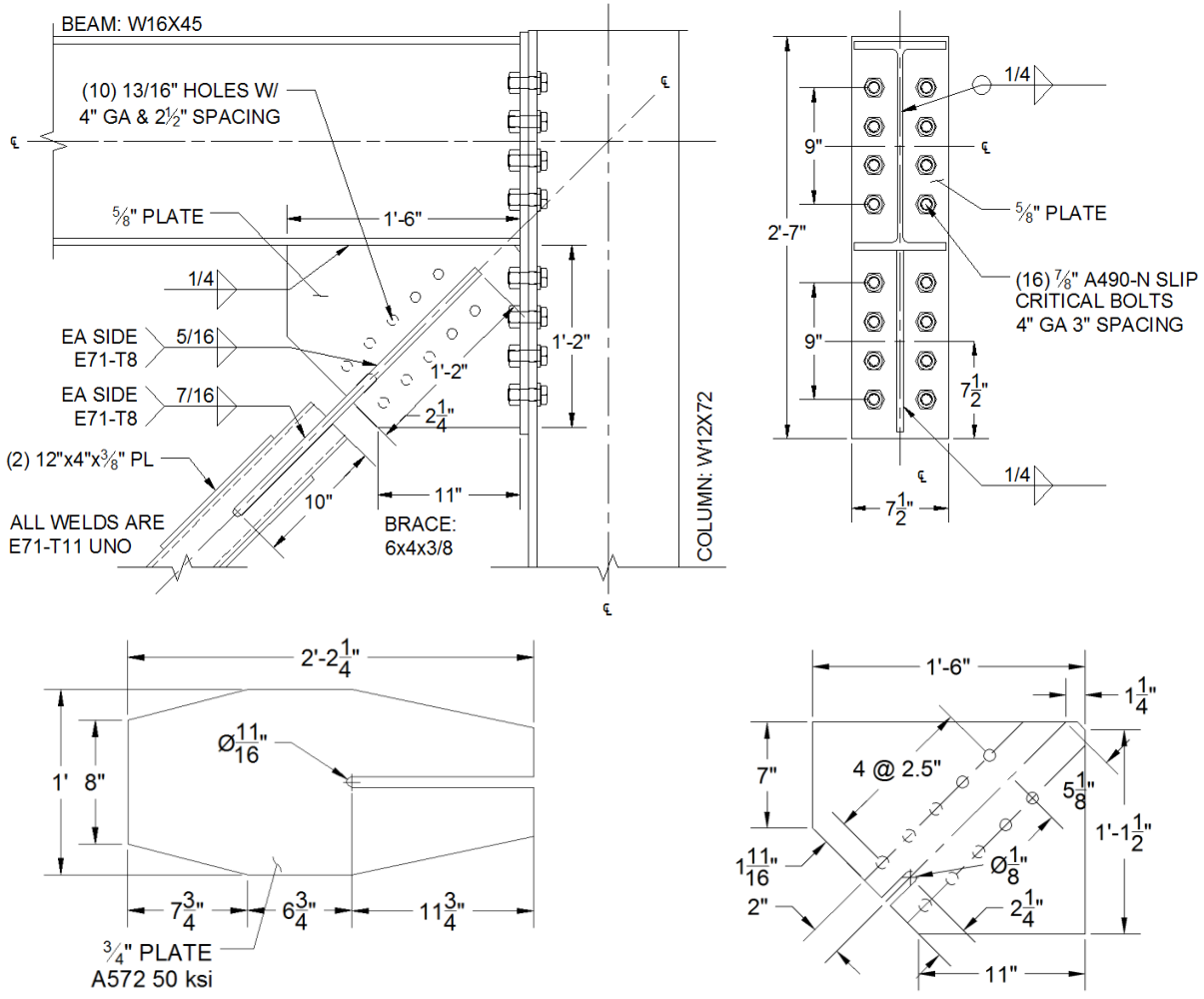

Figure 5-21: Specimen NCBF4-R2 Connection Detail

a. NE Connections

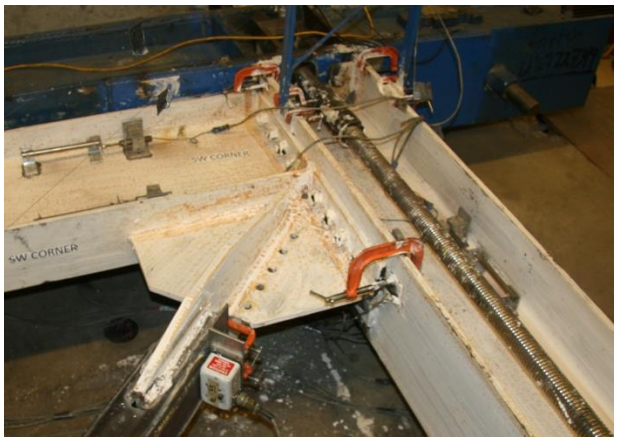

b. SW Connection

Figure 5-22: Specimen NCBF4-R2 Photos Prior to Testing

Table 5-12 shows the connection DCRs for Specimen NCBF4-R2 as calculated in Section 3.3. The primary deficiencies of the connection are beam-to-gusset plate weld fracture (per BDP) and non-ductile welds (also deficiencies in Specimen NCBF4-R1). The knife plate in-plane buckling retrofit was intended to address these deficiencies by limiting the deformation demands on the weld.

Table 5-12: Specimen NCBF4-R2 Demand Capacity Ratios

	Limit State	**NCBF4-R2**
Yielding Mechanisms	Gusset Plate Whitmore Yielding	0.82
	Knife Plate Yielding	*1.12*
	End Plate Bolt Bearing	0.17
Failure Modes	Brace Net Section Fracture	NA
	Brace Splice Fracture	0.75
	Brace Block Shear	0.66
	Gusset Plate Whitmore Fracture	0.60
	Gusset Plate Block Shear	0.64
	Beam-to-Gusset Plate Weld Fracture (GP)	**1.58**
	Beam-to-Gusset Plate Weld Fracture (BR-CVM)	0.64
	Gusset Plate-to-End Plate Weld Fracture (BR-CVM)	0.72
	End Plate Bolt Shear (BR-CVM)	0.42
Geometric Limits	Brace Compactness Ratio $(b/t)/\lambda_{hd}$	**1.21**
	Slenderness Ratio $(KL/r)_{max}$	95.08

The DCR for knife plate yielding was also above 1.0. Originally the knife plate yielding DCR was designed to be less than 1.0, but due to a fabrication error, lower grade steel was used for the knife plate; however, damage of this nature is ductile and was not seen as detrimental to frame performance. The brace compactness ratio is also shown as a deficiency and could potentially limit the deformation capacity of the specimen (relative to a brace with a lower b/t) provided the connection remained in-tact.

5.4.2 Summary of Response and Performance

The frame achieved a drift range of 3.9%, as shown in Figure 5-23. The failure mode was beam-to-gusset plate weld fracture followed by gusset plate-to-end plate weld fracture of the SW corner connection. Note that brace tearing had also developed at the mid-span of the brace. Table 5-12 shows the drift ranges when various performance states were observed. Damage to the frame included (1) severe yielding in both knife plates (PS Y3), (2) moderate yielding of both gusset plates (PS Y2), (3) moderate local buckling in the south beam at the edge of the gusset plate (PS LB2), (4) severe yielding in the east column web (PS Y3-W), (5) moderate yielding in the outer flange of the west column (PS Y2-OF), and (6) initial yielding in the N beam (PS Y1-IF).

The base shear recorded for this test was larger than in previous NCBF tests (~ 30 kips higher). The large actuator loads lead to uplift of the west column and some local damage at the edge of the gusset plate-to-beam connection. Prying action in the end plate occurred at 3.9% drift range but did not seem to help prolong the propagation of the weld tear as it did in Specimen NCBF4-R1. This might be because the out-of-plane rotation of the gusset plate was mostly eliminated. Aside from the weld tearing in the beam-to-gusset plate welds the connection elements and framing members sustained only a moderate level of damage.

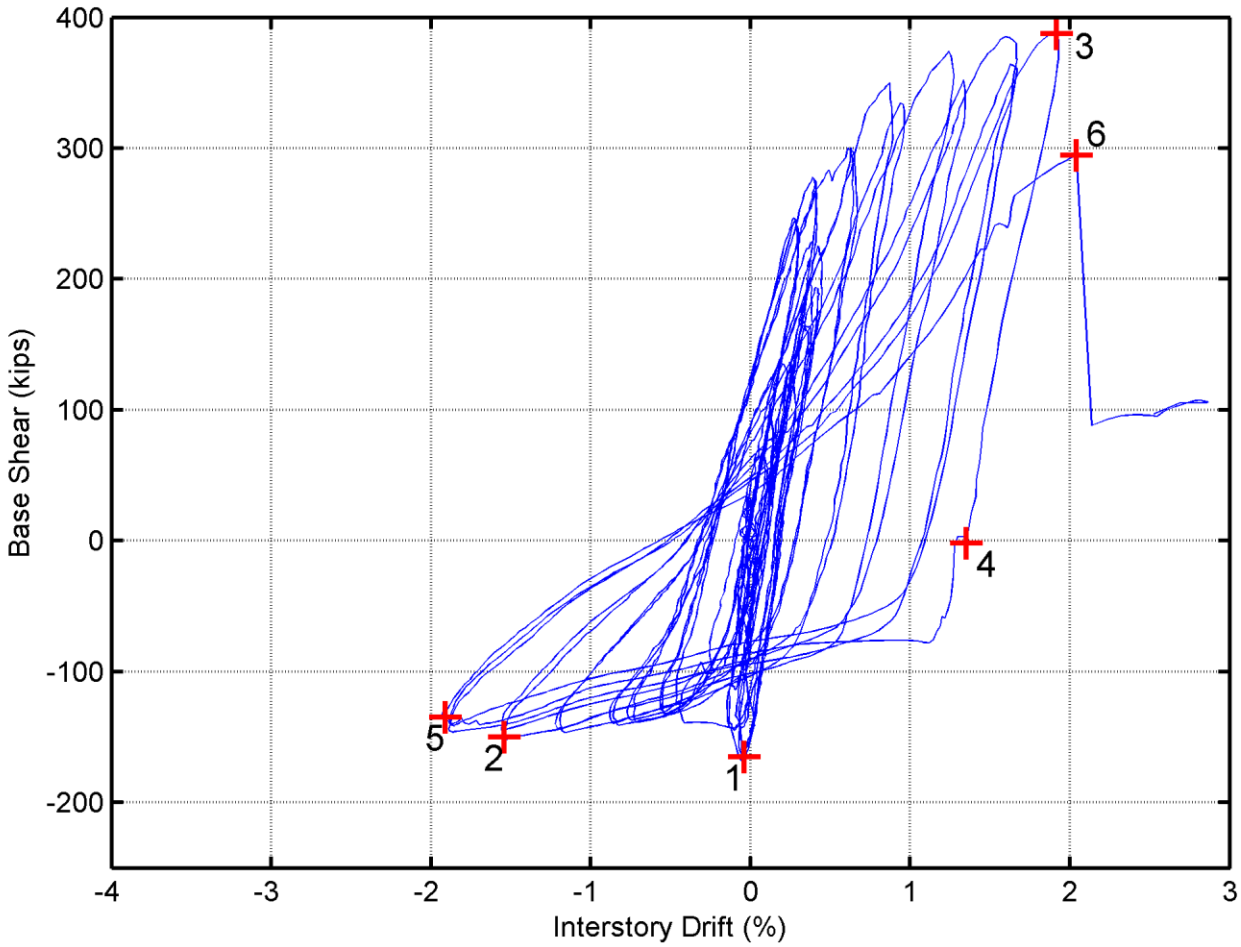

1. Brace begins buckling in-plane
2. Initial weld cracking (PS W1) observed in NE and SW beam-to-gusset welds.
3. Uplift of W column and beam web buckling distort actuator.
4. Test delayed and corrective measures taken to protect actuator.
5. SW beam-to-gusset plate weld fractures (PS W4-WF).
6. SW gusset plate-to-end plate weld fractures (PS W4-WF).

Figure 5-23: Specimen NCBF4-R2 Base Shear vs. Interstory Drift Hysteresis
(See Section 6.3.1 for details on generation of hysteresis.)

Table 5-13: Specimen NCBF4-R2 Performance State Summary Table

Cycle	Drift (%)			Brace	Northeast Connection										Southwest Connection									
	Range	Pos.	Neg.		East Column	North Beam	BR-KP Weld	KP	KP - GP Weld	GP	GP-Beam Weld	GP-EP Weld	Beam-EP Weld	EP	EP bolts	West Column	South Beam	BR-KP Weld	KP	KP-GP Weld	GP	GP-Beam weld	GP-EP Weld	Beam-EP Weld	EP	EP bolts
1	0.0	0.0	0.0																						
2	0.1	0.0	0.0																						
3	0.2	0.1	-0.1																						
4	0.2	0.1	-0.1																						
5	0.3	0.1	-0.1																						
6	0.3	0.1	-0.1																						
7	0.3	0.2	-0.1																						
8	0.3	0.3	0.0																						
9	0.4	0.4	-0.1	B1																					
10	0.4	0.4	-0.1																						
11	0.6	0.4	-0.1					Y1	W1										Y1	W1					
12	0.5	0.4	-0.1																						
13	0.9	0.4	-0.4																						
14	0.9	0.4	-0.5																						
15	0.9	0.3	-0.6																						
16	0.9	0.3	-0.6																						
17	1.1	0.4	-0.7					Y2											Y2						
18	1.2	0.4	-0.8																						
19	1.5	0.6	-0.9																						
20	1.5	0.7	-0.9											Y1											
21	2.1	0.9	-1.2	B2	Y1-PH	Y1-IF				Y1											Y1				
22	2.2	1.0	-1.2																						
23	2.8	1.3	-1.5					Y3			W1					Y1-OF	Y1-OF		Y3			W1				
24	2.9	1.3	-1.6	B3-BH													Y1-W									
25	3.6	1.7	-1.9		Y1-W, Y1-OF					Y2																
26	3.6	1.7	-1.9		LB-1,Y2-W	Y1-W																W2				
27	3.9	1.9	-1.9		Y2-PH						W2						LB1, LB2				Y2	W4-WF			P1	
28	3.9	1.7	NA	B4-BT	Y3-W											Y2-OF, Y1-W							W4-WF			

5.4.3 Test Narrative

Specimen NCBF4-R2 was essentially elastic up to a drift range of 0.4%; at this drift range the brace began visibly buckling in-plane towards the NW corner (PS B1, Figure 5-24). The buckling became more pronounced at a drift range of 0.6% progressing from 1" of in-plane displacement in the previous cycle (at 0.4% drift range) to over 3 ¼". To accommodate the in-plane deformation, the knife plates rotated resulting in yielding on the compression side of the knife plate (PS-Y1, Figure 5-24). Yield lines also extended between the top and bottom brace-to-knife plate splice welds to the knife plate-to-gusset plate splice on the tension side of the knife plates. Weld cracks at the base of both knife plate-to-gusset plate splice welds opened up as a result of knife plate deformation (PS-W1, Figure 5-24). Neither of these weld cracks would propagated beyond 1" during the remainder of the test.

Figure 5-24: Visible In-Plane Brace Buckling (PS B1, 0.4%)

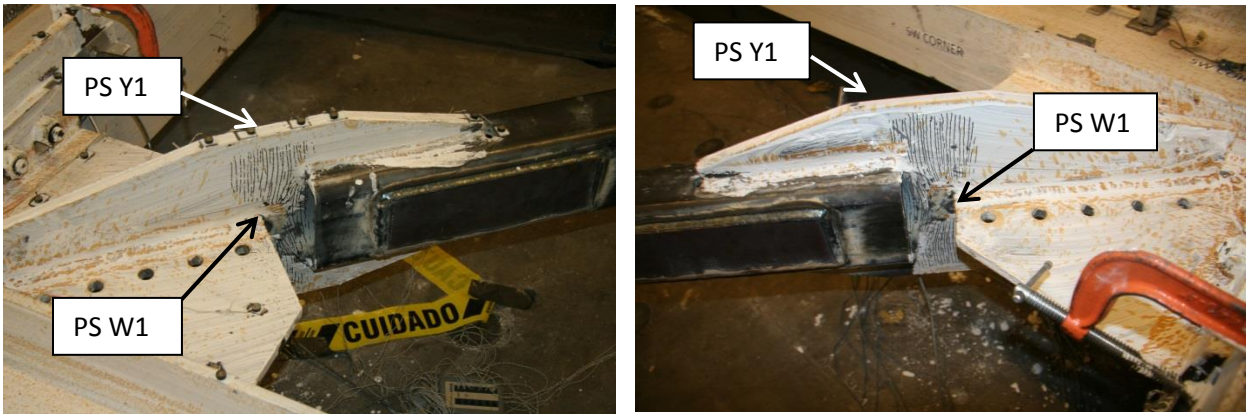

a. NE Corner Knife Plate **b. SW Corner Knife Plate**

Figure 5-25: Initial Damage in Knife Plates and Splice Welds (0.6%)

The actuator was paused momentarily on the way to the next compression peak (0.6% drift range) so that the lab technician could adjust the actuator controls and reduce the amount of air in the hydraulic pressure lines. Upon resuming, the actuator program reset and the target displacement was overshot.

The actuator was paused again to re-program the loading protocol. This event did not have significant impact on the final results except for an irregular cycle in the hysteresis with a drift range of 0.9%.

By a drift range of 1.1%, the knife plates had reached a moderate yield state (PS Y2, Figure 5-26) with concentrated yielding at the top and bottom of the knife plate. By a drift range of 2.1% the brace in-plane displacement had exceeded the brace depth by a factor of two, the threshold for moderate brace buckling (PS B2, Figure 5-27).

a. NE Knife Plate b. SW Knife Plate

Figure 5-26: Moderate Yielding in the Knife Plates (PS Y2, 1.1%)

Figure 5-27: Moderate Brace Global In-Plane Buckling (PS B2, 2.1%)

At a drift range of 2.1% initial yielding in the gusset plates (PS Y1, Figure 5-28) and initial yielding of the NE corner framing members was observed. Yield lines in the gusset plates extended between the existing gusset plate holes and radiated outwards towards the gusset plate welds. Yielding in the N beam was observed along the top of the inner flange (PS Y1-IF, Figure 5-29a) while yielding in the east column was observed in the plastic hinge location near the end of the end plate (PS Y1-PH Figure 5-29b).

a. NE Gusset Plate

b. SW Gusset Plate

Figure 5-28: Initial Yielding in the Gusset Plates (PS Y1, 2.1%)

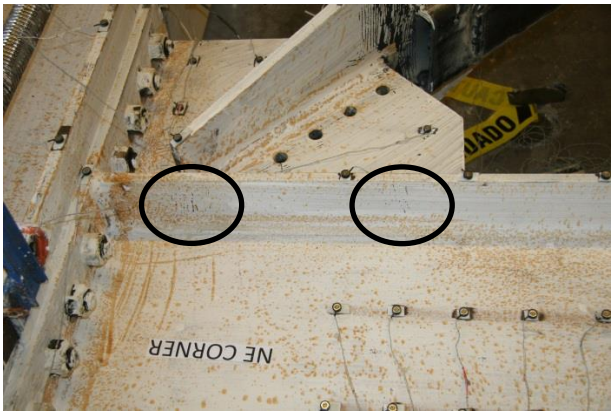

a. N Beam Inner Flange (PS Y1-IF)

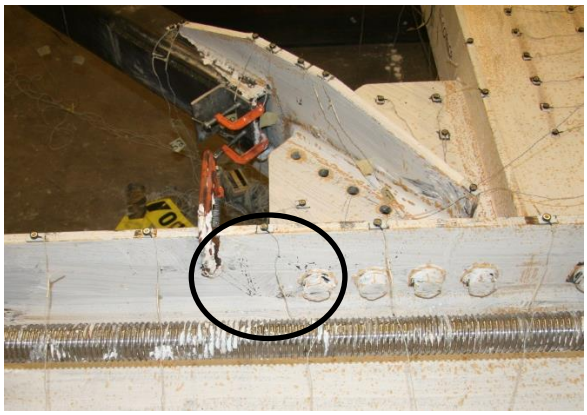

b. E Column Inner Flange (PS Y1-PH)

Figure 5-29: Initial Yielding in NE Corner Framing Members (2.1%)

By a drift range of 2.8%, the knife plates had completely yielded along the compression side and had new yield lines on the tension side signifying severe yielding in the knife plates (PS Y3, Figure 5-30). Weld tearing occurred at the edge of both beams to gusset plate welds (PS W1, Figure 5-31). Some local yielding in the beam flange extended diagonally from the edge of the beam-to-gusset plate weld (PS Y1-IF, Figure 5-31). The weld cracks and yielding in the beam flange at the edge of the connection were most likely induced from the opening and closing of the beam-column joint. Initial yielding on the outside flange of the west column was also observed at a drift range of 2.8% (PS Y1-OF, Figure 5-32).

a. Tension Side of Knife Plate b. Compression Side of Knife Plate

Figure 5-30: Severe Yielding in the NE Knife Plate (PS Y3, 2.8%)

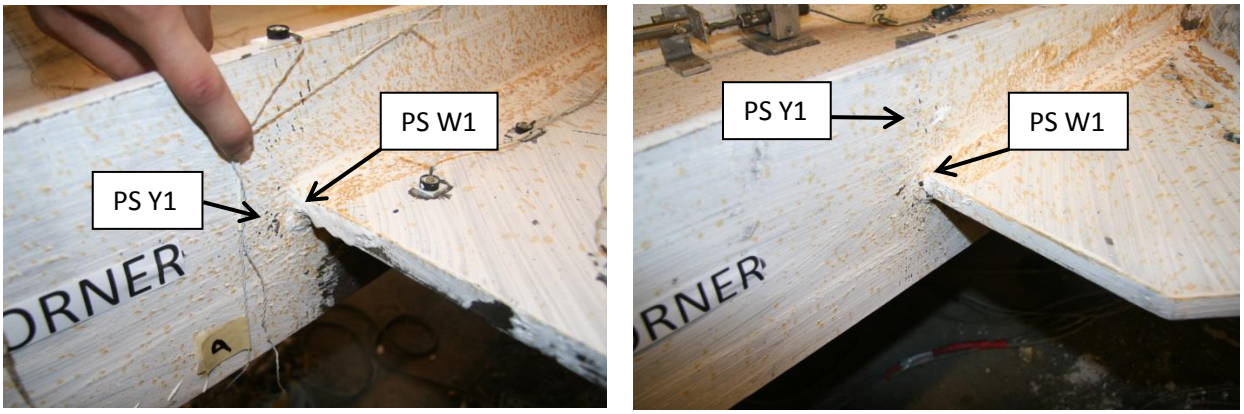

a. NE Beam-to-Gusset Plate Weld b. SW Beam-to-Gusset Plate Weld

Figure 5-31: Damage at the Edge of the Beam-to-Gusset Plate Welds (2.8%)

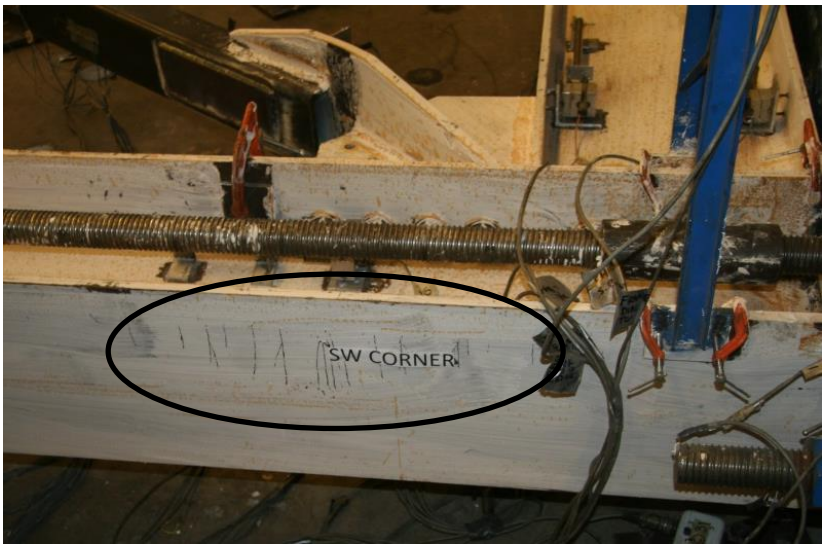

Figure 5-32: Initial Yielding on Outer Flange of W Column (Y1-OF, 2.8%)

The brace began to cup at mid span prior to the next compression peak at a drift range of 2.9%. This cupping increased with each successive compression excursion until the end of the test. Photos of brace hinging from the test are shown in Figure 5-33.

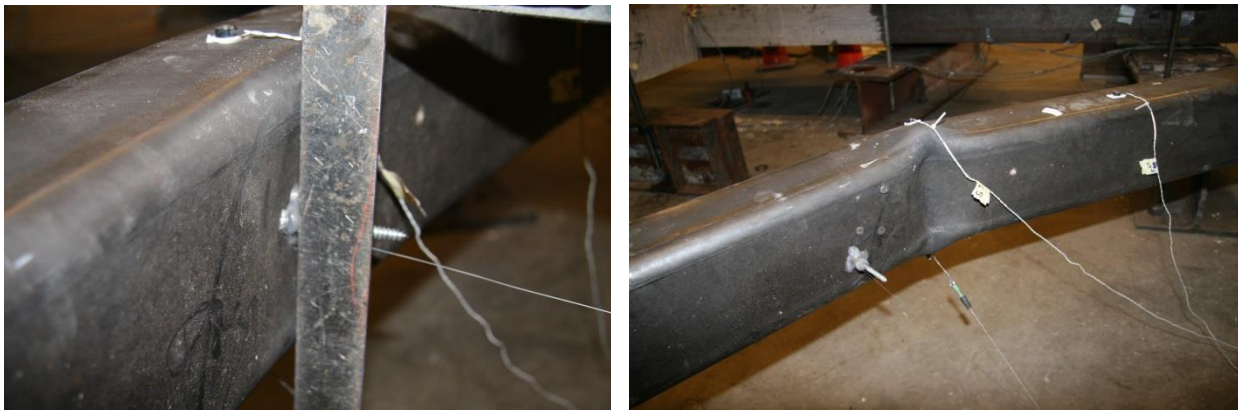

a. Initial Brace Hinging (2.9%) b. Pronounced Brace Hinging – 3.9%-27

Figure 5-33: Brace Hinging at Mid-Span (PS B3-BH)

At a drift range of 3.6%, the NE gusset plate reached a moderate yielding state (PS Y2, Figure 5-34). Yield lines extended from the edge of the gusset plate through all of the bolt holes and around the end of the knife plate. The yield lines were in the same pattern as the rupture lines assumed for calculation of the gusset plate block shear strength. Additional yield lines that were not part of the block shear rupture pattern extended from the bolt holes out to gusset plate welds. A similar yielding pattern also was developing in the SW gusset plate but the performance state did not progress to PS Y2 until a drift range of 3.9%.

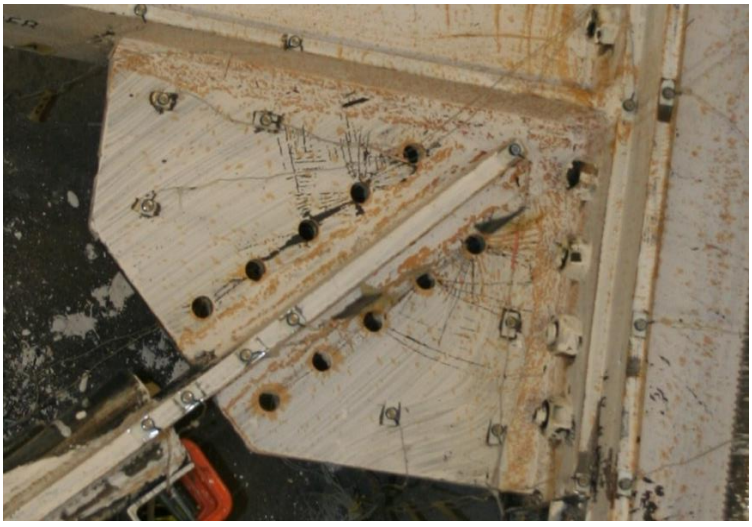

Figure 5-34: Moderate Yielding in NE Gusset Plate (PS Y2, 3.6%)

During the second cycle at 3.6% drift range, the 1” weld crack in the SW beam-to-gusset plate weld propagated to 3 1/8” (18%) at both the top and bottom of the gusset plate. This initiated unstable crack propagation, and the weld tear would grow substantially in the next few cycles.

The yielding of the east column also became much more pronounced during this cycle (Figure 5-35). Yield lines appeared on the outside flange of the column, on the web in the plastic hinge region and in the column web between the end plate bolts. The column flanges and web at the edge of the end plate started to buckle locally out-of-plane and by the end of the compression peak the column had sustained moderate damage throughout. Initial yielding in the N beam web also occurred near the NE end plate.

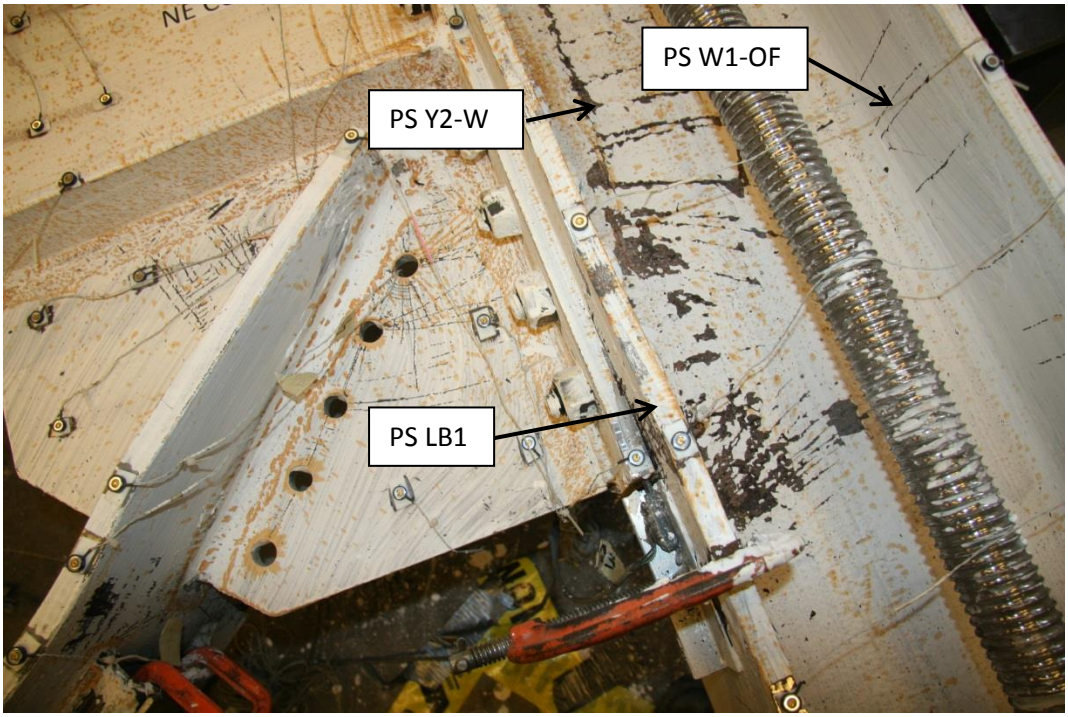

Figure 5-35: Moderate Damage in East Column (3.6%)

At a drift range of 3.9%, both the beam web and inner flange of the S beam buckled locally reaching the LB2 performance state. The lateral load exceeded the overturning capacity of the frame causing the west column to uplift off of the channel assembly. It is anticipated that the uplift and general instability of the frame lead to the local damage in the S beam and, in turn, to out-of-plane rigid body rotation of the column. Damage to the S beam at a drift range of 3.9% is shown in Figure 5-36.

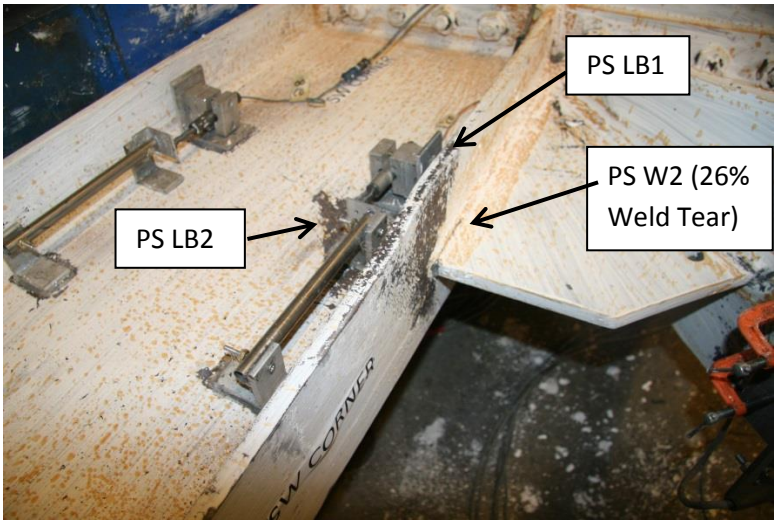

Figure 5-36: Local Buckling of S Beam Flange and Web (3.9%)

The S end of the column displaced over an inch down as a result of the column rigid body rotation. On the other end of the column the actuator clevis became pinched (Figure 5-37). To protect the actuator, the load was returned to zero and the test was put on hold until a solution could be implemented. An additional out-of-plane restraint was installed on the N end of the west column as shown in Figure 5-38 (see Section 4.3 for details on out-of-plane restraints). The new out-of-plane restraint was used to ratchet down the N end of the column and rigidly rotate the S end of the column back most of the way back to its original position. At this point another out-of-plane support was positioned beneath the S end of the column to prevent the column from rigidly rotating out-of-plane again. The post tension rods were re-tensioned to initial values to limit future uplift. The test was resumed the following day.

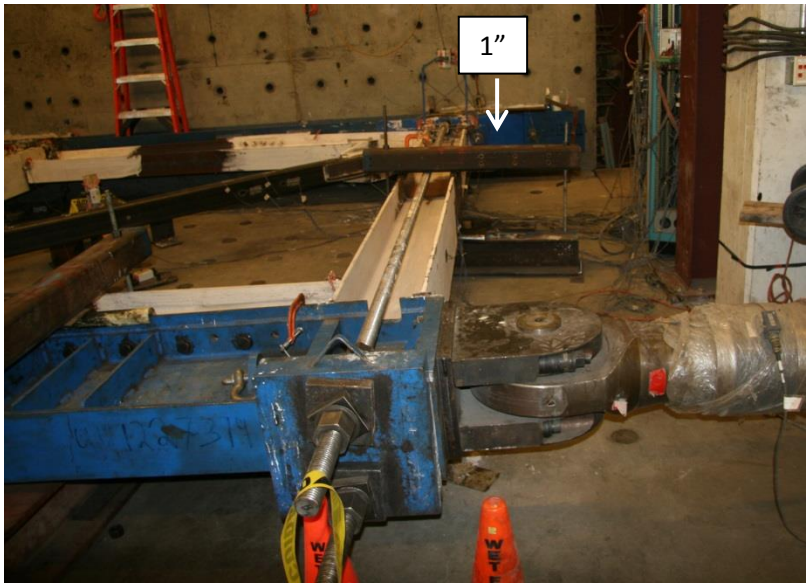

Figure 5-37: Rigid body Rotation of Column and Actuator Distortion (3.9%)

Figure 5-38: New Out-of-Plane Restraints

During the next cycle at 3.9% drift range the SW beam-to-gusset plate weld fractured and the NE beam-to-gusset plate weld tear increased to 3 ¼". A gap between the SW end plate and the column also opened up at the edge of the inner beam flange indicating prying action in the end plate. A picture of the weld tear is shown in Figure 5-39.

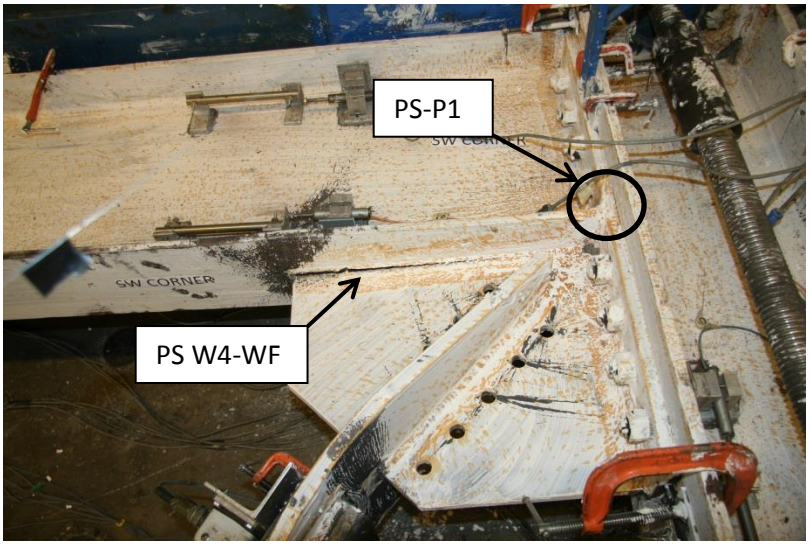

Figure 5-39: Weld Fracture of SE Beam-to-Gusset Plate Weld (PS W4-WF, 3.9%)

The gusset plate to end plate weld fractured completely during to the next tension peak. Simultaneously, additional yielding was observed in the framing members. Final damage of the SW connection is shown in Figure 5-41 while final damage of the NE connection is shown in Figure 5-42. Although weld fracture along the SW beam-to-gusset plate weld was the ultimate failure mode of the specimen it is worth noting that the brace was also close to failure. In fact, the brace had begun tearing prior to fracture of the gusset plate to end plate weld. A picture of the torn brace is shown in Figure 5-40.

Figure 5-40: Brace Tearing (PS B4-BT, 3.9%)

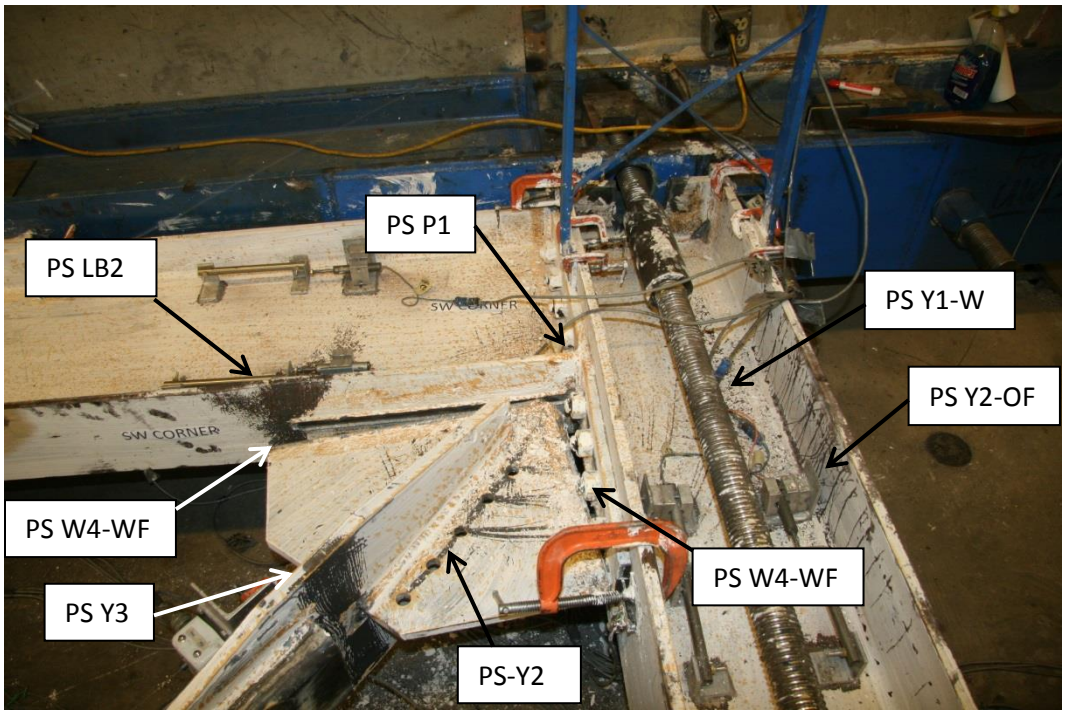

Figure 5-41: Damage in SW Corner at End of Test (3.9%)

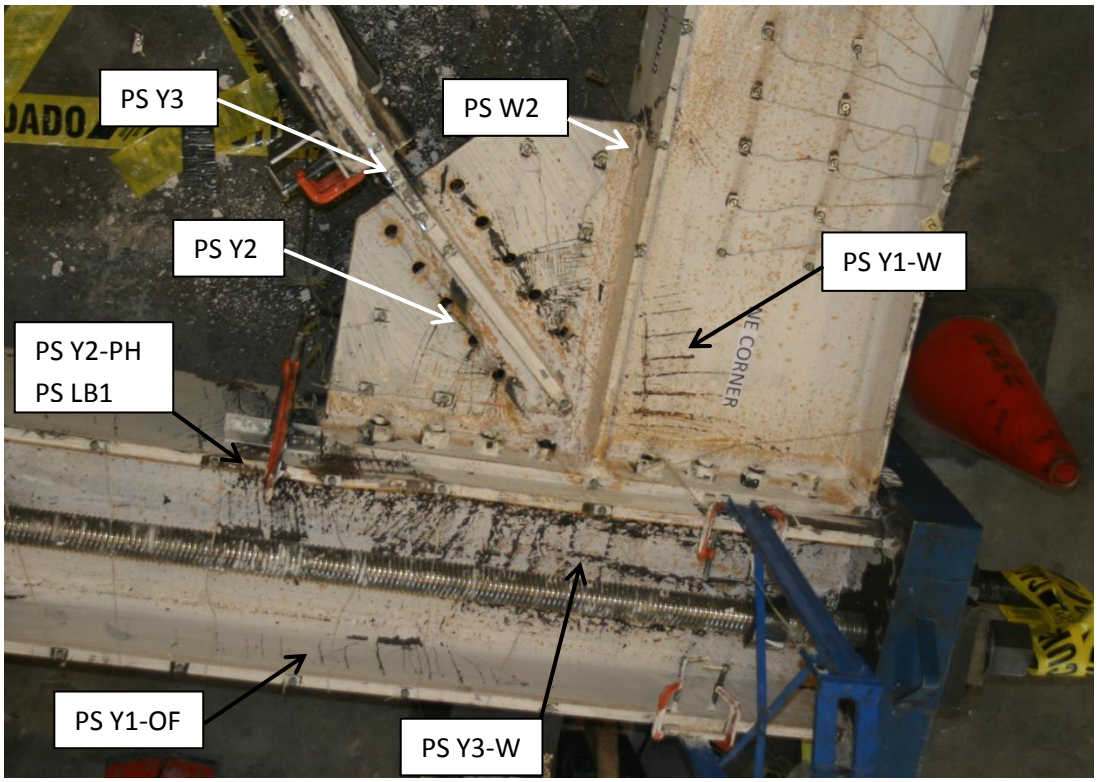

Figure 5-42: Damage in NE corner at End of Test (3.9%)

5.5 Specimen NCBF4-R3: Bolted End Plate – Buckling Restrained Brace

5.5.1 Overview

Specimen NCBF4-R3 was a retrofit design using BRBs for the NCBF with bolted end plate connections as described in Section 3.2and as shown in Figure 5-43 and Figure 5-44. The objective of the test was to test another brace option that could limit the deformation demands on the gusset plate welds. Aspects of the connection geometry were scaled up from the two previous end plate connections (Specimens NCBF4-R1 and NCBF4-R2) to accommodate a BRB with a length of 142". The BRB was not collared; the extension plate was exposed. A bolted connection was used (BRB details in Appendix E).

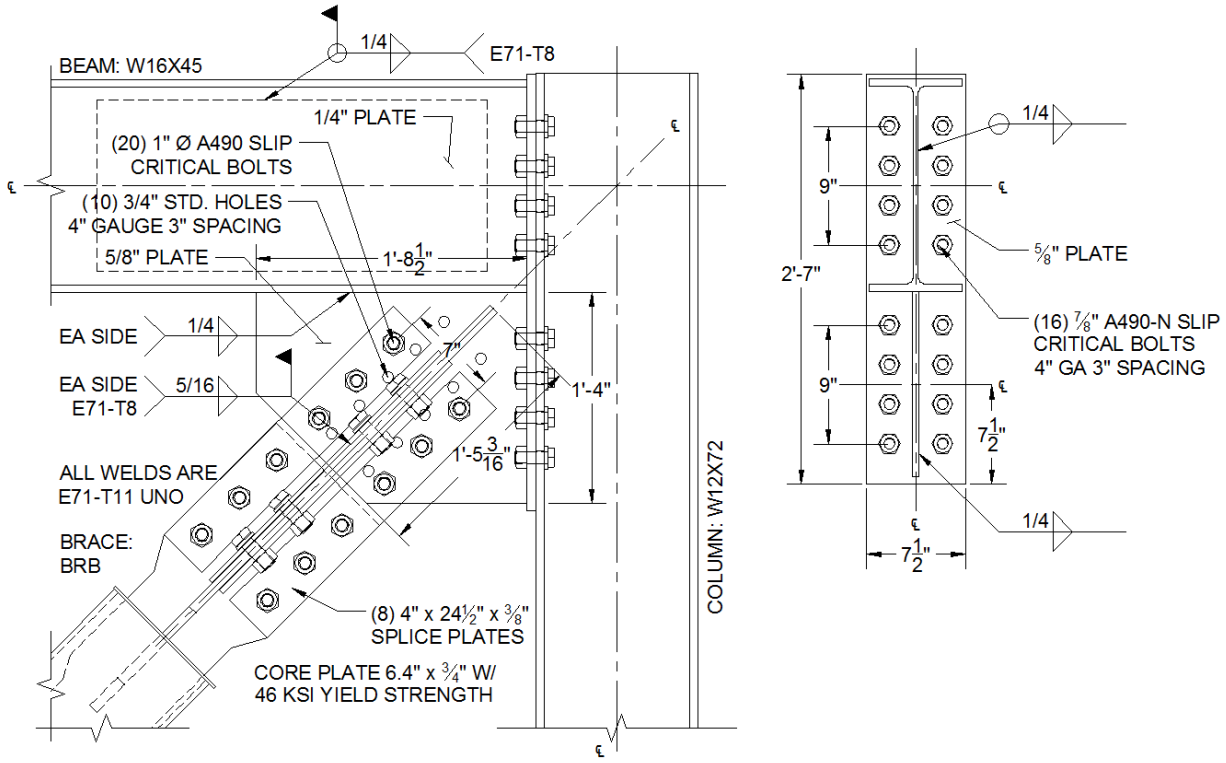

Figure 5-43: Specimen NCBF4-R3 Connection Detail

The BRB was connected to the gusset plate using ten splice plates bolted on either side of each leg of a cruciform section. Two rib plates were welded to the gusset plate to create a matching cruciform shape. Twenty 1" A490 bolts in each corner transferred the load between the BRB and the gusset plate. The bolts were slip critical and prevented dynamic slip of the BRB during the test. The existing NCBF gusset plate of the connection was assumed to be left in place, and all welds were non-notch tough. A 3/8" plate was welded to the beam web to prevent local instabilities in the beam web; this follows the recommendation of Palmer et. all (2011).

a. SW Corner

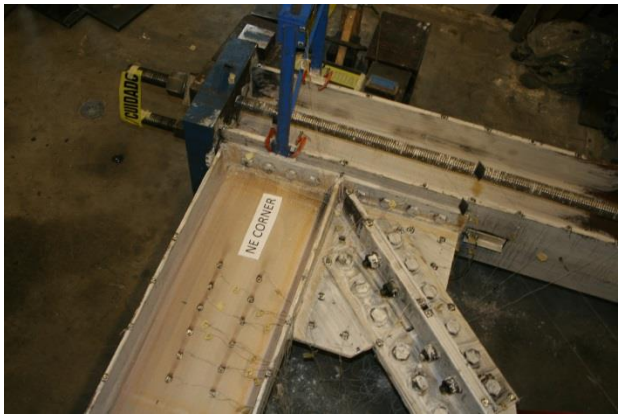

b. NE corner

Figure 5-44: Specimen NCBF4-R3 Photos Prior to Testing

Since the gusset plate dimensions were increased in Specimen NCBF4-R3 (relative to Specimens NCBF4-R1 and NCBF4-R2) and the expected capacity of the BRB (compression and tension) was lower than the HSS braces (tension), most of the calculated DCRs for Specimen NCBF-R3 were well below 1.0 (Table 5-14). Since it takes many cycles to fracture a BRB core plate, it was expected that the frame would sustain a high drift range but with significant damage to the connection and/or framing members. As seen in previous BRB system tests, the damage to the connection and framing elements was expected to contribute to a local instability and ultimately lead to hinging of the BRB.

Table 5-14: Specimen NCBF4-R3 Demand to Capacity Ratios

	Limit State	NCBF4-R3
Yielding Mechanisms	Gusset Plate Whitmore Yielding	0.63
	End Plate Bolt Bearing (BR-CVM)	0.14
Failure Modes	Brace Net Section Fracture	0.56
	Brace Splice Fracture	0.33
	Brace Block Shear	0.36
	Gusset Plate Whitmore Fracture	0.43
	Gusset Plate Block Shear	0.44
	Beam-to-Gusset Plate Weld Fracture (GP)	**1.61**
	Beam-to-Gusset Plate Weld Fracture (BR-CVM)	0.52
	Gusset Plate-to-End Plate Weld Fracture (BR-CVM)	0.56
	End Plate Bolt Shear (BR-CVM)	0.38

5.5.2 Summary of Response and Performance

The frame achieved a drift range of 4.6%, as shown in Figure 5-45. The failure mode was mixed and included fracture of the beam-to-gusset plate weld and BRB core plate hinging outside of the casing. Table 5-15 shows the drift ranges when various performance states were observed. Damage to the frame included (1) severe yielding and local buckling in both columns at the edge of the end plates (PS Y3-PH & PS LB3), (2) initial yielding in the gusset plates (PS-Y1), (3) moderate weld tearing in the SW beam-to-gusset plate weld, (4) and initial yielding in the N beam inner flange (PS Y1-IF).

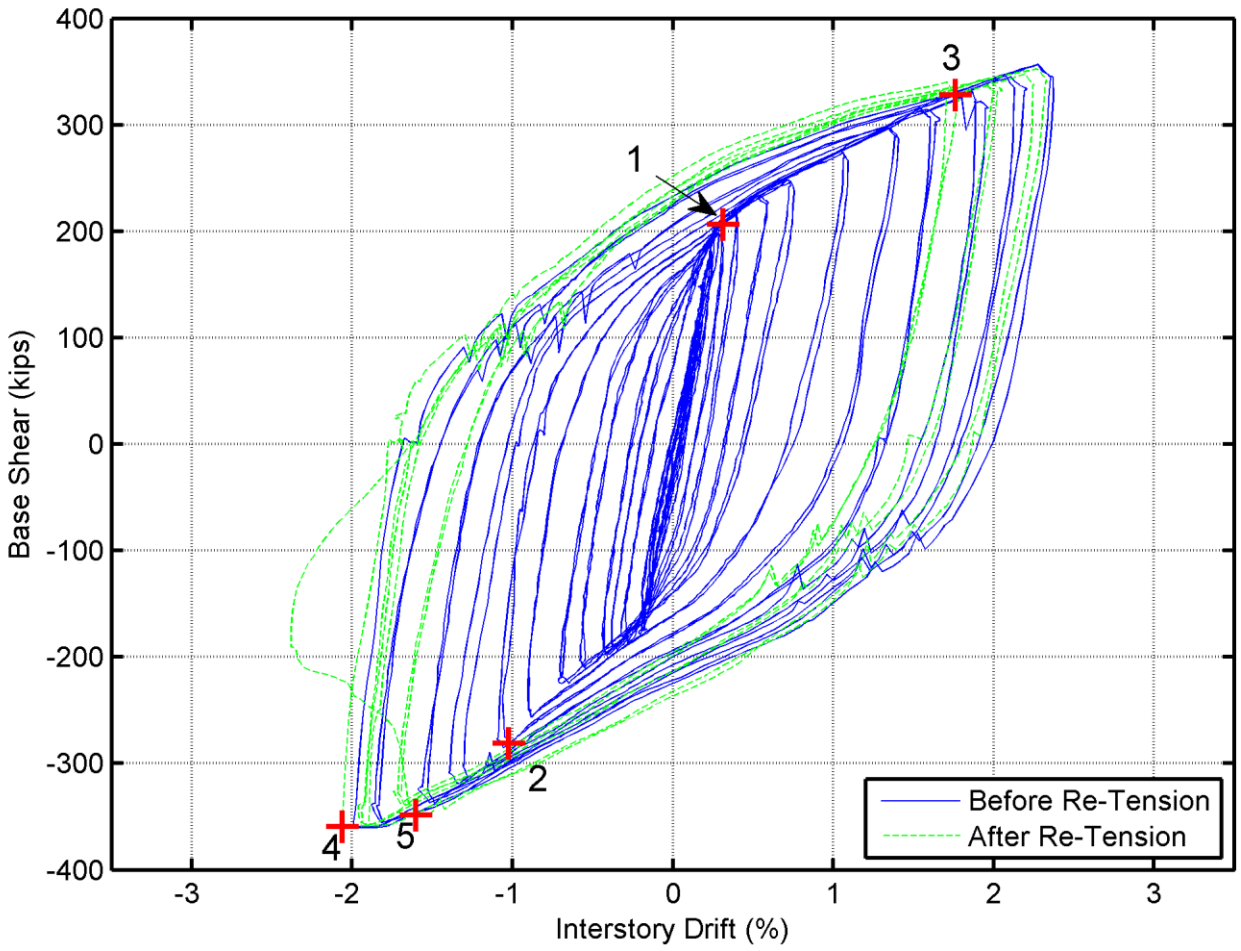

1. BRB core plate begins to yield (PS B1).
2. Initial cracking in NE beam-to-gusset plate weld (PS W1).
3. Slip occurs between NE end plate and E column.
4. Columns develop full plastic hinges at edge of end plates. Columns are re-tensioned and loading protocol restarted from when first uplift occurred.
5. Initial hinging of BRB core plate at NE corner. Full fracture of the NE beam-to-gusset plate weld. Note that hinging of the BRB occurred after the axial load system was re-tensioned.

Figure 5-45: Specimen NCBF4-R3 Base Shear vs. Interstory Drift Hysteresis
(See Section 6.3.1 for details on generation of hysteresis.)

The drift range of 4.5% is similar to the drift range achieved in previous BRB tests conducted at UW (Christopulos 2005). A beam web doubler effectively reduced damage in the beams but severe damage was sustained in both columns leading to plastic hinges at the edge of the end plates in both columns. The beam-to-gusset plate weld sustained moderate damage throughout the test but was generally more stable than in the previous bolted end plate tests (Specimens NCBF4-R1 and NCBF4-R2).

The drifts achieved prior to significant beam-to-gusset plate weld damage and complete weld rupture were larger than those for Specimens NCBF4-R1 and NCBF4-R2. A number of factors could have contributed to this but the most obvious is the low beam-to-gusset plate weld DCR resulting from the change in connection geometry necessary to accommodate the BRB. Comparisons between the weld cracking patterns in the bolted end plate tests will be provided in the data analysis section (Section 6.5.1).

It is unclear how much the re-tensioning of the post tensioning rods contributed to the frame damage; however, it should be noted that the columns were able to develop the full post-tension force when re-tensioned. This indicated that the columns had not yet failed despite severe damage.

Table 5-15: Specimen NCBF4-R3 Performance State Summary Table

Cycle	Drift (%)			Brace	Northeast Connection									Southwest Connection								
	Range	Pos.	Neg.		East Column	North Beam	BRB Conn.	GP	GP-Beam Weld	GP-EP Weld	Beam-EP Weld	EP	EP bolts	West Column	South Beam	BRB Conn.	GP	GP-Beam weld	GP-EP Weld	Beam-EP Weld	EP	EP bolts
1	no data																					
2	no data																					
3	0.2	0.1	-0.1																			
4	0.2	0.1	-0.1																			
5	0.3	0.2	-0.1																			
6	0.3	0.1	-0.1																			
7	0.3	0.2	-0.2																			
8	0.4	0.2	-0.2																			
9	0.5	0.2	-0.2																			
10	0.4	0.2	-0.2																			
11	0.6	0.3	-0.3																			
12	0.6	0.3	-0.3																			
13	0.7	0.3	-0.4	B1																		
14	0.7	0.3	-0.4																			
15	0.8	0.4	-0.4																			
16	0.8	0.4	-0.4																			
17	1.2	0.6	-0.6																			
18	1.2	0.6	-0.6																			
19	1.5	0.8	-0.7		Y1-PH			Y1														
20	1.4	0.7	-0.7																			
21	2.0	1.1	-0.9	B2										Y1-PH			Y1					
22	2.0	1.1	-0.9																			
23	2.5	1.4	-1.1						W1													
24	2.5	1.4	-1.1																			
25	3.0	1.7	-1.3		LB1								Bo1	Y1-OF								
26	3.0	1.6	-1.4																			
27	3.6	2.0	-1.6	B3	Y2-PH	Y1-IF								Y2-PH, Y2-OF, LB1				W1				
28	3.4	1.9	-1.5																			
29	4.1	2.2	-1.9		Y1-W																	
30	4.0	2.1	-1.8		Y3-PH, LB2																	
31	4.4	2.4	-2.0						W2					Y3-PH, LB2								
32	4.5	2.4	-2.1		LB3																	
33-38	4.6	2.3	-2.4	B4-BH					WF			P2		LB3				W2				

5.5.3 Test Narrative

Specimen NCBF4-R3 performed elastically in cycles through a drift range of 0.6%. At a drift range of 0.7% the stiffness of the frame reduced as a result of yielding of the BRB core. Core plate yielding occurred during both the tension and compression cycles as evidenced in the force-drift response curves (Figure 5-45).

At a drift range of 1.5%, yielding occurred in the columns and gusset plates, as indicated in Figure 5-46 and Figure 5-47 for the NE and SW corners respectively, states (PS Y1) and (PS Y1-PH). Note that much of the gusset plate was concealed by the BRB splice plates; the first visible yield lines appeared in the corner of the gusset plates.

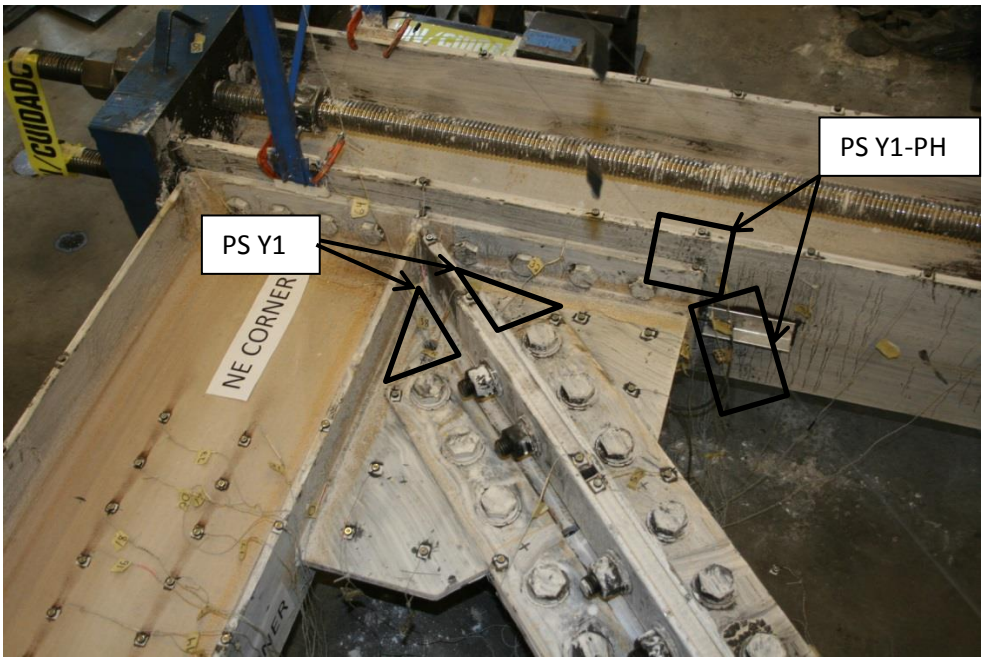

Figure 5-46: Initial Yielding in the NE Corner Gusset Plate and Column (1.5%)

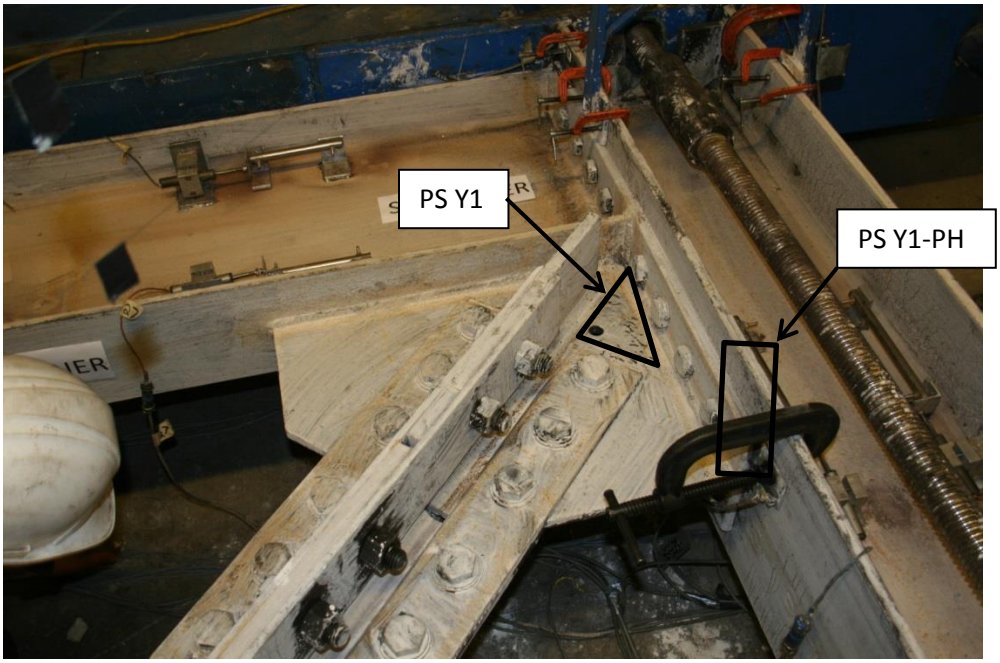

Figure 5-47: Initial Yielding in the SW Column (2.0%)

By a drift range of 2.0%, the BRB had reached a state of moderate yielding (PS B2), as determined by the brace elongation measurements and the yield lines on the exposed portion of the core plate. Figure 5-48 shows the movement of the BRB, which is the gap between the edge of the whitewash and the edge of the BRB casing at the NE corner.

Initial weld cracking in the NE beam-to-gusset plate weld was observed at a drift range of 2.5% (PS W1, Figure 5-49). The weld crack was measured to be ¼".

Figure 5-48: BRB Core Plate Moderate Yielding (PS B2, 2.0%)

Figure 5-49: Initial Weld Cracking in the NE Beam-to-Gusset Plate Weld (PS W1, 2.5%)

At a drift range of 3.0% the NE end plate slipped relative to the column (PS Bo1) reducing the force by approximately 30 kips. This force was recovered quickly as the bolts began to bear against the edge of the bolt holes. Since the slip occurred dynamically and was less than 1/16 of an inch it was difficult to capture the behavior with a photograph. Figure 5-50 shows an image of the NE connection just after slip had occurred with an arrow indicating the initial direction of slip in the end plate.

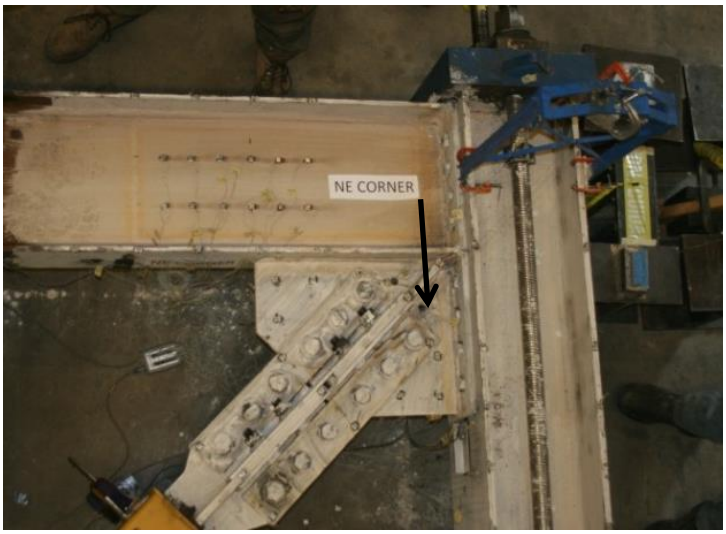

Figure 5-50: Dynamic Slip of the NE End Plate (PS Bo1, 3.0%)

The frame also sustained additional yielding at a drift range of 3.0%, including local buckling in the east column at the plastic hinge location (PS LB1, Figure 5-51) and initial yielding of the west column outer flange (PS Y1-OF, Figure 5-52).

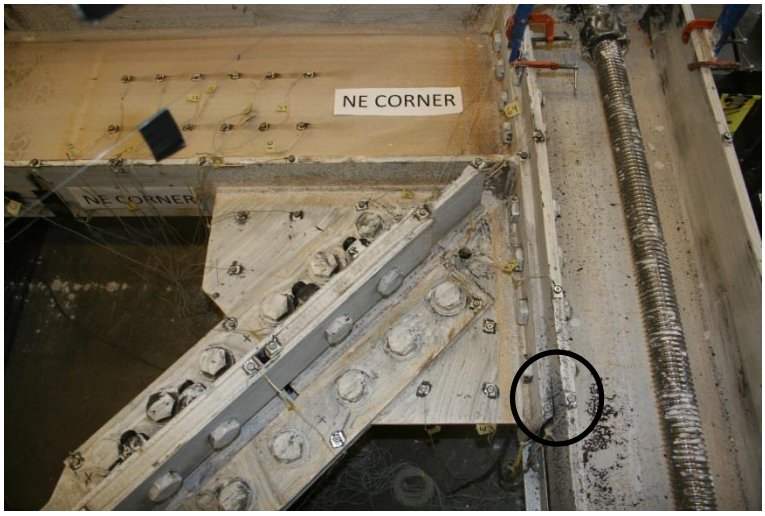

Figure 5-51: Initial Local Buckling in the East Column (PS LB1, 3.0%)

Figure 5-52: Initial Yielding in the West Column Outer Flange (PS Y1-OF, 3.0%)

The frame also sustained additional yielding at several locations by the end of the cycles with a drift range of 3.6%. Damage in the east and west column are shown in Figure 5-53 and Figure 5-54 respectively. The BRB core plate had reached a severe yielding state (PS B3) and both columns had reached moderate performance states. A weld crack had also opened up in the SW beam-to-gusset plate weld.

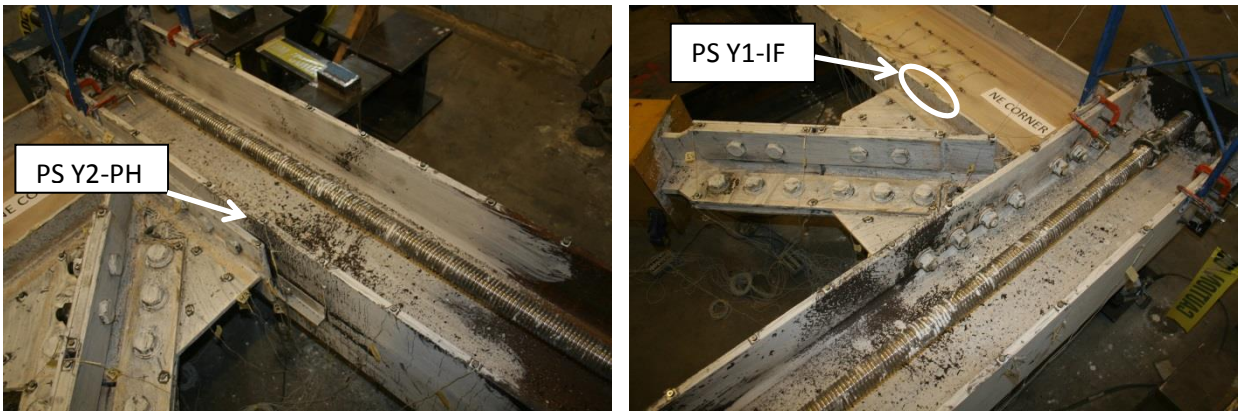

Figure 5-53: Moderate Yielding in E Column (3.6%)

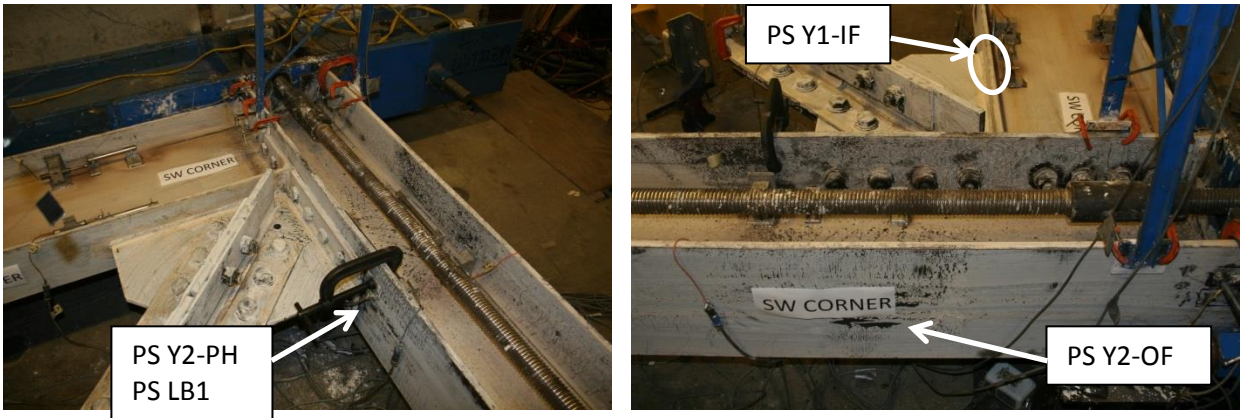

Figure 5-54: Moderate Yielding and Initial Flange Buckling in W Column (3.6%)

Yielding and buckling occurred in the east column while the brace was in tension and the west column while the brace was in compression. Yielding in the endplates, beams, and gusset plates was minimal. The yielding progression in the columns from 3.6% to 4.5% drift range is documented in Figure 5-55. Once the 4.5% drift range was achieved, both columns had developed full plastic hinges.

a. NE Corner (3.6%)

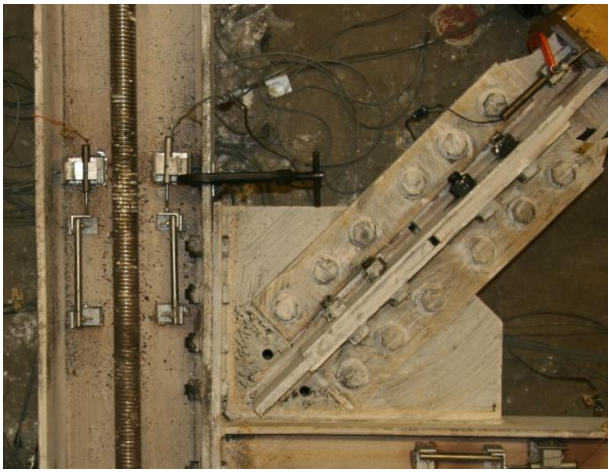

b. SW Corner (3.6%)

c. NE Corner (4.0%)

d. SW Corner (4.0%)

e. NE Corner (4.5%)

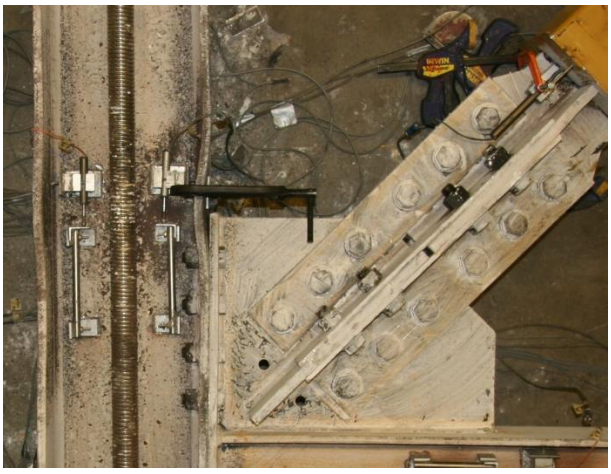

f. SW Corner (4.5%)

Figure 5-55: Damage in the Columns at Increasing Drift Range

After the second cycle at 4.5% drift range, the test was paused because of noticeable uplift at the base of the west column. At that point in the test it was believed that the frame was failing to sustain additional drift in the brace tension excursions; instead deformation of the post-tension rods and rigid body rotation of the frame accommodated the movement. To rectify this, the rods were re-tensioned and the loading protocol was restarted from a point when the uplift initiated (3.6% drift range).

(However, it should be noted that it was determined later that the drift in the brace tension excursions were increasing but the potentiometer mounts used to measure the deformation for the frame along the diagonal were rotating. This issue is discussed further in Section 6.3.1. Although this pause resulted in interruption of the test, it did not alter the performance or failure mode)

Upon resuming the loading protocol, the west column started buckling globally out-of-plane between the out-of-plane supports while the brace was in compression. The second 4.5% drift range cycle resulted in a severe tearing of the NE beam-to-gusset plate weld (PS W3) and the brace moved out-of-plane; a result of hinging of the exposed portion of the core plate at the NE edge of the end of the casing (PS B4-BH).

In the following cycle, the out-of-plane deformation of the BRB tore the remaining length of weld adjoining the beam and gusset plate (PS W4-WF, Figure 5-56) and the test was stopped. Frame damage in the NE and SW corners at the end of the test is shown in Figure 5-56 and Figure 5-57 respectively.

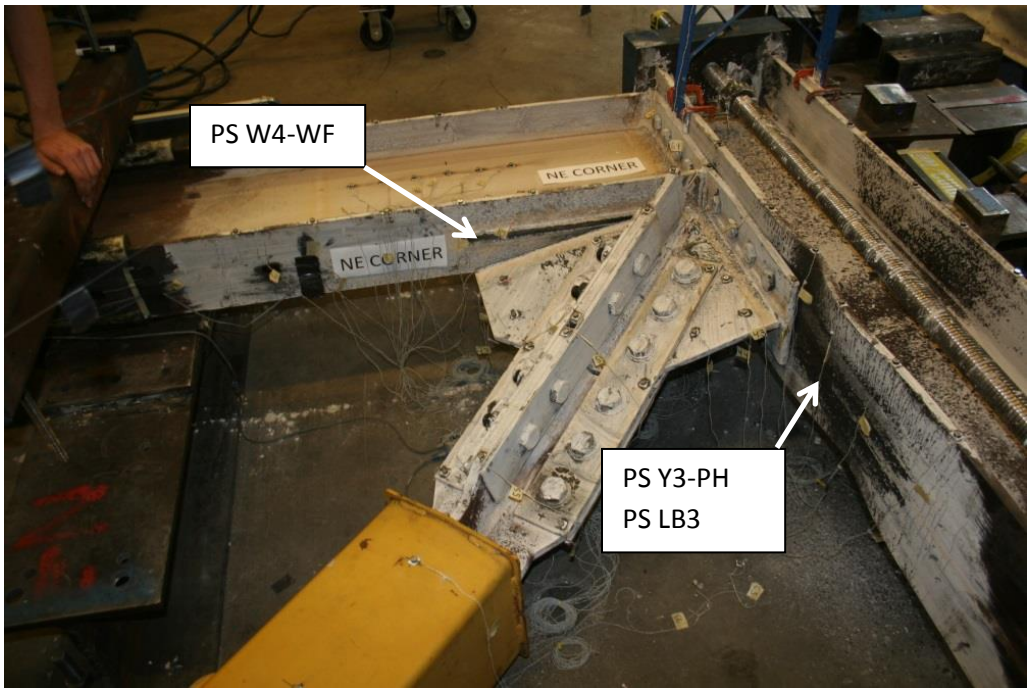

Figure 5-56: Damage in the NE Corner at End of Test (4.6%)

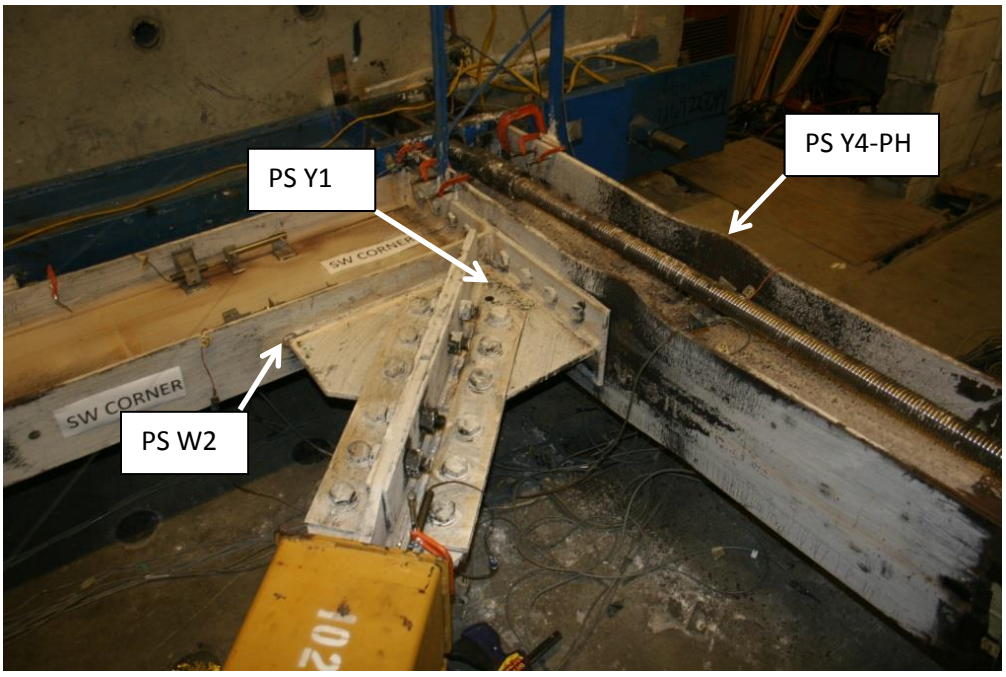

Figure 5-57: Damage in SW Corner at End of Test (4.6%)

5.6 Specimen NCBF5: Integrated Shear Plate – Out-of-Plane Buckling Brace

5.6.1 Overview

Specimen NCBF5, shown in Figure 5-58 and Figure 5-59, was designed to represent a subset of connections analyzed during the infrastructure review that had shared gusset plates, i.e. connections utilizing a single plate as the gusset plate and a bolted shear-tab beam-to-column connection. As shown, the gusset plate is connected to the column with a CJP weld and connected to the beam with a bolt group.

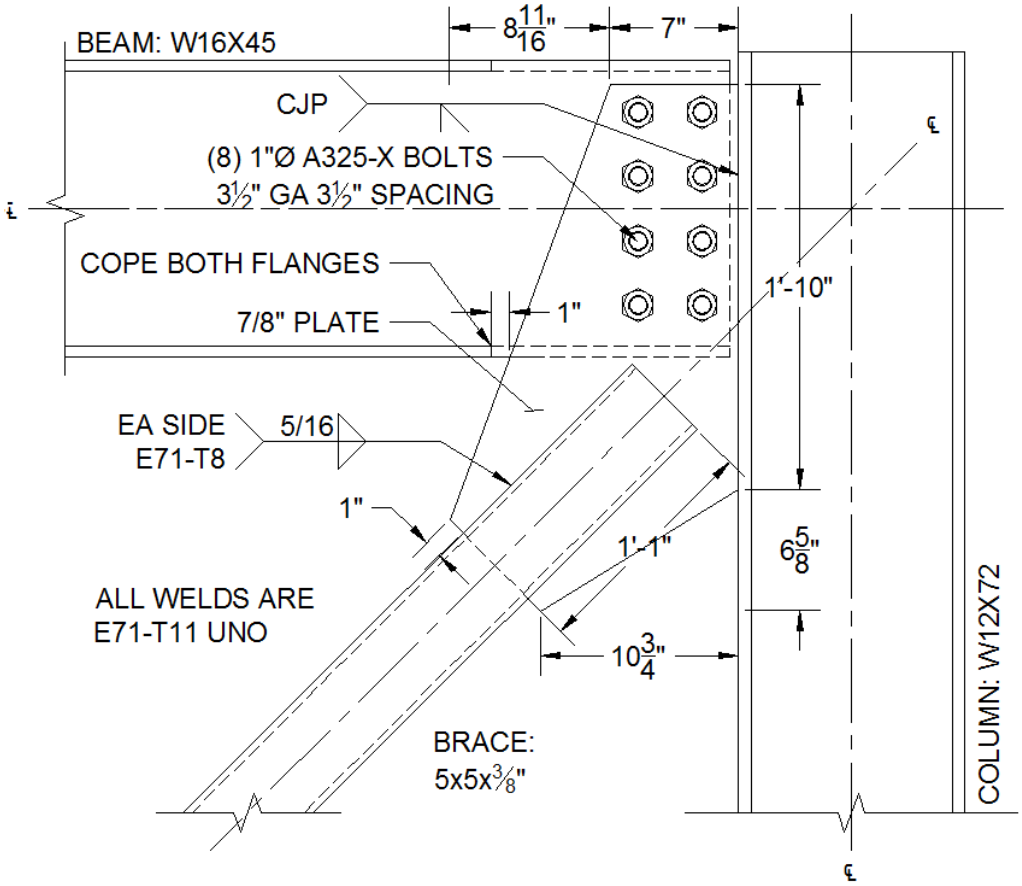

Figure 5-58: Specimen NCBF5 Connection Detail

The gusset plate was 7/8" thick, the brace had limited clearance, and the bolt group was composed of eight A325-X bolts. Both flanges of the beam were coped to allow for construction and to limit the moment capacity of the beam in relation to the bolt group. The brace-to-gusset plate splice weld was detailed as a ductile weld (E71-T8) to reduce the potential for brace slice weld fracture mechanism which was studied in Specimen NCBF0 (Section 2.4.4).

a. SW corner b. NE corner

Figure 5-59: Specimen NCBF5 Photos Prior to Testing

The DCRs for Specimen NCBF5 are shown in Table 5-16. The one calculated deficiency, brace net section fracture was not expected to limit the drift capacity of the frame based on observations from previous tests conducted by Sloat (2014) and Johnson (2014).

Table 5-16: Specimen NCBF5 Demand to Capacity Ratios

NCBF5	Limit States	Specimen
		NCBF5
Yielding Mechanisms	Whitmore Yielding	0.70
	Base Metal Yielding Integrated Shear Plate	0.85
	Bolt Bearing in Beam-to Gusset Plate (BR-CVM)	0.55
Failure Modes	Brace Net Section Fracture	**1.15**
	Brace Splice Fracture	0.79
	Brace Block Shear	0.50
	Gusset Plate Whitmore Fracture	0.40
	Gusset Plate Block Shear	0.31
	Bolt Rupture in Beam-to-Gusset Plate (BR-CVM)	0.63
Geometric Limits	Brace Compactness Ratio $(b/t)/\lambda_{hd}$	0.95
	Slenderness Ratio $(KL/r)_{max}$	93

Although Specimen NCBF5 did not have many calculated deficiencies, there was potential for other failure modes and damage states not explicitly listed with the DCRs. The column CJP was non-ductile and there was little rotational clearance in the gusset plate which was expected to lead to some cracking during out-of-plane rotation of the gusset plate. It was also possible that the beam web could have undesirable damage due to the relatively thin web thickness and large forces being transferred through the bolt group.

5.6.2 Summary of Response and Performance

The frame achieved a drift range of 5.0%, as shown in Figure 5-60. The failure mode was brace fracture. Table 5-15 shows the drift ranges when various performance states were observed. Damage to the frame included (1) severe local buckling of the NE beam web (PS LB3), (2) global buckling of the north beam about the weak axis, (3) moderate yielding in the gusset plates (PS Y2), (4) moderate bolt deformation in the gusset plate-to-beam web bolt group (PS Bo2), and (5) initial weld cracking in the integrated gusset-shear plate-to-column welds (PS W1).

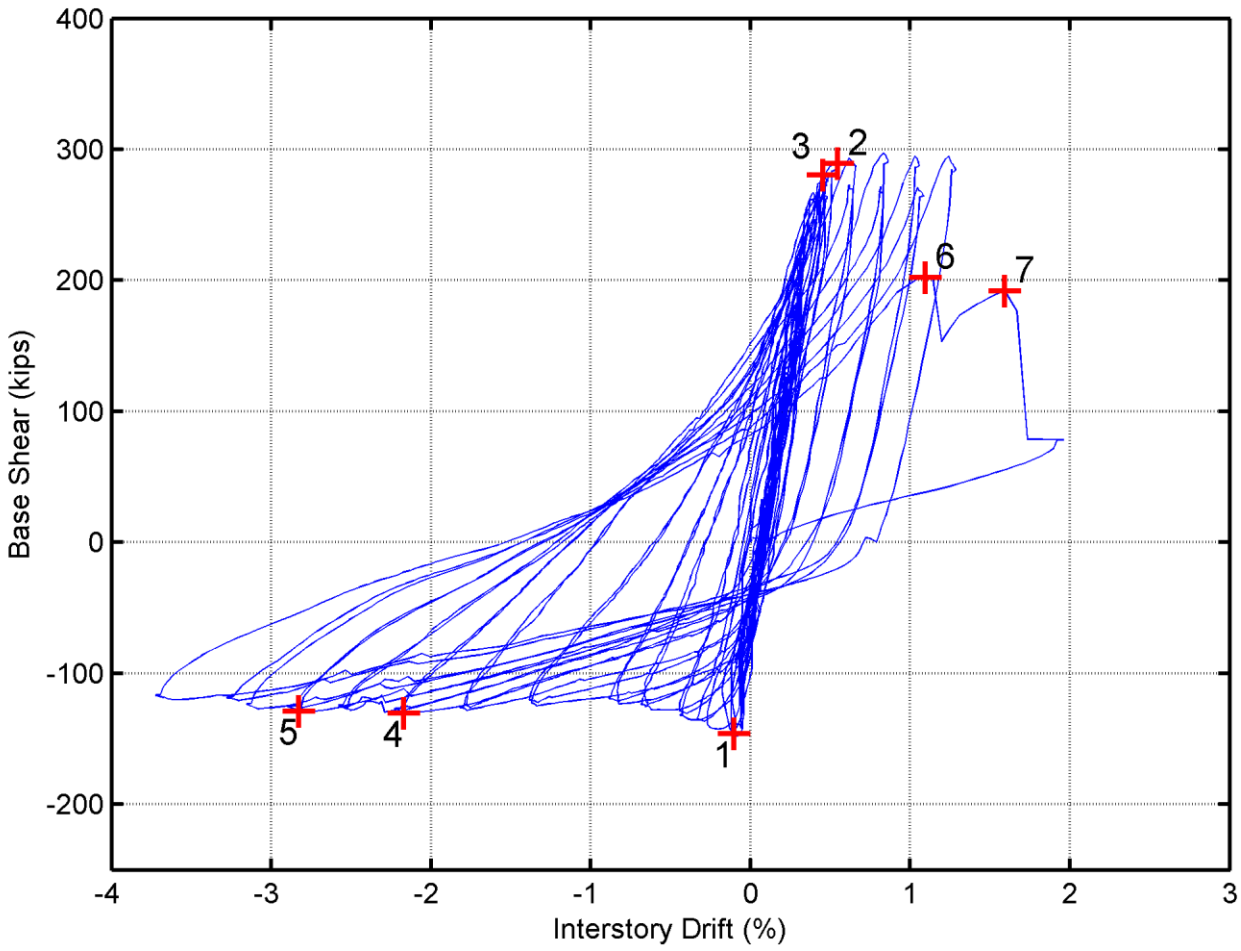

1. Brace begins to buckle out-of-plane (PS B1).
2. NE beam web begins to collapse due to local buckling (PS LB1).
3. The inner flange of the NE beam comes into contact with the gusset plate.
4. Crack initiation in both of the gusset plate-to-column welds (PS W1).
5. Brace begins to hinge at the mid-span (PS B3)
6. Brace tears (PS B4-BT).
7. Brace fractures (PS B4-BF).

Figure 5-60: Specimen NCBF5 Base Shear vs. Interstory Drift Hysteresis
(See Section 6.3.1 for details on generation of hysteresis.)

Contact between the edge of the beam flange and the gusset plate in the NE corner allowed the frame to achieve a modest drift in tension (1.3%) after the initial beam web local buckling. The web local buckling in the beam did not seem to impact the compression behavior of the brace but may have extended the overall brace fracture life by capping the amount of force the brace could develop in tension.

The columns sustained limited yielding. Connection rotation was accommodated by bolt-hole elongation within a single bolt group. The small depth of the bolt group and the reduced brace force limited the moment being transferred into the columns. The gusset plates yielded as a result of out-of-plane buckling of the brace. Although the gusset plate did not meet rules for offset dimensions to accommodate brace buckling, the performance was not impacted.

Table 5-17: Specimen NCBF5 - Performance State Summary Table

Cycle	Drift (%)			Brace	Northeast Connection						Southwest Connection					
	Range	Pos.	Neg.		East Column	North Beam	BR - GP Weld	GP	GP-Col. Weld	GP bolts	West Column	South Beam	BR - GP Weld	GP	GP-Col. Weld	GP bolts
1	0.1	0.1	0.1													
2	0.1	0.1	0.1													
3	0.2	0.1	0.0													
4	0.2	0.1	0.0													
5	0.2	0.2	0.0													
6	0.3	0.2	-0.1													
7	0.3	0.2	-0.1													
8	0.3	0.2	-0.1													
9	0.4	0.3	-0.1													
10	0.4	0.3	-0.1													
11	0.4	0.3	-0.1	B1												
12	0.4	0.3	-0.1													
13	0.6	0.3	-0.3							Bo1						Bo1
14	0.6	0.3	-0.3													
15	0.7	0.3	-0.4					Y1						Y1		
16	0.8	0.3	-0.4													
17	1.1	0.4	-0.7													
18	1.0	0.3	-0.7													
19	1.3	0.4	-0.8													
20	1.3	0.4	-0.9													
21	1.9	0.6	-1.4			LB1										
22	1.9	0.5	-1.4													
23	2.3	0.5	-1.8	B2	LB2, Y1-IF, Y1-OF			Y2		Bo2				Y2		Bo2
24	2.2	0.4	-1.8			LB3										
25	2.7	0.5	-2.2			Contact			W1						W1	
26	2.7	0.5	-2.2													
27	3.2	0.7	-2.5			Y1-IF										
28	3.2	0.6	-2.6													
29	3.7	0.9	-2.8	B3-BH							Y1-OF	LB1				
30	3.7	0.8	-2.9													
31	4.2	1.1	-3.2													
32	4.4	1.1	-3.3													
33	5.0	1.3	-3.7							Bo3						
34	5.0	1.1	NA	B4-BF								LB2				

5.6.3 Test Narrative

The response of Specimen NCBF5 was essentially elastic up to a drift range of 0.4%, after which the brace began to visibly buckle out-of-plane (PS B1, Figure 5-61). This drift coincided with the peak compressive strength of the frame. To accommodate the out-of-plane movement of the brace, the gusset plate rotated out-of-plane.

Initial yielding in both gusset plates was observed at a drift range of 0.8% (PS Y1, Figure 5-62). Yield lines extended from the end of the brace to the edge of the gusset plate-to-column weld. Bolts that connected the gusset plate-to-beam web slipped at a drift range of 0.8%.

Figure 5-61: Initial Brace Global Buckling (PS B1, 0.4%)

a. SW Gusset Plate **b. NE Gusset Plate**

Figure 5-62: Initial Yielding in Gusset Plates (PS Y1, 0.8%)

By a drift range of 1.1% the gusset plate had developed an elliptical yield line on the compression side of the gusset plate as the brace continued to deform out-of-plane. Moderate yielding in the gusset plates was not reached until a drift range of 2.3% (PS Y2, Figure 5-63). This was the maximum performance state achieved. The gusset plate yielding at the end of the test can be seen in Figure 5-76 and Figure 5-77.

a. SW Gusset Plate **b. NE Gusset Plate**

Figure 5-63: Moderate Yielding in the Gusset Plates (2.3%)

At a drift range of 1.9%, the gusset plate separated from the middle of the NE beam web as a result of web buckling. In the next cycle the tension portion of the drift range dropped from 0.5% to 0.4% as the web collapsed. The beam flanges began to buckle, and the associate local deformations induced moderate yielding on both the inner (PS Y2-IF) and outer flange (PS Y2-OF) of the N beam. The progression of damage in the beam web is shown in Figure 5-64 below.

a. Initial Web Local Buckling (PS LB1, 1.9%)

b. Moderate local buckling (PS LB2, 2.3%)

c. Severe Local Buckling (PS LB3, 2.2%)

Figure 5-64: Local Buckling Progression in N Beam Web

Local buckling of the beam web occurred because all of the force from the actuator had to go through an undersized beam web. The issue was exacerbated further by coped flanges of the beam. The local instability in the beam web became a global instability and the N beam bent about its weak axis. The N end of the E column deflected towards the strong floor and visibly twisted about its axis. The global instabilities can be seen in Figure 5-65 and Figure 5-66.

Figure 5-65: Twisting of E Column (2.7%)

Figure 5-66: Global Buckling of N Beam (2.7%)

The severe web buckling in the N beam would not be expected in braced frames in practice as the concrete deck would transfer the lateral force to the beam and restrain its movement. Further, in the experiment forces are not transferred directly to the columns, therefore the axial load in the beam web is at the maximum. Finally, in an actual system with floor slabs and other lateral frames, the columns, are more restrained from out-of-plane movement at the corner and from overall global twisting.

The frame sustained additional drift in tension through contact of the inner beam flange and the gusset plate. The contact of these two elements (shown in Figure 5-67) transferred some of the axial load, reducing the demand on the beam web.

Figure 5-67: Contact Between Inner Beam Flange and Edge of Gusset Plate (2.7%)

Although the tension cycles were accompanied by instabilities and had a limited drift capacity, the performance of the frame in compression remained stable. At a drift range of 2.7%, the brace had surpassed the threshold for PS B2 (Figure 5-68), and weld cracks were present in both gusset plate-to-column CJP welds (PS W1, Figure 5-69). The maximum length of the weld crack was 10% (PS W2) of the weld length. Weld damage at the end of the test is shown in Figure 5-78.

Figure 5-68: Moderate Brace Global Buckling (PS B2, 2.7%)

a. SW Gusset Plate - N End of Weld

b. NE Gusset Plate – S End of Weld

Figure 5-69: Initial Weld Cracking in Column CJP Welds (PS W1, 2.7%)

The buckling of the NE beam web had stabilized and at drift range of 3.7% the contact of the lower flange and gusset plate resulted in local yielding in both the beam flange and the gusset plate (Figure 5-70).

Figure 5-70: Local Yielding from Beam-to-Gusset Plate Contact (3.7%)

Additional damage to the frame at a drift range of 3.7% included buckling of the SW beam web (PS LB1, Figure 5-71), initial yielding in the outer flange of the west column (PS Y1-OF, Figure 5-72), and hinging in the brace (PS B3-BH, Figure 5-73). The lower amount of web buckling in the SW beam web resulted from the restraint of the column in the SW corner by the reaction beam. Although the west column flange was observed to have additional yielding in the remaining compression cycles it would not reach a higher performance state. The N end of the E column did not acquire any damage during the test.

Figure 5-71: Local Web Buckling in SW Corner (PS LB1, 3.7%)

Figure 5-72: Initial Yielding in W Column Outer Flange (PS Y1-OF, 3.7%)

Figure 5-73: Initial Brace Hinging (PS B3-BH, 3.7%)

At a drift range of 5.0%, local cupping at the brace mid-span became more pronounced. Figure 5-74 shows the brace hinging in the compression cycle prior to brace fracture; in the figure the brace out-of-plane deformation had exceeded 17". Prior to reaching the subsequent tension peak, the bottom half of the brace tore. With continued loading, the brace fractured completely. Final drift range was 5.0%.

An image of the fractured brace is shown in Figure 5-75. Damage to the connection immediately after brace fracture is shown in Figure 5-76 and Figure 5-77.

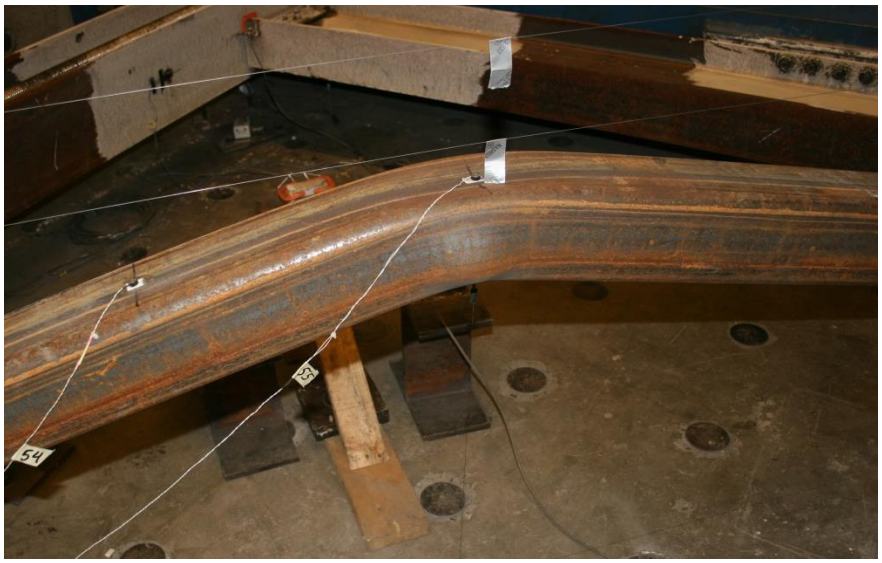

Figure 5-74: Brace Hinging Prior to Fracture (5.0%)

Figure 5-75: Brace Fracture (PS B4-BF, 5.0%)

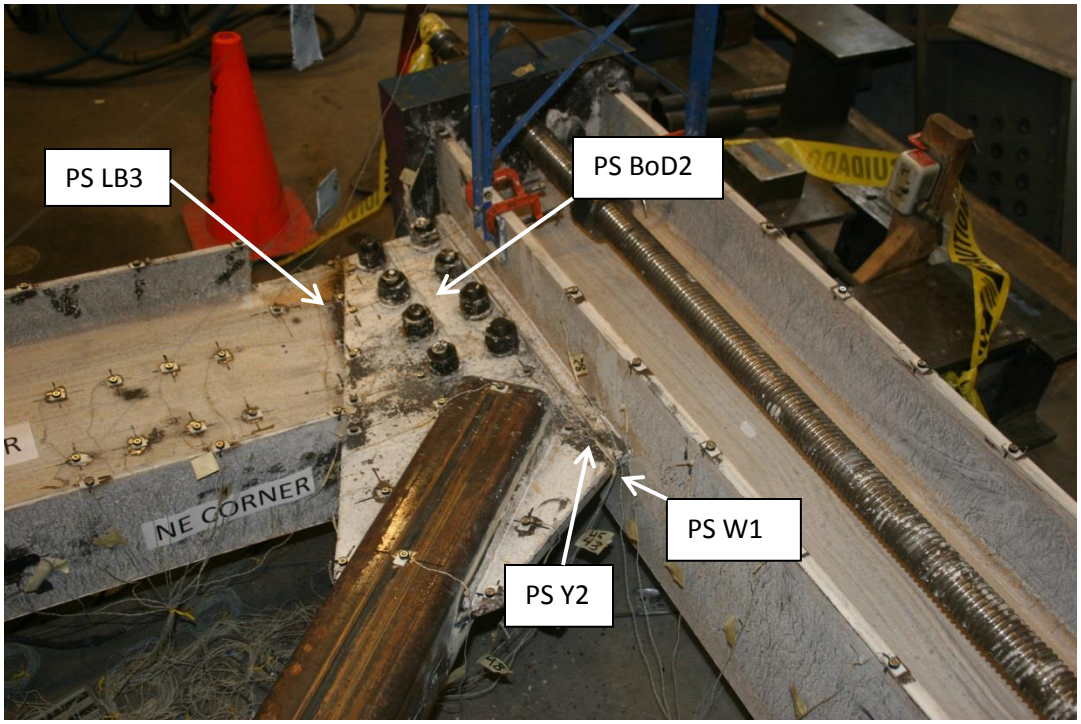

Figure 5-76: NE Connection at Failure (5.0%)

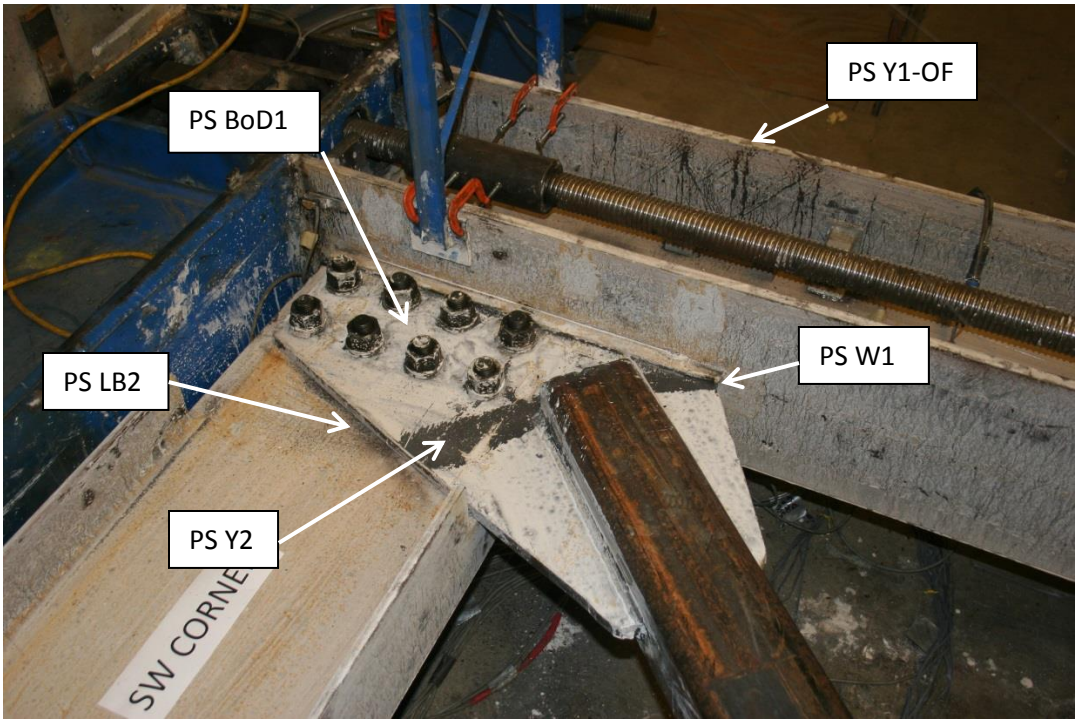

Figure 5-77: SW Connection at Failure (5.0%)

After the test was over several post fracture cycles were run to investigate the post fracture stiffness and strength of the frame. These cycles did not damage the frame.

Figure 5-78 shows the final column to gusset plate weld damage. Both welds had a similar cracking pattern and had the same overall length of 1 ¼" (6% weld tear length). Figure 5-79 and Figure 5-80 show the damage in both beam webs at the end of the test. Values of bolt-hole deformation are recorded in Table 5-18. In general the deformation at the bolt holes were less than ¼".

a. SW Gusset Plate - N End of Weld b. NE Gusset Plate – S End of Weld

Figure 5-78: Weld Damage at End of Test (5.0%)

Figure 5-79: Damage to the NE Beam Web at End of Test (5.0%)

Figure 5-80: Damage to the SW Beam Web at End of Test

Table 5-18: Bolt Hole Elongation Values at End of Test

Bolt Hole Location Key	NE Corner			SW Corner		
NORTH 1 ○ ○ 2 3 ○ ○ 4 5 ○ ○ 6 7 ○ ○ 8	Bolt	Bolt Hole Elongation	Bolt Shear Deformation	Bolt	Bolt Hole Elongation	Bolt Shear Deformation
	1	3/16”	No	1	1/8”	No
	2	3/32”	No	2	5/32”	No
	3	1/16”	No	3	0”	No
	4	0”	No	4	0”	No
	5	1/32”	No	5	0”	No
	6	0”	No	6	0”	No
	7	1/4"	No	7	0”	No
	8	1/8”	No	8	0”	No

5.7 Specimen NCBF2-R1: Continuous Shear Plate – Buckling Restrained Brace

5.7.1 Overview

Specimen NCBF2-R1 was designed as a BRB retrofit of a specimen tested by Johnson (2014) and is shown in Figure 5-81 and Figure 5-82. The BRB was selected as a retrofit option for deficient non-compact braces seen in the infrastructure review. Aspects of the connection geometry were scaled up from the original connection detail (Specimen NCBF2) to accommodate a BRB with a length of 142". The BRB was not collared; the extension plate was exposed. A bolted connection was used (BRB details in Appendix E).

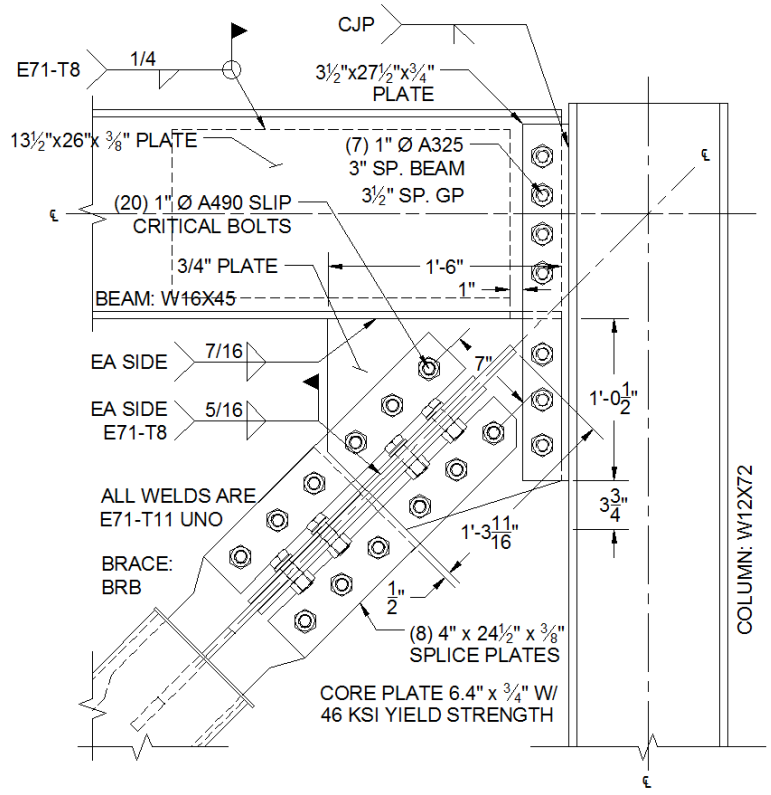

Figure 5-81: Specimen NCBF2-R1 Connection Detail

The beam and gusset plate were connected to the column using a ¾" shared (or continuous) shear plate and seven 1" diameter A325-X bolts (4 bolts in the beam web and 3 bolts in the gusset plate). The shear plate was connected to the column using a CJP weld. The BRB was connected to the gusset plate using ten splice plates bolted on either side of each leg of a cruciform section. Two rib plates were welded to the gusset plate to create a matching cruciform shape. Twenty 1" A490 bolts in each corner transferred the load between the BRB and the gusset plate. The bolts were slip critical and prevented dynamic slip of the BRB during the test. A 3/8" plate was welded to the beam web to prevent local instabilities in the beam web; this follows the recommendation of Palmer et. all (2011).

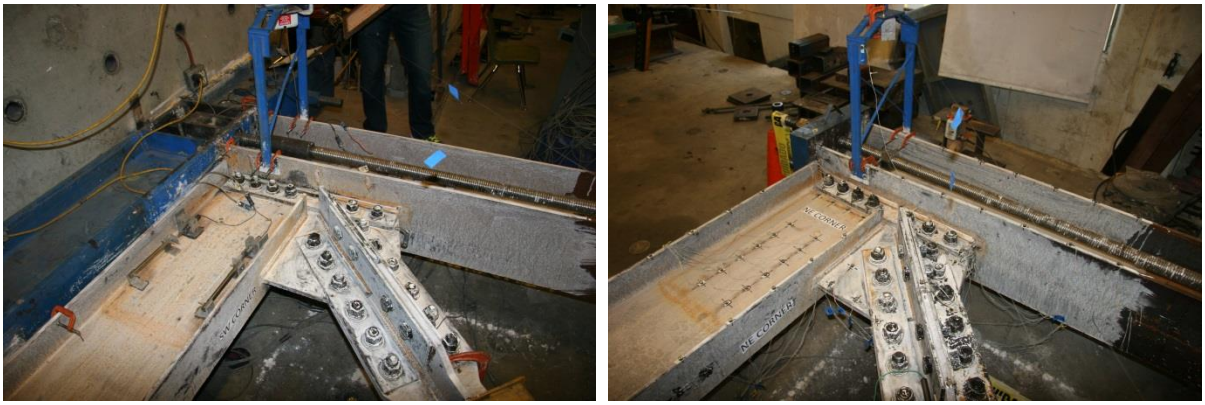

a. SW Connection b. NE Connection

Figure 5-82: Specimen NCBF2-R1 Undamaged Connections

The DCRs for Specimen 2-R1 are shown in Table 5-19. The calculated deficiencies for this test are bolt shear in the shear plate, and gusset plate-to-beam weld fracture using the BDP. Although the bolt group was considered to be deficient for the assumed force distribution, it was possible that it could undergo a significant amount of deformation through bolt shear deformation and bolt hole elongation (as seen in Specimen NCBF2 Johnson 2014) due to the relatively thin thickness of the beam web

It was also anticipated that there would be a large amount of damage in the column since the other BRB test (Specimen NCBF3-R1) had developed plastic hinges; however, it was possible that the column damage would be less severe because the continuous shear plate was less rigid than the end plate and could more easily accommodate rotation at the connection.

Table 5-19: Specimen NCBF2-R1 Demand to Capacity Ratios

	Limit State	**NCBF2-R1**
Yielding Mechanisms	Gusset Plate Whitmore Yielding	0.82
	Shear Plate Yielding	0.67
Failure Modes	Brace Net Section Fracture	0.73
	Brace Splice Fracture	0.33
	Brace Block Shear	0.36
	Gusset Plate Whitmore Fracture	0.44
	Gusset Plate Block Shear	0.33
	Gusset Plate Interface Weld Fracture (GP)	0.74
	Gusset Plate-to-Beam Weld Fracture (BR-CVM)	0.83
	Shear Plate Bolt Fracture (BR-CVM)	**1.05**
Geometric Limits	Brace Compactness Ratio $(b/t)/\lambda_{hd}$	NA
	Slenderness Ratio $(KL/r)_{max}$	NA

5.7.2 Summary of Response and Performance

The frame achieved a drift range of 5.2%, as shown in Figure 5-83. The failure mode was mixed and included fracture of the bolted gusset plate-to-shear plate connection and BRB core plate hinging. Table 5-20 shows the drift ranges when various performance states were observed. Damage to the frame included: (1) severe local buckling of the E column inner flange (PS LB3), (2) moderate yielding of both gusset plates (PS Y2), (3) minor weld cracking in the beam-to-gusset plate connections (PS Y1), (4) severe deformation at the bolt holes of the continuous shear plate connection (PS Bo3), and (5) moderate yielding of the west column outer flange (PS Y1-OF).

Bolt hole elongation was a stable ductile mechanism that alleviated the demands on frame elements particularly the column. This mechanism might look different in an actual building that utilizes a slab because the deformation at the bolt holes was primarily parallel to the column interface and would have been restrained from that direction of displacement.

It appears that the bolts in the shear plate connection can undergo approximately ¼" of shear deformation. If the gusset plate or shear plate had been thinner, this connection may have been able to promote more bolt hole elongation and sustain a higher drift range than it did.

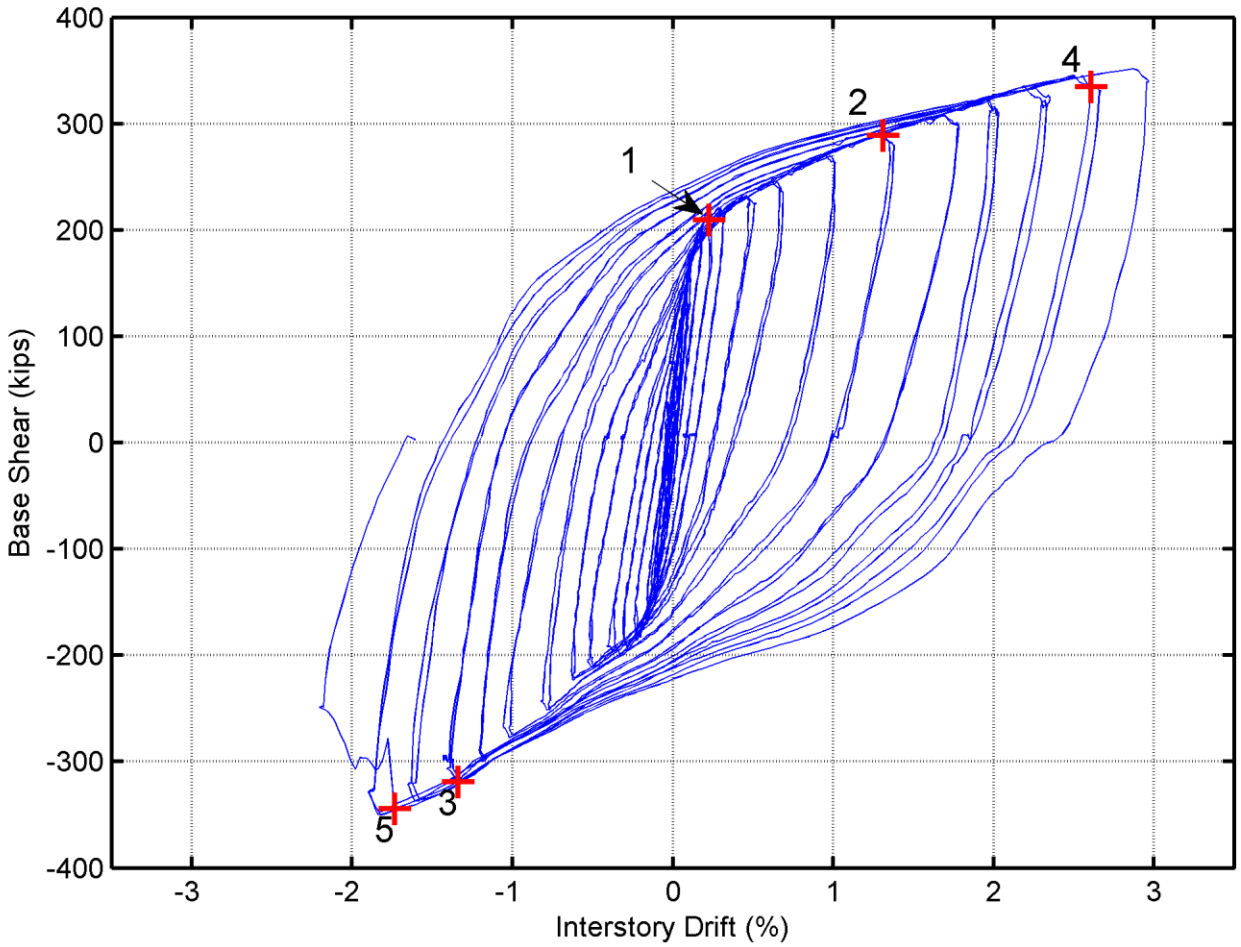

1. Initial yielding in BRB core plate (PS B1).
2. Inner flange of E column begins to buckle locally at edge of the shear plate (PS LB1).
3. Initial crack in NE beam-to-gusset plate weld (PS W1).
4. Severe local buckling in E column flange (PS LB3)
5. Bolts in the NE gusset plate-to-shear plate connection fracture, and the BRB core plate hinges at the edge of the BRB casing (PS B4-BH).

Figure 5-83: Specimen NCBF2-R1 Base Shear vs. Interstory Drift Hysteresis
(See Section 6.3.1 for details on generation of hysteresis.)

Table 5-20: Specimen NCBF2-R1 Performance State Summary Table

Cycle	Drift Range (%)			Brace	Northeast Connection								Southwest Connection							
	Total	Pos.	Neg.		East Column	North Beam	BRB Conn.	GP	GP-Beam Weld	ST	ST-Col. Weld	ST Bolts	West Column	South Beam	BRB Conn.	GP	GP-Beam weld	ST	ST-Col. Weld	ST bolts
1	0.1	0.0	0.0																	
2	0.1	0.0	0.0																	
3	0.1	0.0	-0.1																	
4	0.1	0.0	-0.1																	
5	0.2	0.1	-0.1																	
6	0.2	0.1	-0.1																	
7	0.2	0.1	-0.1																	
8	0.2	0.1	-0.1																	
9	0.3	0.1	-0.2																	
10	0.3	0.1	-0.2																	
11	0.4	0.2	-0.2																	
12	0.4	0.2	-0.2																	
13	0.5	0.2	-0.3	B1								Bo1								
14	0.5	0.2	-0.3																	
15	0.7	0.3	-0.4																	
16	0.7	0.3	-0.4																	
17	1.0	0.5	-0.5		Y1-PH			Y1												Bo1
18	1.0	0.5	-0.5																	
19	1.3	0.7	-0.6																	
20	1.3	0.7	-0.6																	
21	1.8	1.0	-0.8	B2								Bo2								
22	1.8	1.0	-0.8																	
23	2.4	1.4	-1.1		LB1											Y1		Y1		
24	2.4	1.4	-1.0																	
25	3.0	1.8	-1.2																	
26	3.0	1.8	-1.2																	
27	3.4	2.0	-1.4	B3	Y2-PH, LB2				W1		W1		Y1-OF						W1	
28	3.4	2.0	-1.4																	
29	4.0	2.3	-1.6									Bo3								Bo2
30	4.0	2.3	-1.6																	
31	4.6	2.7	-1.9		LB3			Y2					LB1, Y1-PH			Y2				
32	4.5	2.6	-1.9																	
33	5.2	3.0	-2.2	B4-BH							W2	Bo4-BF	Y2-OF							

5.7.3 Test Narrative

Specimen NCBF2-R1 was elastic up to a drift range of 0.4%. At a drift range of 0.5% the BRB core plate began to yield in both tension and in compression (PS B1), and relative slip occurred between the shear plate and gusset plate in the NE corner (PS Bo1). Slip continued to occur at this interface for the remainder of the test; the primary mechanism of bolt-group resistance was bearing.

In contrast to the NE corner, slip in the SW corner did not occur until a drift range of 1.0%. Note that initial slip was identified by a loud noise and cannot be shown with photographs.

Initial yielding in the NE gusset plate (PS Y1, Figure 5-84) and initial yielding in the plastic hinge location of the east column (PS Y1-PH, Figure 5-85) also occurred at a drift range of 1.0%. Yield lines in the NE gusset plate were observed at the edge of the beam-to-gusset plate connection signifying that a large moment was being transferred at the beam-to-gusset plate interface. Yield lines in the column extended diagonally from the edge of the shear plate to the edges of the column flange.

Figure 5-84: Initial Yielding in the NE Gusset Plate (PS Y1, 1.0%)

Figure 5-85: Initial Yielding in the E Column (PS Y1-PH, 1.0%)

At a 1.8% drift range, the BRB core plate had reached a moderate yielding performance state (PS B2). For cycles less than this, the tension and compression excursions were symmetric. Cycles above the 1.8% drift range, were not. Instead the tension excursions exceeded the compression excursions due to relative movement of components at the column interface and deformation of the bolt holes in the NE corner.

At a drift range of 2.4%, initial local buckling of the east column inner flange was observed in the region adjacent to the gusset plate (PS LB1, Figure 5-86). The out-of-plane displacement of the flange exceeded the threshold for moderate buckling at a drift range of 3.4% (PS LB2, Figure 5-88).

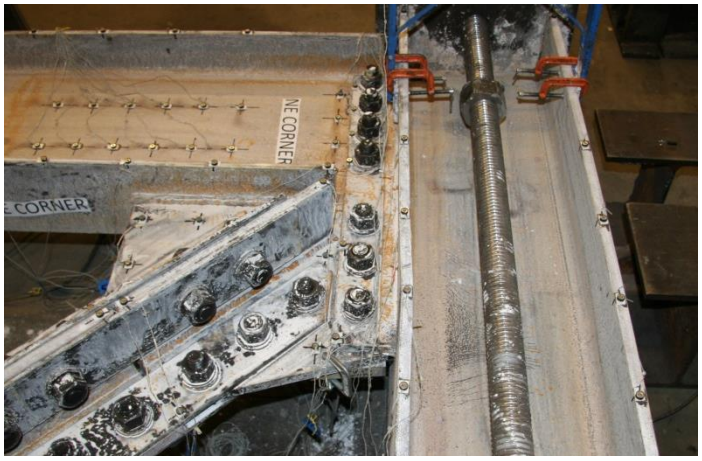

Figure 5-86: Initial Local Buckling in East Column Inner Flange (PS LB1, 2.4%)

Figure 5-87: Moderate Local Buckling of E Column Flange (PS LB2, 3.4%)

Figure 5-88: Initial Yielding in W Column Outer Flange (PS Y1-OF, 3.4%)

Initial weld cracks in both beam-to-gusset plate connections were also observed at a drift range of 3.4% (PS W1, Figure 5-89). The NE beam-to-gusset plate weld cracks would propogate at higher drift ranges, but did exceed 10% of the weld length (PS W2). At the end of the test, the NE beam-gusset plate weld crack had grown to only 1" long. The SW beam-to-gusset plate weld crack did not propogate throughtout the remainder of the test.

Figure 5-89: Weld Cracking in NE Beam-to-Gusset Plate Weld (3.4%-27)

By a drift range of 4.0% deformation at the bolt holes in the NE connection bolt group was visible by comparing the markers for the Optotrak system and the bolts. Figure 5-90 shows the relative vertical displacement of the column and the beam. Optotrak LED markers that had been lined up between the shear plate and the beam web at the beginning of the test had displaced by over ¼" vertically relative to each other.

The rotation of the beam web and gusset plate relative to the column can also be observed in Figure 5-90. The rotation of these two elements exposed base metal of the gusset plate that had not been whitewashed signifying that the connection was accommodating a portion of the rotational demands.

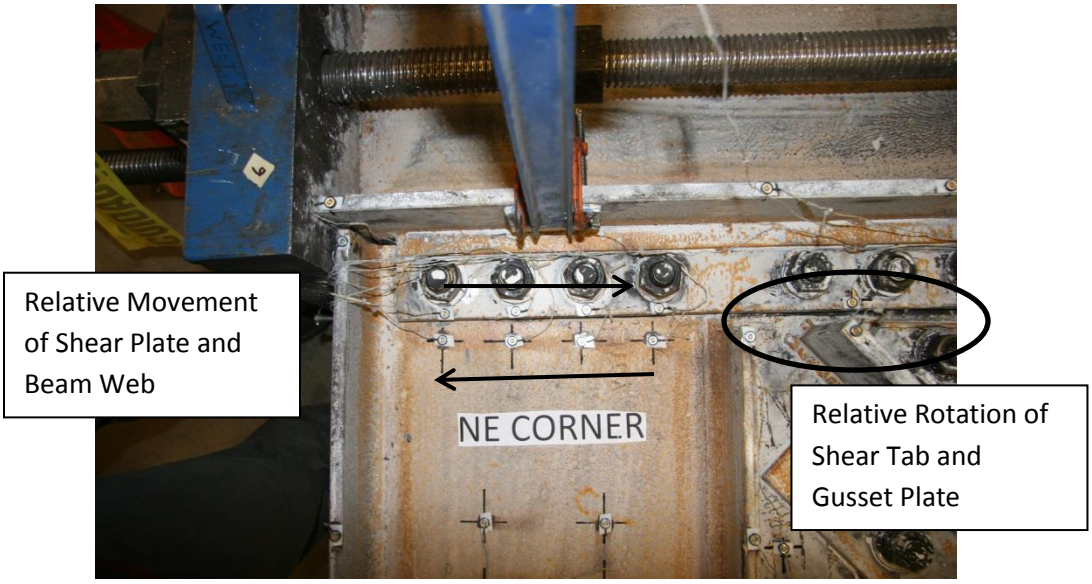

Figure 5-90: Severe Deformation at Bolt Holes (PS Bo3, 4.0%)

At a drift range of 4.6% moderate yielding of gusset plates (PS Y2), severe local buckling of the east column inner flange (PS LB3), and initial local buckling of the west column inner flange (PS LB1) were observed. Yield lines in the gusset plate were concentrated along the length of the base material adjacent to the beam-to-gusset plate weld.

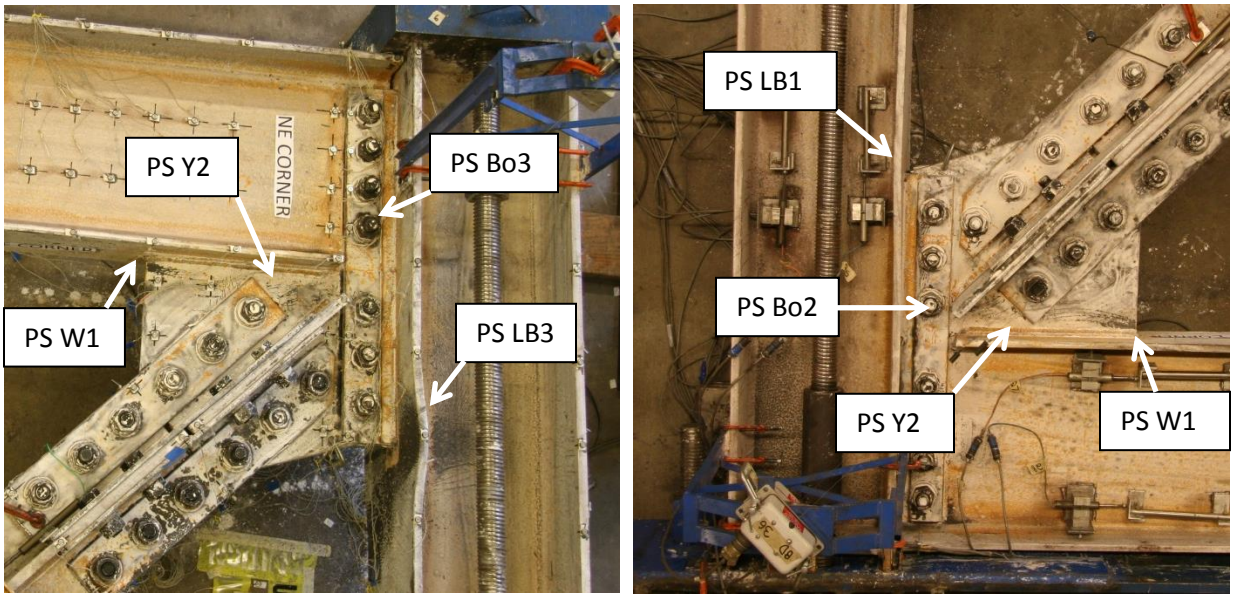

Figure 5-91: Connection Damage (4.6%)

Just prior to reaching a drift range of 5.2%, the three bolts connecting the gusset plate to the shear plate fractured (PS Bo4-BF) and the exposed portion of the BRB core plate began to hinge (PS B4-BH). With increased drift, the hinging became more severe, the beam flange began twisting out-of-plane, and the elongation of the bolt holes in the NE connection increased. At this point the NE connection was considered to be unstable, the actuator load had dropped significantly, and the test was terminated. Damage in the NE and SW corners at the end of the test is shown in Figure 5-92 and Figure 5-93. No post fracture cycles for the test were run.

Figure 5-92: Bolt Fracture of NE Gusset Plate-to-Shear Plate Bolts (5.2%)

Figure 5-93: Damage in SW Corner End of Test (5.2%)

Bolt hole elongation values and bolt damage in the continuous shear plate connections at the end of the test are documented in Figure 5-94 and Figure 5-95. As noted above the high values of bolt hole elongation in the NE connection (bolts 4 and 5) were most likely amplified upon reloading after bolt fracture in the gusset plate (all of the BRB force went through the bolts in the beam web after fracture and placed demands in excess of the bolt bearing capacity). In general the bolts appeared to have deformed a little over a ¼" through a combination of bolt hole elongation and bolt shear deformation. Up to another 1/16" of deformation at the bolt hole may have been provided by rotation of the bolts themselves.

1	1	3	4	5	6	7
						
BHE=5/16”	1/4"	0”	5/8”	1/2"	5/16”	1/4"

Figure 5-94: Bolt Hole Elongation and Bolt Damage in NE Connection

1	2	3	4	5	6	7
						
BHE = 0”	0”	0”	1/4"	3/16”	3/16”	1/8”

Figure 5-95: Bolt Hole Elongation and Bolt Damage in SW Connection

Chapter 6: Data Analysis

6.1 Introduction

This chapter describes data processing and analysis for the tested specimens and presents the results that are used to evaluate braced frame response and performance. Section 6.2 describes processing of the raw data from the various instrumentation systems described in Section 4.5. Section 6.3 presents results related to system response quantities such as overall frame drifts and frame member forces. Section 6.4 and Section 6.5 examine the brace and connection response respectively. This chapter is also intended to be a reference for Chapter 7 which compares the response of the five specimens presented in this chapter with the response of other NCBF specimens tested by Sloat (2014) and Johnson (2014).

Additional plots documenting frame and connection behavior are contained in Appendix D including all computed frame member forces, post-tension loss in both columns, and connection/beam/ column rotation plots.

6.2 Data Processing

6.2.1 Reduction of LabVIEW Data

The data collected from the National Instruments DAQ and LabVIEW Software consists of measurements from potentiometers, strain gauges, actuator load cell, and actuator LVDT. Data was collected continuously at a frequency of 1 HZ during each test including during the pauses in the loading that occurred at the peak positive and negative drifts of each cycle. These pauses ranged in duration from thirty seconds to over five minutes. The data was reduced to eliminate redundant data points at drift peaks and reduce the total number of points to work with. Every channel of data was manually zeroed to remove and unintended offset and was also run through a filter to remove spikes in the potentiometer data that occurred as the instruments got bumped. Table 6-1 shows the algorithm used to process the LabVIEW data in matlab.

The actuator displacement is the most reliable instrument to determine when a test holds occur because it is integral to the actuator control software during testing. Tolerances mentioned in Table 6-1are selected based on the individual instrument measurement range, instrument type, and accuracies. Some manual corrections to the data sets were made after applying the algorithm in circumstances where an instrument was either replaced or repositioned during testing.

Table 6-1: Outline of LabVIEW Processing Algorithm

Objective		Algorithm
1	Remove Data During Test Holds	For each point in the actuator displacement history 1. Compare current displacement reading to previous reading. - If difference is greater than a predefined tolerance[1] keep the point - If difference is less than the tolerance discard data point. There must be at least nine consecutive points where the difference is less than the tolerance to discard a data point. 2. All points that are discarded from the actuator displacement history are also discarded from the potentiometer and strain gauge data.
2	Zero Initial Data	1. Determine the initial reading for an individual instrument using the first data point 2. Subtract the initial reading from all readings in the data set 3. Repeat steps 1 and 2 for all potentiometers and strain gauges.
3	Identify and Correct Erroneous Discontinuities in String Potentiometer Data.	For each point in a selected potentiometer data series 1. Find the difference between current reading and previous reading. - If difference is less than a tolerance[2] keep the point and go to next point in the data set. - If difference is greater than the tolerance go to step 3. 2. Compare the difference between consecutive readings for the next 10 data points. Find the maximum absolute difference of opposite sign to the difference computed in step 2. - If maximum is greater than the tolerance the reading is erroneous. Set the current reading to equal the previous reading. - If maximum is less than the tolerance, the discontinuity is not erroneous. Go to next point in data set. 3. Repeat procedure for each potentiometer.

1 – tolerance = 0.004 in + (displacement reading)*0.005 in

2 – tolerance = 0.06 in

A sample set of raw and reduced data from a string potentiometer is shown in Figure 6-1. As shown, the data reduction eliminates redundant points at pauses in the loading and removes large spikes that are clearly not a result of specimen behavior. The algorithm was applied to all data from the main and post-fracture loading protocols and was done after the system had been post-tensioned. The number of total data points is reduced by up to a factor of 4.

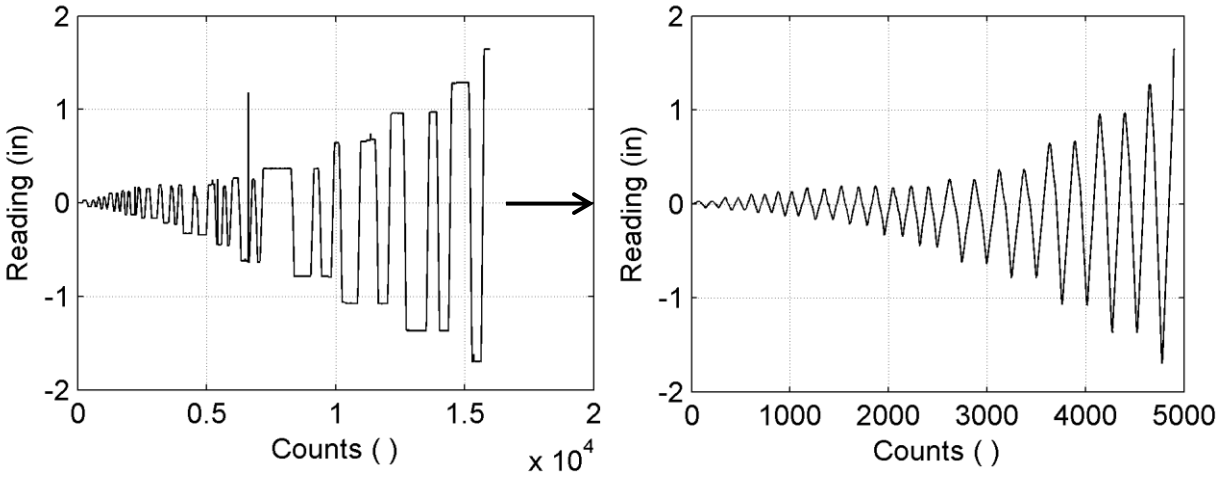

a. Example Raw Data Set b. Reduced Data Set

Figure 6-1: Example of LabVIEW Data Reduction

6.2.2 OptoTrak Data Transformation and Reduction

The Optotrak system as described in Section 4.5.3 tracks the position of LED markers in three dimensional space throughout the test. The recorded coordinates of each LED marker are based on a pre-defined Cartesian coordinate system (shown Figure 6-2a) that is arbitrarily chosen during setup. To make the data sets easier to work with, they were transformed to a new Cartesian coordinate system (shown in Figure 6-2b) with the origin at the SW work point, the x and y axis oriented parallel the centerline of the beam and column respectively, and the z-axis in the out-of-plane direction of the frame.

The coordinate system transformation procedure is outlined in Table 6-2 below. Although the specimens were not perfectly square to start, they were within ±0.7˚of 90˚ for all five specimens tested. Units were also converted from mm to in.

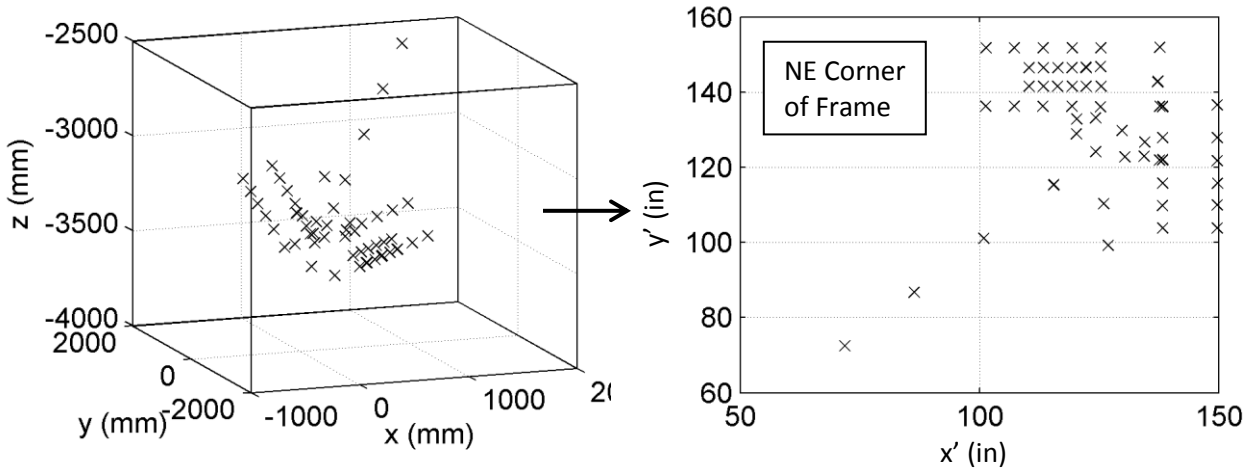

a. Original Coordinate System (x,y,z) b. New Coordinate System (x',y',z')

Figure 6-2: Optotrak Coordinate Transformation

Table 6-2: Optotrak Transformation Procedure

Step	Description	Figure
1	Identify markers to use in the new x'-axis and y'-axis definition (1-4) in adjacent figure.	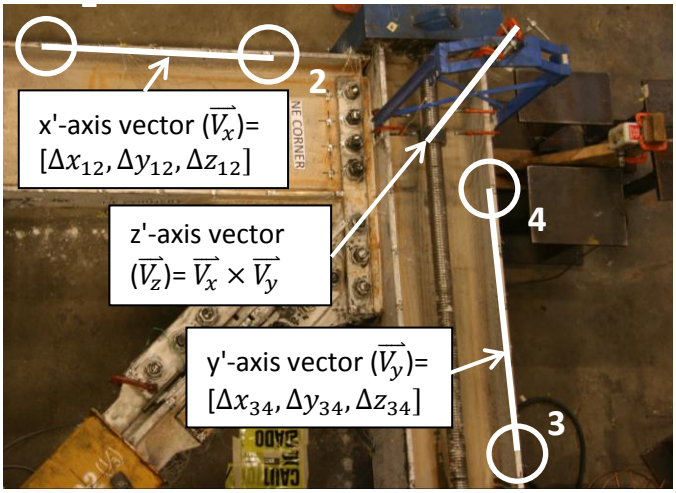
2	Determine vectors for x-axis and y-axis in the original coordinate system.	
3	Compute the z-axis vector by taking the cross product of x and y-axis	
4	Build transformation matrix using the newly defined vectors.	
5	Use transformation matrix to convert data to x', y', z' coordinate system for all Optotrak LED markers.	

After the data was transformed it was then reduced to remove data acquired during test holds and to remove erroneous spikes from the LEDs going in and out of view of the cameras. The data reduction procedure for the Optotrak is similar to the LabVIEW filter, but was run several times using different markers as a reference. The tolerance values and reference markers were different for each test and were selected to achieve the best result. An example of a raw and reduced data set for an Optotrak LED reading is shown in Figure 6-3.

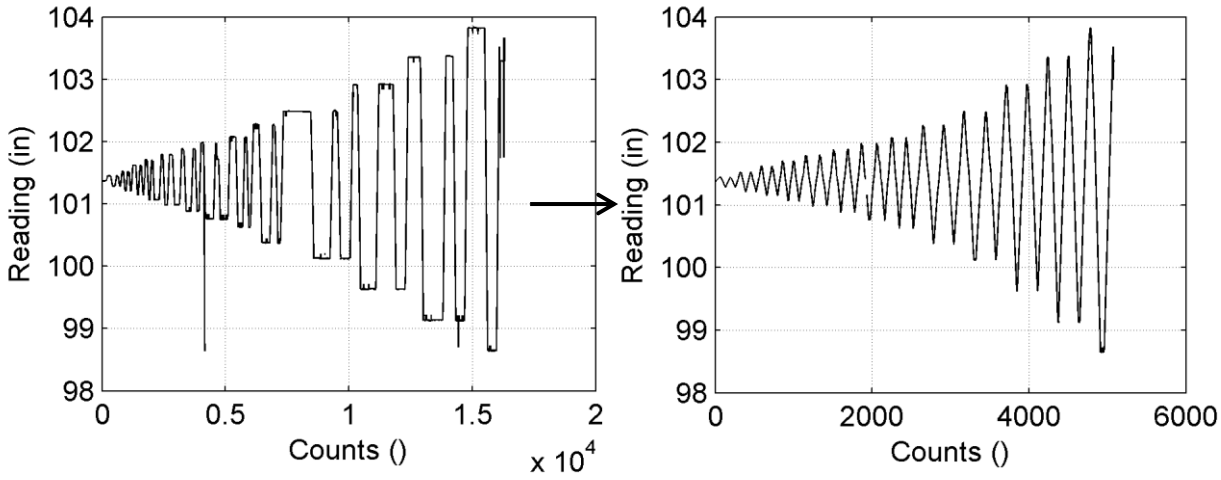

a. Example Raw Optotrak Data b. Example Reduced Optotrak Data Set

Figure 6-3: Example of Optotrak Data Reduction

6.3 Calculation of System Performance Quantities

6.3.1 Interstory Drift

The interstory drift was calculated using the displacement measurements from the string potentiometers that extended from work-point to work-point along the diagonal of the frame as illustrated in Figure 6-4. An algorithm for computing the interstory frame drift is shown in Table 6-3. The two string potentiometers used in the frame drift calculation are labeled as FD1 for the top and FD2 for the bottom in Figure 6-4. Interstory drift was calculated from these measurements because they eliminate slip at boundary conditions and the contribution to lateral displacement from uplift. Since the potentiometers were mounted at a relatively high distance above the frame work points the rotation of the mounts was considered in the calculation procedure.

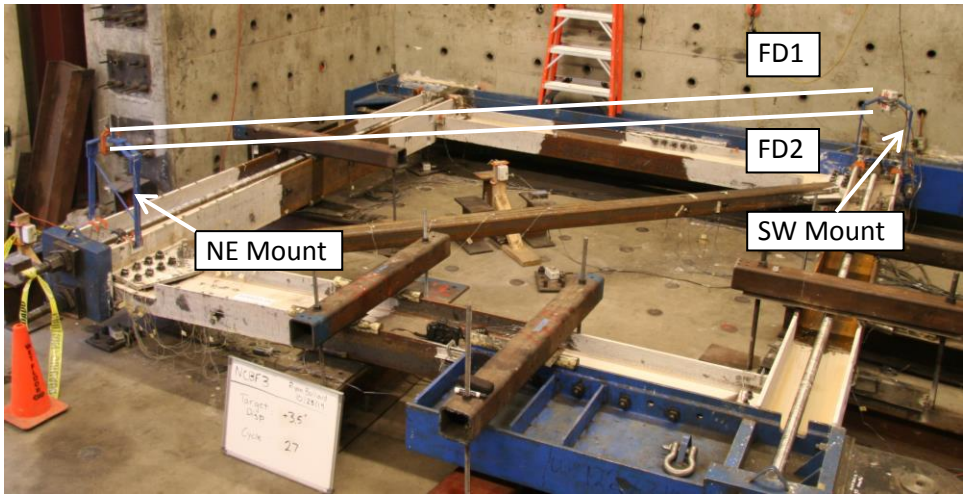

Figure 6-4: Frame Diagonal Elongation Measurement

Table 6-3: Outline of Frame Drift Calculation Procedure

Step	Description	Section/ Figure
1	Filter raw data. Remove erroneous data spikes and data during test holds.	Section 6.2.1
2	Apply a nine point moving average to each of the two frame diagonal potentiometer measurements (FD1 and FD2).	NA
3	Calculate the difference between the two frame diagonal measurements throughout the test and compute a rotation angle.	Figure 6-5
4	Use the computed rotation angle to calculate the frame diagonal elongation.	Figure 6-5
5	Use the computed frame diagonal elongation to compute the interstory drift.	Figure 6-6

Steps 3 and 4 of the frame drift calculation procedure (Table 6-3) are illustrated in Figure 6-5 for a case when the NE potentiometer rotates in the EW direction. Both of the potentiometers deflect inwards and would give a reading less than the actual deformation between the work points; however, since these measurements are taken at different known heights above the work points, a difference between the measurements can be used to calculate the rotation angle, α. Knowing α, the elongation along the diagonal of the frame between the work points can be computed.

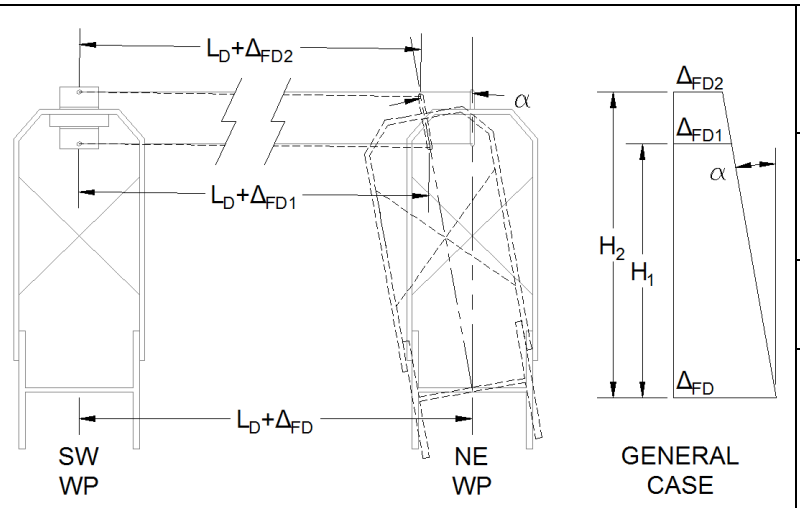

H_1 H_2	Height from Work Point to Potentiometer
Δ_{FD1} Δ_{FD2}	Measurement from Frame Diagonal Potentiometers
Δ_{FD}	Frame Diagonal Elongation

$$\alpha = \tan^{-1}\left(\frac{\Delta_{FD2} - \Delta_{FD1}}{H_2 - H_1}\right)$$

$$\Delta_{FD} = \Delta_{FD1} - \tan(\propto) H_1$$

Figure 6-5: Determination of Frame Diagonal Elongation

Figure 6-5 depicts the case when only the NE potentiometer mount is rotating. However, the procedure for computing the frame diagonal elongation is applicable for many other scenarios including rotation of both potentiometer mounts, and rotation of the mounts in either the NS or EW direction. In some cases the differences between the potentiometers readings in Figure 6-5 were very small, near the instrument resolution. In these cases the angle calculated included a good deal of noise. To correct for this, a nine point moving average was applied to each potentiometer prior to determining the corrected frame diagonal measurement as mentioned in step 2 of Table 6-3.

Lateral displacement of the frame is directly related to the interstory drift and can be calculated using the computed frame diagonal elongation measurement as shown in Figure 6-6. The results of the interstory drift calculation procedure for Specimen NCBF5 is shown in Figure 6-7b. Figure 6-7a shows what the drift would be calculated using raw individual potentiometer data from FD1 and FD2. The difference between Figure 6-7a and Figure 6-7b show that the rotation of the frame diagonal potentiometer mounts had a large impact on the frame diagonal measurements and highlight the necessity of the calculation procedure.

H	Frame Height Between Work Points
W	Frame Width Between Work points
L_D	Initial Diagonal Distance Between Work Points
Δ_{FD}	Displacement Along the Diagonal Measured from String Potentiometers
Δ	Lateral Frame Displacement
δ	Interstory Drift

$$\Delta = \sqrt{(L_D + \Delta_{FD})^2 - H^2}$$

$$\delta = \Delta / H$$

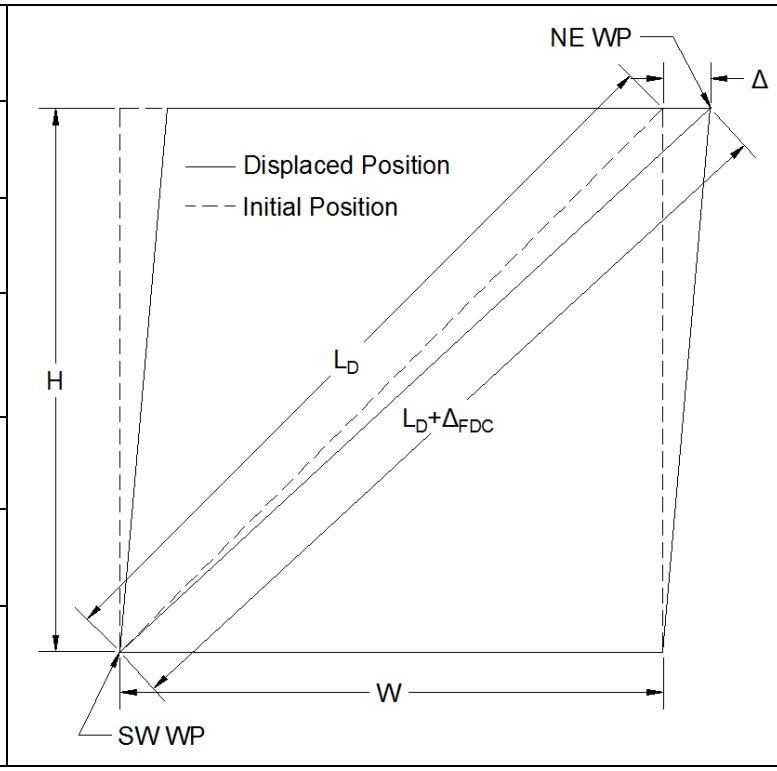

Figure 6-6: Calculation of Frame Drift from Frame Diagonal Measurement

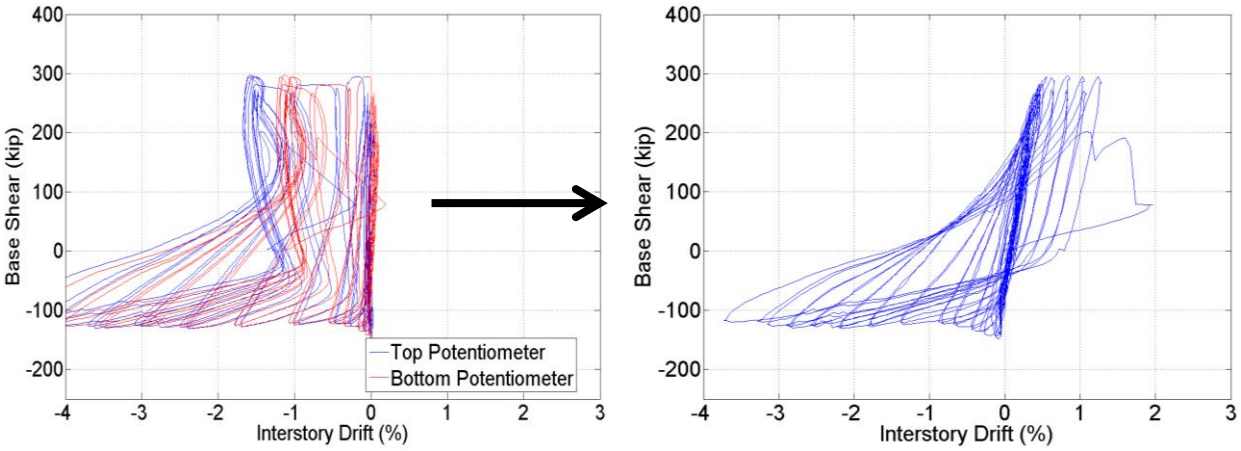

a. Raw Potentiometer Data b. Interstory Drift

Figure 6-7: Potentiometer Readings vs. Interstory Drift

The base shear vs. interstory drift hysteresis for the five experiments are shown in Figure 6-8. Base shear for the plots is equivalent to the actuator force reading, and interstory drift was calculated as described previously. A summary of the system performance for each specimen is shown in Table 6-4. The individual hystereses are also presented in Sections 5.3-5.6 with the test observations.

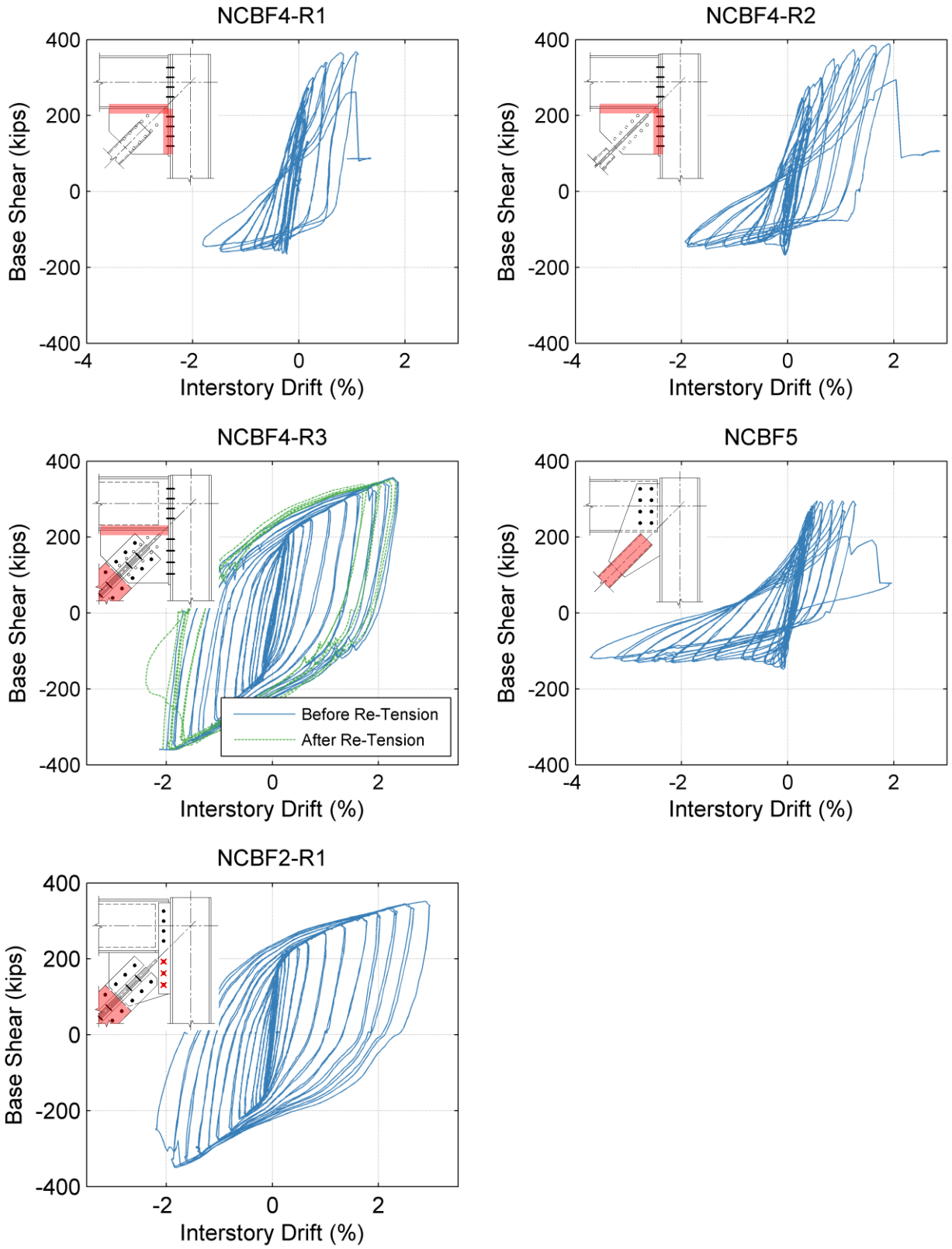

Figure 6-8: Base Shear Vs. Interstory Drift Hysteresis

Table 6-4: System Response Summary

Specimen Name	Connection Type	Brace Type	Drift Range	Max Forces		Failure Mode
				T	C	
NCBF4-R1	Bolted End Plate	HSS 5x5x3/8" Out-Of-Plane	2.9%	368	-166	Beam-To-Gusset Plate Weld Fracture
NCBF4-R2	Bolted End Plate	HSS 6x4x3/8" In-Plane	3.9%	389	-168	Beam-To-Gusset Plate Weld Fracture
NCBF4-R3	Bolted End Plate	BRB	4.6%	357	-360	Weld Tearing → BRB Brace Hinging
NCBF5	Integrated Gusset-Shear Plate	HSS 5x5x3/8" Out-Of-Plane	5.0%	297	-148	Brace Fracture
NCBF2-R1	Bolted Continuous Shear Plate	BRB	5.2%	351	-350	Bolt Fracture in Gusset Plate-to-Shear Plate→ BRB Brace Hinging

For the bolted end plate connections, the brace type had an impact on the system response of the frame in terms of drift range, but did not seem to impact the failure mode. The out-of-plane buckling brace developed the least amount of frame drift (2.9%) due to premature weld tearing in the beam-to-gusset plate weld. The in-plane buckling brace developed more frame drift (3.9%) but still caused the beam-to-gusset plate weld to fail. The BRB developed the most drift range (4.6%). These results show that the in-plane buckling and BRB retrofit are a better retrofit scheme for the bolted end plate connection with a deficient beam-to-gusset plate weld than the highly ductile out-of-plane buckling brace retrofit.

Specimen NCBF5 was the only specimen to achieve brace fracture and was able to attain a drift range of 5.0% using an out-of-plane buckling brace. Although this test exhibited high ductility, the beam web limited the drift in tension for the specimen.

Specimen NCBF2-R1 achieved a drift range of 5.2% but failed in part due to a connection fracture. This shows that the connection is capable of attaining a high drift range but can be vulnerable to bolt shear failure at high levels of joint rotation.

The connection type also had an impact on both the drift range and the failure modes. The drift ranges and failure modes shown for these experiments are compared with other NCBF experiments conducted by Sloat (2014) and Johnson (2014) in Chapter 7.

6.3.2 Frame Member Forces – Columns and Beams

This section discusses how forces in the beams and columns are computed and presents column shear vs. drift hysteresis for all five experiments along with a summary of the maximum forces achieved in each member relative to the plastic moment capacity. The strain gauges used to compute member forces for both columns and the north beam are shown in Figure 6-9. Brace forces were back-calculated using the actuator force and the computed column shears and is discussed in Section 6.4.1. Forces in the south beam cannot be directly calculated using the instrumentation plan (as described in Section 4.5.2). Two strain gauge pairs and a known distance apart are needed to compute the axial forces, moments, and shear forces at the two locations. Three pairs of gauges are provided for the columns in case of gauge malfunction and can be used to compute a second set of forces for comparison.

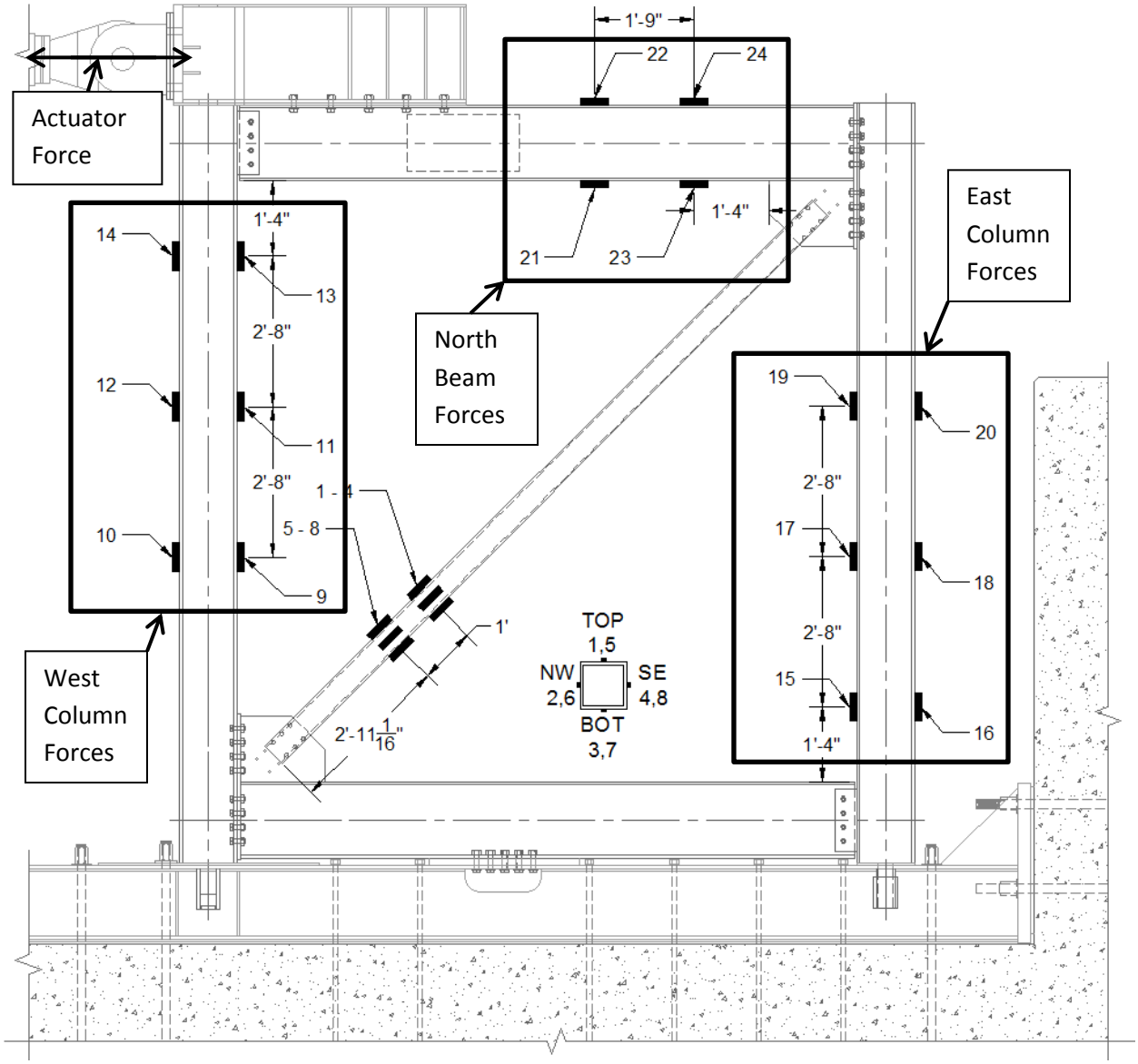

Figure 6-9: Strain Gauges Used to Compute Member Forces

The procedure for calculating member forces for the beams and columns is outlined in Table 6-5. An example of the procedure is depicted in Figure 6-10 for the east column. At each strain gauge location, strains were converted to stresses using Hooke's Law. The stress was used to compute axial force and moment at each strain gauge pair. Column shear was then calculated using the moment from two strain gauge pairs and the distance between them. Moments at edge of the connections can be computed by projecting the shear and moment distribution as shown in Figure 6-10. The calculation procedure assumes that the stress profile at each strain gauge pair remains linear elastic during the test and the out-of-plane restraints do not contribute to the shear and moment distribution (i.e. column shear is constant between the edge of the connections).

Note that the member forces computed here represent the change in force from when the test was started (i.e. after post-tensioning forces were applied). Initial frame member forces from post-tensioning the columns to the reaction beam can also be calculated using the methods presented in this section. However, data for this calculation was only available for three of the tests. Initial frame forces such as the column axial load are discussed in more detail in Appendix Section D.2.

Table 6-5: Procedure for Calculating Member Forces

Step	Description	Variable	Calculations
1	Determine strain at each strain gauge location.	ε_i	Processed strain gauge data (see Section 6.2.1)
2	Compute stress at strain gauge location using Hooke's Law	σ_i	$\sigma_i = \varepsilon_i E$
3	Compute moment at each strain gauge pair.	$M_{i,j}$	$M_{ij} = S_x\left(\frac{\sigma_i - \sigma_j}{2}\right)$
4	Compute axial force at each strain gauge pair.	P	$P = A\left(\frac{\sigma_i + \sigma_j}{2}\right)$
5	Compute shear force in member.	V	$V = \frac{M_{12} - M_{56}}{h}$
6	Compute moment in column at edge of gusset plate.	M_{North}	$M_{North} = M_{56} + V \cdot b$

Where E is the modulus of elasticity of steel (29000 ksi), S_x is the elastic section modulus of the member, and A is the gross cross sectional area of the member.

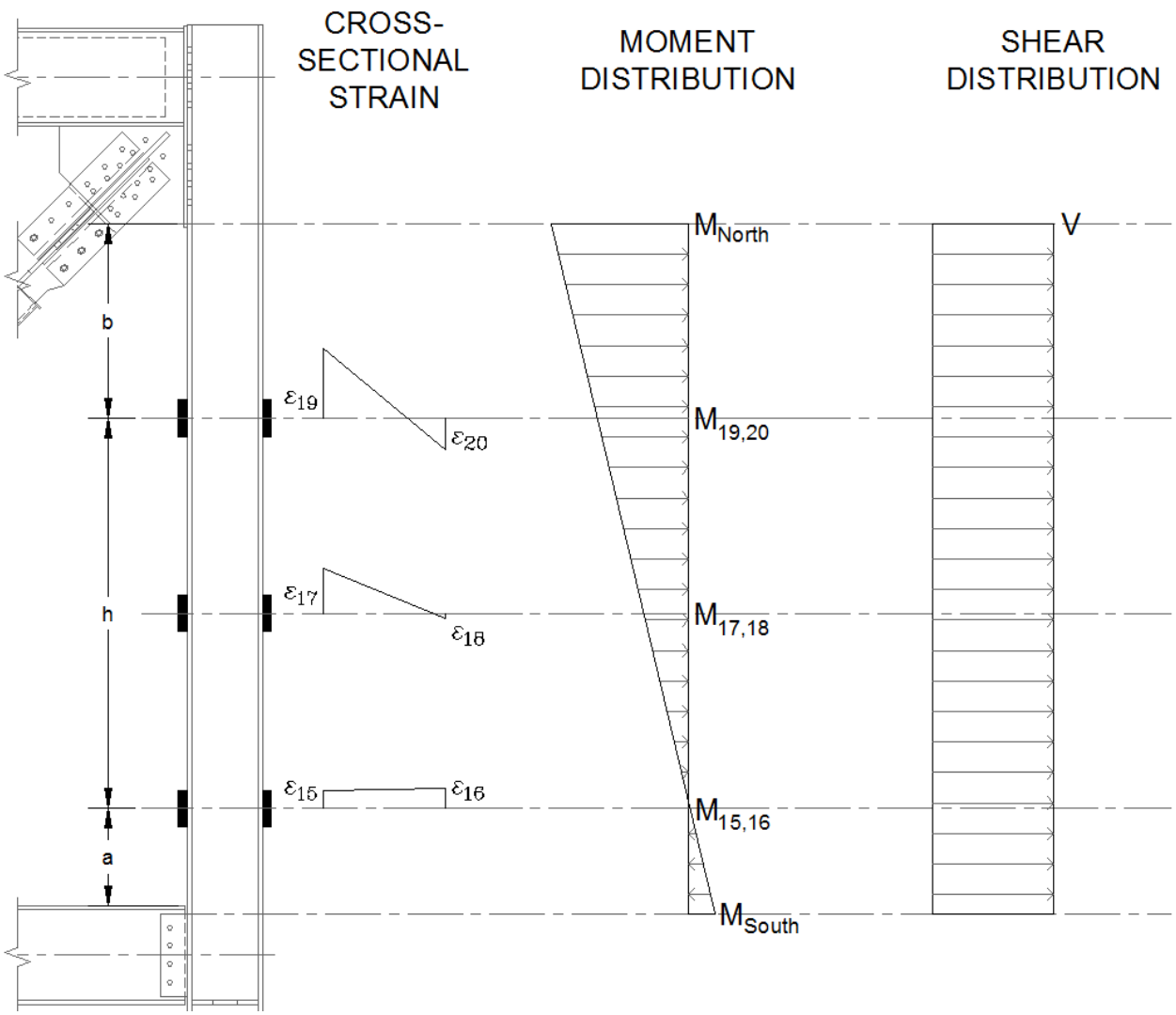

Figure 6-10: Member Force Calculation Procedure Example

The column shear force vs interstory drift hysteresis for each experiment is shown in Figure 6-11. Column shear includes the shear from both columns while the interstory drift is computed from the previous section (Section 6.3.1). Other frame forces computed using the procedure presented in this section are presented in Appendix D for each of the specimens. Forces in the columns are discussed in more detail in Chapter 7.

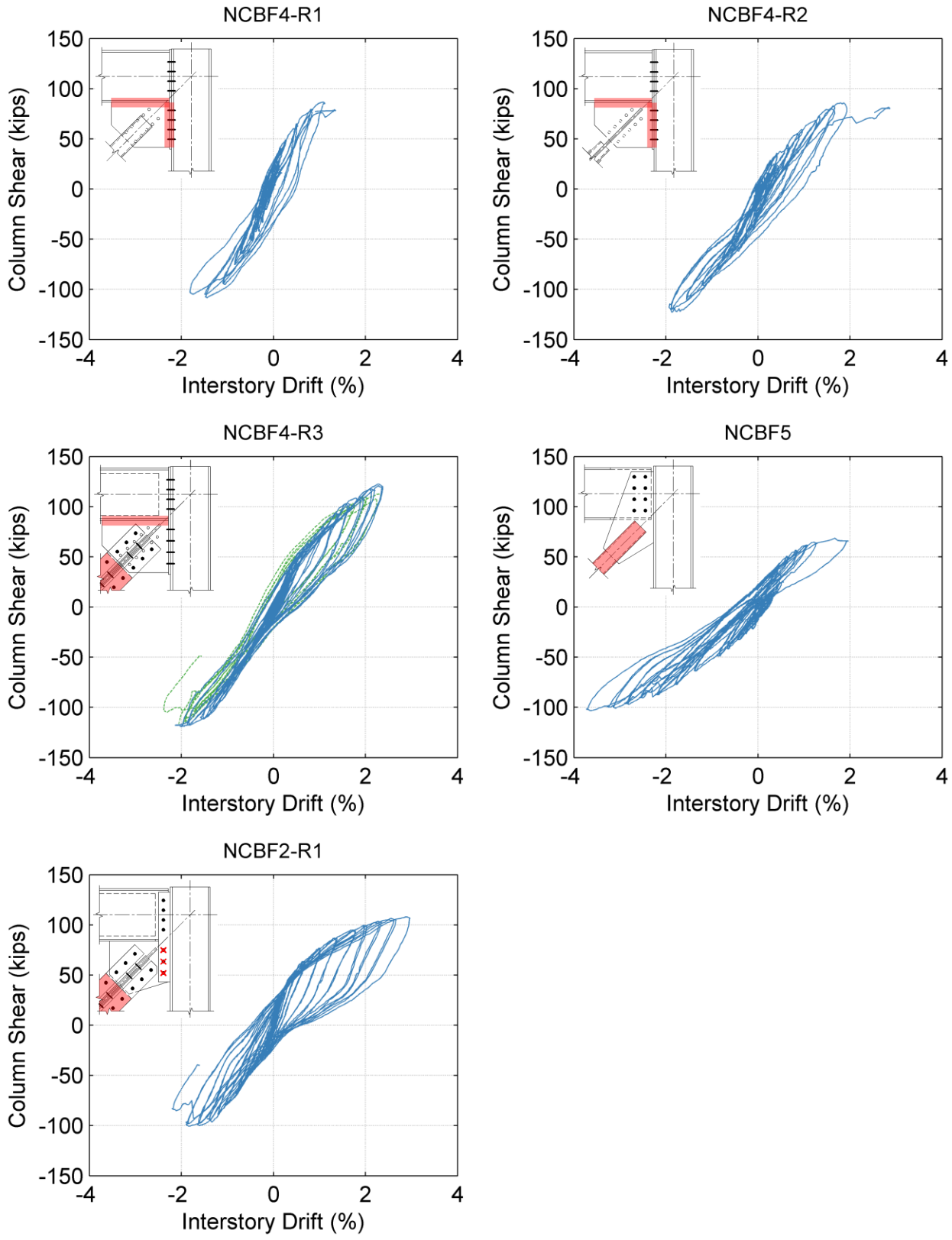

Figure 6-11: Column Shear vs. Interstory Drift Hysteresis

6.3.3 Energy Dissipation

Energy dissipation is another way to measure system performance of a braced frame as input energy from earthquakes must be dissipated in part through inelastic work done by the lateral force resisting system. Eq. 6-1 shows the general form of the cumulative energy dissipation equation, while Eq. 6-2 shows the numerical trapezoidal summation.

$$W = \int F \cdot d\Delta \quad \textbf{Eq. 6-1}$$

$$W = \sum_{i=2}^{n} \frac{F_i - F_{i-1}}{2} (\Delta_i - \Delta_{i-1}) \quad \textbf{Eq. 6-2}$$

Where

W = Work or Cumulative Energy Dissipation

F = Force

Δ = Lateral Displacement of Frame

The cumulative energy dissipation was computed for each cycle over the interstory drift range using both the actuator force and the horizontal component of the computed brace force (see Section 6.4.1) and are presented in Figure 6-12. The difference between the two represents the energy dissipated by the columns. The value of cumulative energy dissipation at the end of each test is also tabulated in Table 6-6.

Table 6-6: Energy Dissipation Values

Specimen Name	Maximum Drift Range	Cumulative Energy Dissipation (kip-in)		
		System	Brace	Columns
NCBF4-R1	2.9%	2880	2370	510
NCBF4-R2	3.9%	5250	4390	860
NCBF4-R3	4.6%	21330	19750	1580
NCBF5	5.0%	6960	5630	1330
NCBF2-R1	5.2%	22670	19000	3640

There are some limitation of the cumulative energy dissipation calculation presented in Figure 6-12 and Table 6-6. For instance, the energy dissipation from the brace may be overestimated because it is computed using the interstory drift instead of the brace elongation. This means that the measurement includes the energy dissipation of the connection. Brace elongation would have been used but it could only be calculated reliably at the peaks (see Section 6.4.3 for more on brace elongation). Also, the energy dissipation values presented are for a specific loading protocol and frame geometry. They are not directly comparable to energy dissipation values from tests with different loading protocols or frame geometry.

As shown in Figure 6-12, the cumulative energy dissipation values increase with higher drift ranges. In all tests, the energy dissipation from the brace accounts for a majority of the total cumulative energy dissipation. The magnitude of cumulative energy dissipation is much greater for a BRB than a buckling brace because it achieves higher forces in compression than a buckling brace in compression and has a

much fuller hysteresis. The columns did not provide much energy dissipation in comparison to the brace for any of the tests despite sustaining moderate to severe damage in the plastic hinge location in specimens NCBF4-R2, NCBF4-R3, and NCBF2-R1.

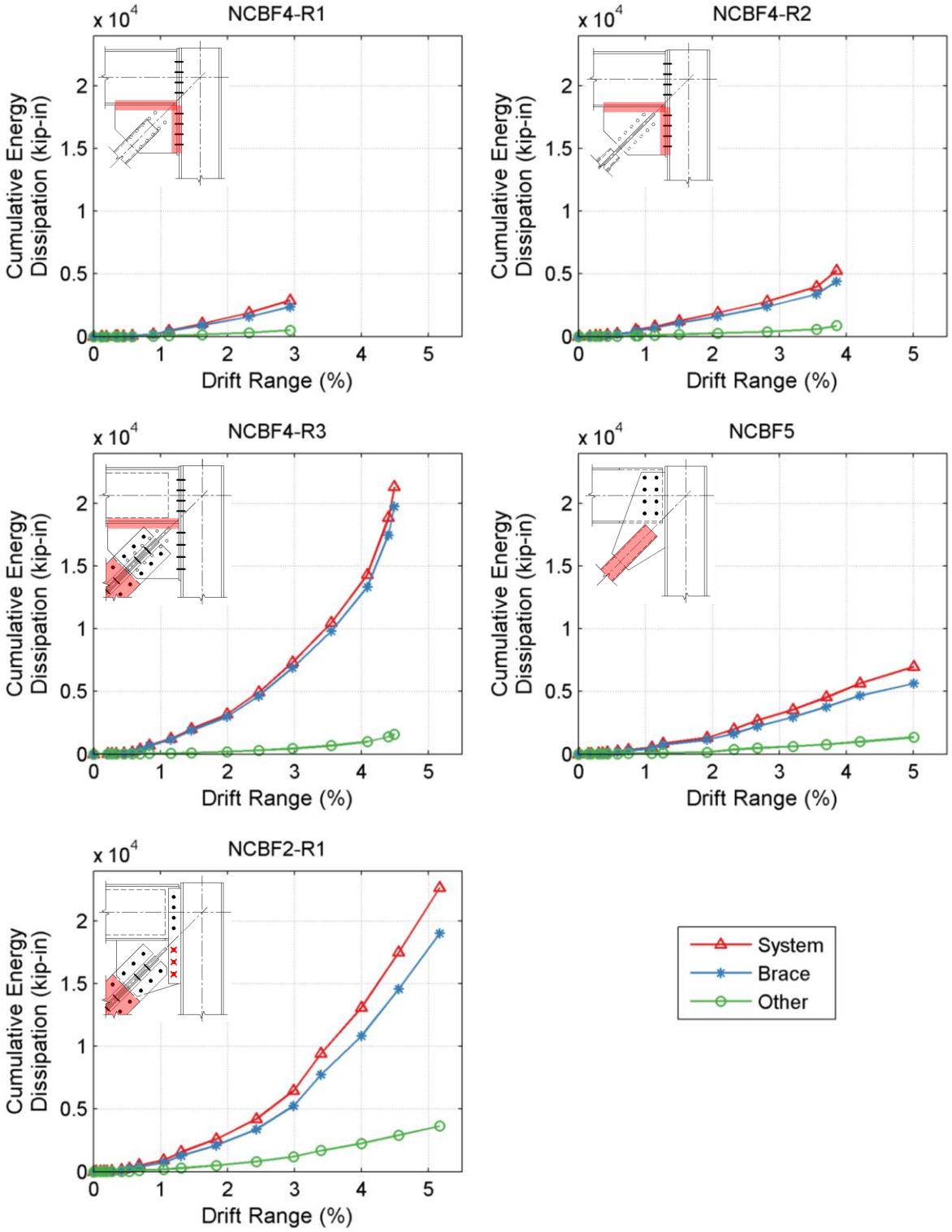

Figure 6-12: Energy Dissipation

6.4 Brace Performance

6.4.1 Brace Force vs. Interstory Drift Hysteresis

Brace force was determined using computed column shear forces (Section 6.3.2) and the actuator load cell reading to calculate the brace force from horizontal force equilibrium. This approach is reliable because the strain gauges on the column are in elastic regions with a well-defined stress distribution. This method was used to determine the brace force for all of the experiments.

Brace force vs. interstory drift hysteresis for all five experiments are shown in Figure 6-8. Maximum tension and compression forces in the brace are tabulated in Table 6-7 and are compared to their expected capacities $(P_y \ \& \ P_{cr})$ as computed in Section 2.3.2. Note that the expected capacities were computed using the material strengths from coupon tests (Appendix C).

Table 6-7: Comparison of Maximum Brace Forces to Expected Capacities (P_y and P_{cr})

Specimen Name	Brace Type	Tension Capacity			Comp. Capacity		
		Max (kip)	P_y (kip)	Max/ P_y	Max (kip)	P_{cr} (kip)	Max/ P_{cr}
NCBF4-R1	HSS5x5x3/8	408	382	1.07	190	190	1.00
NCBF4-R2	HSS6x4x3/8	432	390	1.11	198	184	1.08
NCBF4-R3	BRB	340	340	1.00	356	358	1.00
NCBF5	HSS5x5x3/8	381	383	1.00	181	173	1.04
NCBF2-R1	BRB	345	340	1.01	355	358	1.00

In general, the experimental maximum brace force matched the expected capacity of the brace in both tension and compression (< 11% difference in all cases). This was particularly true for the BRBs (within 1% of the expected capacities). These results suggest that the prediction method for brace capacity is relatively good for the specimens tested, and that the computed capacities can be used as normalization quantities. The maximum tensile brace force for Specimens NCBF4-R1 and NCBF4-R2 slightly exceed the expected capacity. This occurred due to post-yield strain hardening as seen in the hysteresis of Figure 6-13.

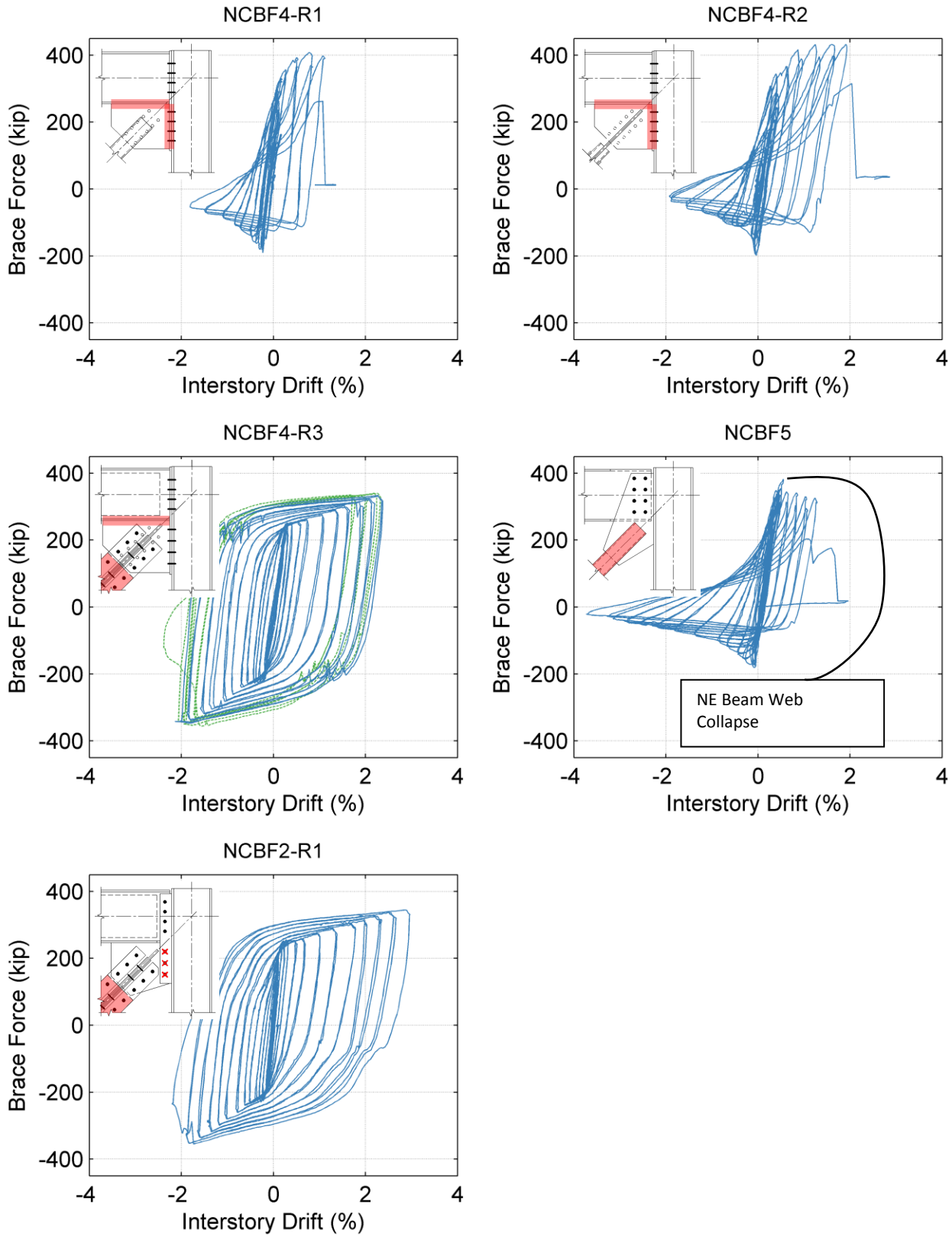

Figure 6-13: Brace Force vs. Interstory Drift

6.4.2 Brace Deflected Shape

The brace deflected shape indicates deformation demand for the brace plastic hinge at mid-span and gusset plates at each end of the brace. The displacement of the brace at mid-span is a good measure of brace ductility and is of particular importance when evaluating the overall performance of the braced frame. Brace end rotation is strongly correlated with the brace mid span deflection (Sloat 2014) and can be used to quantify the demands on beam-to-gusset plate welds.

The brace deflected shape was determined by tracking the relative position of all LED markers placed on the brace as shown in Figure 6-14 and Figure 6-15. The out-of-plane deflection of the frame at the NE corner and the lateral displacement of the frame in the x direction were accounted for in the calculation by projecting a line between brace ends[2] as shown in Figure 6-14 and Figure 6-15 respectively. The resulting deflection quantities for brace out-of-plane and in-plane deflection are represented by the variables $d_{i\ OOP}$ and $d_{i\ IP}$ respectively. For both cases it was assumed that the location of the SW work point was constant, the brace deflected shape was symmetric about the mid-span.

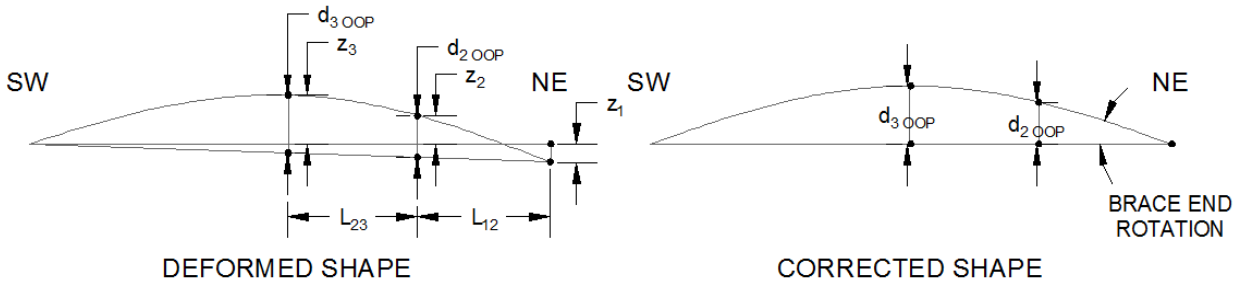

Figure 6-14: Brace Out-Of-Plane Displacement Calculation

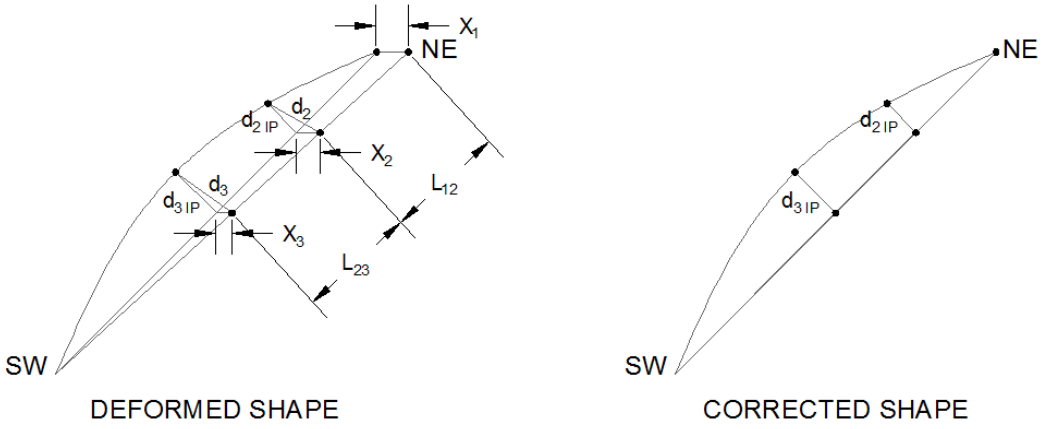

Figure 6-15: Brace In-Plane Displacement Calculation

Note that each test used more markers than shown in Figure 6-14 and Figure 6-15 and that the variables z_i and x_i represent the measurements from the Optotrak system (as discussed in Section 6.2.2). The variable L_{ij} represents the original distance between brace Optotrak markers.

[2] For in-plane buckling braces with knife plate retrofit, the measurement was taken from the far edge of the knife plates.

Brace end rotation in the out-of-plane direction was computed by considering the relative angle change in the vertical plane using the two LED markers on the brace closest to the NE corner. This measurement was taken after the brace deflected shape had been determined.

The brace deflected shape for the out-of-plane and in-plane buckling cases at specified drift ranges are shown in Figure 6-16. The maximum values of mid-span deflection are listed in Table 6-8. Due to the limited viewing space of the Optotrak cameras, LED markers were not visible past the mid-span of the brace and the deflected shape on the SW portion of the brace was assumed to be symmetric.

Table 6-8: Brace Mid-Span Deflections

Specimen Name	Brace Length (in)	Brace Out-Of-Plane Deformation (in)	Brace In-Plane Deformation (in)
NCBF4-R1	164.3	12.6	0.7
NCBF4-R2	142.8	0.4	12.1
NCBF5	174.8	17.0	0.7

Each of the three specimens achieved over 12” of mid-span displacement in the intended direction of buckling. They also had deflections in the orthogonal direction; however, these deflections were all under 1” and did not seem to impact the performance. Notably the only specimen that achieved a brace fracture failure mode, Specimen NCBF5, had the largest brace mid-span deflection.

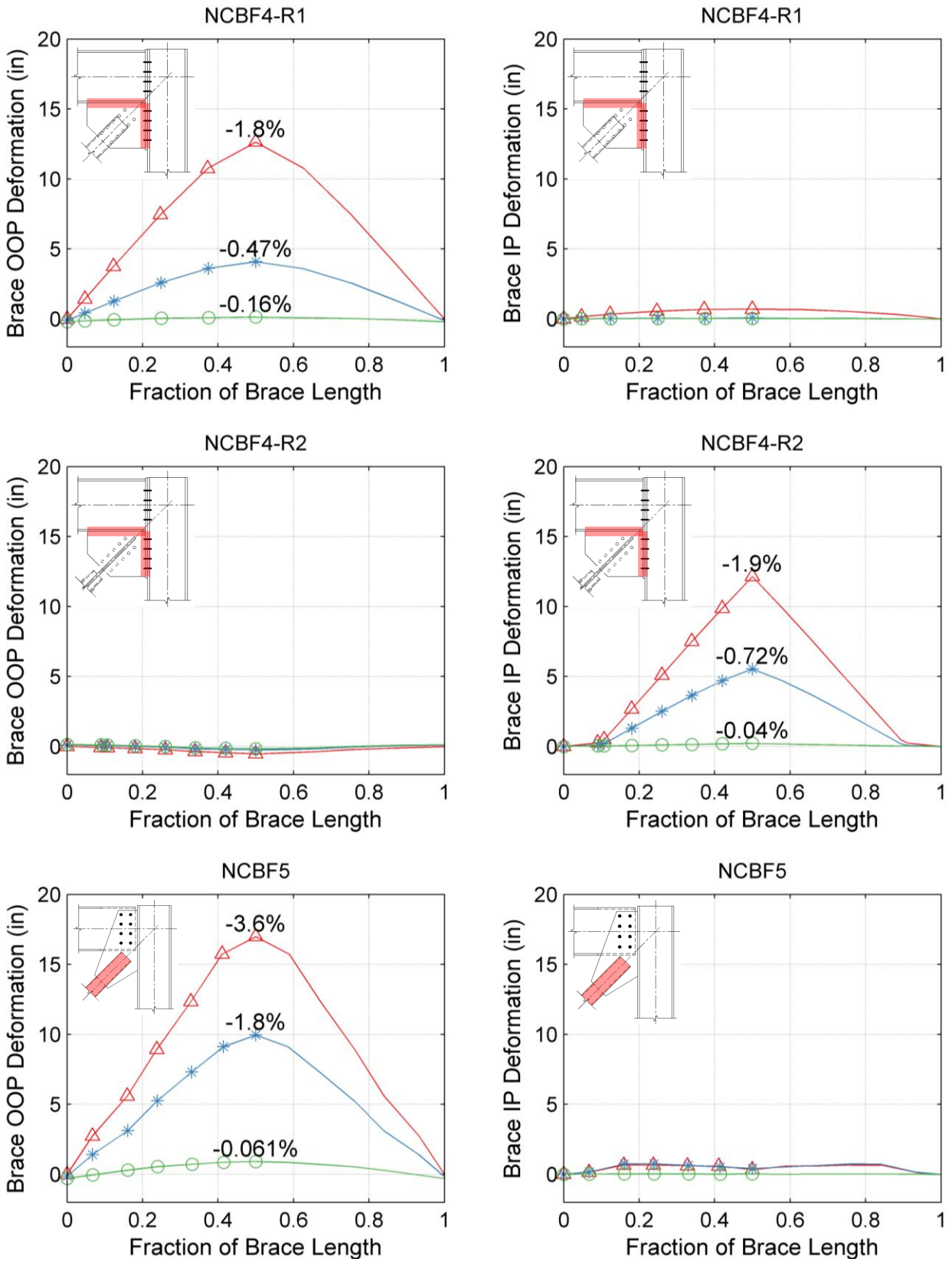

Figure 6-16: Brace Deflected Shape

6.4.3 Brace Elongation

Brace elongation, ε_B, is a direct measurement of brace ductility demand and typically provides a majority of the overall frame ductility in CBFs. Other sources of inelastic deformation capacity such as Whitmore yielding of the gusset plate, bolt hole elongation, and frame member yielding can also contribute to the overall ductility.

For buckling braces, brace elongation was measured using a string potentiometer mounted to the brace ends as shown in Figure 6-17. In this configuration, the potentiometer mount rotated as the brace end rotation increased. For a highly ductile out-of-plane buckling brace these rotation can be significant and must be accounted for to get a reliable measurement for the overall brace elongation. The brace elongation measurement was calculated using Eq. 6-3 where the rotation at both ends of the brace has been accounted for.

$$\varepsilon_B = \frac{L' - L}{L} = \frac{\Delta_{BE} + 2\Delta_{\emptyset}}{L} \qquad \textbf{Eq. 6-3}$$

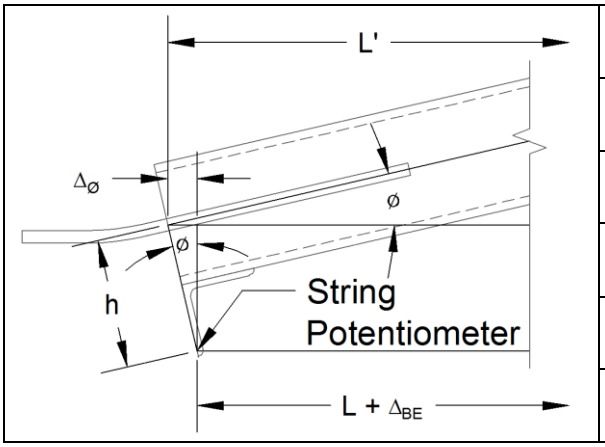

$\emptyset$	Brace end rotation measured from the brace deflected shape
Δ_{BE}	Brace elongation reading
$\Delta_{\emptyset}$	Rotational adjustment to brace elongation measurement at one brace end
h	Distance between center of brace and measurement location
L	Original length of the brace
L'	Current brace length

Figure 6-17: Brace Elongation Measurement BRB

The brace elongation for a BRB is determined by summing the relative displacements measured at each end of the BRB between the core plate and BRB casing as shown in Eq. 6-4 and Figure 6-18. This calculation is a direct measurement of the core plate and does not include the elastic deformation of the cruciform section or the rib plates.

$$BRB \qquad \varepsilon_B = \frac{L' - L}{L} = \frac{\Delta_{NE} + \Delta_{SW}}{L} \qquad \textbf{Eq. 6-4}$$

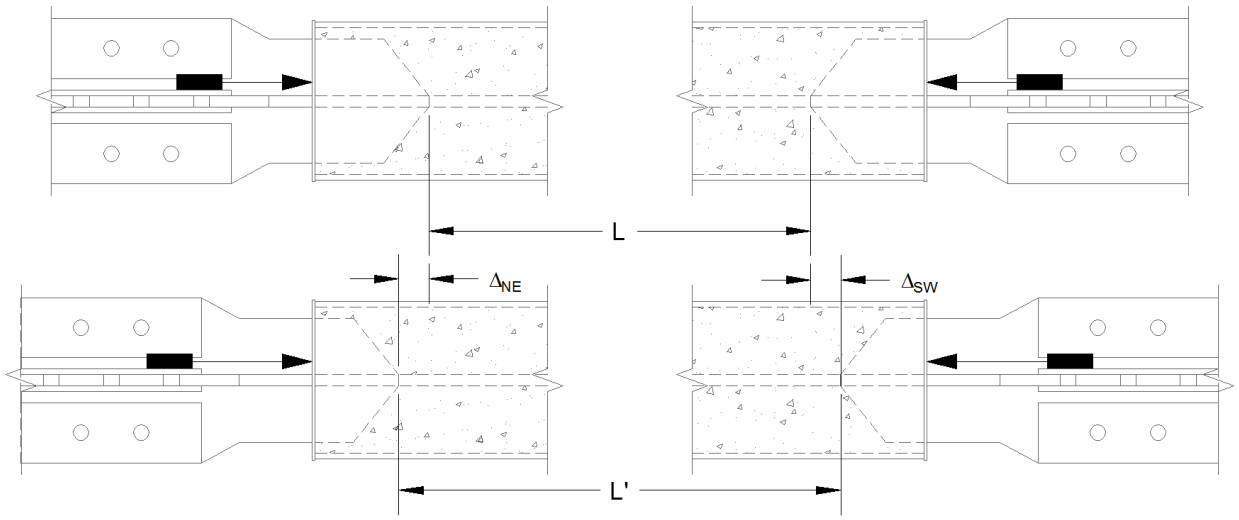

Figure 6-18: Brace Elongation Measurement BRB

Figure 6-19 shows the brace elongation vs. the elongation between the frames NE and SW work points (frame diagonal elongation computed in Section 6.3.1). Both quantities are normalized by the distance between the NE and SW points and are expressed as percentages. The solid line represents a theoretical relationship where the elongation between the work points is provided entirely by the brace.

As seen in Figure 6-19, the brace elongation is nearly equivalent to the overall elongation between the frame work points when the brace is in compression (negative elongation values). In tension, the brace elongation values tend to be less than the elongation between the frame work points as other components of the frame contribute to the overall frame diagonal elongation. In Specimen NCBF4-R2 the difference between the elongation values is largely due to the yielding of the knife plates and gusset plates. In Specimen NCBF2-R1 the difference is largely due to deformation at the bolt holes. Specimens NCBF4-R1 and NCBF4-R3 have similar values of elongation in tension indicating that the connection did not contribute much ductility to the frame.

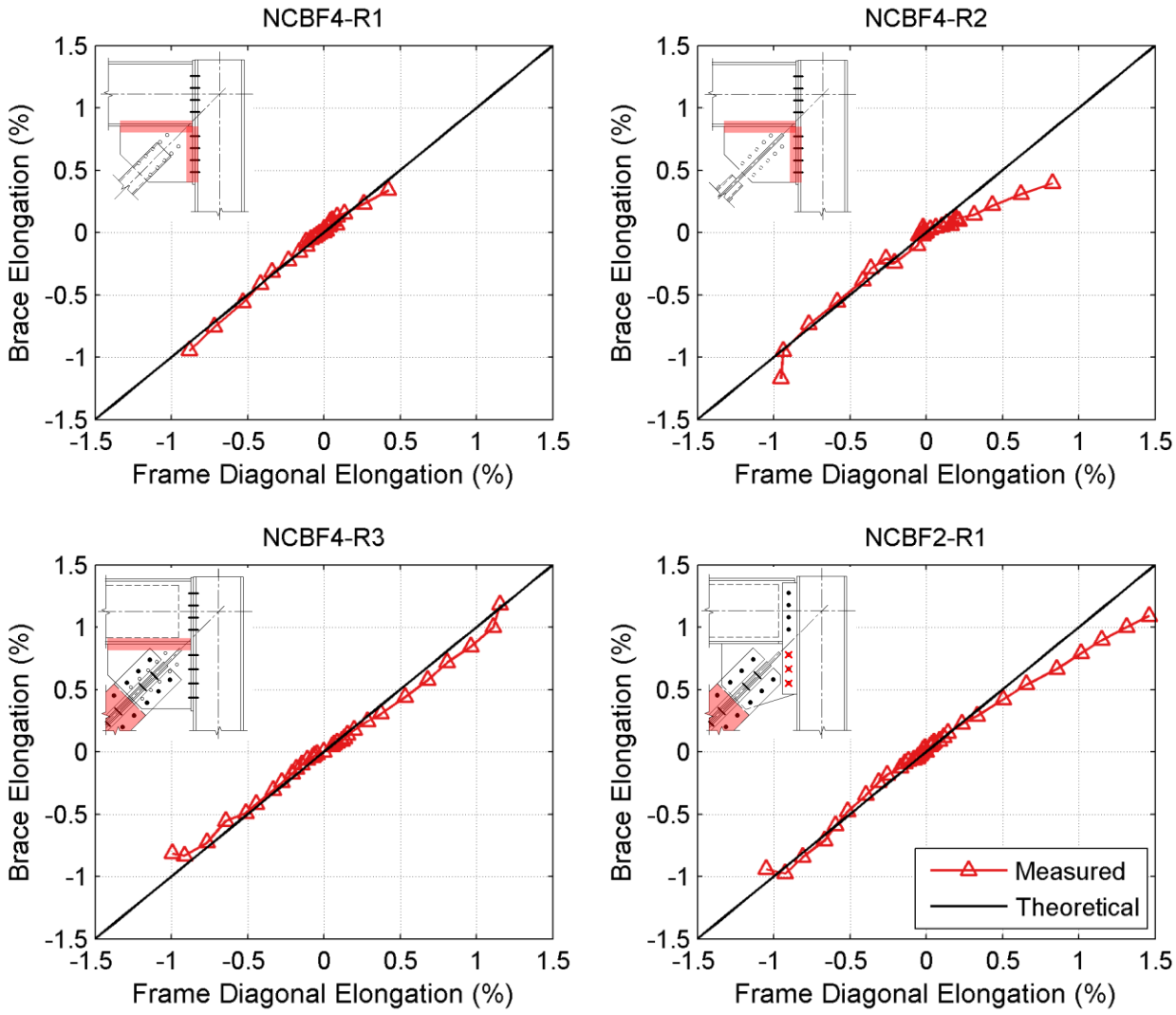

Figure 6-19: Brace Elongation vs. Frame Diagonal Measurement

Brace elongation for Specimen NCBF5 could not be accurately computed using the method presented and is not presented with Figure 6-19 because of poor Optotrak data near the brace end coupled with significant out-of-plane deformations of the entire frame.

6.5 Connection Performance

6.5.1 Beam-to-Gusset Plate Weld Damage

The progression of beam-to-gusset plate weld damage for four of the five specimens (in both the NE and SW corner connections) is shown in Figure 6-20 and is based on measurements of crack lengths made during the tests (crack lengths are normalized by the length of the weld). A summary of each specimens weld details, DCRs, and performance is tabulated in Table 6-9. Note that all beam-to-gusset plate welds did not meet demand-critical requirements. Performance states listed in Table 6-9 are originally defined in Section 5.2 and correspond to the crack length percentage presented in Figure 6-20. Specimen NCBF5 did not have a beam-to-gusset plate weld.

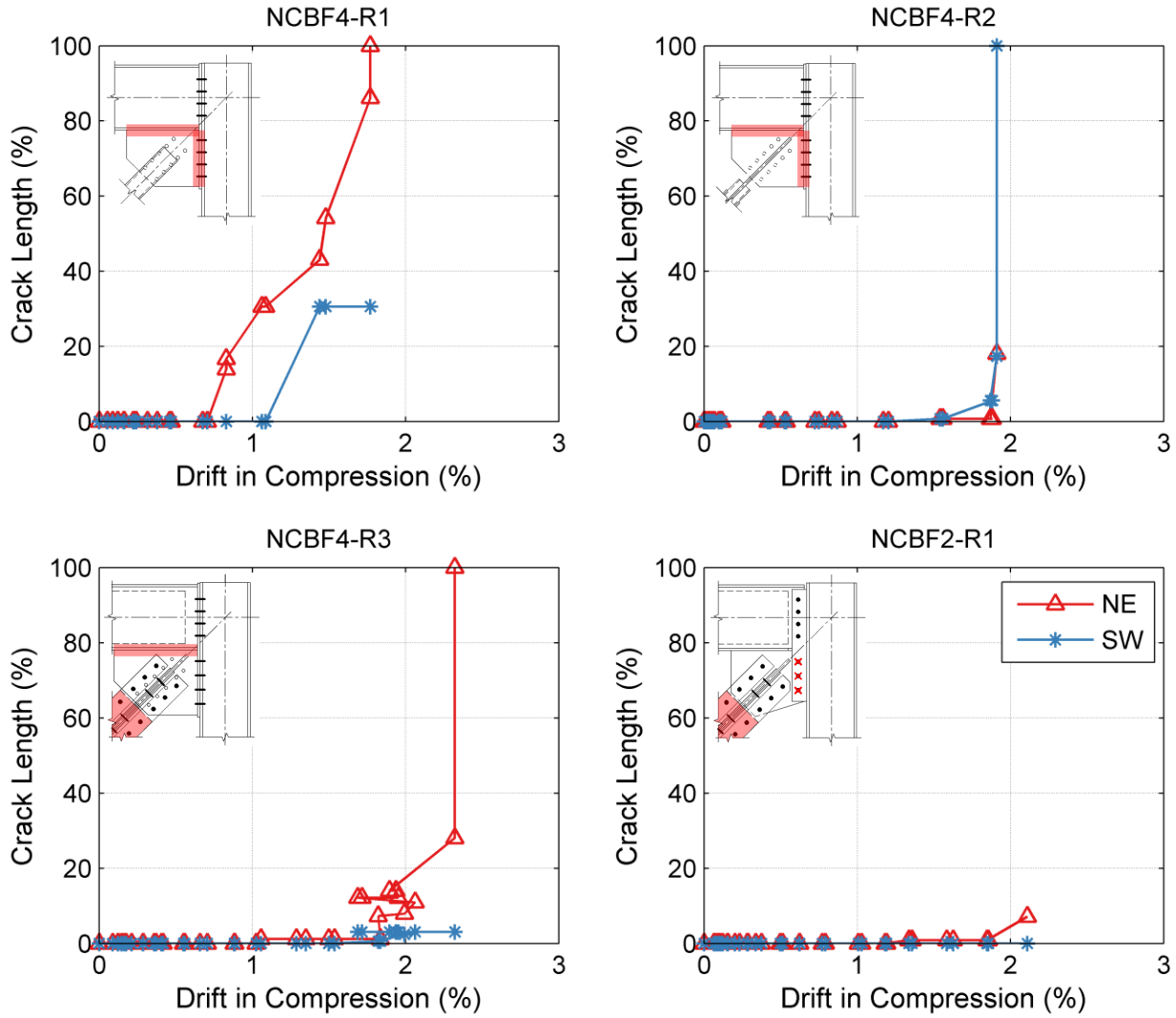

Figure 6-20: Beam-to-Gusset Plate Weld Damage

Table 6-9: Weld Damage Summary

Specimen Name	Gusset Plate		Weld Thick.	DCRs		Drift Range at Given PS (%)			
	Thick.	Length		BR-CVM	GP	W1	W2	W3	WF
NCBF4-R1	5/8”	18”	1/4"	0.63	1.58	-0.8	-0.8	-1.1	-1.8
NCBF4-R2	5/8”	18”	1/4"	0.64	1.58	-1.5	-1.9	-1.9	-1.9
NCBF4-R3	5/8”	20-1/2"	1/4"	0.52	1.61	-1.1	-2.0	-2.4	-2.4
NCBF2-R1	3/4”	14”	7/16”	0.83	1.06	-1.4	NA	NA	NA

Three of the specimens failed due to the beam-to-gusset plate weld fracture despite having enough nominal strength to develop the yield capacity of the brace. This indicates that other approaches are needed to quantify the level of deficiency in the beam-to-gusset plate weld. Checking the weld capacity equation using the yield capacity of the gusset plate was a better indication of the level of deficiency but does not account for limited brace end clearance and non-demand critical welds.

For Specimen NCBF4-R1 weld crack initiation and propagation occurred at a smaller compressive drift than Specimens NCBF4-R2 and NCBF4-R3. This occurred because of high localized stresses induced by out-of-plane buckling that were not present in Specimens NCBF4-R2 and NCBF4-R3. The weld failure shown for Specimen NCBF4-R2 occurred rapidly and was likely induced by opening/ closing of the joint in the SW corner. Although the beam-to-gusset plate weld contributed to the failure of Specimen NCBF4-R3, the weld fracture shown in the final cycle of Specimen NCBF4-R3 occurred as a result of out-of-plane brace hinging. The only specimen to have minimal beam-to-gusset plate weld damage was Specimen NCBF2-R1 which had the lowest DCR using the BDP capacity. The weld cracking of the BEP connections is compared in more detail in 7.3.1.2.

Chapter 7: NCBF Performance Comparison

7.1 Introduction

This chapter compares the performance of the five specimens presented in this document (tested specimens) with several other specimens (reference specimens) tested by Sloat (2014) and Johnson (2014) using parameters calculated as described in Chapter 6. The reference specimens share similarities in either brace type or connection type with the tested specimens and are shown in a connection test matrix Table 7-1. By comparing these specimens, conclusions about the impact of the brace and connection on system performance (yielding hierarchy and failure mode) can be drawn.

The connection and brace test matrix is shown in Table 7-1 and provides context for the comparisons made in the chapter. The top row of the table indicates the specific categories of the connections; the row below provides general geometric characteristics. The leftmost column provides the brace type: highly ductile, moderately ductile, or buckling restrained brace (BRB). Each cell provides the abbreviated specimen name, location of the failure mode signified by the highlighted regions, the drift range achieved in the last cycle prior to failure, and the plot marker used in the plots throughout this chapter. Specific connection details and demand capacity ratios for each specimen are documented in more detail in Chapters 2 for the reference specimens and Chapter 3 for the tested specimens.

Section 7.2 will make comparisons between the connection types by looking at tests with the same brace while Section 7.3 compares the brace types for specimens with the same connection type. Section 7.4 will summarize the main conclusions.

Table 7-1: Connection Test Matrix for NCBF Comparisons

Connection Matrix	Welded Continuous Shear Plate (WC)	Bolted Continuous Shear Plate (BC)	Bolted Split Shear Plate (BS)	Bolted End Plate (BE)	Integrated Gusset-Shear Plate (I)
Beam/Gusset-to-Column Conn. Details	3/8" Gusset Plate 3/8" Shear Plate w/ 5/16" Single Fillet	3/4" Gusset Plate 3/4" Shear Plate w/ 7-A325X 1" Φ Bolts	1/2" Gusset Plate 3/4" Shear Plates w/ 7-A325X 1"Φ Bolts	5/8" Gusset Plate 5/8" End Plate w/ 16-A490N 7/8"Φ Bolts	7/8" Gusset/ Shear Plate w/ 8-A325X 1"Φ Bolts & CJP weld
Highly Ductile 5x5x3/8" HSS Brace (OOP)	NCBF1-R2 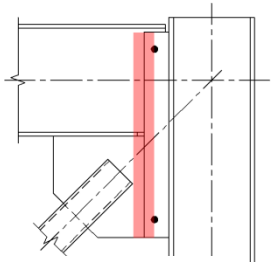 **Drift Range: 3.3%**	NCBF2 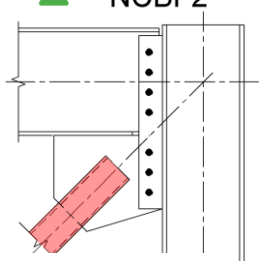 **Drift Range: 4.7%**	NCBF3-2 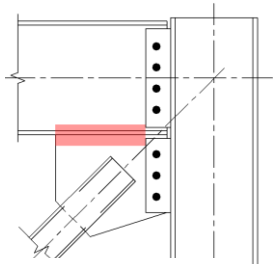 **Drift Range: 2.7%**	NCBF4-R1 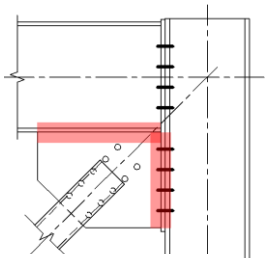 **Drift Range: 2.9%**	NCBF5 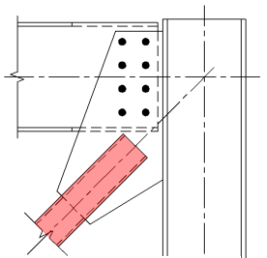 **Drift Range: 5.0%**
Moderately Ductile 6x4x3/8" HSS Brace with Knife Plate Retrofit (IP)	NCBF1-R4 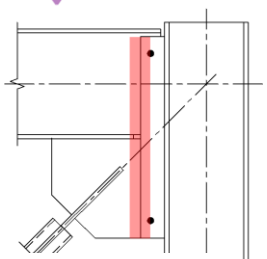 **Drift Range: 2.3%**	NA	NA	NCBF4-R2 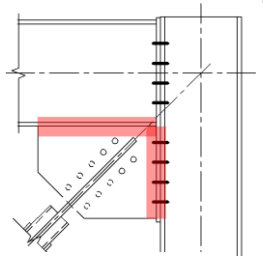 **Drift Range: 3.9%**	NA
Buckling Restrained Brace Retrofit (BRB)	NA	NCBF2-R1 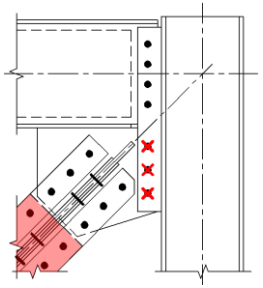	NA	NCBF4-R3 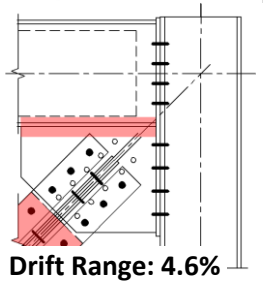 **Drift Range: 4.6%**	NA

7.2 Connection Comparisons by Brace Type

7.2.1 NCBF Specimens with Out-of-Plane Buckling Brace

All five specimens in the first row of Table 7-1 used a seismically compact HSS 5x5x3/8" with an out-of-plane buckling brace but all used a different connection type. Table 7-2 summarizes some of the important response parameters measured from each experiment. As shown, the drift range for the specimens varied from 2.7% for specimens with a connection failure to approximately 5.0% for specimens that achieved brace fracture. These results indicate that the connection type can have an impact on the overall response of the frame in terms of drift and failure mode.

Table 7-2: Summary of Response Parameters - Connection with Out-of-Plane Buckling Brace

Specimen Name	Drift Range	Frame Response		Brace Response			Failure Location
		Moment (% of 2Mp)		OOP disp. (in)	Normalized Brace Force[1]		
		Tension	Comp.		Tension	Comp.	
NCBF1-R2	3.3%	31%	49%	12.2	0.92	0.77	Connection
NCBF2[2]	4.7%	NM	NM	17.3	NM	NM	Brace
NCBF3-2	2.7%	32%	35%	11.0	1.03	1.08	Connection
NCBF4-R1	2.9%	50%	59%	12.9	1.07	1.00	Connection
NCBF5	5.0%	22%	50%	17.3	1.00	1.04	Brace

1 – Ratio between the maximum brace force and the expected capacity of the brace
2 – Column shears and brace force could not be calculated due to inadequate strain gauge data (indicated as NM for Not Measured)

7.2.1.1 Frame Response

Figure 7-1 shows the maximum moments developed in the column versus interstory drift for four of the connection types. The moment is expressed as a percentage of the plastic moment capacity and includes both the east and west columns. At drifts less than ±0.25% the percentage of moment developed at the edge of the gusset plates is similar and has a linear relationship with the drift; at these drift levels the frame is elastic. At drifts > ±0.25%, the relationship becomes nonlinear as the connection and frame undergo inelastic action. The drift at which the relationship switches from linear to non-linear behavior can be controlled by any number of ductile mechanisms in each of the different connection types. Examples of possible mechanisms include flexural yielding of the gusset plate at the column interface due to moment, shear yielding of the gusset plate at the column interface due to shear, or yielding of the framing members. Note that although the moments do not reach the plastic moment capacity there can still be yielding in the columns from flexural/ axial interaction.

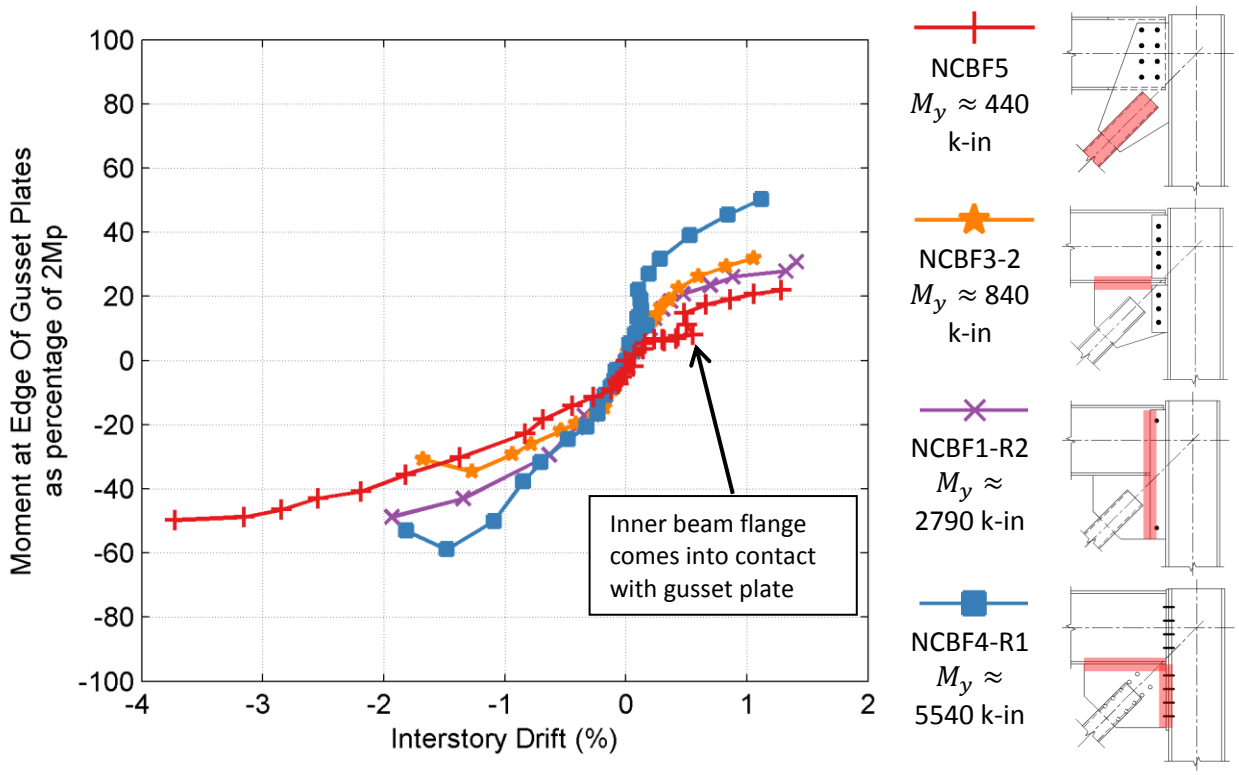

Figure 7-1: Column Moments vs. Interstory Drift - Connections w/ 5x5x3/8" Brace

An estimation of the yield moment (connection strength), M_y, for each connection type is shown in Figure 7-1[3]. When the brace is in compression, the connection with the highest yield capacity goes on to develop the highest moment in the column. Among the connections, the bolted end plate connection (Specimen NCBF4-R1, highest M_y) developed the highest moments in both tension and compression drifts and it did so at a smaller drift range than other connection types such as the integrated gusset-shear plate (Specimen NCBF5, lowest M_y). This relationship also holds up when the brace is in tension except for the continuous welded shear plate (Specimen NCBF1-R2). In this case, severe tensile yielding in the gusset plate was a controlling ductile mechanism in the connection and likely was part of the mechanism that lead to lower moments in the column while the brace was in tension.

From these results it appears that a weaker connection at the column interface limits the amount of force being delivered into the columns. This is also observed when comparing the two BRB specimens discussed in 7.2.3.

[3] The yield moment is the lesser of the column yield moment and the connection yield moment. The connection yield moment is obtained by assuming a linear stress distribution across the elements transferring forces from the beam/gusset to the column and finding the moment that causes the farthest element to reach the measured yield capacity $\sigma_y = M_y/S$.

7.2.1.2 Brace Response

The specimens achieved 11" to 17.3" of brace out-of-plane mid-span displacement. As shown in Figure 7-2, the out-of-plane displacement is strongly correlated to the drift in compression and as expected appears to be independent of connection type.

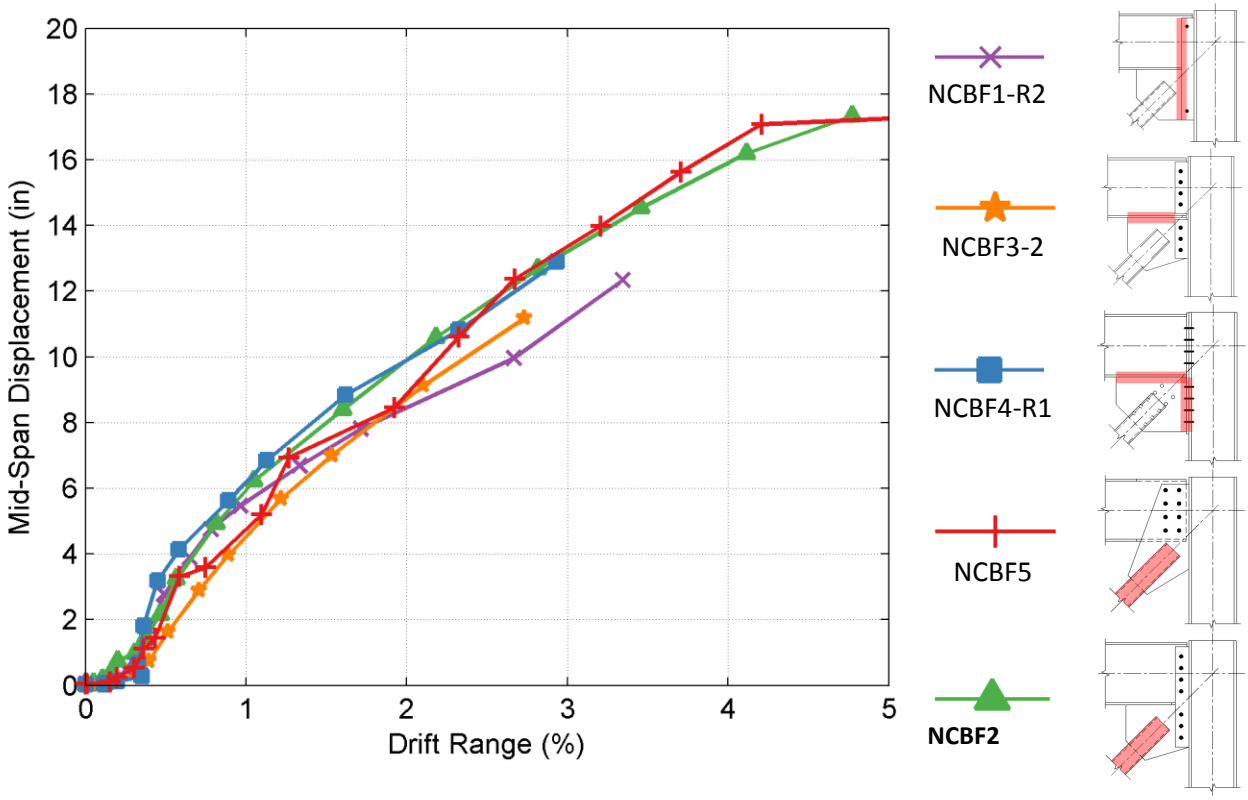

Figure 7-2: Brace Out-of-Plane Displacement vs Drift – Connections w/ 5x5x3/8" Brace

The expected capacities in tension, P_y, and compression, P_{cr}, for each test were computed using the measured material parameters following the procedure in Section 2.3.2. All of braces achieved the theoretical brace capacities in tension and compression except for the specimen with continuous welded shear plate connections (Specimen NCBF1-R2), as shown in Table 7-2 and in Figure 7-3.

The brace force in the integrated gusset-shear plate connection (Specimen NCBF5) was able to achieve the expected yield capacity of the brace in tension, but may have exceeded the expected capacity if not for premature local web buckling in the beam web. Beam web buckling limited the amount of force that could be transferred through the beam from the actuator to the NE corner connection until the beam flange came into contact with the gusset plate. The point where web buckling begins is indicated with 1* in Figure 7-3.

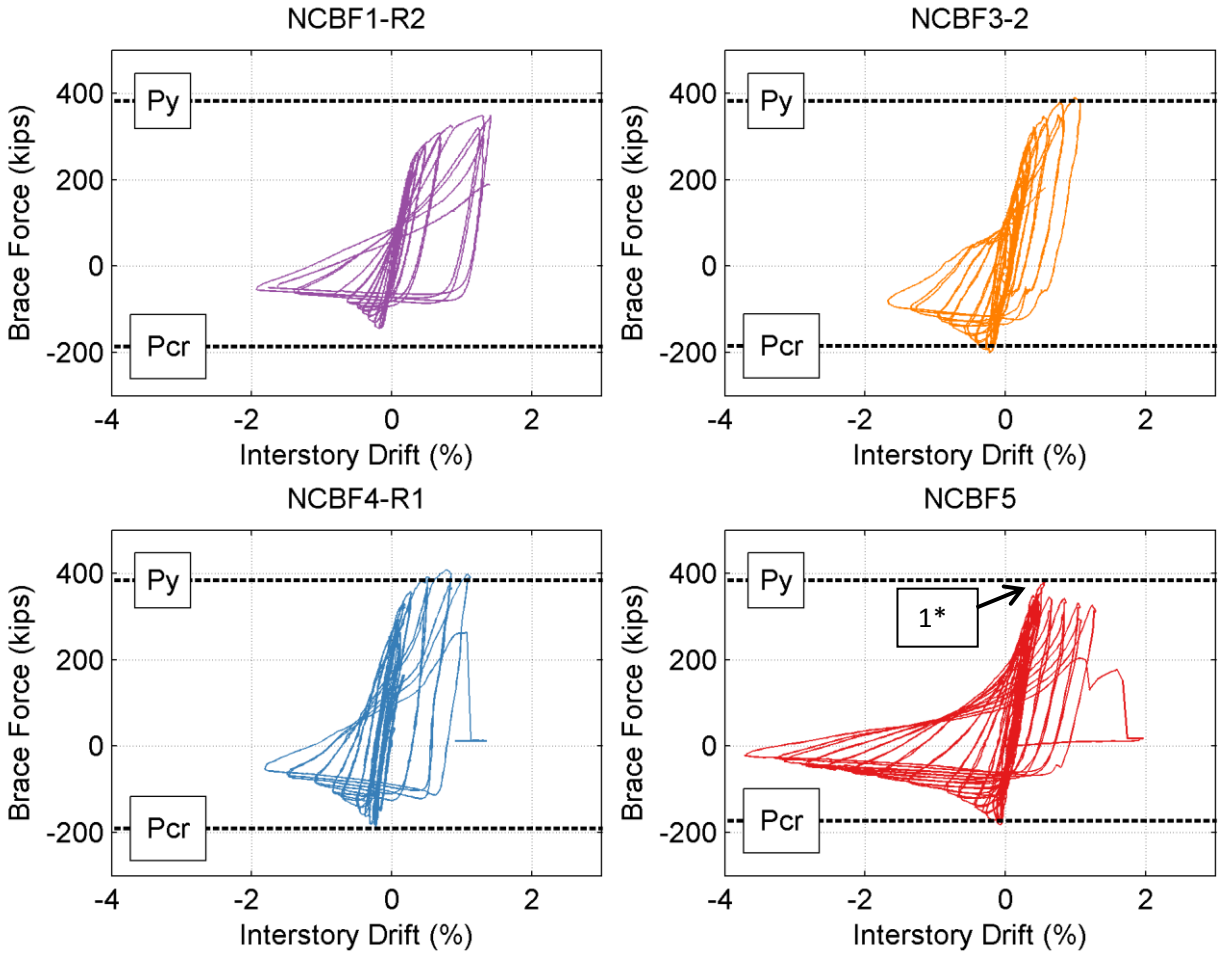

Figure 7-3: Brace Force vs. Interstory Drift – Connections w/ 5x5x3/8" Braces

1* - Severe local web buckling in NE beam reduces amount of force that can be transferred from the actuator to the NE corner connection.

7.2.1.3 Failure Modes

Although the beam-to-gusset plate welds were nominally strong enough to develop the expected capacity of the brace (BR-CVM or BR-UFM <1.0), three of the five connections suffered weld fractures at drift ranges less than 3%. The beam-to-gusset plate weld was particularly vulnerable in most of these connections due to limited brace end clearance, non-demand critical welds, and deficient weld size when checked against the yield capacity of the gusset plate. A summary of the gusset plate weld details and damage is shown in Table 7-3.

Table 7-3: Gusset Plate Weld Damage – Connections with Out-of-Plane Buckling Brace

Specimen Name	Gusset Plate			Weld Thick.	DCRs		Drift Range at Given PS[1] (%)			
	Thick.	Length	Clear		BR	GP	W1	W2	W3	WF
NCBF2	3/4”	11-3/4”	3.8	7/16"	0.8	1.1	-1.5	-1.9	-2.7	NA
NCBF3-2	3/4”	16-1/8”	1.1	5/16"	0.6	1.1	-1.3	-1.1	-1.1	-1.1
NCBF4-R1	5/8”	18”	4.1	1/4"	0.6	1.6	-0.8	-0.8	-1.1	-1.8

1- Performance State (PS) definitions for weld damage given in Section 5.2.

Figure 7-4 and Figure 7-5 show the normalized beam-to-gusset plate weld crack length vs drift in compression for the tests that sustained severe weld tearing and/or fracture for two cases looking at the connection continuity and the beam-to-gusset plate deficiencies.

For the two tests (Specimens NCBF2 and NCBF3-1) with a weld fracture DCR (GP) of 1.1 (Figure 7-4) weld cracking initiated when the brace was in compression at approximately 1.4% drift. In the split shear plate connection (Specimen NCBF3-2) the weld crack propagated and resulted in weld fracture three cycles later. For the continuous bolted shear plate (Specimen NCBF2), the weld crack propagated at a slower rate and the weld did not fracture. It is believed that the continuity of the continuous shear plate allowed for the redistribution of forces (especially when the brace is in tension) as the weld tore and allowed the specimen to achieve brace fracture.

For the two continuous connections (Specimens NCBF2 and NCBF4-R1) with different weld fracture DCRs (GP) (Figure 7-5) the inability of the welds to develop the capacity of the gusset plate led to premature weld fracture in Specimen NCBF4-R1. This shows that for an out-of-plane buckling brace it is important to consider this DCR.

There was also a weld fracture in the continuous welded shear plate connection specimen, but it occurred in the vertical weld connecting the shear plate to the gusset plate and beam web. This weld was also deficient considering AISC weld fracture equation and was not directly comparable to the beam-to-gusset plate weld damage in the other specimens.

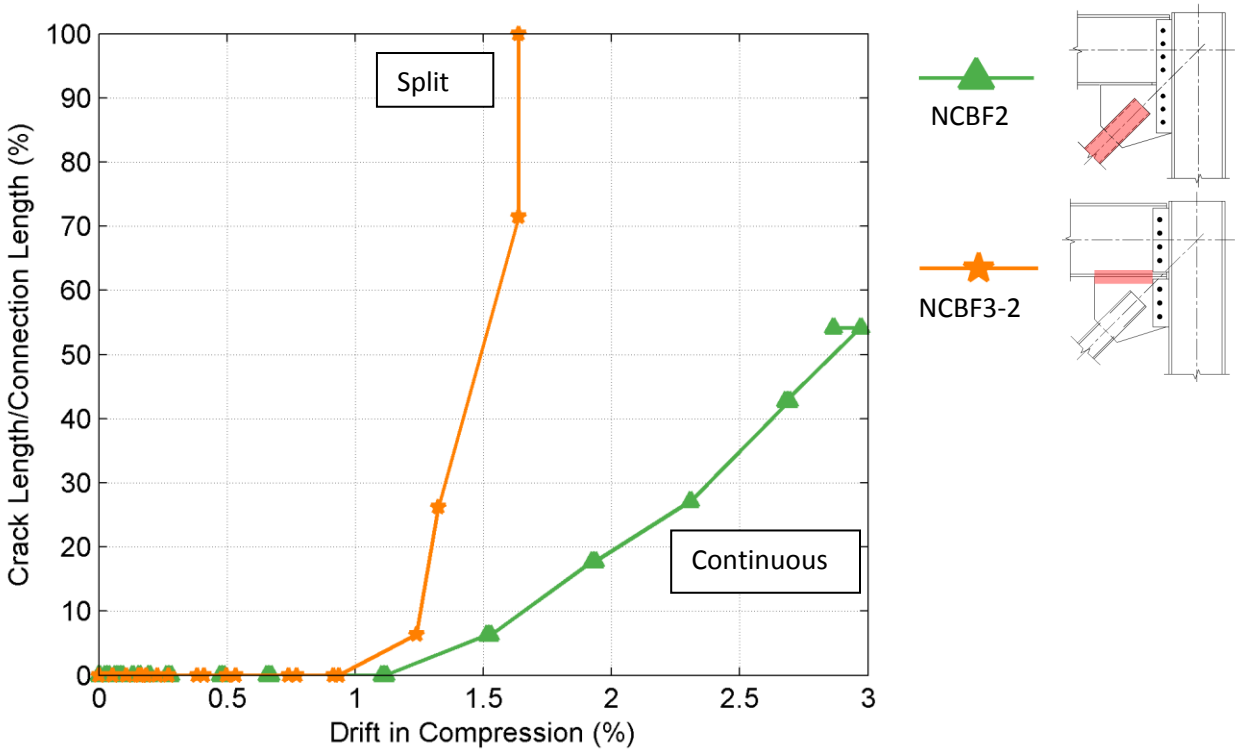

Figure 7-4: Beam-to-Gusset Plate Weld Crack Length Vs. Drift (Connection Continuity)

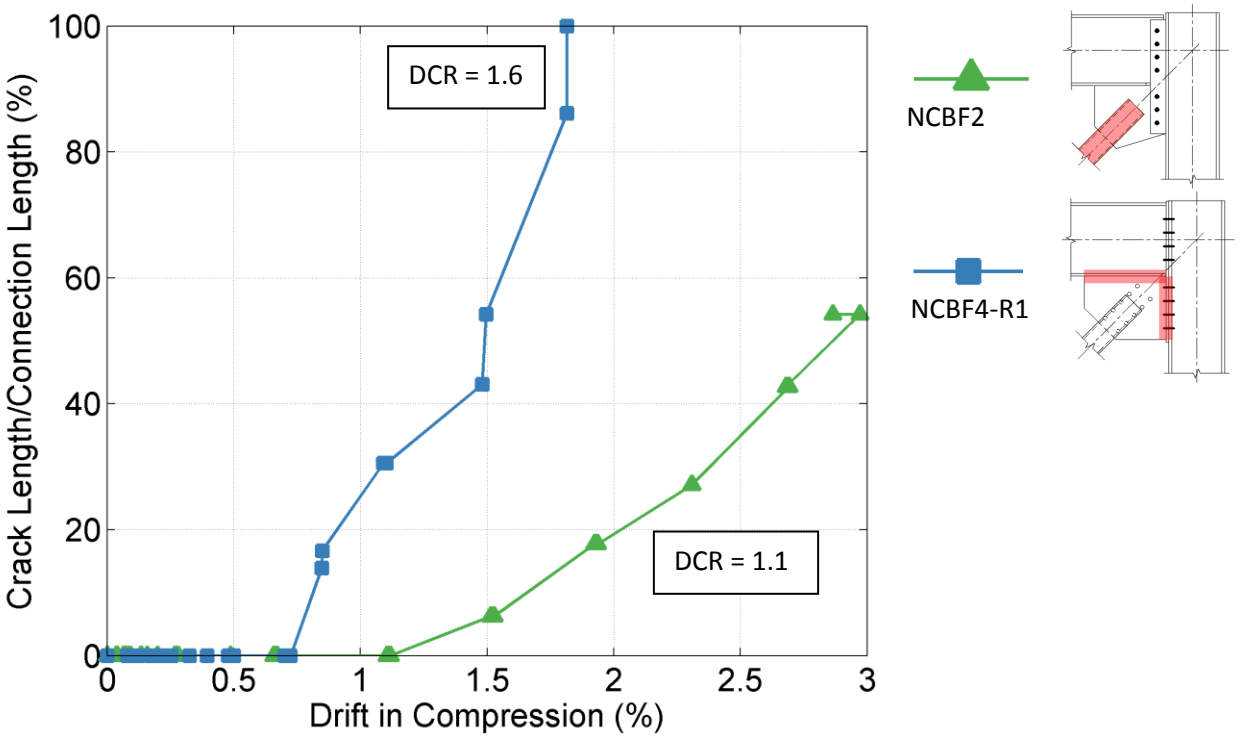

Figure 7-5: Beam-to-Gusset Plate Weld Crack Length Vs. Drift (Connection Deficiency)

7.2.2 NCBF Connections with Knife Plate In-Plane Buckling Retrofit

This section compares the two connections that utilized a knife-plate, in-plane-buckling retrofit (2nd row of the connection test matrix (Table 7-1). The in-plane retrofit was intended to limit damage resulting from out-of-plane deformations. A summary of the both specimens is given in Table 7-4. Although a connection fracture is noted for the bolted end plate connection (Specimen NCBF4-R1), note that the brace began tearing just prior to connection fracture.

Table 7-4: Summary of Response Parameters - Connections with In-Plane Buckling Brace

Specimen Name	Drift Range	Frame Response		Brace Response			Failure Location
		Moment (% of 2Mp)		In-Plane disp. (in)	Brace Force[1]		
		Tension	Comp.		Tension	Comp.	
NCBF1-R4	2.3%	28	-54	9.9	0.89	1.06	Connection
NCBF4-R1	3.9%	51	-71	12.1	1.11	1.08	Connection

1 – Ratio between the maximum brace force and the expected capacity of the brace

7.2.2.1 Frame Response

The column moments vs. interstory drift for the two knife-plate retrofit specimens is shown in Figure 7-6. The moment developed in the two specimens is similar in both tension and compression over a limited drift range. In Specimen NCBF1-R4 connection failure occurred at a drift range of 2.3% compared to the drift range of 3.9% that was achieved by Specimen NCBF4-R2 indicating that the bolted end plate connection was a better candidate for the knife plate retrofit.

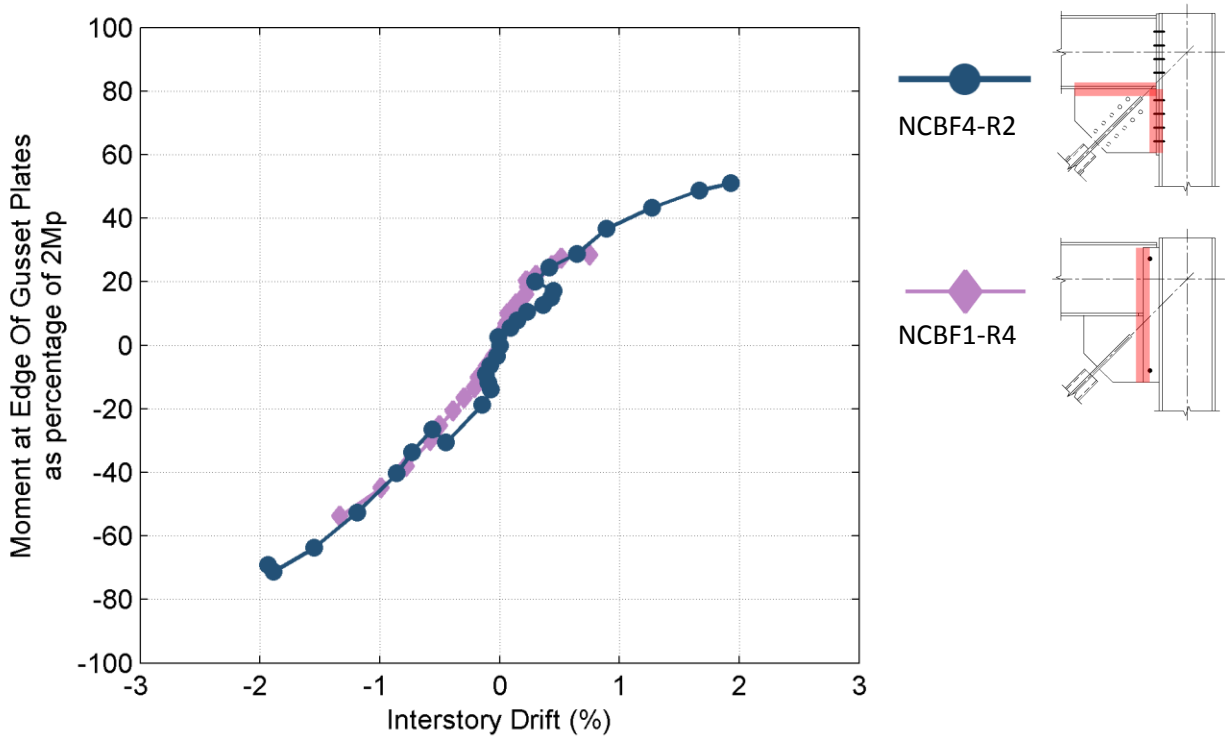

Figure 7-6: Column Moment vs. Interstory Drift - Connections with In-Plane Buckling Brace

7.2.2.2 Brace Response

The brace force vs interstory drift for each of the knife plate retrofit specimens is shown in Figure 7-7. Both specimens developed compression forces slightly higher than the expected buckling capacity, P_{cr}, suggesting that an effective length factor of 1.0 might under estimate the actual buckling capacity of the brace for this type of connection. Due to the number of uncertainties in determining the experimental and expected buckling capacities, it is possible that this difference is a coincidence. Either way, a 10% difference between the actual and expected buckling capacities is not large enough to justify the use of a different effective length factor in the prediction of expected buckling capacity of other knife plate specimens. The maximum tension brace force is different for the two specimens. The continuous welded shear plate Specimen NCBF1-R4 did not develop the expected tensile brace capacity (also seen in Specimen NCBF1-R2, Section 7.2.1).

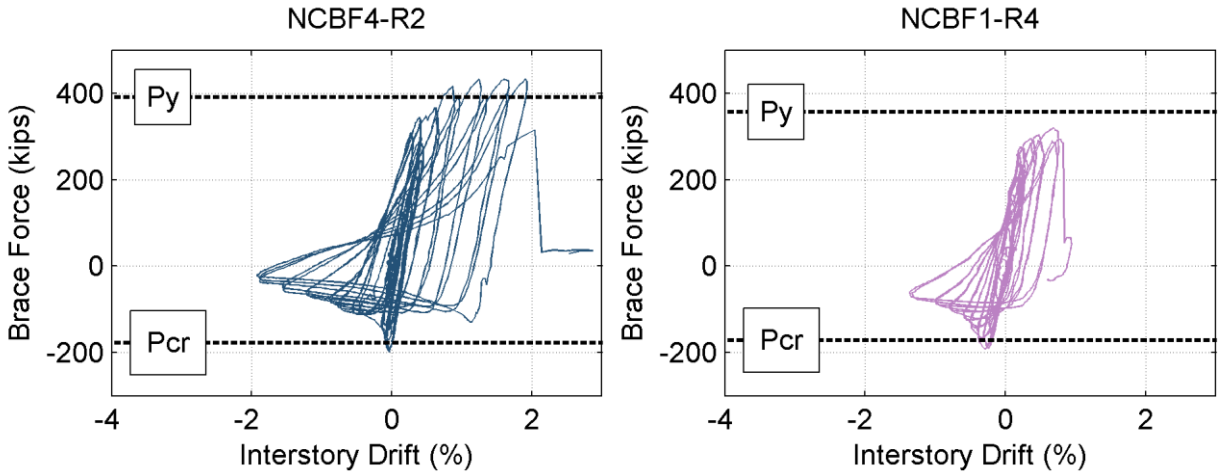

Figure 7-7: Brace Force vs. Interstory Drift - Connections w/ In-Plane Retrofit

The brace mid-span in-plane deflection vs. drift for the two specimens at the peaks of the first drift cycle to a specified drift level is shown in Figure 7-8. It appears that the continuous welded shear plate (Specimen NCBF1-R4) is able to develop a higher level of in-plane displacement than the bolted end plate connection (Specimen NCBF4-R2); however, it is difficult to determine the source of the difference considering brace deformation mechanics, and no conclusions from this difference can be drawn.

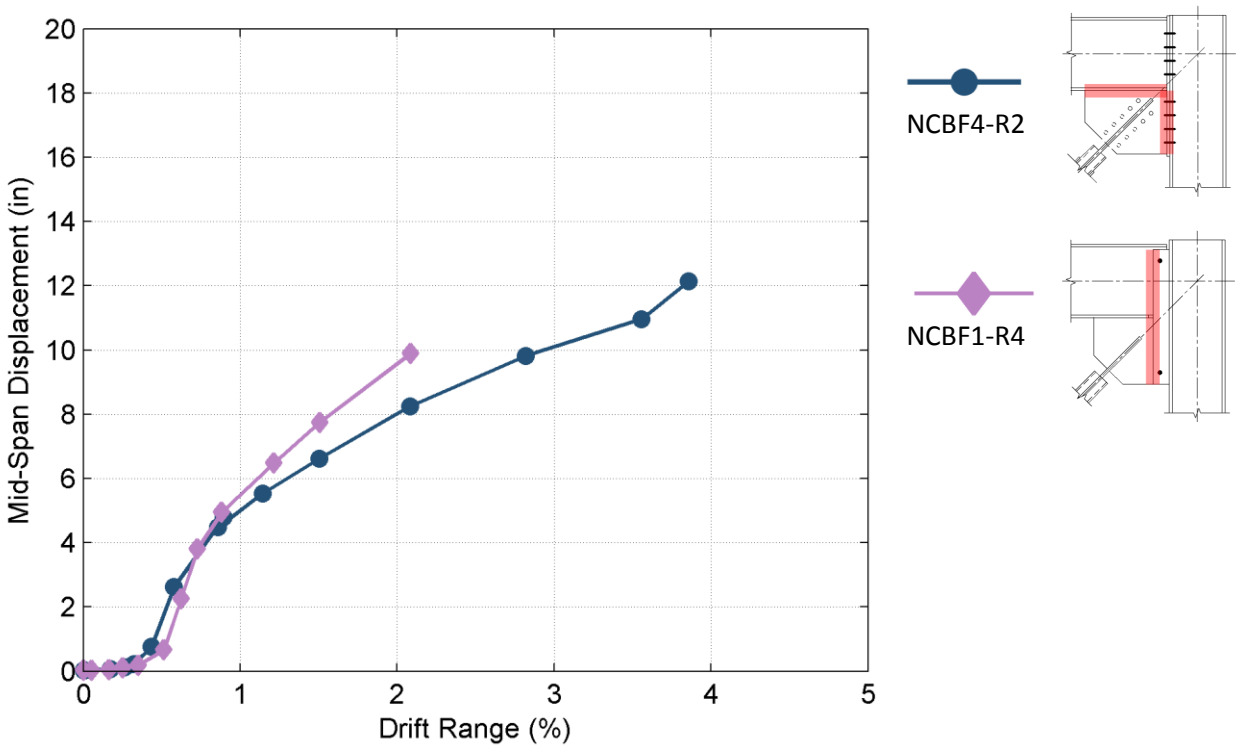

Figure 7-8: Brace In-Plane Displacement vs. Drift Range - Connections w/ In-Plane Retrofit

7.2.3 NCBF Connections with BRBs

This section compares the two connections that utilized a BRB retrofit (5th row of the connection test matrix, Table 7-1). A summary of the response is provided in Figure 7-9. Both specimens achieved a high drift range (>4.5%) and lost lateral resistance when the BRB core plate hinged. Note that prior to this failure mode, both specimens also sustained instability in the connection (beam-to-gusset plate weld tearing in Specimen NCBF4-R3 and bolt fracture in Specimen NCBF2-R1).

Figure 7-9: Summary of Response Parameters for Connections with BRBs

Specimen Name	Drift Range	Frame Response		Brace Response		Failure Location
		Column Shear		Brace Force		
		Tension	Comp.	Tension	Comp.	
NCBF2-R1	5.2%	52	65	1.01	1.00	Brace
NCBF4-R3	4.6%	65	82	1.00	1.00	Brace

1 – Ratio between the maximum brace force and the expected capacity of the brace

7.2.3.1 Frame Response

Both specimens developed a drift range of greater than 4.5% and column moments in excess of 50% of the plastic moment capacity in both brace tension and compression. This drift range is similar to BRBF connections designed using ductile detailing and full strength connections (Christopulos 2005).

The column moment vs. interstory drift for the two specimens is shown in Figure 7-7. At drift levels between -0.9% and 0.9%, the moment developed in the columns is similar and is approximately linear with drift. Beyond this drift range, the amount of the column moment developed in Specimen NCBF2-R1 (bolted continuous shear plate connection) declines relative to the bolted end plate because the connection reaches its yield capacity. The point when the curves begin to diverge corresponds to the point when bolt hole elongation (from observation) begins in the continuous shear plate (Specimen NCBF2-R1). The drift at which this occurs is consistent with the observations made in Section 5.7.3.

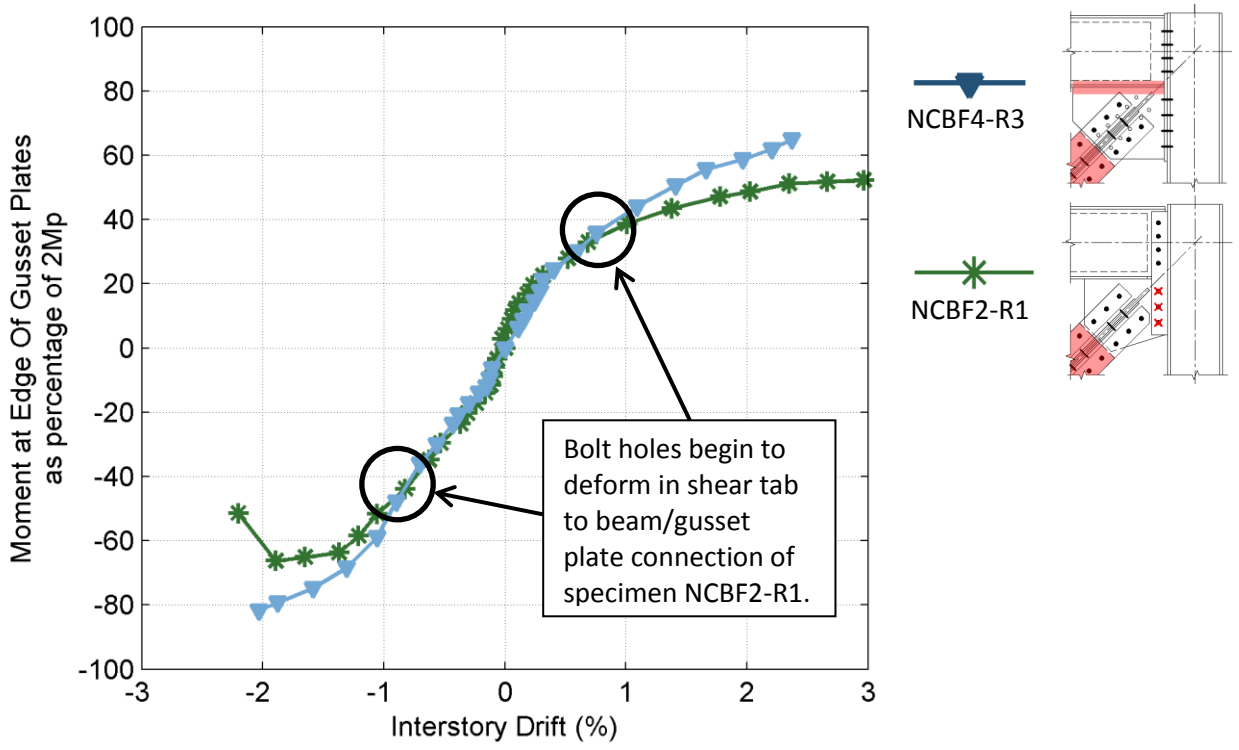

Figure 7-10: Column Shear vs. Interstory Drift for Connections with BRBs

The difference between the connection moment strengths has an impact on the yielding hierarchy. Figure 7-11 shows that the bolted end plate connection (Specimen NCBF4-R3) sustained much more yielding in the plastic hinge region than Specimen NCBF2-R1 at a similar level of drift in both columns. These results suggest that a ductile mechanism at the connection interface can limit the forces transferred to the columns. This observation is consistent to the conclusions made in Section 7.2.1.1 for frames using out-of-plane buckling braces.

Note that the beam web was reinforced for both BRB connections and beam damage for both specimens was limited.

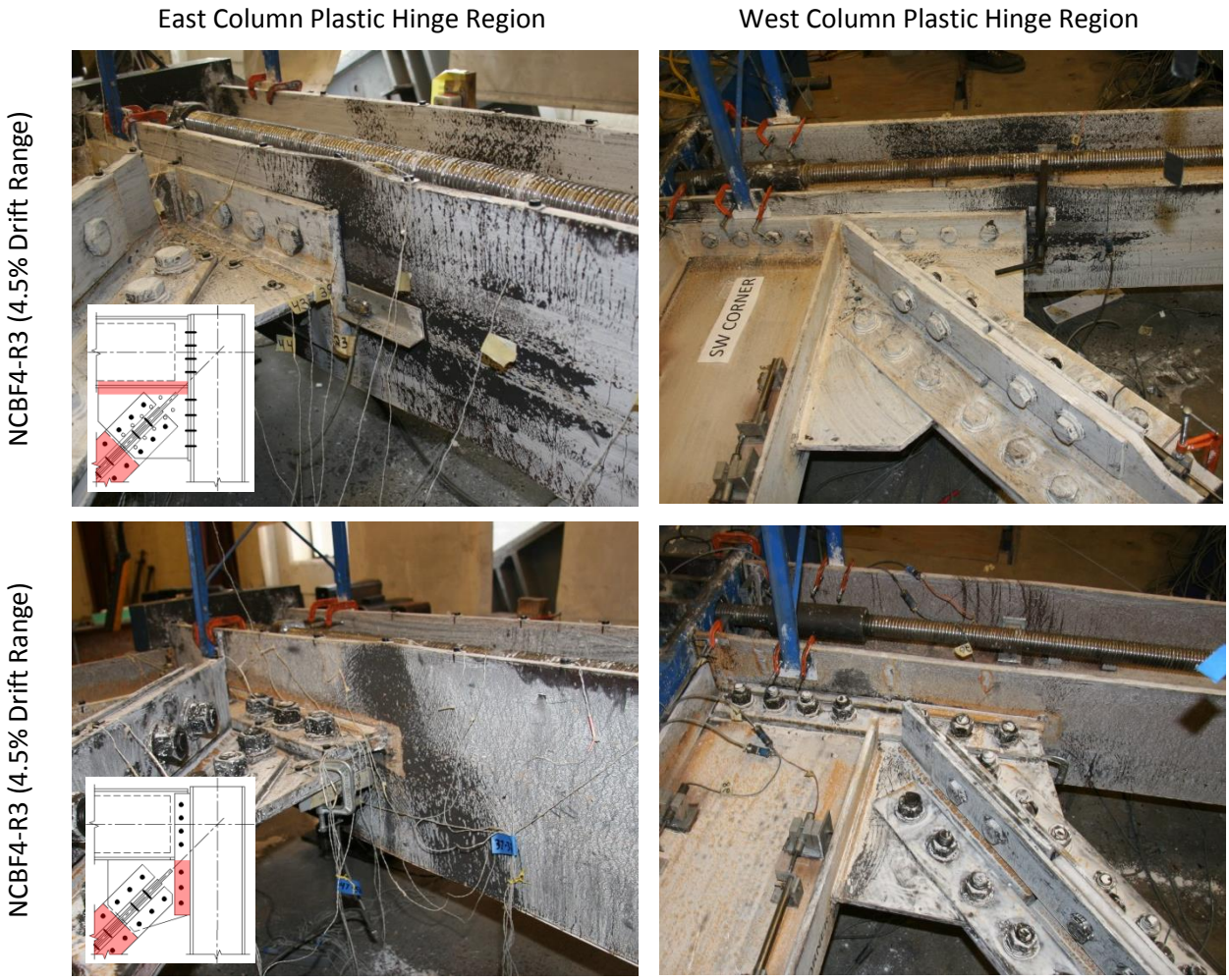

Figure 7-11: Column Damage in Plastic Hinge Locations for BRB Retrofit Tests

7.2.3.2 Brace Response

The brace force versus interstory drift response for Specimens NCBF2-R1 and NCBF4-R3 is shown in Figure 7-11. Both BRBs developed their expected capacities (also shown Figure 7-9) and had nearly identical load-drift behavior despite the difference in the connection type.

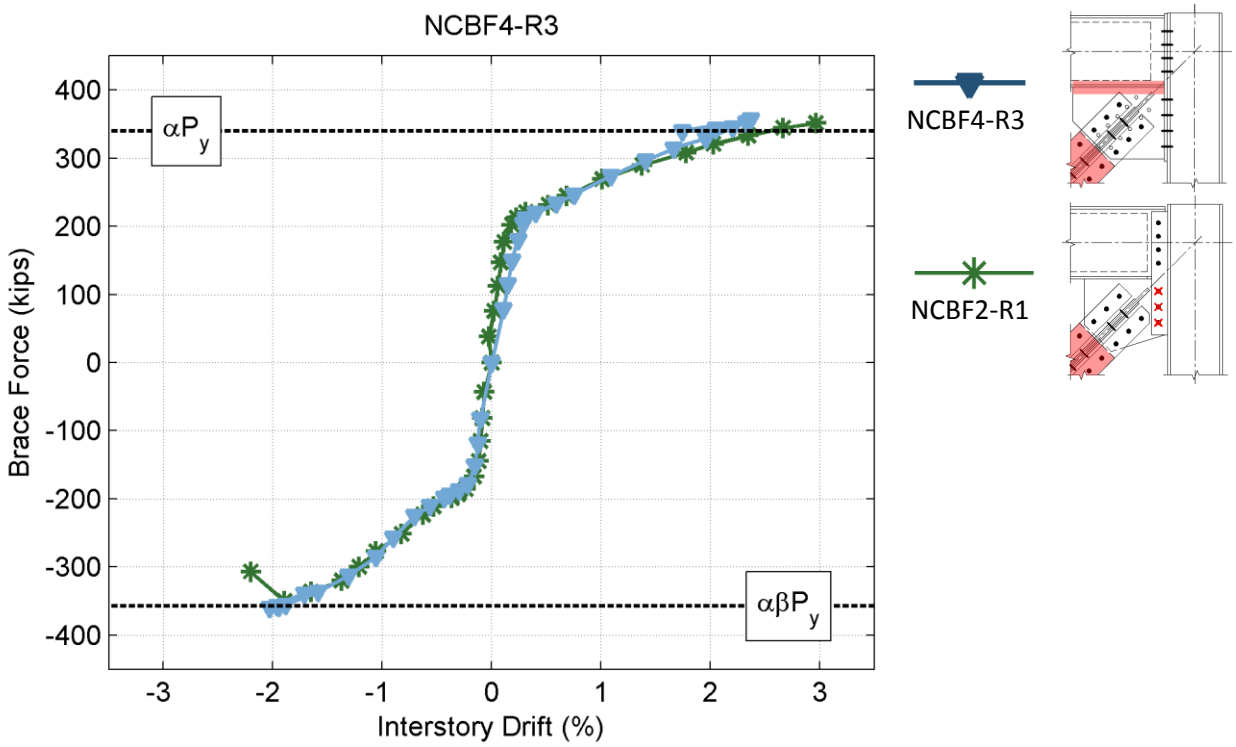

Figure 7-12: Brace Force vs. Interstory Drift BRB Braces

7.3 Connection Response by Brace Type

7.3.1 Bolted End Plate Connections

The bolted end plate connection was the only connection to be tested using all three brace retrofit options (1- out-of-plane buckling brace, 2- in-plane buckling brace, 3-BRB retrofit). A summary of the response for the bolted end plate connections is shown in Table 7-5. As shown, the brace type had an impact on overall specimen response in the terms of drift range.

Table 7-5: Summary of Bolted End Plate Response

Specimen Name	Brace Type	Frame Response			Brace Response		Failure Location
		Drift Range	Moment (% of $2M_p$)		Brace Force[1]		
			Tension	Comp.	Tension	Comp.	
NCBF4-R1	Out-of-Plane Buckling	2.9%	50	59	1.07	1.00	Connection
NCBF4-R2	In-Plane Buckling	3.9%	51	71	1.11	1.08	Connection
NCBF4-R3	BRB	4.6%	65	82	1.00	1.00	Brace Hinge

1 – Ratio between the maximum brace force and the expected capacity of the brace

7.3.1.1 Frame Response

Figure 7-13 shows the amount of moment developed in the columns at a given drift range as discussed previously in Sections 7.2.1.1. As shown, there are only slight differences between the curves, and it is difficult to determine the sources of these differences. These results suggest that the forces in the framing members are dependent primarily on the connection.

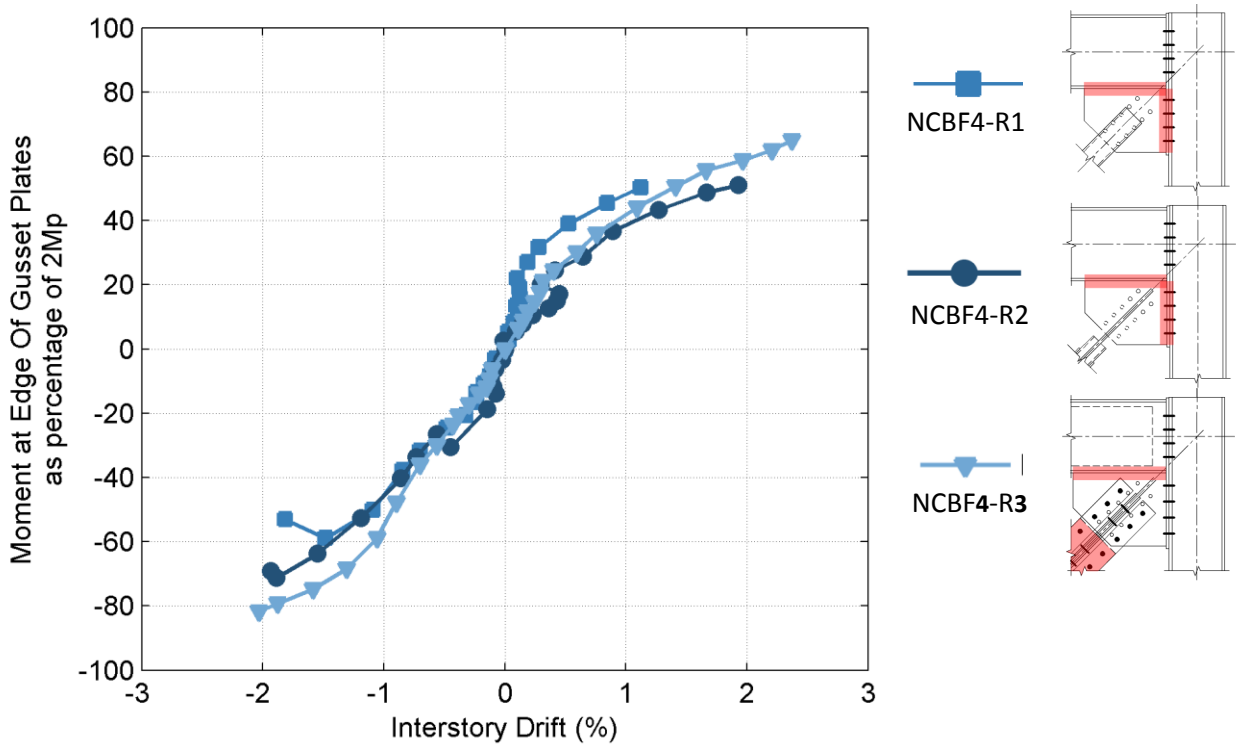

Figure 7-13: Column Moment vs. Interstory Drift for Bolted End Plate Connections

7.3.1.2 Failure Modes

All three bolted end plate connections experienced complete fracture of a beam-to-gusset plate weld during the test. Figure 7-14 shows a normalized beam-to-gusset plate weld crack length vs. the drift in compression. Although these tests sustain complete weld fracture, the cause of weld fracture varied in each test. For the out-of-plane buckling brace (Specimen NCBF4-R1), weld crack initiation occurred at a small drift of 0.6% while the brace was in compression and the weld crack length continued to propagate with each cycle until weld fracture. For the in-plane knife plate retrofit (Specimen NCBF4-R2), weld crack initiation occurred at a larger deformation, but once formed; the weld crack propagated quickly leading to an abrupt failure of the weld just a few cycles later. The weld crack propagation was most likely due to joint opening. In the BRB retrofit (Specimen NCBF4-R3), the weld crack length remained relatively stable up until the last cycle (4.6% drift range) where the BRB core plate began to hinge and the weld tore the remaining length as the BRB deflected out-of-plane. A summary of this information along with the weld DCRs is shown in Table 7-6.

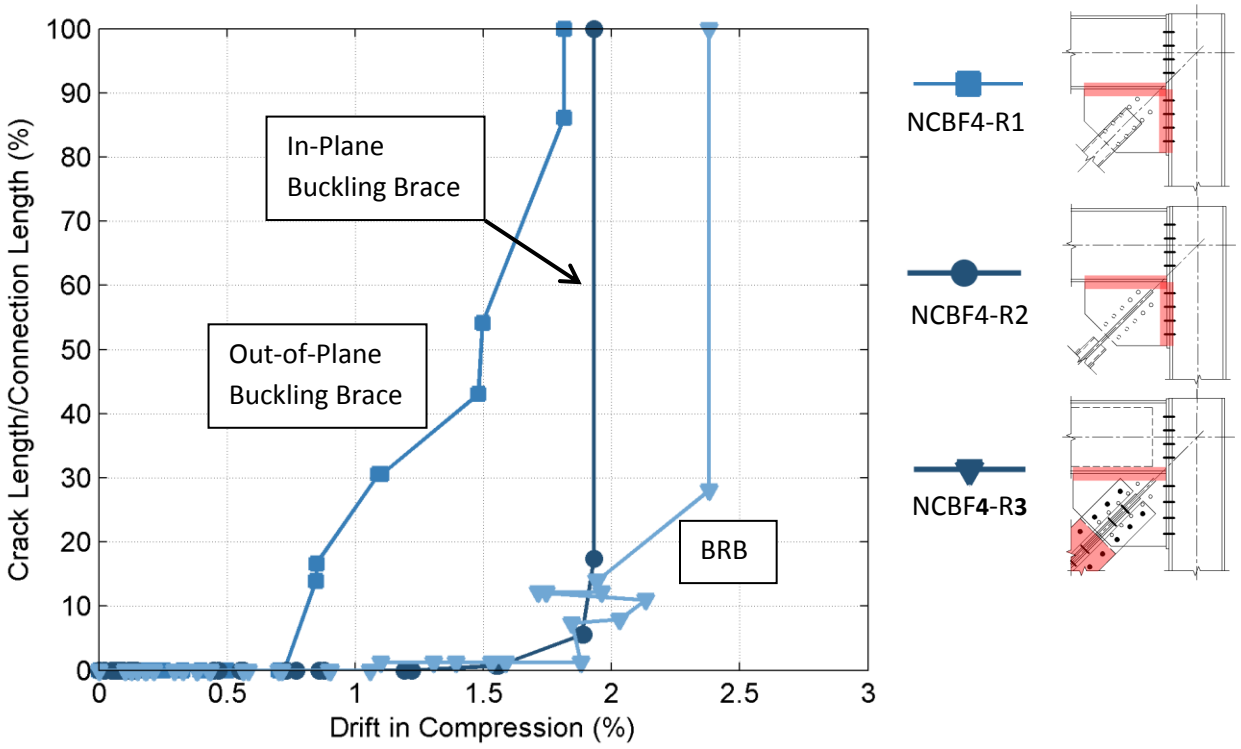

Figure 7-14: Beam-to-Gusset Plate Weld Crack Length vs. Drift in Compression Bolted End Plate Connections.

Table 7-6: Gusset Plate Weld Damage

Specimen Name	Mechanism that Caused Weld Fracture	DCRs		Drift Range at Given PS (%)			
		AISC	BDP	W1	W2	W3	WF
NCBF4-R1	Out-Of-Plane Brace Buckling	0.63	1.58	-0.8	-0.8	-1.1	-1.8
NCBF4-R2	In-Plane Connection Rotation	0.64	1.58	-1.5	-1.9	-1.9	-1.9
NCBF4-R3	In-Plane Connection Rotation - Initial Out-Of-Plane Brace Hinging - Final	0.52	1.61	-1.1	-2.0	-2.4	-2.4

These results show that the weld for the bolted end plate connections was vulnerable to out-of-plane brace deflection as indicated by the BDP weld fracture DCR (~1.6). Although the knife plate retrofit (Specimen NCBF4-R2) seemed to have protected the weld from out-of-plane rotations, the weld was still vulnerable from deformation demands introduced by connection rotation and beam-to-column joint opening. The BRB retrofit (Specimen NCBF4-R3) was also vulnerable to this mechanism but may have been able to resist severe weld crack propagation due to the longer beam-to-gusset connection length (20.5” instead of 18” for Specimens NCBF4-R1 and NCBF4-R2).

7.4 Summary

This chapter compared the response of nine test specimens that shared similarities in connection type and brace type. Each specimen group as outlined in Table 7-1 was compared by considering the frame response (column moments and drift range), brace response (expected capacity and mid-span deflection, and failure modes. By comparing these quantities conclusions about the interdependency of the framing members, the connection, and the brace were determined. The important findings of this effort are summarized below.

- The connection type and connection deficiencies can have a significant impact on the overall drift range a frame can achieve and the failure mode that is observed even when using braces that are considered to be highly ductile.

- Stable yielding mechanisms at the column interface such as bolt hole elongation and gusset plate yielding can help to limit deformation demands on the columns and reduce the amount of forces delivered across the connection interface. Stronger connections such as the bolted end plate connection can transfer forces in excess of the framing members capacity and cause significant column damage depending on the axial flexural interaction.

- The expected capacity of the brace as calculated in Section 2.3.2 provides a good indication of the actual brace capacities in both tension and compression (within 10%) as long as the brace is the controlling yielding mechanism.

- The response of the brace does not depend significantly on the connection type.

- The beam-to-gusset plate weld In an NCBF connection with limited clearance and non-ductile welds is especially vulnerable using an out-of-plane buckling brace. The weld can be protected by providing a continuous connection at the column interface, by making sure that welds can develop the yield capacity of the gusset plate.

- The beam-to-gusset plate weld is also vulnerable considering in-plane deformation demands as evidenced by beam-to-gusset plate weld fractures in Specimens NCBF4-R2 and NCBF4-R3; however, the weld fractures occurred at higher drift ranges near the deformation capacity of the braces.

Chapter 8: Evaluation and Retrofit

8.1 Introduction

This chapter documents and compares the response of all NCBF tests conducted at UW to date using experimentally derived backbone curves. Section 8.2 will describe how the backbone curves are generated for each test and discuss their relevance in evaluation of seismically deficient braced frame structures. Section 8.3 presents the computed experimental backbone curves of 16 tests and tabulates backbone parameters. Section 8.4 compares the individual backbone curves for specimens with similar geometry and failure modes. Comparisons between these backbone curves highlight the failure modes observed in each of the specimens and are used to set up discussion of general retrofit strategies. The observations here are intended to provide guidance and motivation for future testing of NCBFs.

8.2 Evaluation of System Response

Evaluation and retrofit of existing NCBF infrastructure is typically done using procedures outlined in ASCE41 (2013). The current procedures for evaluation and retrofit of NCBF structures in ASCE 41 are presented in more detail in Section 2.2.3, but are revisited here to provide context for the development of experimental backbone curves.

Figure 8-1 shows a general force-deformation backbone curve. These backbone curves can be used to model individual component performance (brace, column, connection, etc.) in nonlinear static and dynamic models. Due to the lack of experimental research on NCBFs, the nonlinear modeling parameters provided depend on the brace and are only slightly modified for connection deficiencies. More work to include connection deficiencies in the modeling is necessary to help engineers determine expected performance of NCBFs and retrofits.

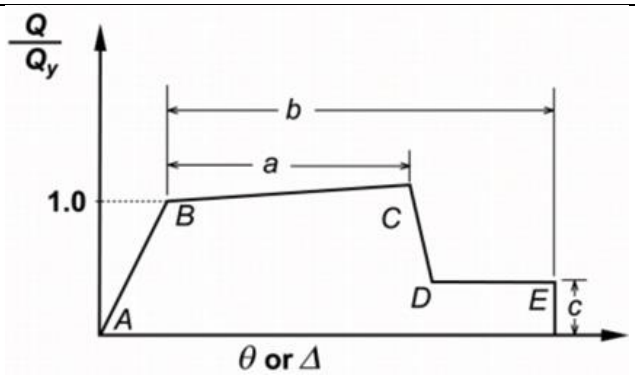

Q/Q_y	Normalized Capacity
θ or Δ	Component Deformation
A	Origin
B	Yield Capacity
C	Ultimate Capacity
D	Residual Capacity
E	Complete Failure
a	Inelastic Deformation Capacity
b	Inelastic Deformation Capacity
c	Residual Capacity

Figure 8-1: Generalized Force-Deformation Relation for Steel Elements or Components (Fig. 9-1 ASCE 2014)

The generalized force-deformation relation shown in Figure 8-1 can be calibrated to represent system and brace force-drift behavior using experimental data as shown in Figure 8-2. This model will be used to represent all of the NCBF experiments tested during the research project.

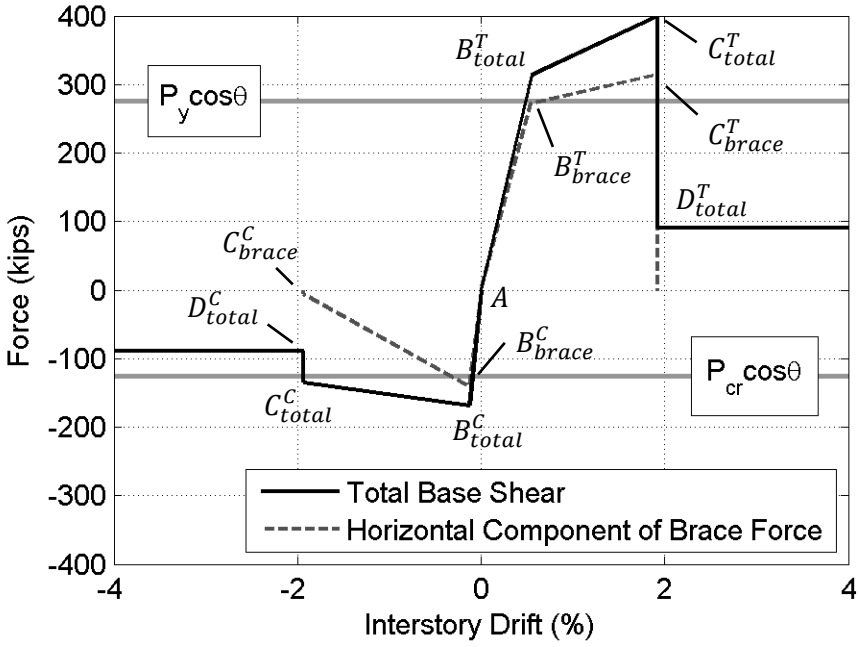

Superscript – indicates if brace is in tension or compression.
Subscript – total base shear or horizontal component of the brace force.
Point B – is the limit of the elastic behavior.
Point C – is the point of rapid degradation (from brace or connection fracture
Point D – is the residual strength after failure.

Figure 8-2: Example BackBone Curve Tabulated Points

Note that point E could not be determined for any of the experiments because the actuator used to load the system did not have adequate stroke capacity to reach the systems deformation at full strength deterioration. A majority of specimens tested using a post-fracture loading protocol were tested until a drift range of at least 4%. In some cases the post-fracture cycles of the frame were run to drift range greater 6% (3 tests, Specimens NCBF0, NCBF3-2, and NCBF4-R1), and in one case up to an 8% drift range (Specimen NCBF0).

Backbone curves for each experiment follow the model presented in Figure 8-2 and are computed for both compression behavior (-drift) and tension behavior (+ drift). The procedure used to calculate experimental backbone parameters is detailed in the list below. Each step of the procedure is represented graphically in Figure 8-3 $(A, B, \& C)$ and Figure 8-4 (D).

1. Generate Base Shear vs. Interstory Drift Hysteresis using procedure defined in Section 6.3.1.
2. Find the maximum force and drift during the first tension and compression peak of each cycle.
3. Find the backbone parameters in tension
   a. Find a least squares linear fit for points[4] on elastic portion of the tension curve. The fit is constrained to pass through the origin.
   b. Find a least squares linear fit for the points on inelastic portion of the tension curve.
   c. Compute B^T - the intercept of the two linear fits.
   d. Compute C^T – value of the second linear fit computed at maximum tensile drift.
4. Find the backbone parameters in compression
   a. Find a least squares linear fit for points on elastic portion of the compression curve. The linear fit is constrained to pass through the origin.
   b. Compute B^C
   c. Find a least squares linear fit for points on inelastic portion of the tension curve. The linear fit is constrained to pass through B_C
   d. Compute C^C – value of the second linear fit computed at compressive drift prior to fracture

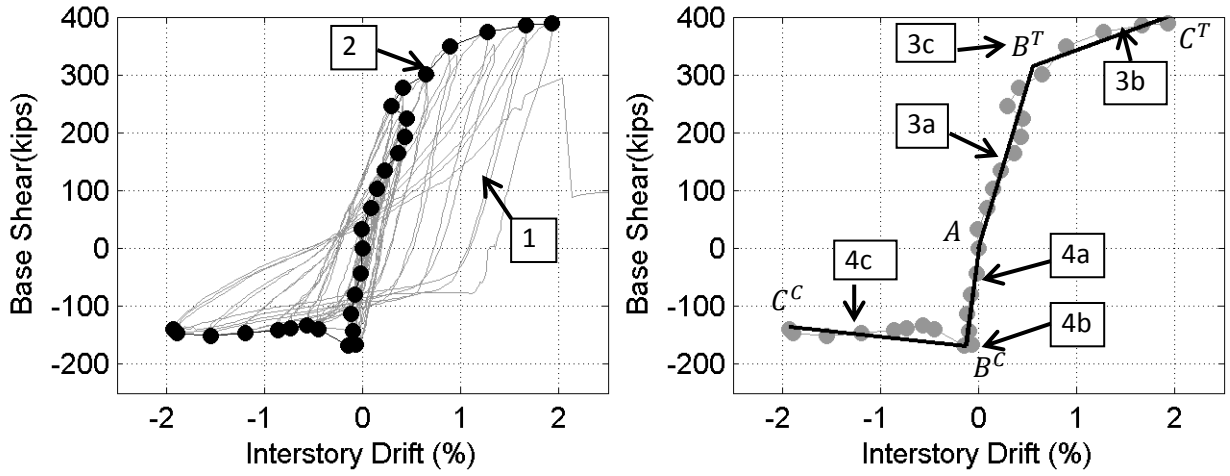

Figure 8-3: Determination of Backbone Parameters B and C

5. Compute the residual frame capacity.
   a. Determine the residual inter-story drift from post-fracture cycles – drift at the x-intercept.

[4] The points used to fit the line segments for the elastic and inelastic portion of the curve are selected such that the intercept (yield point) occurs at a drift level between the drift at the last "elastic" point and the first "inelastic point". For this example 9 points (not including the origin) were selected to represent the elastic portion of the curve while 5 points were selected for the inelastic portion.

b. Find the residual capacity at ±2%[5] of the residual interstory drift using linear interpolation between the peaks.
c. Compute D^T – Residual tension capacity from step 5b at the tension drift just after fracture.
d. Compute D^C – Residual compression capacity from step 5b at the compressive drift just after fracture.

6. Repeat steps 1-6 to find the backbone parameters for the brace. Use the horizontal component of the brace force instead of the total base shear. Note that the brace does not typically have residual capacity.

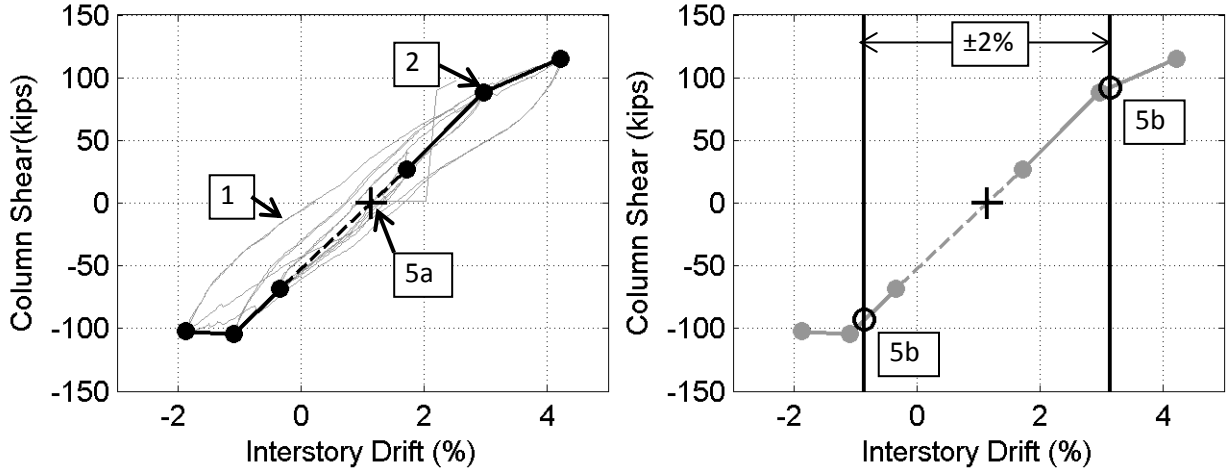

Figure 8-4: Determination of Residual Frame Capacity

8.3 Results

Each test has a unique experimental backbone curve calculated in accordance with Section 8.2. Table 8-1 through Table 8-4 document the computed experimental backbone curves for 14 NCBF tests, 1 reference SCBF test, and 1 reference BRBF test. Interstory drift and force for each of the points on the backbone curves are tabulated for both the system (solid line) and the brace (dashed line). A dash-dot line after fracture in the system backbone curve indicates that there was no post-fracture data available and the residual capacity was inferred. Note that not all tests had adequate data to determine the brace backbone curves.

Each table also contains basic information about each test including the specimen name, type of connection, brace type, connection detail, failure mode (highlighted in the connection detail), and expected tension and compression capacities computed using material test data. More detailed information about the specimens can be found in Chapter 2 or in the individual thesis that the test was originally presented in.

[5] This drift was selected for all of the tests so that the reported values of residual capacity would be consistent. Ideally a larger drift would have been selected because it could be a better representation of the residual capacity; however, the post-fracture data was limited at higher drift ranges and did not allow for consistent calculation beyond the selected drift.

Table 8-1: Experimental BackBone Curve (1 of 4)

Specimen	NCBF1 (Sloat 2014)			NCBF1-R2 (Sloat 2014)			NCBF1-R3 (Sloat 2014)			NCBF1-R4 (Sloat 2014)		
Conn. Type	Continuous Welded Shear Plate			Continuous Welded Shear Plate			Continuous Welded Shear Plate			Continuous Welded Shear Plate		
Brace Type	HSS 7x7x1/4			HSS 5x5x3/8			HSS 5x5x3/8" w/ Knife Plate			HSS 6x4x3/8" w/ Knife Plate		
Connection Detail	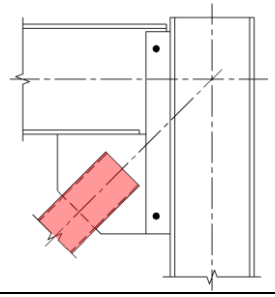			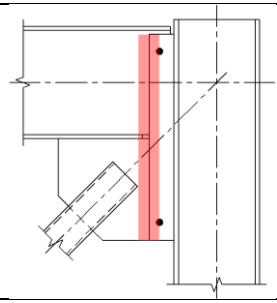			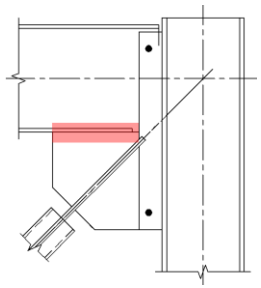			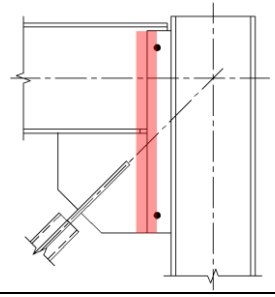		
Backbone Curve	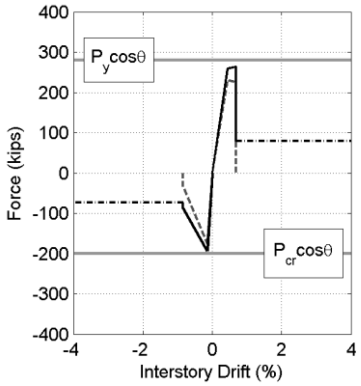			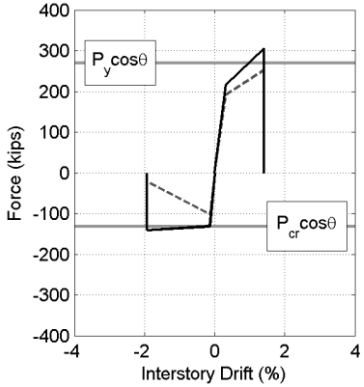			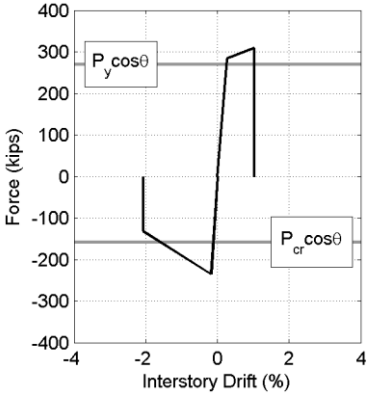			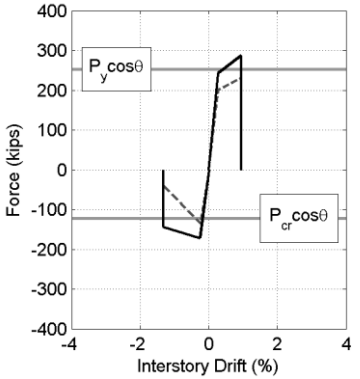		
BackBone Points	δ (%)	Base Shear (kip)		δ (%)	Base Shear (kip)		δ (%)	Base Shear (kip)		δ (%)	Base Shear (kip)	
		Total	Brace		Total	Brace		Total	Brace		Total	Brace
B^T	0.43	259	231	0.33	217	192	0.27	284	-	0.27	243	199
C^T	0.69	264	224	1.41	306	253	1.02	309	-	0.94	287	231
D^T	0.69	80	0	1.41	0	0	1.02	0	-	0.94	0	0
B^C	-0.14	-193	-175	-0.14	-131	-101	-0.18	-234	-	-0.26	-172	-134
C^C	-0.84	-88	-34	-1.93	-140	-21	-2.06	-132	-	-1.33	-143	-39
D^C	-0.84	-73	0	-1.93	0	0	-2.06	0	-	-1.33	0	0

Expected Brace Capacity	Tension (kip)	Comp. (kip)	Tension (kip)	Comp. (kip)	Tension (kip)	Comp. (kip)	Tension (kip)	Comp. (kip)
	281	199	270	132	270	158	250	122

Table 8-2: Experimental BackBone Curves (2 of 4)

Specimen	NCBF1-R5 (Sloat 2014)			NCBF2 (Johnson 2014)			NCBF3-1 (Johnson 2014)			NCBF3-2 (Johnson 2014)		
Conn. Type	Continuous Welded Shear Plate			Continuous Bolted Shear Plate			Split Bolted Shear Plate			Split Bolted Shear Plate		
Brace Type	HSS 7x7x1/4" – Concrete In-Fill			HSS 5x5x3/8"			HSS 6x6x1/4"			HSS 5x5x3/8"		
Connection Detail	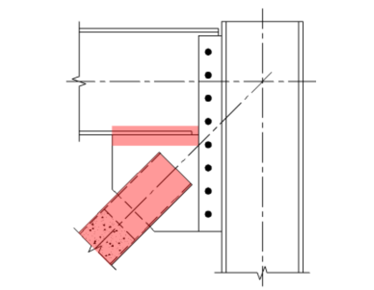			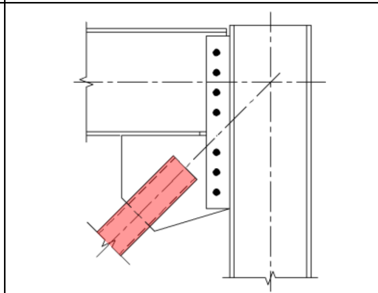			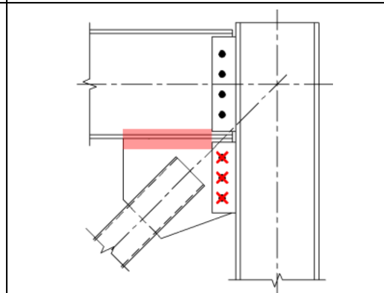			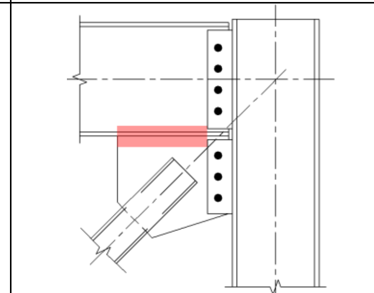		
Backbone Curve	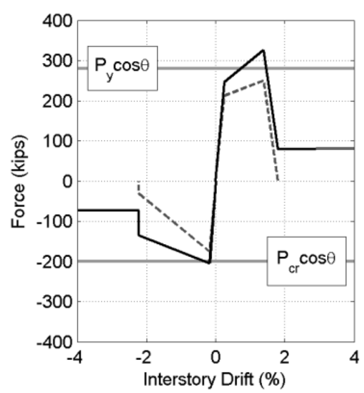			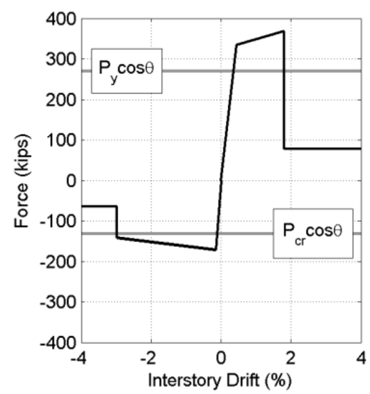			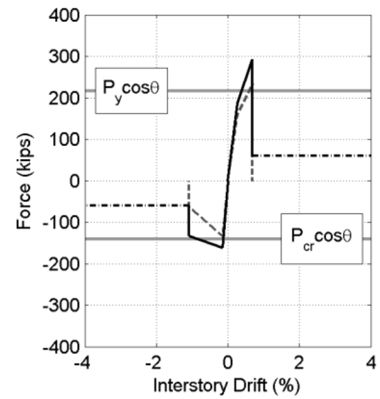			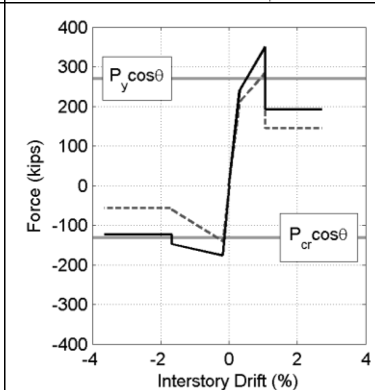		
BackBone Points	δ (%)	Base Shear (kip)		δ (%)	Base Shear (kip)		δ (%)	Base Shear (kip)		δ (%)	Base Shear (kip)	
		Total	Brace		Total	Brace		Total	Brace		Total	Brace
B^T	0.25	245	212	0.44	335	-	0.27	186	159	0.31	241	211
C^T	1.38	326	250	1.80	369	-	0.69	292	235	1.06	350	284
D^T	1.80	80	0	1.80	78	-	0.69	60	0	1.06	192	145
B^C	-0.18	-204	-175	-0.15	-171	-	-0.15	-161	-134	-0.18	-176	-140
C^C	-2.22	-134	-31	-2.97	-141	-	-1.08	-133	-62	-1.67	-147	-61
D^C	-2.22	-73	0	-2.97	-65	-	-1.08	-60	0	-1.67	-124	-58

Expected Capacity	Tension (kip)	Comp. (kip)	Tension (kip)	Comp. (kip)	Tension (kip)	Comp. (kip)	Tension (kip)	Comp. (kip)
	281	199	270	131	217	140	270	131

Table 8-3: Experimental BackBone Curves (3 of 4)

Specimen	NCBF4-R1		NCBF4-R2		NCBF5		NCBF0 (Powell 2010)	
Conn. Type	Bolted End Plate		Bolted End Plate		Integrated Shear Plate		Bolted Angle Connection	
Brace Type	HSS 5x5x3/8”		HSS 6x4x3/8” – w/ Knife Plate		HSS 5x5x3/8”		HSS 6x6x1/4”	
Connection Detail	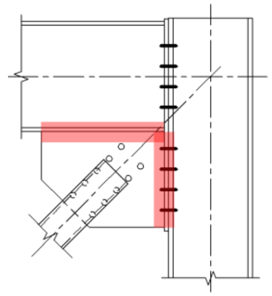		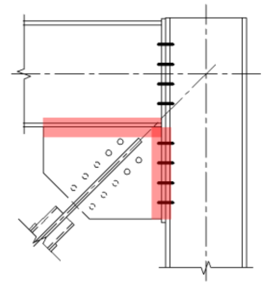		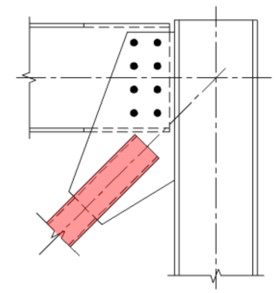		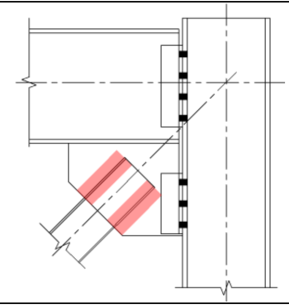	
BackBone Curve	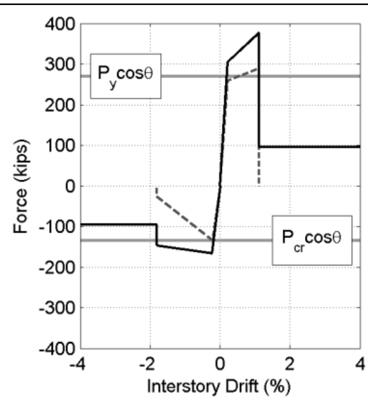		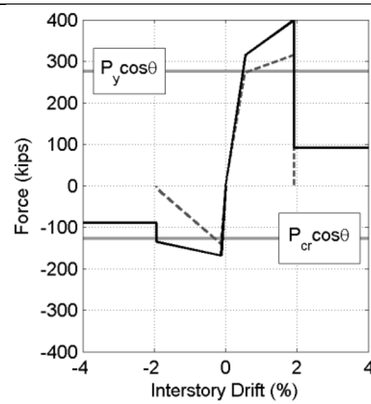		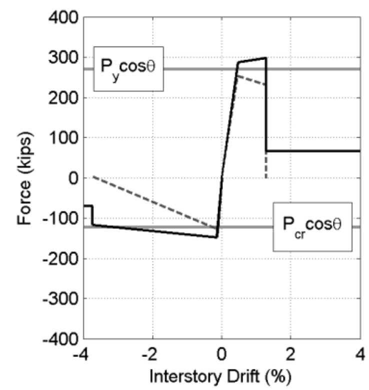		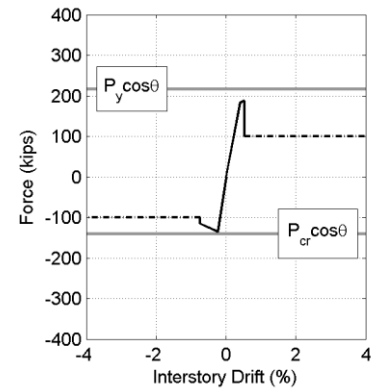	

BackBone Points	δ (%)	Base Shear (kip)		δ (%)	Base Shear (kip)		δ (%)	Base Shear (kip)		δ (%)	Base Shear (kip)	
		Total	Brace		Total	Brace		Total	Brace		Total	Brace
B^T	0.22	306	258	0.56	315	272	0.48	287	253	0.36	177	0.36
C^T	1.12	378	290	1.93	400	315	1.28	298	231	0.53	183	0.53
D^T	1.12	96	0	1.93	91	0	1.28	66	0	0.53	102	0.53
B^C	-0.23	-166	-133	-0.13	-168	-140	-0.14	-148	-127	-0.22	-131	-0.22
C^C	-1.81	-147	-25	-1.93	-135	-6	-3.73	-116	3	-0.79	-91	-0.79
D^C	-1.81	-96	0	-1.93	-89	0	-3.73	-71	0	-0.79	-111	-0.79

Expected Brace Capacity	Tension (kip)	Comp. (kip)	Tension (kip)	Comp. (kip)	Tension (kip)	Comp. (kip)	Tension (kip)	Comp. (kip)
	271	134	276	126	271	123	217	-140

Table 8-4: Experimental BackBone Curve (4 of 4)

Specimen	HSS08 (Herman 2007)	BRB05 (Christopulos 2005)	NCBF2-R1	NCBF4-R3
Conn. Type	Fully Restrained Moment Conn.	Fully Restrained Moment Conn.	Continuous Bolted Shear Plate	Bolted End Plate
Brace Type	HSS 5x5x3/8”	BRB A = 4.8in^2	BRB A = 4.8in^2	BRB A = 4.8in^2
Connection Detail	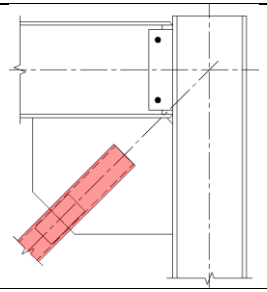	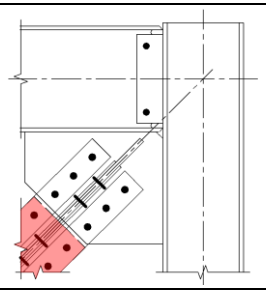	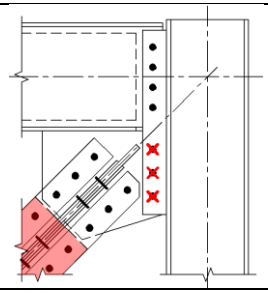	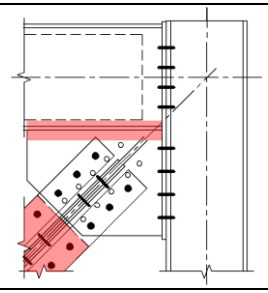
Backbone Curve	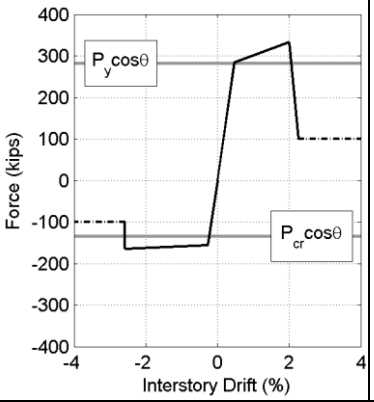	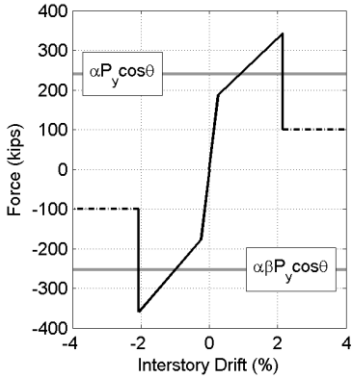	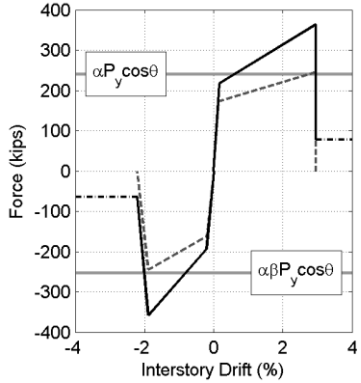	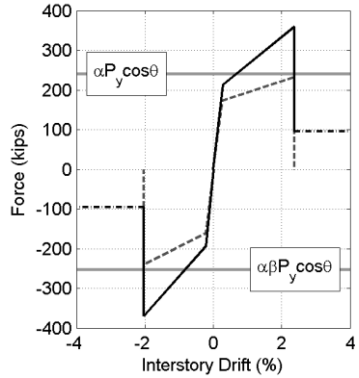

BackBone Points	δ (%)	Base Shear (kips)		δ (%)	Base Shear (kips)		δ (%)	Base Shear (kips)		δ (%)	Base Shear (kips)	
		Total	Brace		Total	Total		Total	Total		Total	Total
B^T	0.48	287	253	0.26	187	-	0.17	218	172	0.29	214	173
C^T	1.28	298	231	2.16	343	-	2.97	364	245	2.37	360	232
D^T	1.28	66	0	2.16	100	-	2.97	78	0	2.37	96	0
B^C	-0.14	-148	-127	-0.25	-176	-	-0.21	-193	-162	-0.22	-194	-159
C^C	-3.73	-116	3	-2.06	-359	-	-1.89	-358	-244	-2.03	-369	-240
D^C	-3.73	-71	0	-2.06	-100	-	-2.20	-65	0	-2.03	-96	0

Expected Brace Capacity	Tension (kip)	Comp. (kip)	Tension (kip)	Comp. (kip)	Tension (kip)	Comp. (kip)	Tension (kip)	Comp. (kip)
	271	123	240	253	240	252	240	253

8.4 Evaluation of Failure Modes and Retrofit Strategies

Table 8-5 lists all of the brace types used in the 14 NCBF specimens and indicates the number of braces that failed in each category along with the drift range achieved prior to brace fracture. For brace types that had multiple brace fractures the average drift range was taken. As shown, only 6 of 14 specimens had a brace failure mode. All the other connections failed to develop the full deformation capacity of the brace and suffered from premature connection fracture. The failure modes of the connections are of particular interest when considering retrofit.

Table 8-5: Brace Type and Failures

Brace Type	# of Specimens	# of Brace Failures	Drift Range at Fracture
Highly Ductile 5x5x3/8"	5	2	4.8%
Non Compact 7x7x1/4"	3	1	1.5%
Non Compact 7x7x1/4" Concrete In-Fill	1	1	3.6%
Highly Ductile 5x5x3/8" In-Plane	1	0	(3.1%)[1]
Moderately Ductile 6x4x3/8" In-Plane	2	0	(3.9%)[1]
BRB Retrofit	2	2	4.9%

1 – Maximum Drift Range Achieved Before Connection Fracture

Table 8-6 lists each of the potential failure modes for all NCBF baseline and retrofit tests and shows the number of frames that were deficient considering that failure mode along with the number of frames that failed by that failure mode. Average DCRs and average drifts are taken only for the specimens that experienced the specified failure mode. The most prevalent failure modes included gusset plate weld fracture (BDP), brace fracture, bolt shear rupture, and splice weld fracture. Each of these failure modes will be discussed in the Sections 8.4.1 - 8.4.5.

Table 8-6: Failure Modes Observed in All NCBF Specimens

Connection Failure Modes	Deficient		Average Drift Range at Failure	Not Deficient		NA # Specimens
	Deficient Specimens	Failures Observed		Compliant Specimens	Failures Observed	
Gusset Plate Weld Fracture (BDP)	13	8	2.9%	1	0	0
Gusset Plate Weld Fracture (AISC)	5	3	2.9%	9	5	0
Bolt Shear Rupture	6	2	3.5%	4	0	4
Brace Splice Weld Fracture	1	1	1.3%	13	0	0
Net Section Fracture	11	0	NA	1	0	2
Whitmore Fracture	1	0	NA	13	0	0
Block Shear Rupture	5	0	NA	9	0	

8.4.1 Splice Weld Fracture

Figure 8-5 shows the backbone curves for the one NCBF test to experience brace-to-gusset splice weld fracture. Splice weld fracture is a failure mode upon which the weld (or bolt group) connecting the brace to the gusset plate ruptures. For a welded splice (used in all of the NCBF tests), this is a brittle failure mode and leads to an abrupt loss of capacity. Specimen NCBF0 was the only NCBF test in the testing program to have a splice weld fracture deficiency (DCR = 1.7) and non-coincidentally was the only specimen to experience splice weld fracture. This failure mode developed at a drift range of only 1.3%. Note that the frame was still able to achieve a modest residual capacity at negative drifts because the brace developed compressive force from contact between the brace and gusset plate while the brace was in compression.

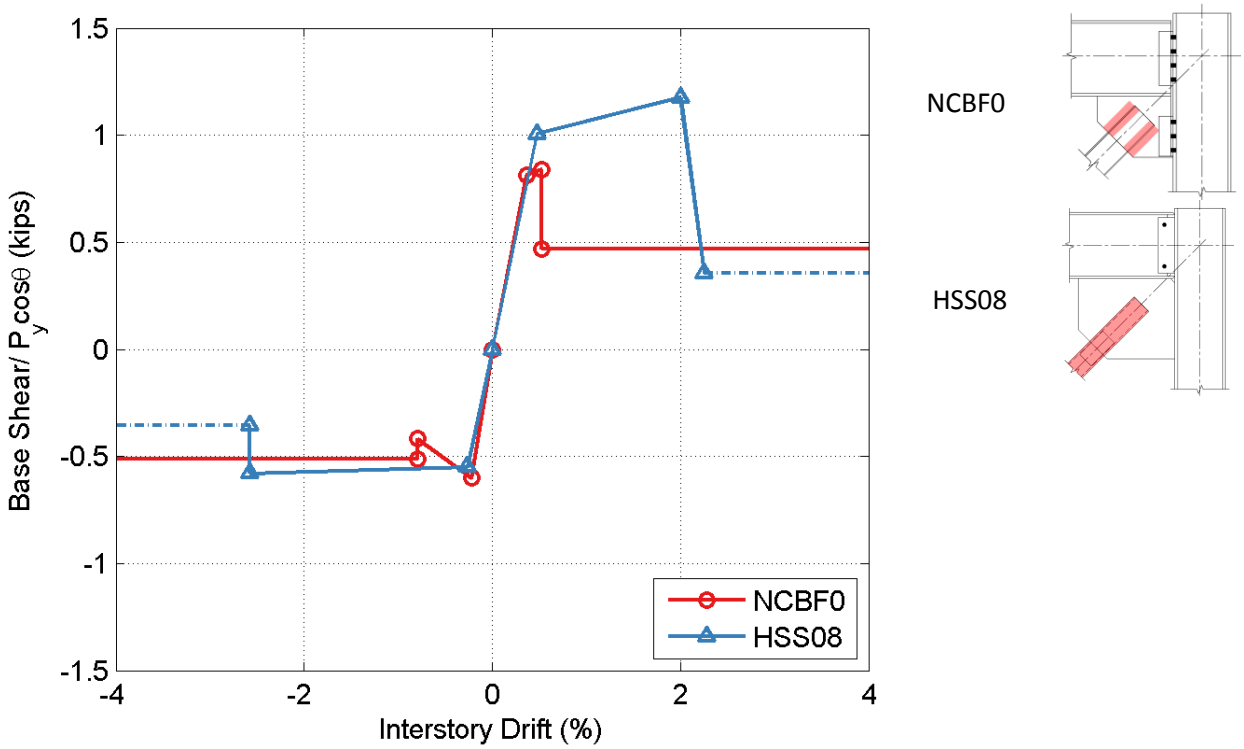

Figure 8-5: Splice Weld Fracture

These results indicate that a splice connection deficiency can severely limit the drift capacity and lateral resistance of the frame. Retrofit strategies for a splice weld include brace replacement with a compliant splice detail, or weld reinforcement/overlay of the splice weld. There are no tests of the latter, which could be a topic of future research, and there are also no tests of deficient bolted splice connections.

8.4.2 Brace Fracture

Figure 8-6 shows the backbone curves for three of the six specimens that achieved brace fracture. Specimen NCBF1 used a non-compact 7x7x1/4" brace that fractured at a drift range of 1.5%. Specimen NCBF1-R5 was nominally the same as Specimen NCBF1 except that the shear plate was reinforced with bolts and the brace was filled with concrete and represents a retrofit strategy for non-compact braces. The concrete fill prolonged the fracture life of the brace and achieved a drift range of 3.6%. Specimen HSS08 (Herman 2007) (highly ductile 5x5x3/8" brace) is shown for reference and represents the frame performance of an SCBF specimen.

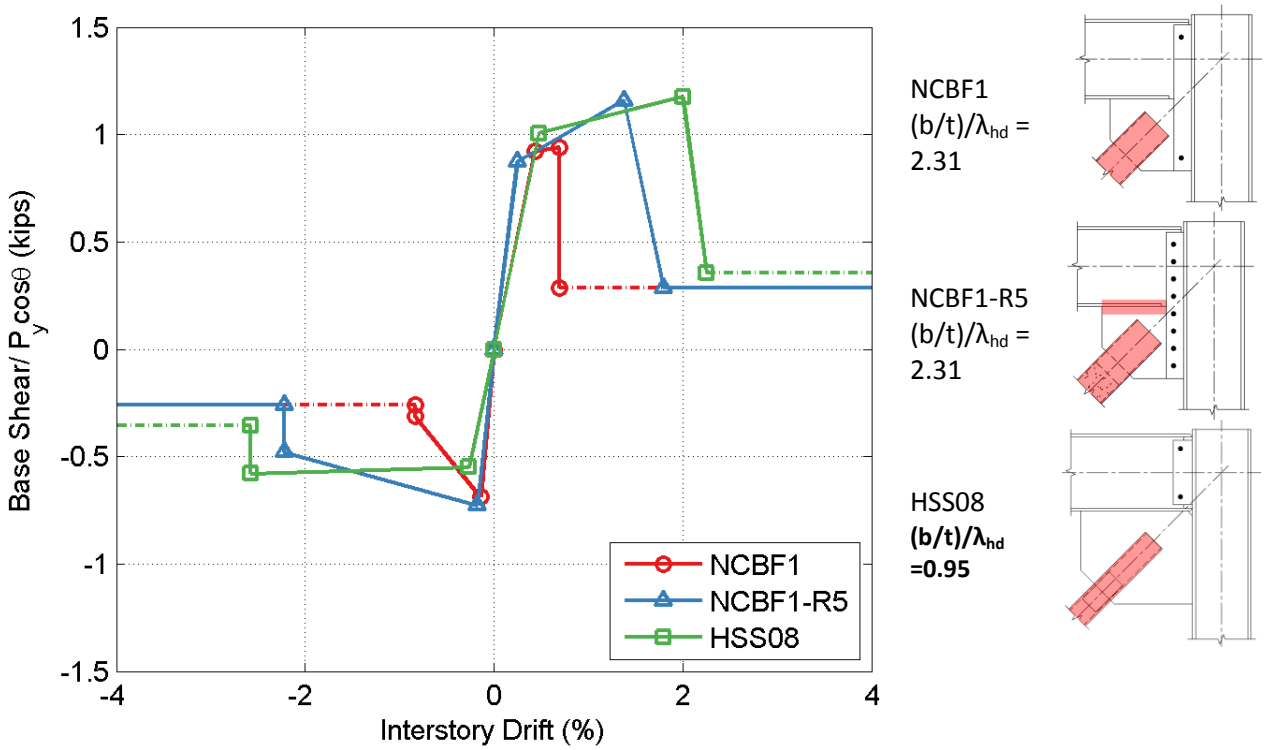

Figure 8-6: Non-Compact Brace

These results show that a non-compact brace can severely limit the deformation capacity and lateral resistance of the frame. Retrofit strategies include filling the brace with concrete (specimen NCBF1-R5), replacing the brace with a highly ductile brace, and replacing the brace with a BRB. Often times, non-compact braces cannot simply be retrofit with a highly ductile brace because of slenderness concerns, while retrofitting with BRBs can be costly. Filling the non-compact brace with a concrete infill is a promising retrofit strategy for existing infrastructure because it does not require removal of the brace for retrofit and is applicable to a significant portion of existing infrastructure that utilize non-compact braces. For the connection tested in Specimens NCBF1 and NCBF1-R5, this retrofit increased the drift range from 1.5% to 3.6%. This type of retrofit has only been tested in one connection configuration and should be tested using a different connection type to verify its deformation capacity.

8.4.3 Gusset Plate Weld Fracture

Complete weld fracture of the beam-to-gusset plate weld or the column interface weld occurred in 8 of the 14 NCBF specimens tested. Table 8-7 shows all of the gusset plate welds that fractured and contains information about the weld DCRs, clearance, drift range, and brace type. Since all of the specimens have non-ductile welds, limited brace end clearance, inability to develop the capacity of the gusset plate, and different connection types it is difficult to pinpoint which variable is the most important when considering gusset plate weld fracture at the beam or column interfaces. These variables are also analyzed in more detail in Chapter 7, but are presented here to show the importance of the failure mode.

Table 8-7: NCBF Gusset Plate Weld Details

Specimen Name	Location of the Weld	Fracture	DCR		Clearance (elliptical)	Drift Range	Brace Type
			GP	BR			
NCBF0	Beam-to-Gusset Plate	No	1.26	0.62	$1.4t_{gp}$	1.3	OOP
	Gusset Plate-to-angle	No	1.26	0.91			
NCBF1	Beam-to-Gusset Plate	No	0.67	0.65	2.9 t_{gp}	1.5	OOP
	Column Interface Weld	No	1.35	1.28			
NCBF1-R2	Beam-to-Gusset Plate	No	0.67	0.63	3.8 t_{gp}	3.3	OOP
	Column Interface Weld	Yes	1.35	1.22			
NCBF1-R3	Beam-to-Gusset Plate	Yes	0.67	0.63	-	3.1	IP[1]
	Column Interface Weld	Yes	1.35	1.22			
NCBF1-R4	Beam-to-Gusset Plate	No	0.67	0.59	2.5 t_{gp}	2.3	IP
	Column Interface Weld	Yes	1.35	1.14			
NCBF1-R5	Beam-to-Gusset Plate	Yes	0.67	0.65	1.4 t_{gp}	3.6	OOP
	Column Interface Weld	No	1.35	1.28			
NCBF2	Beam-to-Gusset Plate	No	1.06	0.76	1.5 t_{gp}	4.7	OOP
NCBF2-R1	Beam-to-Gusset Plate	No	0.74	0.83	-	5.2	BRB
NCBF3-1	Beam-to-Gusset Plate	Yes	1.62	0.38	1.1 t_{gp}	1.8	OOP
NCBF3-2	Beam-to-Gusset Plate	Yes	1.12	0.64	1.8 t_{gp}	2.7	OOP
NCBF4-R1	Beam-to-Gusset Plate	Yes	1.58	0.63	4.1 t_{gp}	2.9	OOP
	Gusset-to-End Plate	Yes	1.58	0.71			
NCBF4-R2	Beam-to-Gusset Plate and	Yes	1.58	0.64	-	3.9	IP
	Gusset-to-End Plate	Yes	1.58	0.72			
NCBF4-R3	Beam-to-Gusset Plate	Yes	1.58	0.52	-	4.6	BRB
	Gusset-to-End Plate	No	1.58	0.56			

1 – Specimen NCBF1-R3 was designed to buckle in-plane, but actually buckled out-of-plane.
Elliptical clearances that are not marked are negative.

Retrofit strategies for the beam-to-gusset plate weld include gusset plate replacement with properly detailed demand critical weld, weld reinforcement, an in plane buckling brace, or a buckling restrained brace. Retrofit of a deficient beam-to-gusset plate with in-plane and BRB retrofit strategies weld was

studied with Specimens NCBF4-R2 and NCBF4-R3 respectively and is discussed in 7.3.1.2. Weld reinforcement of the gusset plate has been studied with mixed results, but could be of interest for future testing because it is a more cost effective retrofit than gusset plate and/or brace replacement.

8.4.4 Bolt Shear Fracture

Four of the specimens had deficiencies in bolt shear (represented in Table 8-8), and three of these specimens experienced bolt fracture in the gusset plate-to-shear plate connections (highlighted in Table 8-8). For Specimen NCBF2-R1 bolt fracture did not occur until a drift range of 5.2% and is not much of concern. For Specimen NCBF3-1 bolt fracture occurred at a drift range of 1.8% and is of more interest. Bolt fracture for Specimen NCBF3-2 occurred after beam-to-gusset plate weld fracture. All bolts for these four specimens were 1" diameter A325-X.

Table 8-8: Bolt Shear/ Bolt Bearing

Connection Type	Specimen Name	Thicknesses			DCR (bolts in beam web)		DCR (bolts in gusset plate)		Drift Range at Bolt Fracture
		Beam Web	Gusset Plate	Shear Plate	Bearing	Shear	Bearing	Shear	
Continuous Bolted Shear Plate	NCBF2	0.345"	3/4"	3/4"	0.76	1.14	0.76	1.14	NA
	NCBF2-R1	0.345"	3/4"	3/4"	0.69	1.05	0.69	1.05	5.2
Split Bolted Shear Plate	NCBF3-1	0.345"	3/4"	3/4"	1.17	0.82	0.60	1.04	1.8
	NCBF3-2	0.345"	1/2"	3/4"	1.35	0.94	0.88	1.12	6.4

1 – Specimen NCBF1-R5 is actually a welded continuous shear plate reinforced with bolts.

To help understand the bolt shear failure in Specimen NCBF3-1, consider the two split bolted shear plate connections (Specimens NCBF3-1 and NCBF3-2) shown in Figure 8-7. Both specimens experienced beam-to-gusset plate weld fracture at a drift range less than three percent. In Specimen NCBF3-1 (3/4" gusset plate), the three bolts connecting the shear plate and gusset plate failed in shear the cycle after weld fracture. In Specimen NCBF3-2 (1/2" gusset plate), those same three bolts went into bearing, and a significant amount of bolt hole elongation (>1/2") developed in the ensuing cycles. Figure 8-8 shows the two split bolted shear plate connections after fracture. In Specimen NCBF3-2 the photo is taken at a drift range greater than 6%.

Since the connection for Specimen NCBF3-2 was able to remain in-tact the brace could still contribute to the lateral resistance leading to a post-fracture residual strength over twice that of Specimen NCBF3-1. Bolt hole elongation continued in Specimen NCBF3-2 until a drift range of 6.4% upon which the bolts fractured. These results show that bolt bearing as a yielding mechanism can delay bolt shear fracture in connections that are considered to be deficient in bolt shear. This is especially relevant when considering collapse prevention performance state in ASCE 41 evaluation and retrofit.

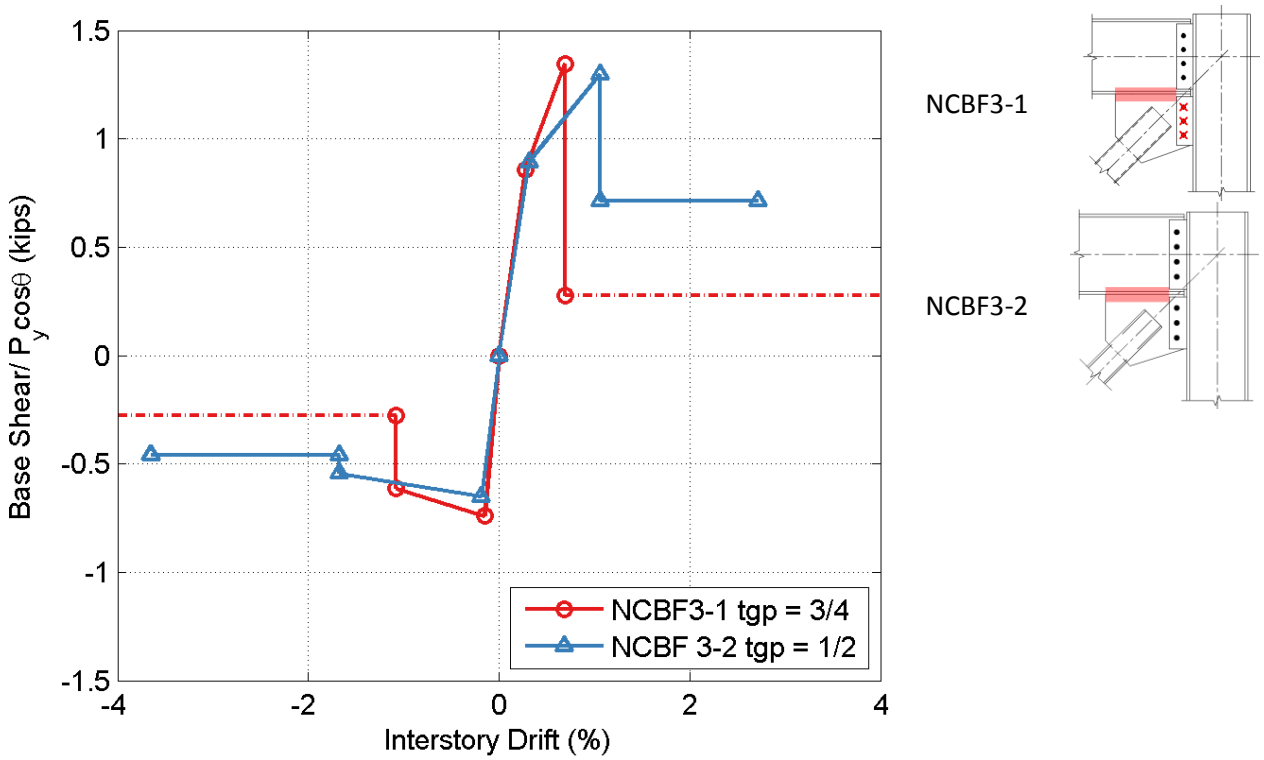

Figure 8-7: Bolt Shear Fracture

a. NCBF3-1 b. NCBF3-2

Figure 8-8: Split Shear Plate Connections After Weld Fracture

Retrofit strategies for bolt shear deficiencies include the addition of more bolts and replacing bolts with higher strength bolts. This deficiency may not need to be addressed if bolt bearing is a controlling mechanism over bolt shear

8.4.5 Buckling Restrained Brace Retrofit

Figure 8-9 shows the backbone curves for the two BRB retrofit specimens and the reference BRBF connection. As shown the backbone curves for all three are similar for both tension and compression behaviors except for Specimen NCBF2-R1 which had a larger interstory drift while the brace was in tension. The difference between the drifts is related to the bolt hole deformation in the shear plate bolts and is discussed in Section 6.3.1. Additionally, the ultimate failure mode of each specimen was hinging of the BRB core plate that resulted due to instability in the connection. This comparison shows that the BRB can be used successfully as a retrofit option and achieve drift ranges compared to a BRBF.

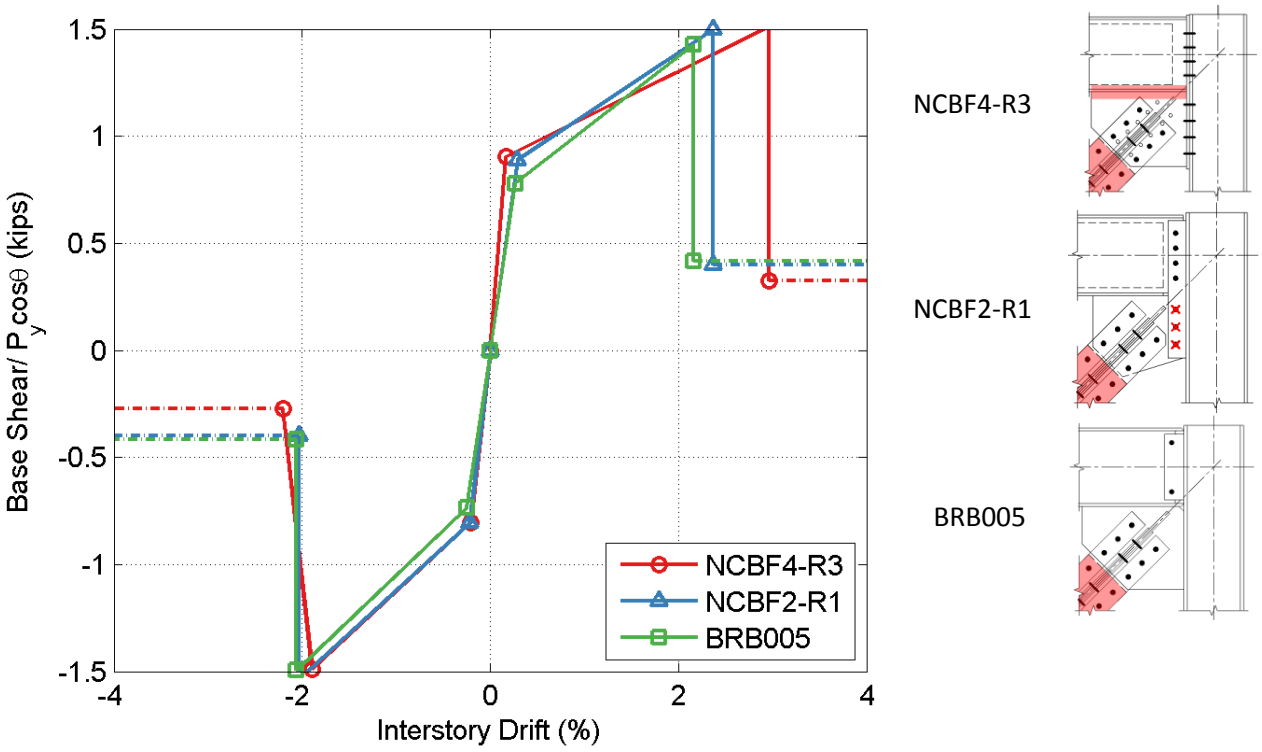

Figure 8-9: BackBone Comparison for BRB Tests

Chapter 9: Summary and Conclusions

9.1 Introduction

This chapter provides a summary of the work completed for this thesis and offers conclusions and recommendations for future work based on the results and comparisons of 14 single bay NCBF and NCBF retrofit experiments. Section 9.2 summarizes the results of five experiments conducted uniquely for this thesis and discusses how they were compared to the other nine experiments conducted by Hsiao et. all (2012), Sloat (2014) and Johnson (2014). Section 9.3 goes through the important conclusions made about the interdependencies of the brace, connection, and frame performance as well as the impact the variance of these elements can have on the yield hierarchy and failure modes observed. Section 9.4 discusses recommendations for future work both analytically and experimentally and is based on the results of this study.

9.2 Summary

The research presented in this thesis builds on work done by Hsiao (2012), Sloat (2014), and Johnson (2014) and is part of a larger research collaboration to develop a better understanding of the behavior of NCBFS. A total of five experiments were conducted to evaluate the behavior of different NCBF connection types with different brace types. Among the five tests, three tests used a bolted end plate connection, one used an integrated gusset-shear plate, and one used a bolted continuous shear plate. Each specimen had a unique combination of deficiencies, brace type, connection type and as a result different yield hierarches and failure modes were observed. The goals and results of each experiment are summarized below.

- **Specimen NCBF4-R1: Bolted End Plate with Out-of-Plane Buckling Brace**
  Goals: Determine the deformation capacity, yield hierarchy, and failure mode of a single-bay frame using a bolted end plate connection that was similar to bolted end plate reference connections found in a review of existing NCBFs. Provide an evaluation of the bolted end plate connections with a common brace type (highly ductile out-of-plane buckling brace) for a comparison point to other tests (Specimens NCBF1-R2, NCBF2, and NCBF3) conducted by Sloat (2014) and Johnson (2014).

  Results: Specimen NCBF4-R1 developed beam-to-gusset plate weld cracking at a drift range of 1.1% as a result of out-of-plane buckling. The continuity provided by a continuous end plate along with prying action at the inner beam flange at the center of the end plate facilitated the redistribution of forces as the weld tore and ultimately allowed the specimen to achieve a final drift range of 2.9% despite having a high BDP weld fracture deficiency (1.58), a non-demand critical weld, limited brace end elliptical clearance (4.1 times the thickness of the gusset plate) and significant tearing of the beam-to-gusset plate weld. Fracture of the beam-to-gusset plate

weld led to weld fracture of the gusset plate-to-end plate weld ending the test. The bolted end plate connection was able to develop the yield capacity of the brace and transferred a relatively high amount of forces across the connection interface into the column. Primary yielding mechanisms include brace buckling, brace tensile yielding, and gusset plate yielding.

- **Specimen NCBF4-R2: Bolted End Plate with In-Plane Buckling Brace**
  Goals: Determine if an in-plane buckling brace retrofit would improve the ductility of Specimen NCBF4-R1. In-plane buckling reduces the gusset plate stresses and strains at the welds by eliminating gusset plate out-of-plane rotation.

  Results: The in-plane knife plate buckling retrofit of Specimen NCBF4-R2 successfully protected the beam-to-gusset plate from out-of-plane deformation demands but was not able to completely prevent beam-to-gusset plate weld damage from occurring. Weld fracture of the beam-to-gusset plate weld occurred at a drift range of 3.9% and was induced by the in-plane connection rotations from opening and closing of the connection joint. Although weld fracture was the final failure mode, brace tearing had also begun developing at the mid-span of the brace just prior to weld fracture. Primary yielding mechanisms include brace in-plane buckling, brace tensile yielding, knife plate yielding, gusset plate yielding, and some local compressive column buckling/ yielding as a result of axial/moment interaction in the column.

- **Specimen NCBF4-R3: Bolted End Plate with Buckling Restrained Brace**
  Goals: Test an alternative brace retrofit option (BRB) that could limit the deformation demands on the deficient gusset plate welds of an existing gusset plate in a bolted end plate connection. Determine the response and performance of a specimen having a bolted end plate connection over the maximum deformation and force ranges of a highly ductile BRB.

  Results: Specimen NCBF4-R3 achieved the highest drift range of the three bolted end plate connections (4.6%) and failed due to hinging of the BRB core plate at the edge of its casing. This failure mode developed after a significant amount of yielding and deformation was observed in the columns. The deformation in the plastic hinge region of the column caused the columns to shorten and reduced the post-tension force in the columns. Prior to reaching brace hinging the columns had to be re-tensioned twice in an effort to prevent uplift. The primary yielding mechanisms in Specimen NCBF4-R3 include BRB core plate yielding in tension and compression along with local compressive column buckling/ yielding as a result of axial/moment interaction in the column.

- **Specimen NCBF5: Integrated Gusset-Shear Plate with Out-of-Plane Buckling Brace**
  Goals: Determine the deformation capacity of a single-bay frame having an integrated gusset-shear plate connection that was representative of the integrated connections found in a review of existing infrastructure. Provide an evaluation of the integrated gusset-shear plate connections with a common brace type (highly ductile out-of-plane buckling brace) for a

comparison point to other tests (Specimens NCBF1-R2, NCBF2, and NCBF3) conducted by Sloat (2014) and Johnson (2014).

Results: Specimen NCBF5 suffered from severe local buckling of the beam web at a drift range of 2.3% which limited the amount of force that could be transferred from the actuator to the connection until the inside of a coped flange came into contact with the gusset plate. After that point, the frame was able to develop a total drift range of 5.0% (1.3% in tension 3.7% in compression) and achieved brace fracture. Damage in the connection aside from beam web local buckling was limited and the columns were virtually undamaged. This specimen developed the smallest amount of column shear forces in part due to the beam web local buckling but also because it was the most flexible connection and weakest connection. Bolt hole elongation in the beam web accommodated most of the connection rotation.

- **Specimen NCBF2-R1: Bolted Continuous Shear Plate with Buckling Restrained Brace**
  Goal: Test brace retrofit option (BRB) that could be used to replace deficient non-compact braces seen in the infrastructure review. Provide comparison point to the other BRB retrofit test Specimen NCBF4-R3 to determine the impact of the connection type on the system performance.

  Results: Specimen NCBF2-R1 achieved a drift range of 5.2% and failed due to a combination of bolt fracture in the gusset plate-to-shear plate bolts and out-of-plane hinging of the BRB core plate at the edge of the casing. Bolt hole elongation in the beam web allowed the beam/gusset to displace vertically relative to the column and develop higher drifts in tension than in compression (3.0% drift in tension and 2.2% drift in compression). Bolt shear deformation also contributed to this mechanism, but the deformation demands on the bolts eventually caused them to fracture at a drift range of 5.2% leading to BRB out-of-plane core plate hinging. The columns also developed local buckling at the edge of the gusset plates but in general sustained an acceptable amount of damage.

The experimental results for the specimens were analyzed and compared to previous NCBF tests conducted by Sloat (2014) and Johnson (2014) using a connection test matrix of five connection types and 3 brace retrofit options. Observations and conclusions of these comparisons are contained in Section 9.3.

Backbone curves were generated for the five tested specimens as well as nine previous NCBF tests. These backbone curves follow the format of ASCE 41 generalize force-deformation relationships for steel and were used to compare common failure modes and deficiencies of all NCBF specimens. Quantities were normalized by expected brace capacities and facilitated the comparison of similar specimens. This comparison highlighted the relative importance of limit states in being able to predict specimen performance. Gaps in the research and areas of interest were also identified and are used in part to guide the recommendations for future work contained in 9.4.

9.3 Conclusions

9.3.1 Evaluation of Brace Retrofit Options

Retrofit of NCBFs with a highly ductile brace can achieve a performance level similar to SCBFs depending on the connection type, deficiencies, and other factors such as beam and column sizes. A total of three brace retrofit options were examined and the important considerations for each type of brace retrofit option are discussed below.

- **Highly ductile out-of-plane buckling HSS braces:** Out-of-plane buckling braces can induce high deformation demands at the edges of the gusset plates. Using these braces with existing gusset plates can lead to premature weld fracture due to limited brace end clearance, inability of the welds to develop the yield capacity of the gusset plate, and the non-ductile welds typically used in older construction.

- **Moderately ductile in-plane buckling HSS braces:** Retrofit with an in-plane buckling brace, achieved with knife plates, can be used successfully to reduce or eliminate out-of-plane deformation demands on existing gusset plate interface welds. A non-symmetric brace section may be necessary to force in-plane buckling for this type of retrofit.

- **Buckling restrained braces:** Retrofit with BRBs is a versatile solution that enables an engineer to replace non-ductile braces over large bay dimensions and provides a balanced response that eliminates out-of-plane deformation demands on connection relative to a similar set of buckling braces. BRBs develop increasing levels of force with increasing drift and can place large force demands on the connection and framing elements. Care must be taken to ensure an appropriate level of joint rotation is accommodated by both the connection and the framing members to develop a desired yielding hierarchy.

9.3.2 Evaluation of Connection Type

All five connection types tested during the experimental program had a wide variety of connection deficiencies, connection geometry, and connection strengths. These differences influenced the yielding hierarchy and failure modes observed in each of the tests.

The beam-to-gusset plate weld was a common failure mode observed but was more vulnerable for certain combinations of connection type, connection deficiency, and brace type. Beam-to-gusset plate welds for frames with continuous connection elements at the column interface seemed to perform better than frames with split connection elements with similar beam-to-gusset plate DCRs. Connections with beam-to-gusset plate welds not able to develop the yield capacity of the gusset plate were vulnerable when using an out-of-plane buckling brace but were less vulnerable using an in-plane buckling brace or BRB. Limited brace end rotational clearance and non-ductile gusset plate interface

welds also played a role in the beam-to-gusset plate weld fracture, but their individual impacts were not evaluated.

At a given drift level, a braced frame must accommodate the drift at each connection through connection and framing member rotations. The force and deformation demands on the frame components are based on the relative strength of the connection, beam, and column. For the experimental setup at the UW SRL, braced frame connections that have stronger connection (e.g. bolted end plate) at the column interface tend to develop more shear force, bending moments, and rotations in the column at the edge of the gusset plate than connections that are weaker (e.g. integrated gusset-shear plate) at similar levels of drift. For NCBFs with adequate column strength and compactness this may be beneficial since some yielding has been shown to increase overall frame ductility before brace fracture as well as improve frame contribution to lateral drift before and after fracture.

For NCBFs with undersized columns and stiff gussets, the interaction between bending moment and column axial load can lead to significant yielding in the column at the edge of the gusset plate especially for stronger connections. A weaker connection may alleviate some of the deformation demands on the framing members by accommodating rotation and developing a stable yielding mechanism (e.g. bolt hole elongation) at the column interface connection, but the weaker connection may not able to develop as much lateral resistance as a stronger connection with the same frame geometry.

9.4 Recommendations for Future Work

9.4.1 Experimental Work

Experimental work recommendations are based on the limitations and gaps in the current testing program.

- Gusset plate interface weld fracture was a controlling failure mode for a majority of the NCBFs tested to date. Cost effective retrofit schemes of these interface welds such as weld reinforcement over existing non-ductile welds, particularly the beam-to-gusset plate weld should be investigated.

- The Integrated shear plate connection should be tested in a multi-story test setup with more realistic boundary conditions to evaluate importance of the limiting beam web buckling.

- Some deficiencies have not been fully investigated and future tests should be conducted to isolate and determine their impact and relative importance on system performance. These limit states include Whitmore yielding, bolted brace-to-gusset deficiencies, and bolt tension/ prying action in either a bolted end plate or bolted split shear plate connection.

- Although there are many tests on a large variety of brace types, quadruple angle bracing seems to be absent from this list despite their prevalence in both existing and new structures. A test should be done to determine performance of this type of brace when subjected to cyclic loading in a braced frame system.

9.4.2 Analytical Work

Over the past few years there have been a significant number of tests on NCBF infrastructure, and although this thesis compares many of these tests, analytical work is needed to fill in gaps that cannot be addressed with the experimental program.

- The observed yielding hierarchy observed in each of the tests seems to be dependent on the relative strength of the beam, the column, and the connection, yet all of the tests conducted at UW have used the same beam, column, column orientation, and frame dimensions. Analytical models looking at this flexibility of these components should be evaluated to determine the effect changing one or more of these parameters have on the yielding hierarchy and eventual failure mode for each of the connection types.

- Nonlinear evaluation of NCBF structures in ASCE 41 does not explicitly define modeling parameters or techniques to model deficient NCBF connections. The experimental backbone curves generated in this thesis could be the first step in determining a consistent approach to this task.

References

1. AISC “Seismic Design Manual,” American Institute of Steel Construction, Chicago, IL, 2010a
2. AISC “Seismic Provisions for Structural Steel Buildings,” American Institute of Steel Construction Chicago, IL, 2010b
3. AISC “Steel Construction Manual,” 14th Edition, American Institute of Steel Construction, Chicago, IL, 2010c
4. ASCE41 “Seismic Evaluation and Retrofit of Existing Buildings,” American Society of Civil Engineers, Reston, VA, 2014
5. ATC24, “Guidelines for Cyclic Seismic Testing of Components of Steel Structures,” Applied Technology Council, Redwood City, CA, 1992
6. Christopulos, A., “Seismic Performance of Special Concentrically Brace Frames with Buckling Restrained Braces,” MS Thesis, Department of Civil and Environmental Engineering, University of Washington, Seattle, WA, 2005
7. FEMA 274, “NEHRP Commentary on the Guidelines for the Seismic Rehabilitation of Buildings,” Federal Emergency Management Agency, D.C., WA, 1997
8. Herman, D. J., “Further Improvements on and Understanding of Special Concentrically Braced Frame Systems,” MS Thesis, University of Washington Department of Civil Engineering, Seattle, WA, 2007
9. Hsiao, P.C., “Seismic Performance Evaluation of Concentrically Braced Frames,” PHD dissertation, Department of Civil and Environmental Engineering, University of Washington, Seattle, WA, 2012
10. Hsiao, P.C., Lehman, D., Berman, J.W., Roeder, C. W., & Powell, J, “Seismic Vulnerability of Older Braced Frames,” Journal of Performance of Constructed Facilities, 108-120, 2012.
11. Johnson, M. M., “Seismic Evaluation of Bolted Connections in Non-Seismic Concentrically Braced Frames,” MS Thesis, Department of Civil and Environmental Engineering, University of Washington, Seattle, WA, 2014
12. Johnson, S. M., “Improved Seismic Performance of Special Concentrically Braced Frames,” MS Thesis, Department of Civil and Environmental Engineering, University of Washington, Seattle, WA, 2005

13. Kotulka, B. A., “Analysis for a Design Guide on Gusset Plates used in Special Concentrically Braced Frames,” MS Thesis, Department of Civil and Environmental Engineering, University of Washington, Seattle, WA, 2007
14. Lumpkin, E. J., “Enhanced Seismic Performance of Multi-Story Special Concentrically Brace Frames using a Balanced Design Procedure,” MS Thesis, Department of Civil and Environmental Engineering, University of Washington, Seattle, WA, 2009
15. NEES (2014). "NEEShub." Project Warehouse, <https://nees.org/> (June. 9, 2015).
16. Palmer, K. D., Christopulos, A. S., Lehman, D. E., & Roeder, C. W., “Experimental Evaluation of Cyclically Loaded, Large-Scale, Planar and 3-D Buckling-Restrained Braced Frames,” Journal of Constructional Steel Research, 2011, 415-425
17. Powell, J., “Evaluation of Special Concentrically Braced Frames for Improved Seismic Performance and Constructability,” MS Thesis, Department of Civil and Environmental Engineering, University of Washington, Seattle, WA, 2010
18. RCSC “Specification for Structural Joints Using High-Strength Bolts,” Research Council on Structural Connections, Chicago, IL, 2009
19. Roeder, C. W., Lumpkin, E. J., Lehman, D. E., “A Balanced Design Procedure for Special Concentrically Braced Frame Connections,” Journal of Constructional Steel Research, 2011, 1760-1772
20. Sloat, D., “Evaluation and Retrofit of Non-Capacity Designed Braced Frames,” MS Thesis, Department of Civil and Environmental Engineering, University of Washington, Seattle, WA, 2014
21. Sloat, D., Roeder, C. W., Lehman D. E., & Berman, J. W., “Survey and Testing of Pre-1988 Braced Frame Structures From The West Coast of the United States,” 5th International Conference on Advances in Experimental Structural Engineering, Taipei, Taiwan, 2013
22. Sabelli, R., Roeder, C.W., Hajjar, J.F., “Seismic Design of Steel Special concentrically Braced Frame Systems,” NEHRP Seismic Design Technical Brief No. 8, National Institute of Standards and Technology, 2013
23. Tsia et al., “Seismic Design and Hybrid Tests of a Full-Scale Three Story concentrically Braced Frame Using In-Plane Buckling Braces,” Earthquake Spectra, Earthquake Engineering Research Institute, Vol. 29, No. 3, pp. 1043-1067. 2013

Appendix A: Instrumentation Plans

A.1: NCBF4-R1 Instrumentation Plan

This appendix contains detailed instrumentation plans for all of the tested specimens. For each specimen there are three figures and three tables that detail the instruments purpose, location, instrument type, and calibration factors. An in depth description of each type of instrumentation type (potentiometers, strain gauges, and Optotrak) is given in Chapter 4. Raw and corrected data sets for all of the instruments can be found on the NEEShub website (https://nees.org/warehouse/project/1157).

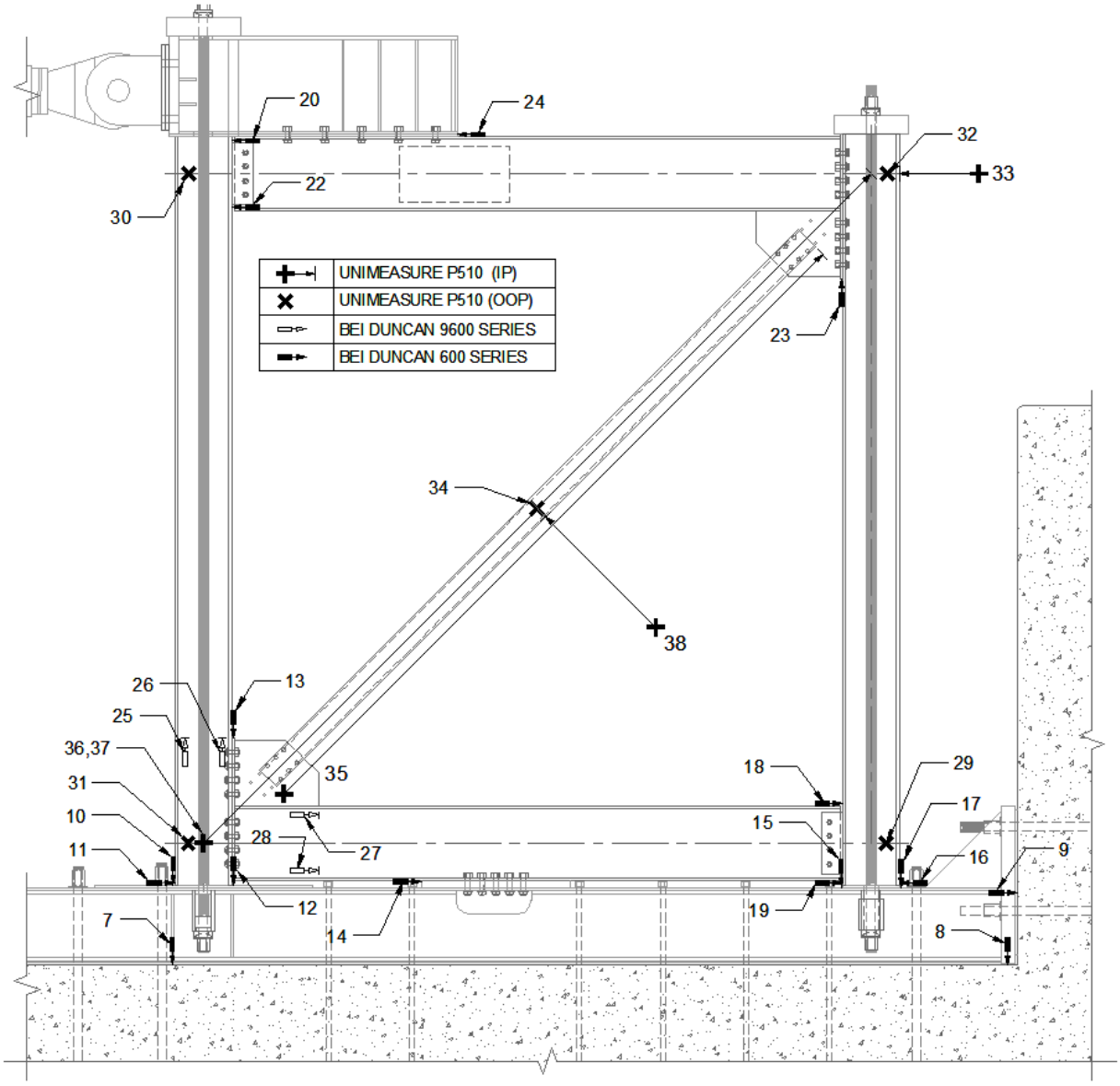

Figure A-1: NCBF4-R1 Potentiometer Layout

Table A-1: NCBF4-R1 Potentiometer Location and Description

Ch. #	Instrument Description	Location			Axis	Length	Instrument Type	Calibration Factor
		x (in)	y (in)	z (in)				
0	Resistor	NA	NA	NA	NA	NA	Resistor	120
1	Actuator Load	NA	NA	NA	NA	NA	Load Cell	50
2	Actuator Displacement	NA	NA	NA	NA	NA	LVDT	1
3	Reaction Block Slip - South	-127.0	105.3	-17.0	X-	0.2	D600	0.0495
4	Actuator Base Slip	-127.0	161.8	14.0	X-	0.2	D600	0.0494
5	Reaction Block Slip - Middle	-127.0	151.3	-17.0	X-	0.2	D600	0.0493
6	Reaction Block Slip - North	-127.0	189.3	-17.0	X-	0.2	D600	0.0497
7	Channel Assembly Uplift - West	-6.8	-26.3	6.4	Y-	0.2	D600	0.0501
8	Channel assembly Uplift - East	174.5	-26.3	8.4	Y-	0.2	D600	0.0501
9	Channel Assembly Slip	175.5	-9.8	8.4	X+	0.7	D600	0.1501
10	West Column West Flange Uplift	-6.4	-9.1	5.0	Y-	0.7	D600	0.1503
11	West Column Slip	-6.2	-8.9	3.0	X+	0.2	D600	0.0491
12	West Column East Flange Uplift	6.5	-9.1	4.0	Y-	0.2	D600	0.0498
13	SW End Plate Slip	6.4	22.6	-0.5	Y-	0.7	D600	0.1501
14	Beam Slip at Shear Release	45.0	-8.3	3.0	X+	0.2	D600	0.0496
15	East Column West Flange Uplift	137.6	-9.1	4.0	Y-	0.7	D600	0.1508
16	East Column Slip	150.2	-8.8	5.0	X-	0.7	D600	0.0993
17	East Column East Flange Uplift	150.4	-9.1	2.0	Y-	0.7	D600	0.0986
18	SE Shear Tab Rotation - North	137.9	8.3	1.8	X+	0.7	D600	0.1492
19	SE Shear Tab Rotation - South	137.9	-8.3	3.0	X+	0.7	D600	0.1509
20	NW Shear Tab Rotation - South	6.2	136.8	2.0	X-	0.7	D600	0.1496
21	Resistor	NA	NA	NA	NA	NA	Resistor	120
22	NW Shear Tab Rotation - North	6.2	151.2	2.0	X-	0.7	D600	0.1522
23	NE Endplate Slip	137.6	121.4	0.0	Y+	0.5	D600	0.1005
24	Load Transfer Beam Slip	54.7	152.3	1.0	X-	0.7	D600	0.1490
25	West Column Plastic Hinge Rotation - West	-3.0	22.6	1.2	Y+	2.0	D9600	0.2027
26	West Column Plastic Hinge Rotation - East	3.0	22.6	1.2	Y+	2.0	D9600	0.2008
27	South Beam Plastic Hinge Rotation - North	24.8	5.0	1.2	X+	2.0	D9600	0.2028
28	South Beam Plastic Hinge Rotation - South	24.8	-5.0	1.2	X+	2.0	D9600	0.2011
29	SE Out-of-Plane Frame Displacement	147.0	0.0	-0.2	Z+	14.7	P510	2.0081
30	NW Out-of-Plane Frame Displacement	-3.0	144.0	-0.2	Z+	14.7	P510	2.0004
31	SW Out-of-Plane Frame Displacement	-3.0	0.0	-0.2	Z+	14.7	P510	2.0010
32	NE Out-of-Plane Frame Displacement	147.0	144.0	-0.2	Z+	14.7	P510	2.0109
33	Frame Lateral Displacement	150.2	144.0	0.0	X-	18.0	P510	1.9922
34	Brace Out-of-Plane Displacement	72.0	72.0	15.4	Z+	12.4	P510	4.0140
35	Brace Elongation	13.9	13.9	-4.7	X+Y+	164.3	P510	3.2632
36	Frame Diagonal Measurement - Bottom	0.0	0.0	24.4	X+Y+	203.6	P510	4.6554
37	Frame Diagonal Measurement - Top	0.0	0.0	29.4	X+Y+	203.6	P510	4.6914
38	Brace In Plane Displacement	73.8	70.2	0.2	X-Y+	30.0	P510	4.3675
39	Terminator	NA	NA	NA	NA	NA	Terminator	NA

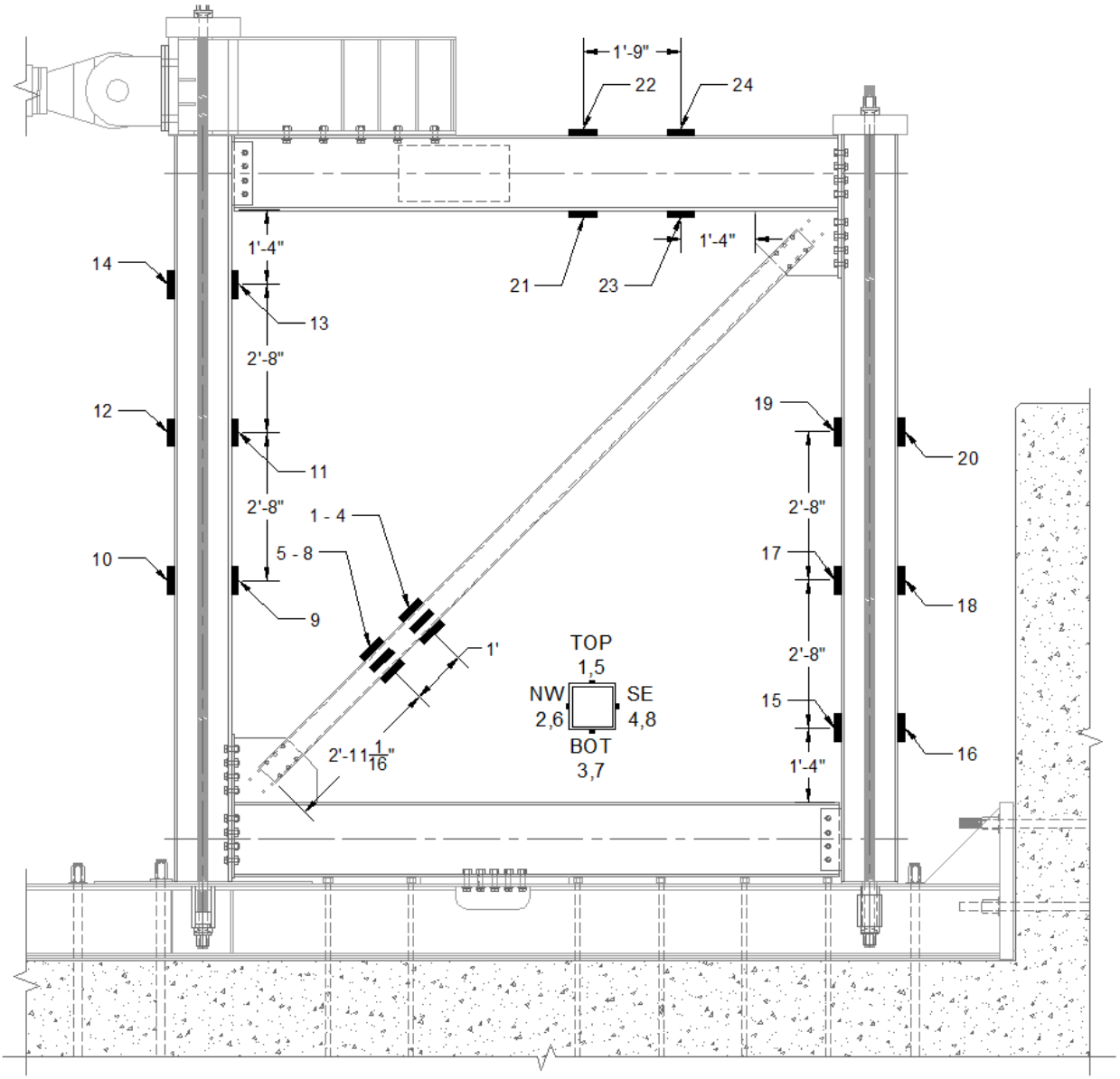

Figure A-2: NCBF4-R1 Strain Gauge Layout

Table A-2: NCBF4-R1 Strain Gauge Location and Description

Ch. #	Instrument Description	Location			Axis	Resistance
		x (in)	y (in)	z (in)		
0	Resistor	NA	NA	NA	NA	NA
1	SG1 - Brace Group 1 - Top	38.7	38.7	2.7	+X+Y	121.36
2	SG2 - Brace Group 1 - Side NW	37.0	40.5	0.2	+X+Y	121.12
3	SG3 - Brace Group 1 - Side SE	40.5	37.0	0.2	+X+Y	121.21
4	SG4 - Brace Group 1 - Bottom	38.7	38.7	-2.4	+X+Y	121.15
5	SG5 - Brace Group 2 - Top	47.2	47.2	2.7	+X+Y	121.13
6[1]	SG6 - Brace Group 2 - Side NW	45.4	49.0	0.2	+X+Y	121.39
7	SG7 - Brace Group 2 - Side SE	49.0	45.4	0.2	+X+Y	121.10
8	SG8 - Brace Group 2 - Bottom	47.2	47.2	-2.4	+X+Y	121.05
9	SG9 - West Column SE	6.2	56.0	0.0	+Y	121.02
10	SG10 - West Column SW	-6.2	56.0	0.0	+Y	120.80
11	SG11 - West Column E	6.2	88.0	0.0	+Y	121.47
12	SG12 - West Column W	-6.2	88.0	0.0	+Y	120.80
13	SG13 - West Column NE	6.2	120.0	0.0	+Y	120.98
14	SG14 - West Column NW	-6.2	120.0	0.0	+Y	121.15
15	SG15 - East Column SW	137.9	24.1	0.0	+Y	121.62
16	SG16 - East Column SE	150.2	24.1	0.0	+Y	121.71
17	SG17 - East Column W	137.9	56.1	0.0	+Y	121.59
18	SG18 - East Column E	150.2	56.1	0.0	+Y	121.48
19	SG19 - East Column NW	137.9	88.1	0.0	+Y	121.62
20	SG20 - East Column NE	150.2	88.1	0.0	+Y	121.55
21	SG21 - North Beam SW	82.3	136.0	0.0	+X	121.58
22	SG22 - North Beam NW	82.3	152.0	0.0	+X	121.40
23	SG23 - North Beam SE	103.3	136.0	0.0	+X	121.10
24	SG24 - North Beam NE	103.3	152.0	0.0	+X	121.41
25	Terminator	NA	NA	NA	NA	NA

1 – Strain gauge was accidently pulled off prior to the end of the test

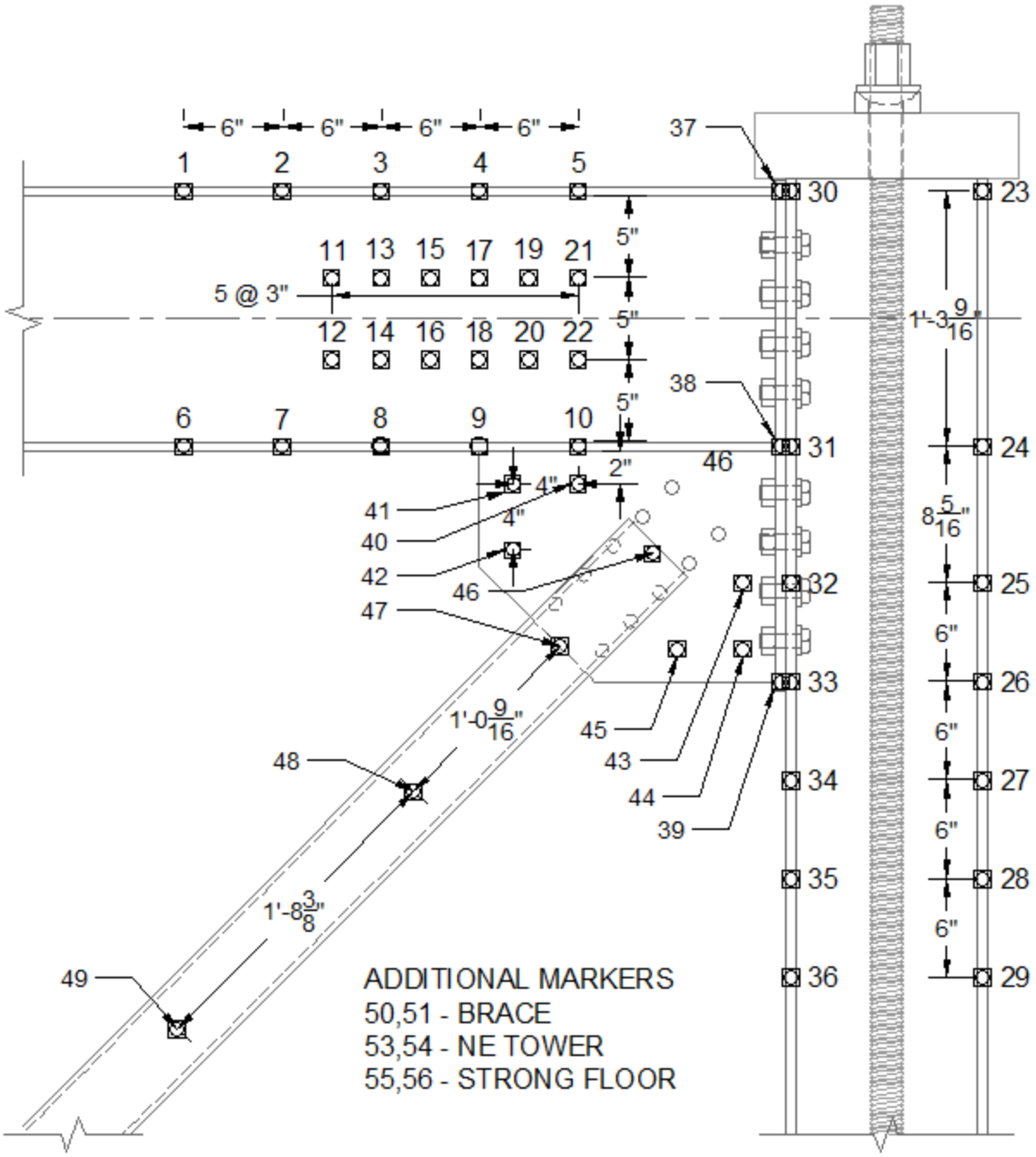

Figure A-3: NCBF4-R1 OptoTrak Layout

Table A-3: NCBF4-R1 OptoTrak Location and Description

Marker	Coordinates			Location
	x (in)	y (in)	z (in)	
1	101.4	151.8	3.6	North Beam North Flange
2	107.3	151.8	3.6	North Beam North Flange
3	113.3	151.8	3.6	North Beam North Flange
4	119.4	151.8	3.6	North Beam North Flange
5	125.4	151.8	3.6	North Beam North Flange
6	101.3	136.2	3.6	North Beam South Flange
7	107.3	136.2	3.6	North Beam South Flange
8	113.3	136.2	3.5	North Beam South Flange
9	119.3	136.2	3.5	North Beam South Flange
10	125.3	136.1	3.5	North Beam South Flange
11	110.4	146.4	0.2	North Beam Web
12	110.4	141.6	0.2	North Beam Web
13	113.4	146.4	0.2	North Beam Web
14	113.4	141.6	0.2	North Beam Web
15	116.4	146.5	0.2	North Beam Web
16	116.3	141.6	0.2	North Beam Web
17	119.4	146.5	0.2	North Beam Web
18	119.4	141.5	0.2	North Beam Web
19	122.3	146.6	0.2	North Beam Web
20	122.3	141.5	0.2	North Beam Web
21	125.3	146.8	0.2	North Beam Web
22	125.4	141.6	0.2	North Beam Web
23	NaN	NaN	NaN	East Column East Flange
24	149.7	136.6	6.0	East Column East Flange
25	149.7	127.9	6.0	East Column East Flange
26	149.7	121.7	6.0	East Column East Flange
27	149.8	115.7	6.0	East Column East Flange
28	149.7	110.0	6.0	East Column East Flange

Marker	Coordinates			Location
	x (in)	y (in)	z (in)	
29	149.7	103.8	6.0	East Column East Flange
30	NaN	NaN	NaN	East Column West Flange
31	138.3	136.2	6.1	East Column West Flange
32	138.3	127.9	6.1	East Column West Flange
33	138.3	122.0	6.1	East Column West Flange
34	138.3	115.8	6.1	East Column West Flange
35	138.3	109.9	6.1	East Column West Flange
36	138.3	103.8	6.1	East Column West Flange
37	137.7	151.9	3.8	End Plate
38	137.7	136.2	3.7	End Plate
39	137.6	121.9	3.7	End Plate
40	124.3	133.1	0.3	Gusset Plate
41	120.3	132.9	0.2	Gusset Plate
42	120.3	128.8	0.2	Gusset Plate
43	134.5	126.7	0.3	Gusset Plate
44	134.4	123.0	0.2	Gusset Plate
45	130.4	122.8	0.2	Gusset Plate
46	129.8	129.7	2.6	Brace
47	124.3	124.2	2.5	Brace
48	115.5	115.3	2.5	Brace
49	100.9	101.0	2.4	Brace
50	86.4	86.7	2.3	Brace
51	71.8	72.5	2.2	Brace
52	NaN	NaN	NaN	Brace - Not Visible
53	137.3	142.7	22.5	NE Frame Diagonal Mount
54	137.3	142.9	8.3	NE Frame Diagonal Mount
55	126.0	110.4	-17.7	Strong Floor Reference
56	126.9	99.2	-17.7	Strong Floor Reference

A.2: NCBF4-R2 Instrumentation Plan

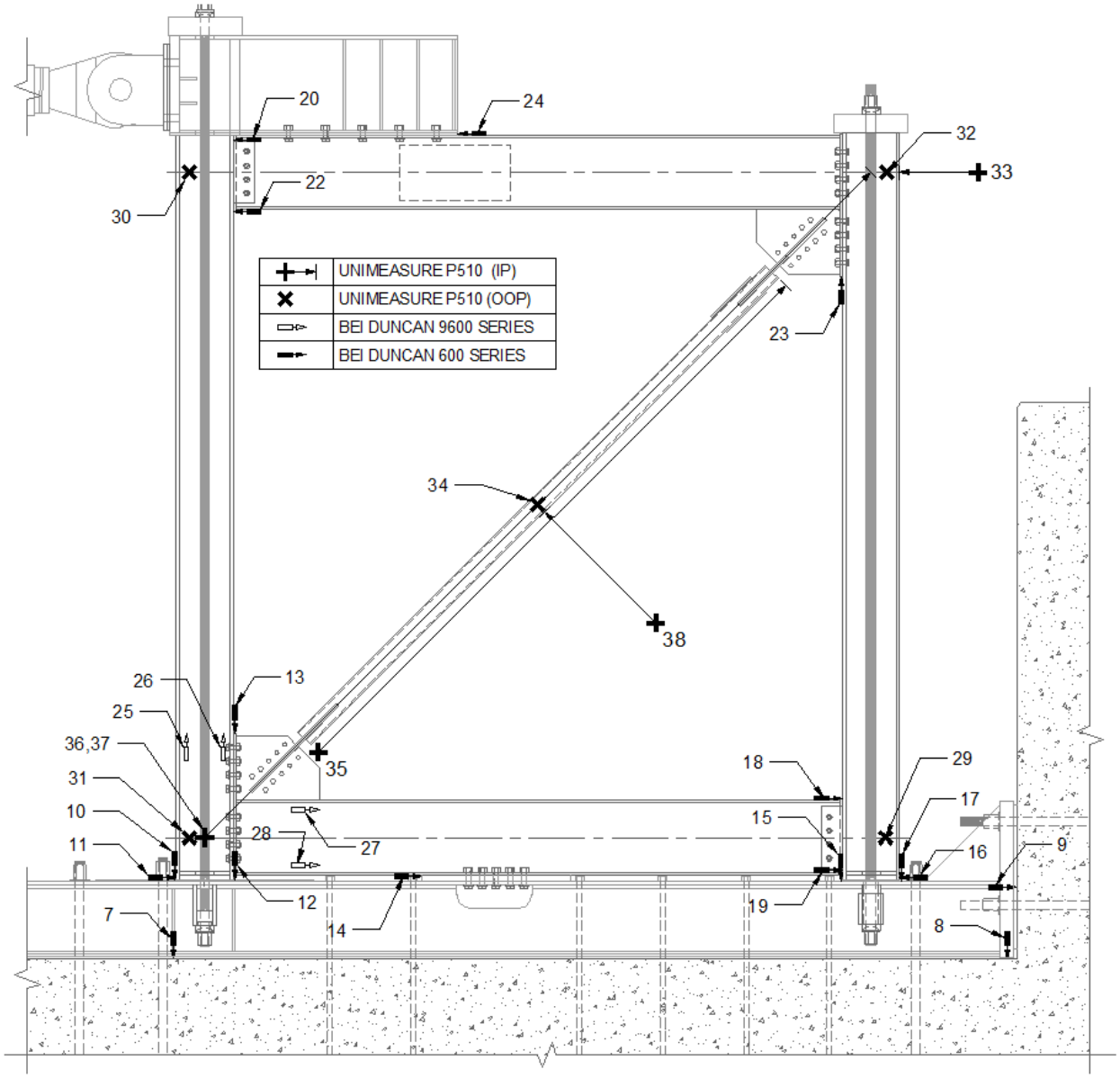

Figure A-4: NCBF4-R2 Potentiometer Layout

Table A-4: NCBF4-R2 Potentiometer Location and Description

Ch. #	Instrument Description	Location			Axis	Length	Instrument Type	Calibration Factor
		x (in)	y (in)	z (in)				
0	Resistor	NA	NA	NA	NA	NA	Resistor	1
1	Actuator Load	NA	NA	NA	NA	NA	Load Cell	50
2	Actuator Displacement	NA	NA	NA	NA	NA	LVDT	1
3	Reaction Block Slip - South	-127.0	105.3	-17.0	X-	0.2	D600	0.04954
4	Actuator Base Slip	-127.0	161.8	14.0	X-	0.2	D600	0.04944
5	Reaction Block Slip - Middle	-127.0	151.3	-17.0	X-	0.2	D600	0.04929
6	Reaction Block Slip - North	-127.0	189.3	-17.0	X-	0.2	D600	0.04974
7	Channel Assembly Uplift - West	-6.8	-26.3	6.4	Y-	0.2	D600	0.05008
8	Channel assembly Uplift - East	174.5	-26.3	8.4	Y-	0.2	D600	0.05009
9	Channel Assembly Slip	175.5	-9.8	8.4	X+	0.7	D600	0.15009
10	West Column West Flange Uplift	-6.4	-9.1	5.0	Y-	0.7	D600	0.1503
11	West Column Slip	-6.2	-8.9	3.0	X+	0.2	D600	0.0491
12	West Column East Flange Uplift	6.5	-9.1	4.0	Y-	0.2	D600	0.04978
13	SW End Plate Slip	6.4	22.6	2.0	Y-	0.7	D600	0.1501
14	Beam Slip at Shear Release	45.0	-8.3	3.0	X+	0.2	D600	0.04959
15	East Column West Flange Uplift	137.6	-9.1	5.0	Y-	0.7	D600	0.15084
16	East Column Slip	150.2	-8.8	2.0	X-	0.7	D600	0.09933
17	East Column East Flange Uplift	150.4	-9.1	5.0	Y-	0.7	D600	0.09862
18	SE Shear Tab Rotation - North	137.9	8.3	1.8	X+	0.7	D600	0.14916
19	SE Shear Tab Rotation - South	137.9	-7.2	1.8	X+	0.7	D600	0.15093
20	NW Shear Tab Rotation - South	6.2	135.7	2.0	X-	0.7	D600	0.14963
21	Resistor	NA	NA	NA	NA	NA	Resistor	120
22	NW Shear Tab Rotation - North	6.2	151.2	2.0	X-	0.7	D600	0.1522
23	NE Endplate Slip	137.6	121.4	3.0	Y+	0.5	D600	0.10053
24	Load Transfer Beam Slip	54.7	152.3	1.5	X-	0.7	D600	0.14904
25	West Column Plastic Hinge Rotation - West	-3.0	22.6	1.2	Y+	2.0	D9600	0.20271
26	West Column Plastic Hinge Rotation - East	3.0	22.6	1.2	Y+	2.0	D9600	0.2008
27	South Beam Plastic Hinge Rotation - North	24.8	5.0	1.2	X+	2.0	D9600	0.20277
28	South Beam Plastic Hinge Rotation - South	24.8	-5.0	1.2	X+	2.0	D9600	0.2011
29	SE Out-of-Plane Frame Displacement	147.0	0.0	-0.2	Z+	14.7	P510	2.00805
30	NW Out-of-Plane Frame Displacement	-3.0	144.0	-0.2	Z+	14.7	P510	2.00041
31	SW Out-of-Plane Frame Displacement	-3.0	0.0	-0.2	Z+	14.7	P510	2.00102
32	NE Out-of-Plane Frame Displacement	147.0	144.0	-0.2	Z+	14.7	P510	2.01094
33	Frame Lateral Displacement	150.2	144.0	0.0	X-	18.5	P510	1.99215
34	Brace Out-of-Plane Displacement	72.0	72.0	15.4	Z+	10.5	P510	4.01401
35	Brace Elongation	18.4	24.6	0.0	X+Y+	143.0	P510	3.26321
36	Frame Diagonal Measurement - Bottom	0.0	0.0	24.4	X+Y+	203.6	P510	4.65537
37	Frame Diagonal Measurement - Top	0.0	0.0	29.4	X+Y+	203.6	P510	4.6914
38	Brace In Plane Displacement	73.8	70.2	0.2	X-Y+	30.5	P510	4.36751
39	Terminator	NA	NA	NA	NA	NA	Terminator	NA

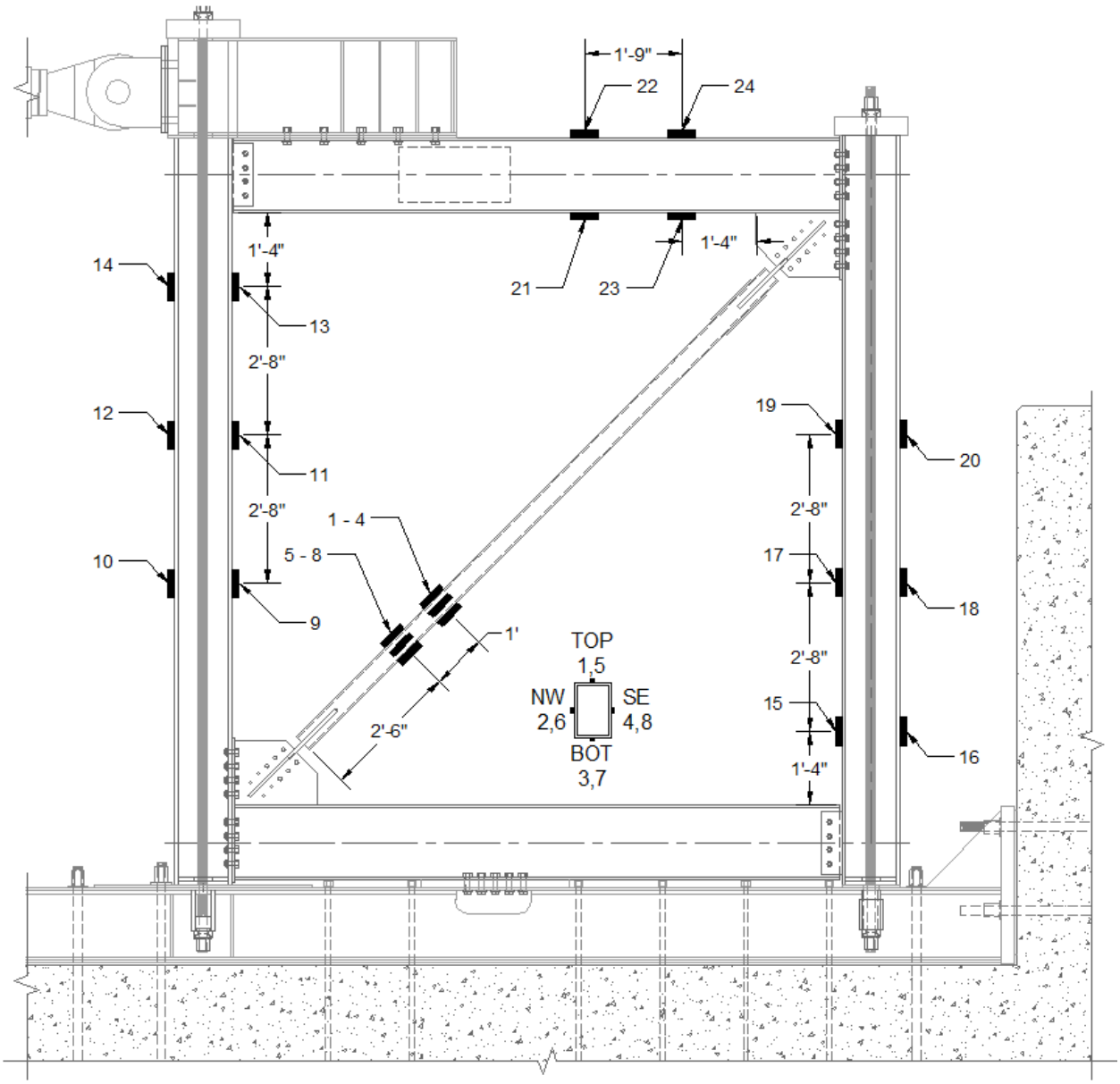

Figure A-5: NCBF4-R2 Strain Gauge Layout

Table A-5: NCBF4-R2 Strain Gauge Location and Description

Ch. #	Instrument Description	Location			Axis	Resistance
		x (in)	y (in)	z (in)		
0	Resistor	NA	NA	NA	NA	NA
1	SG1 - Brace Group 1 - Top	42.7	42.7	3.0	+X+Y	121.42
2	SG2 - Brace Group 1 - Side NW	41.3	44.2	0.0	+X+Y	121.12
3	SG3 - Brace Group 1 - Side SE	44.2	41.3	0.0	+X+Y	121.2
4	SG4 - Brace Group 1 - Bottom	42.7	42.7	-3.0	+X+Y	121.35
5	SG5 - Brace Group 2 - Top	51.2	51.2	3.0	+X+Y	121.31
6	SG6 - Brace Group 2 - Side NW	49.8	52.6	0.0	+X+Y	121.28
7	SG7 - Brace Group 2 - Side SE	52.6	49.8	0.0	+X+Y	121.23
8	SG8 - Brace Group 2 - Bottom	51.2	51.2	-3.0	+X+Y	121.33
9	SG9 - West Column SE	6.2	56.0	0.0	+Y	121.24
10	SG10 - West Column SW	-6.2	56.0	0.0	+Y	121.16
11	SG11 - West Column E	6.2	88.0	0.0	+Y	121.23
12	SG12 - West Column W	-6.2	88.0	0.0	+Y	121.4
13	SG13 - West Column NE	6.2	120.0	0.0	+Y	121.13
14[1]	SG14 - West Column NW	-6.2	120.0	0.0	+Y	121.3
15	SG15 - East Column SW	137.9	24.1	0.0	+Y	121.54
16	SG16 - East Column SE	150.2	24.1	0.0	+Y	122.05
17	SG17 - East Column W	137.9	56.1	0.0	+Y	121.82
18	SG18 - East Column E	150.2	56.1	0.0	+Y	121.83
19	SG19 - East Column NW	137.9	88.1	0.0	+Y	122.54
20	SG20 - East Column NE	150.2	88.1	0.0	+Y	122.43
21	SG21 - North Beam SW	82.3	136.0	0.0	+X	122.49
22	SG22 - North Beam NW	82.3	152.0	0.0	+X	122.47
23	SG23 - North Beam SE	103.3	136.0	0.0	+X	121.84
24	SG24 - North Beam NE	103.3	152.0	0.0	+X	121.79
25	Terminator	NA	NA	NA	NA	NA

1- Strain gauge was accidently pulled off prior to the end of the test.

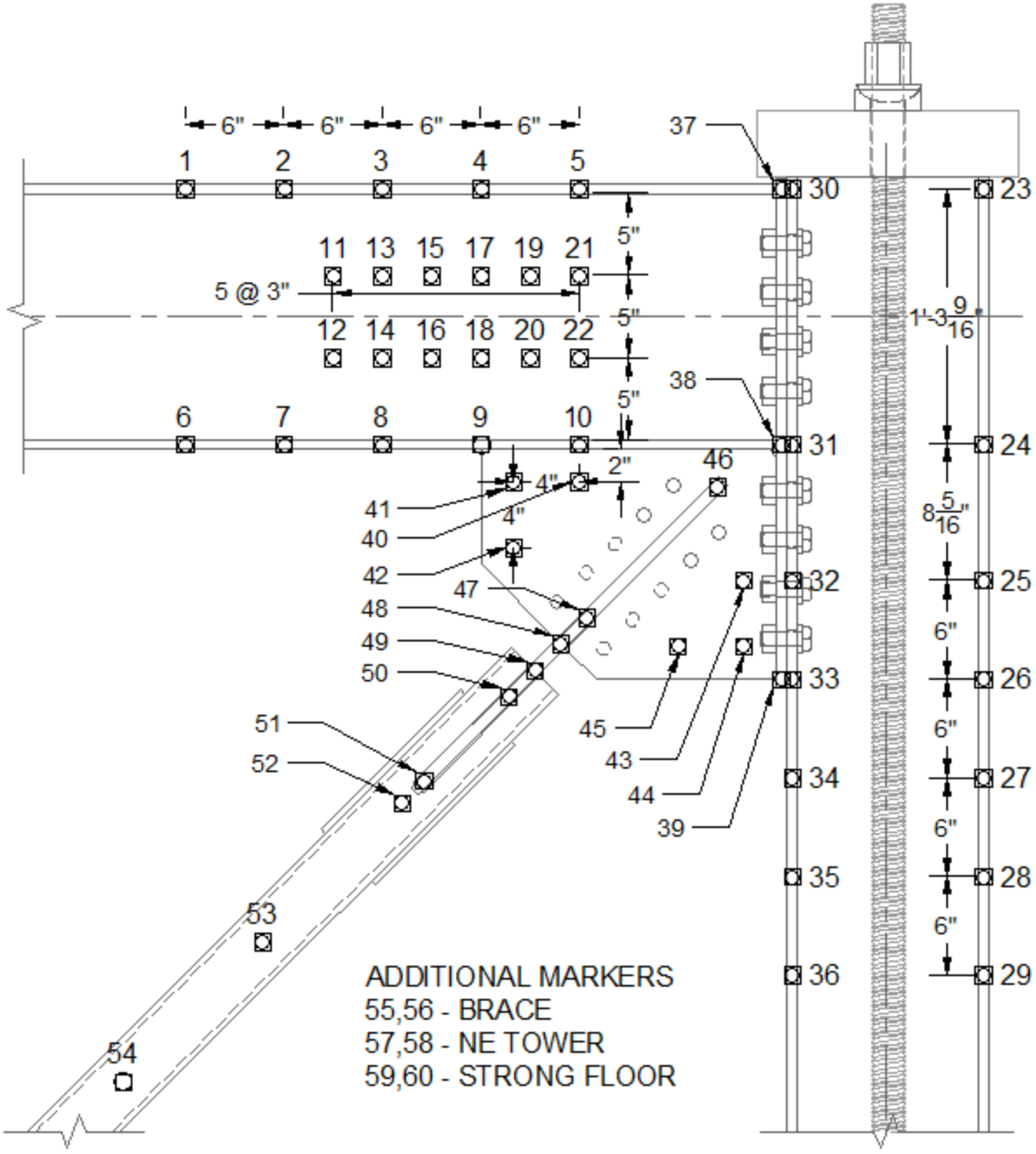

Figure A-6: NCBF4-R2 OptoTrak Layout

Table A-6: NCBF4-R2 OptoTrak Location and Description

Marker	Coordinates			Location
	x (in)	y (in)	z (in)	
1	100.8	151.8	3.5	North Beam North Flange
2	107.0	151.8	3.5	North Beam North Flange
3	112.9	151.8	3.5	North Beam North Flange
4	119.0	151.8	3.5	North Beam North Flange
5	125.1	151.8	3.5	North Beam North Flange
6	101.0	136.2	3.6	North Beam South Flange
7	106.9	136.2	3.6	North Beam South Flange
8	112.9	136.2	3.6	North Beam South Flange
9	119.0	136.2	3.6	North Beam South Flange
10	124.7	136.1	3.6	North Beam South Flange
11	110.0	146.4	0.1	North Beam Web
12	110.0	141.5	0.2	North Beam Web
13	113.0	146.4	0.1	North Beam Web
14	112.9	141.4	0.2	North Beam Web
15	116.2	146.5	0.1	North Beam Web
16	116.1	141.5	0.2	North Beam Web
17	119.2	146.6	0.1	North Beam Web
18	119.1	141.5	0.2	North Beam Web
19	122.1	146.5	0.1	North Beam Web
20	122.1	141.5	0.2	North Beam Web
21	125.0	146.5	0.1	North Beam Web
22	124.9	141.5	0.2	North Beam Web
23	149.8	152.0	6.0	East Column East Flange
24	149.8	135.6	6.0	East Column East Flange
25	149.8	127.7	6.0	East Column East Flange
26	149.8	121.7	6.0	East Column East Flange
27	149.8	115.7	6.0	East Column East Flange
28	149.8	109.5	6.0	East Column East Flange
29	149.8	103.6	6.0	East Column East Flange
30	138.2	151.8	6.0	East Column West Flange

Marker	Coordinates			Location
	x (in)	y (in)	z (in)	
31	138.2	136.3	6.0	East Column West Flange
32	138.2	127.6	6.0	East Column West Flange
33	138.2	121.8	6.0	East Column West Flange
34	138.2	115.7	6.0	East Column West Flange
35	138.2	109.6	6.0	East Column West Flange
36	138.2	103.5	6.0	East Column West Flange
37	137.5	151.8	3.6	End Plate
38	137.6	136.2	3.7	End Plate
39	137.5	122.1	3.8	End Plate
40	124.8	133.9	0.4	Gusset Plate
41	120.9	133.9	0.4	Gusset Plate
42	120.9	130.0	0.4	Gusset Plate
43	135.2	128.1	0.3	Gusset Plate
44	135.1	124.0	0.3	Gusset Plate
45	131.0	124.0	0.3	Gusset Plate
46	133.5	133.8	3.6	Knife Plate
47	125.5	125.7	6.0	Knife Plate
48	124.0	124.2	6.0	Knife Plate
49	122.2	122.5	6.0	Knife Plate
50	121.0	121.3	6.0	Knife Plate
51	115.7	115.7	4.1	Knife Plate
52	114.5	114.7	2.9	Brace
53	106.0	106.2	2.9	Brace
54	97.6	97.8	2.9	Brace
55	89.2	89.3	2.9	Brace
56	80.7	80.9	2.9	Brace
57	71.7	71.9	2.9	Brace
58	137.6	142.9	24.3	NE Frame Diagonal Mount
59	137.3	142.8	6.1	NE Frame Diagonal Mount
60	125.1	110.2	-17.8	Strong Floor Reference

A.3: NCBF4-R3 Instrumentation Plan

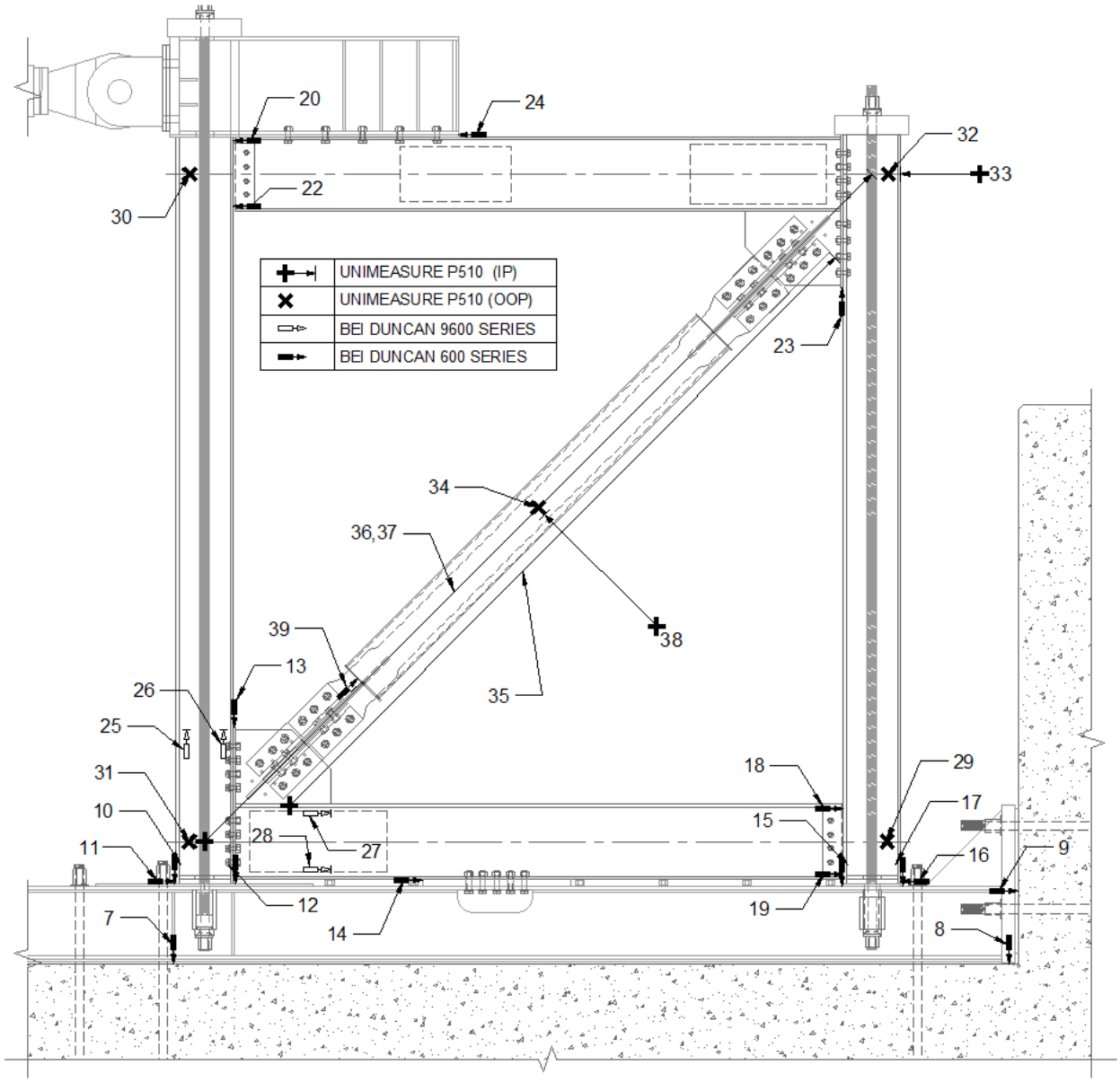

Figure A-7: NCBF4-R3 Potentiometer Layout

Table A-7: NCBF4-R3 Potentiometer Location and Description

Ch. #	Instrument Description	Location			Axis	Length	Instrument Type	Calibration Factor
		x (in)	y (in)	z (in)				
0	Resistor	NA	NA	NA	NA	NA	Resistor	1
1	Actuator Load	NA	NA	NA	NA	NA	Load Cell	50
2	Actuator Displacement	NA	NA	NA	NA	NA	LVDT	1
3	Reaction Block Slip - South	-127.0	105.3	-17.0	X-	0.2	D600	0.04954
4	Actuator Base Slip	-127.0	161.8	14.0	X-	0.2	D600	0.04944
5	Reaction Block Slip - Middle	-127.0	151.3	-17.0	X-	0.2	D600	0.04929
6	Reaction Block Slip - North	-127.0	189.3	-17.0	X-	0.2	D600	0.04974
7	Channel Assembly Uplift - West	-6.8	-26.3	6.4	Y-	0.2	D600	0.05008
8	Channel assembly Uplift - East	174.5	-26.3	8.4	Y-	0.2	D600	0.05009
9	Channel Assembly Slip	175.5	-9.8	8.4	X+	0.7	D600	0.15009
10	West Column West Flange Uplift	-6.4	-9.1	5.0	Y-	0.7	D600	0.1503
11	West Column Slip	-6.2	-8.9	3.0	X+	0.2	D600	0.0491
12	West Column East Flange Uplift	6.5	-9.1	4.0	Y-	0.2	D600	0.04978
13	SW End Plate Slip	6.4	22.6	2.0	Y-	0.7	D600	0.1501
14	Beam Slip at Shear Release	45.0	-8.3	3.0	X+	0.2	D600	0.04959
15	East Column West Flange Uplift	137.6	-9.1	5.0	Y-	0.7	D600	0.15084
16	East Column Slip	150.2	-8.8	5.0	X-	0.7	D600	0.09933
17	East Column East Flange Uplift	150.4	-9.1	2.0	Y-	0.7	D600	0.09862
18	SE Shear Tab Rotation - North	137.9	7.2	2.5	X+	0.7	D600	0.14916
19	SE Shear Tab Rotation - South	137.9	-7.2	1.5	X+	0.7	D600	0.15093
20	NW Shear Tab Rotation - South	6.2	136.8	2.5	X-	0.7	D600	0.14963
21	Resistor	NA	NA	NA	NA	NA	Resistor	NA
22	NW Shear Tab Rotation - North	6.2	151.2	2.5	X-	0.7	D600	0.1522
23	NE Endplate Slip	137.6	121.4	0.0	Y+	0.5	D600	0.10053
24	Load Transfer Beam Slip	54.7	152.3	2.5	X-	0.7	D600	0.14904
25	West Column Plastic Hinge Rotation - West	-3.0	22.6	1.2	Y+	2.0	D9600	0.20271
26	West Column Plastic Hinge Rotation - East	3.0	22.6	1.2	Y+	2.0	D9600	0.2008
27	South Beam Plastic Hinge Rotation - North	24.8	5.0	1.2	X+	2.0	D9600	0.20277
28	South Beam Plastic Hinge Rotation - South	24.8	-5.0	1.2	X+	2.0	D9600	0.2011
29	SE Out-of-Plane Frame Displacement	147.0	0.0	-0.2	Z+	14.7	P510	2.00805
30	NW Out-of-Plane Frame Displacement	-3.0	144.0	-0.2	Z+	14.7	P510	2.00041
31	SW Out-of-Plane Frame Displacement	-3.0	0.0	-0.2	Z+	14.7	P510	2.00102
32	NE Out-of-Plane Frame Displacement	147.0	144.0	-0.2	Z+	14.7	P510	2.01094
33	Frame Lateral Displacement	150.2	144.0	0.0	X-	25.8	P510	1.99215
34	Brace Out-of-Plane Displacement	72.0	72.0	12.7	Z+	8.9	P510	4.01401
35	Brace Elongation – BAD DATA	18.4	24.6	0.0	X+Y+	143.0	P510	3.26321
36	Frame Diagonal Measurement - Bottom	0.0	0.0	28.5	X+Y+	203.6	P510	4.65537
37	Frame Diagonal Measurement - Top	0.0	0.0	23.4	X+Y+	203.6	P510	4.6914
38	Brace In Plane Displacement	75.4	68.5	0.0	X-Y+	25.75	P510	4.36751
39a[1]	BRB Core Elongation SW (first)	33.1	35.2	1.2	X+Y+	0.5	D600	0.09858
39b[1]	BRB Core Elongation SW (replaced)	33.1	35.2	1.2	X+Y+	4	D9600	0.41669
40	Terminator	NA	NA	NA	NA	NA	Terminator	NA

1 – This potentiometer was replaced mid-test due to limited instrument measurement stroke

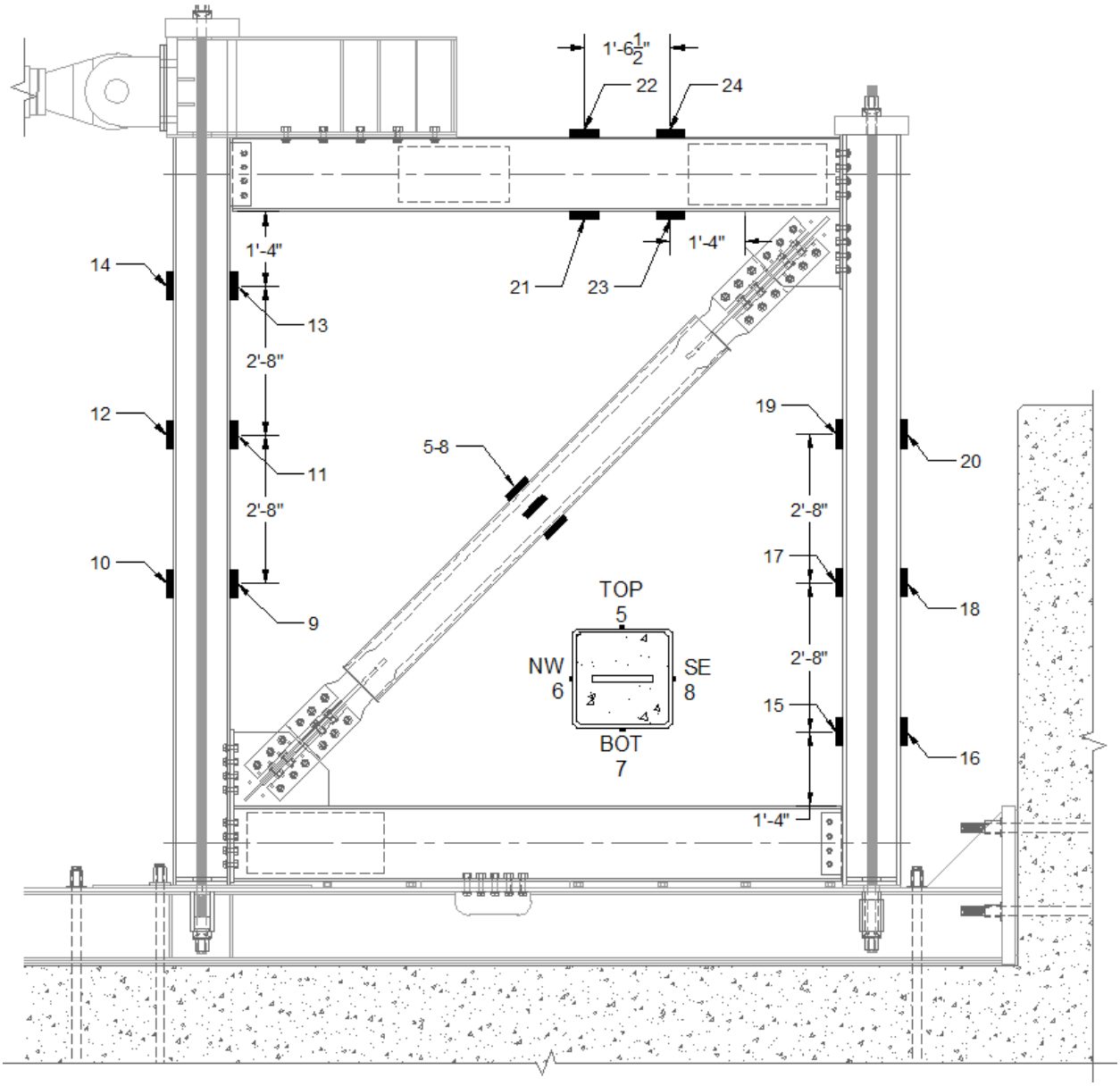

Figure A-8: NCBF4-R3 Strain Gauge Layout

Table A-8: NCBF4-R3 Strain Gauge Location and Description

Ch. #	Instrument Description	Location			Axis	Calibration Factor
		x (in)	y (in)	z (in)		
0	Resistor	NA	NA	NA	NA	NA
1	Resistor	NA	NA	NA	NA	NA
2	Resistor	NA	NA	NA	NA	NA
3	Resistor	NA	NA	NA	NA	NA
4	Resistor	NA	NA	NA	NA	NA
5	SG5 - Brace Group 1 - Top	72.0	72.0	5.1	+X+Y	121.31
6	SG6 - Brace Group 1 - Side NW	68.3	75.4	0.0	+X+Y	121.10
7	SG7 - Brace Group 1 - Side SE	75.4	68.3	0.0	+X+Y	121.20
8	SG8 - Brace Group 1 - Bottom	72.0	72.0	-5.1	+X+Y	121.16
9	SG9 - West Column SE	6.2	56.0	0.0	+Y	121.19
10	SG10 - West Column SW	-6.2	56.0	0.0	+Y	121.19
11	SG11 - West Column E	6.2	88.0	0.0	+Y	121.13
12	SG12 - West Column W	-6.2	88.0	0.0	+Y	121.19
13	SG13 - West Column NE	6.2	120.0	0.0	+Y	121.17
14	SG14 - West Column NW	-6.2	120.0	0.0	+Y	121.09
15	SG15 - East Column SW	137.9	24.1	0.0	+Y	122.83
16	SG16 - East Column SE	150.2	24.1	0.0	+Y	122.81
17	SG17 - East Column W	137.9	56.1	0.0	+Y	122.86
18	SG18 - East Column E	150.2	56.1	0.0	+Y	123.00
19	SG19 - East Column NW	137.9	88.1	0.0	+Y	122.70
20	SG20 - East Column NE	150.2	88.1	0.0	+Y	123.11
21	SG21 - North Beam SW	82.2	136.0	0.0	+X	122.90
22	SG22 - North Beam NW	82.2	152.0	0.0	+X	122.96
23	SG23 - North Beam SE	100.7	136.0	0.0	+X	122.71
24	SG24 - North Beam NE	100.7	152.0	0.0	+X	122.51
25	Terminator	NA	NA	NA	NA	NA

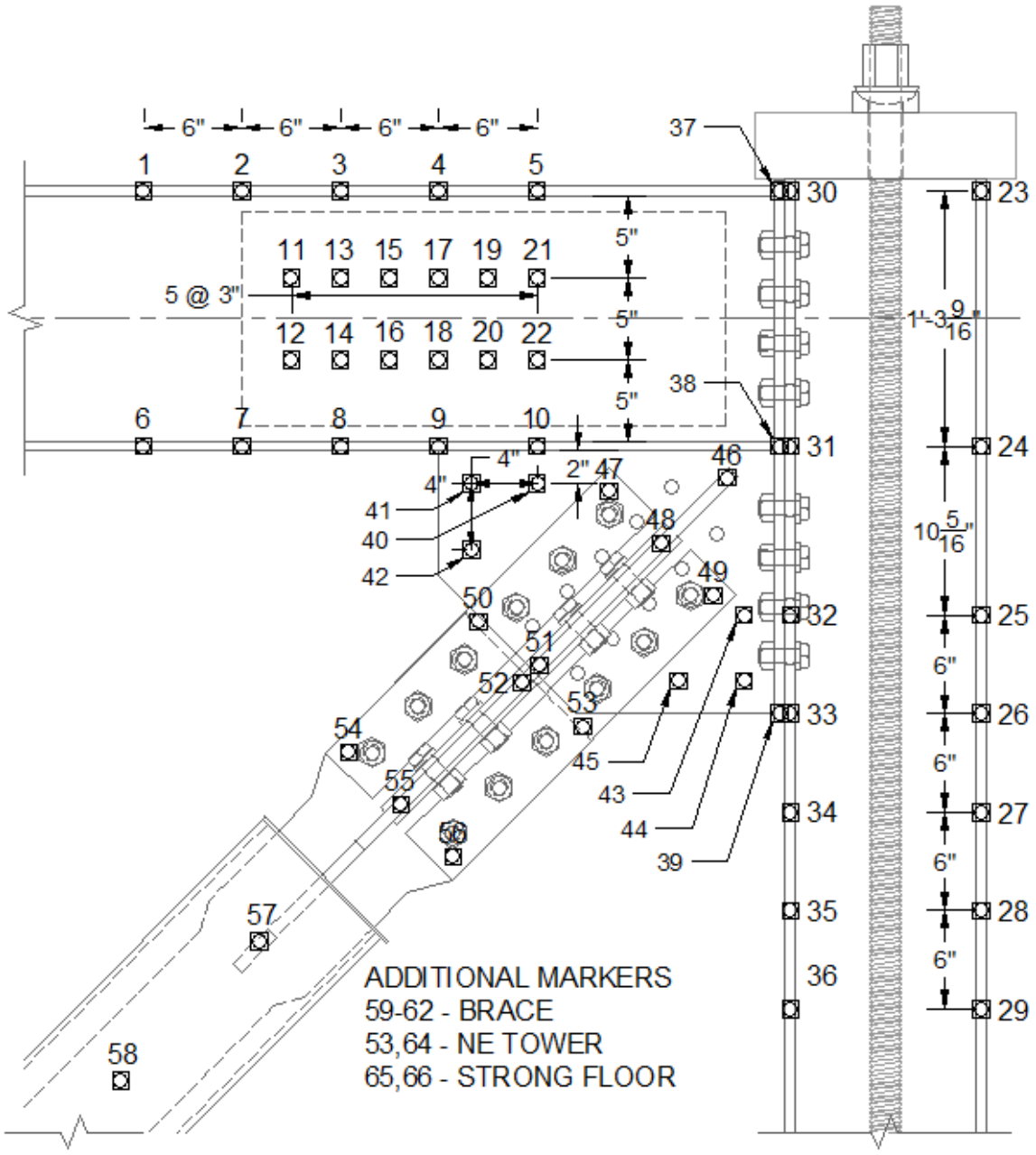

Figure A-9: NCBF4-R3 OptoTrak Layout

Table A-9: NCBF4-R3 OptoTrak Location and Description

Marker	Coordinates			Location
	x (in)	y (in)	z (in)	
1	98.6	151.9	3.5	North Beam North Flange
2	104.6	151.9	3.5	North Beam North Flange
3	110.6	151.9	3.5	North Beam North Flange
4	116.6	151.9	3.5	North Beam North Flange
5	122.6	151.9	3.5	North Beam North Flange
6	98.7	136.2	3.4	North Beam South Flange
7	104.8	136.2	3.4	North Beam South Flange
8	110.7	136.1	3.4	North Beam South Flange
9	116.6	136.1	3.5	North Beam South Flange
10	122.6	136.1	3.5	North Beam South Flange
11	107.6	141.5	0.1	North Beam Web
12	107.5	146.5	0.2	North Beam Web
13	110.5	141.5	0.1	North Beam Web
14	110.4	146.5	0.2	North Beam Web
15	113.6	141.5	0.1	North Beam Web
16	113.3	146.5	0.2	North Beam Web
17	116.5	141.5	0.2	North Beam Web
18	116.5	146.6	0.2	North Beam Web
19	119.4	141.5	0.2	North Beam Web
20	119.3	146.5	0.2	North Beam Web
21	122.3	141.5	0.2	North Beam Web
22	122.4	146.5	0.2	North Beam Web
23	NaN	NaN	NaN	East Column East Flange
24	149.9	136.1	6.1	East Column East Flange
25	149.8	125.7	6.1	East Column East Flange
26	149.9	119.8	6.1	East Column East Flange
27	149.9	113.9	6.1	East Column East Flange
28	149.9	107.9	6.1	East Column East Flange
29	149.8	101.9	6.1	East Column East Flange
30	138.2	151.7	6.0	East Column West Flange
31	138.1	136.0	6.0	East Column West Flange
32	138.1	125.9	6.0	East Column West Flange
33	138.1	120.0	6.0	East Column West Flange

Marker	Coordinates			Location
	x (in)	y (in)	z (in)	
34	138.1	114.1	6.0	East Column West Flange
35	138.2	108.1	6.0	East Column West Flange
36	138.1	102.1	6.0	East Column West Flange
37	137.5	151.9	3.9	End Plate
38	137.5	136.1	3.9	End Plate
39	137.5	120.0	3.9	End Plate
40	122.6	133.8	0.2	Gusset Plate
41	118.7	133.9	0.2	Gusset Plate
42	118.7	129.8	0.2	Gusset Plate
43	135.2	125.9	0.3	Gusset Plate
44	135.0	121.9	0.3	Gusset Plate
45	131.1	122.0	0.3	Gusset Plate
46	134.3	134.3	5.6	BRB Connection
47	127.1	134.3	0.7	BRB Connection
48	131.0	130.9	5.5	BRB Connection
49	134.4	127.2	0.8	BRB Connection
50	119.2	125.9	0.6	BRB Connection
51	123.0	122.9	5.4	BRB Connection
52	121.9	121.8	5.4	BRB Connection
53	126.1	119.0	0.6	BRB Connection
54	110.8	117.2	0.5	BRB Connection
55	114.2	114.1	5.2	BRB Connection
56	NaN	NaN	NaN	BRB Connection
57	107.6	107.5	4.5	BRB Casing
58	100.5	100.3	4.4	BRB Casing
59	93.4	93.3	4.3	BRB Casing
60	86.3	86.3	4.2	BRB Casing
61	79.3	79.2	4.1	BRB Casing
62	72.3	72.2	4.0	BRB Casing
63	138.0	142.6	24.7	NE Frame Diagonal Mount
64	137.3	142.5	6.3	NE Frame Diagonal Mount
65	130.1	111.6	-17.5	Strong Floor Reference
66	126.4	110.3	-17.5	Strong Floor Reference

A.4: NCBF5 Instrumentation Plan

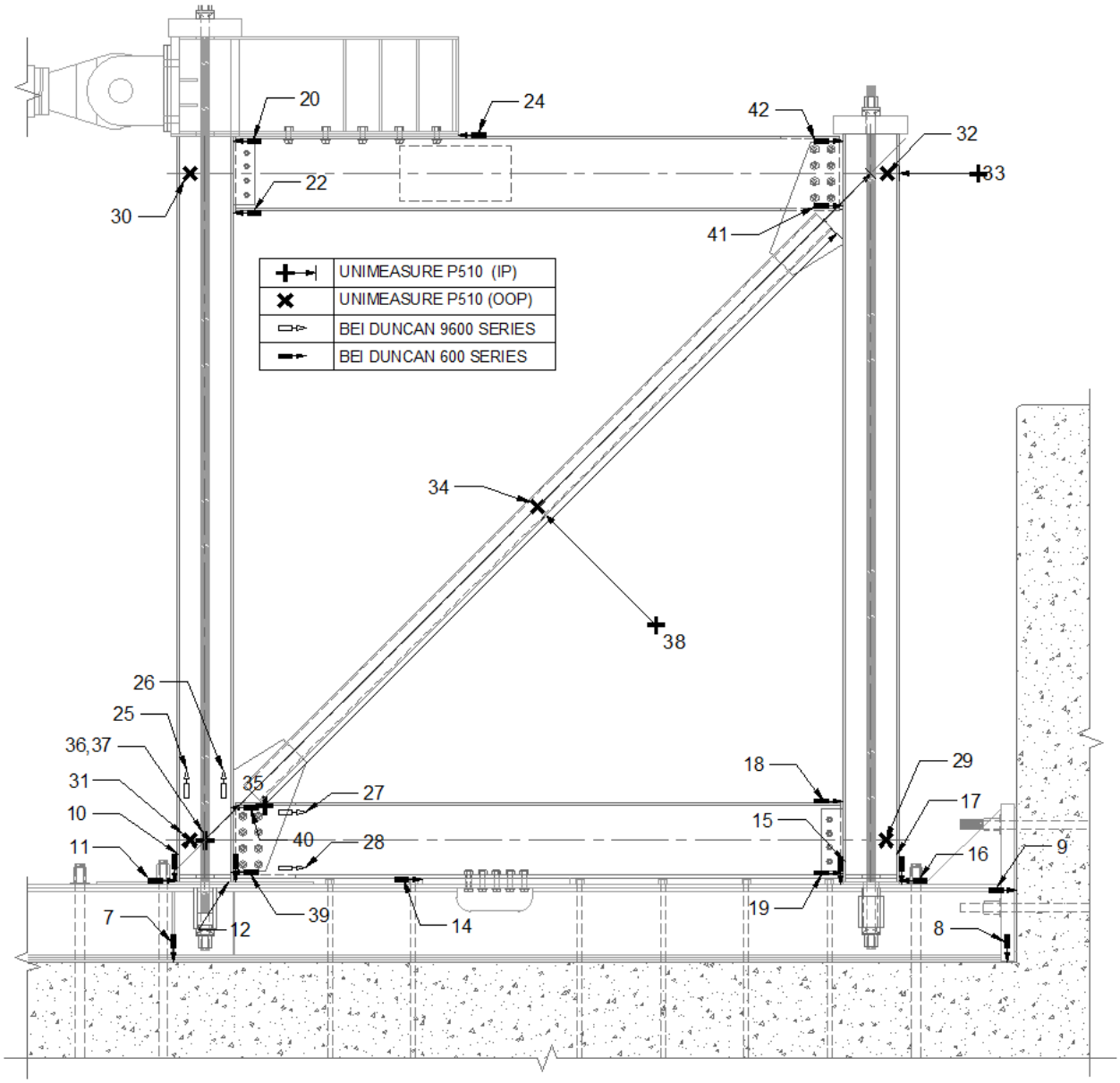

Figure A-10: NCBF5 Potentiometer Layout

Table A-10: NCBF5 Potentiometer Location and Description

Ch. #	Instrument Description	Location			Axis	Length	Instrument Type	Calibration Factor
		x (in)	y (in)	z (in)				
0	Resistor	NA	NA	NA	NA	NA	Resistor	1
1	Actuator Load	NA	NA	NA	NA	NA	Load Cell	50
2	Actuator Displacement	NA	NA	NA	NA	NA	LVDT	1
3	Reaction Block Slip - South	-127.0	105.3	-17.0	X-	0.2	D600	0.04954
4	Actuator Base Slip	-127.0	161.8	14.0	X-	0.2	D600	0.04944
5	Reaction Block Slip - Middle	-127.0	151.3	-17.0	X-	0.2	D600	0.04929
6	Reaction Block Slip - North	-127.0	189.3	-17.0	X-	0.2	D600	0.04974
7	Channel Assembly Uplift - West	-6.8	-26.3	6.4	Y-	0.2	D600	0.05008
8	Channel assembly Uplift - East	174.5	-26.3	8.4	Y-	0.2	D600	0.05009
9	Channel Assembly Slip	175.5	-9.8	8.4	X+	0.7	D600	0.15009
10	West Column West Flange Uplift	-6.4	-9.1	5.0	Y-	0.7	D600	0.1503
11	West Column Slip	-6.2	-8.9	3.0	X+	0.2	D600	0.0491
12	West Column East Flange Uplift	6.5	-9.1	4.0	Y-	0.2	D600	0.04978
13	Resistor	NA	NA	NA	NA	NA	Resistor	NA
14	Beam Slip at Shear Release	45.0	-8.3	2.4	X+	0.2	D600	0.04959
15	East Column West Flange Uplift	137.6	-9.1	5.0	Y-	0.7	D600	0.15084
16	East Column Slip	150.2	-8.8	2.0	X-	0.7	D600	0.09933
17	East Column East Flange Uplift	150.4	-9.1	5.0	Y-	0.7	D600	0.09862
18	SE Shear Tab Rotation - North	137.9	8.3	1.2	X+	0.7	D600	0.14916
19	SE Shear Tab Rotation - South	137.9	-7.2	1.2	X+	0.7	D600	0.15093
20	NW Shear Tab Rotation - South	6.2	135.7	1.4	X-	0.7	D600	0.14963
21	Resistor	NA	NA	NA	NA	NA	Resistor	NA
22	NW Shear Tab Rotation - North	6.2	151.2	1.4	X-	0.7	D600	0.1522
23	Resistor	NA	NA	NA	NA	NA	Resistor	NA
24	Load Transfer Beam Slip	54.7	152.3	0.9	X-	0.7	D600	0.14904
25	West Column Plastic Hinge Rotation - West	-3.0	22.6	1.2	Y+	2.0	D9600	0.20271
26	West Column Plastic Hinge Rotation - East	3.0	22.6	1.2	Y+	2.0	D9600	0.2008
27	South Beam Plastic Hinge Rotation - North	24.8	5.0	-2.1	X+	2.0	D9600	0.20277
28	South Beam Plastic Hinge Rotation - South	24.8	-5.0	-2.1	X+	2.0	D9600	0.2011
29	SE Out-of-Plane Frame Displacement	147.0	0.0	-0.2	Z+	14.7	P510	2.00805
30	NW Out-of-Plane Frame Displacement	-3.0	144.0	-0.2	Z+	14.7	P510	2.00041
31	SW Out-of-Plane Frame Displacement	-3.0	0.0	-0.2	Z+	14.7	P510	2.00102
32	NE Out-of-Plane Frame Displacement	147.0	144.0	-0.2	Z+	14.7	P510	2.01094
33	Frame Lateral Displacement	150.2	144.0	0.0	X-	18.5	P510	1.99215
34	Brace Out-of-Plane Displacement	72.0	72.0	14.9	Z+	11.5	P510	4.01401
35	Brace Elongation	10.2	10.2	-4.7	X+Y+	143.0	P510	3.26321
36	Frame Diagonal Measurement - Bottom	0.0	0.0	23.4	+X+Y	203.6	P510	4.65537
37	Frame Diagonal Measurement - Top	0.0	0.0	28.6	+X+Y	203.6	P510	4.6914
38	Brace In Plane Displacement	73.8	70.2	0.2	X-Y+	27.75	P510	4.36751
39	SW Connection Rotation - South	6.2	-7.2	-3.5	X-	0.5	D600	0.10111
40	SW Connection Rotation - North	6.2	7.2	-3.5	X-	0.5	D600	0.10086
41	NE Connection Rotation -South	137.9	136.8	-3.5	X+	0.75	D600	0.14882
42	NE Connection Rotation - North	137.9	151.2	-3.5	X+	0.75	D600	0.1503
43	Terminator	NA	NA	NA	NA	NA	Terminator	NA

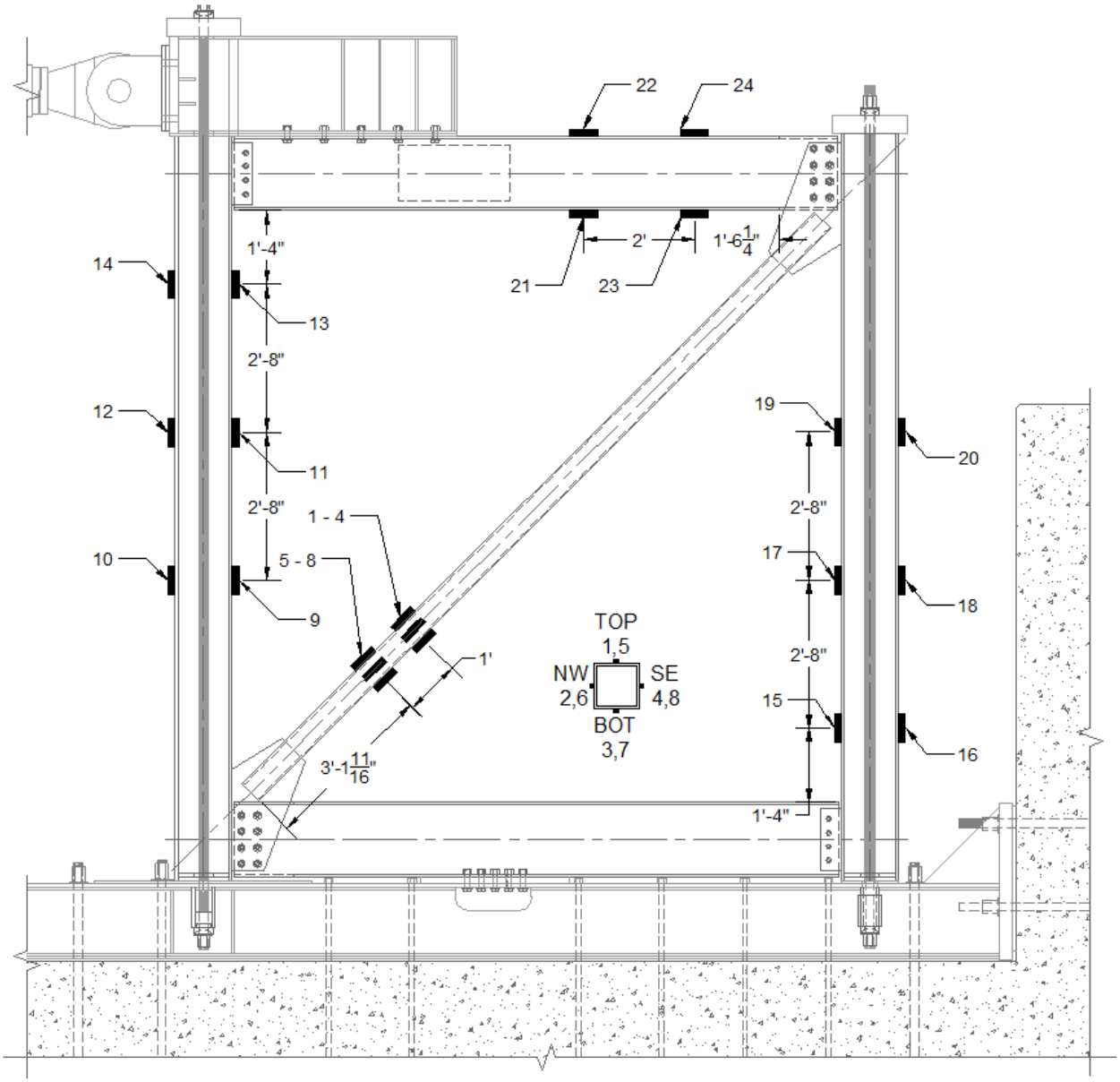

Figure A-11: NCBF5 Strain Gauge Layout

Table A-11: NCBF5 Strain Gauge Location and Description

Ch. #	Instrument Description	Location			Axis	Calibration Factor
		x (in)	y (in)	z (in)		
0	Resistor	NA	NA	NA	NA	NA
1	SG1 - Brace Group 1 - Top	36.9	36.9	2.7	+X+Y	121.16
2	SG2 - Brace Group 1 - Side NW	35.1	38.6	0.2	+X+Y	121
3	SG3 - Brace Group 1 - Side SE	38.6	35.1	0.2	+X+Y	121.05
4	SG4 - Brace Group 1 - Bottom	36.9	36.9	2.3	+X+Y	120.99
5	SG5 - Brace Group 2 - Top	45.3	45.3	2.7	+X+Y	120.9
6	SG6 - Brace Group 2 - Side NW	43.6	47.1	0.2	+X+Y	120.94
7	SG7 - Brace Group 2 - Side SE	47.1	43.6	0.2	+X+Y	120.96
8	SG8 - Brace Group 2 - Bottom	45.3	45.3	2.3	+X+Y	121.2
9	SG9 - West Column SE	6.2	56.0	0.0	+Y	121.12
10	SG10 - West Column SW	-6.2	56.0	0.0	+Y	121.29
11	SG11 - West Column E	6.2	88.0	0.0	+Y	121.1
12	SG12 - West Column W	-6.2	88.0	0.0	+Y	121.23
13	SG13 - West Column NE	6.2	120.0	0.0	+Y	121.32
14	SG14 - West Column NW	-6.2	120.0	0.0	+Y	121.2
15	SG15 - East Column SW	137.9	24.1	0.0	+Y	122.14
16	SG16 - East Column SE	150.2	24.1	0.0	+Y	122.72
17	SG17 - East Column W	137.9	56.1	0.0	+Y	122.72
18	SG18 - East Column E	150.2	56.1	0.0	+Y	122.7
19	SG19 - East Column NW	137.9	88.1	0.0	+Y	123.25
20	SG20 - East Column NE	150.2	88.1	0.0	+Y	123.04
21	SG21 - North Beam SW	82.2	136.0	-0.6	+X	122.01
22	SG22 - North Beam NW	82.2	152.0	-0.6	+X	121.98
23	SG23 - North Beam SE	106.2	136.0	-0.6	+X	122.25
24	SG24 - North Beam NE	106.2	152.0	-0.6	+X	122.06
25	Terminator	NA	NA	NA	NA	NA

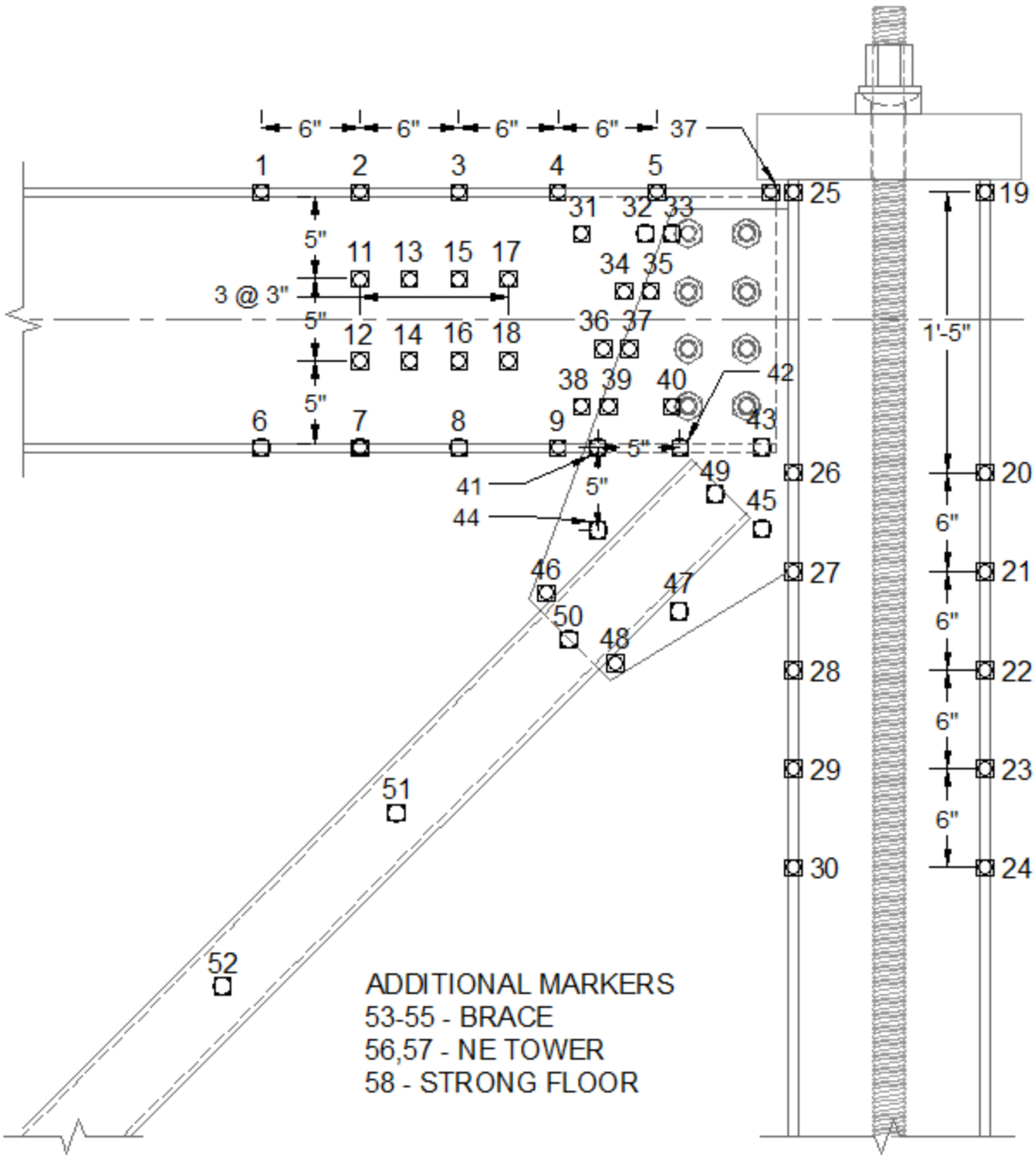

Figure A-12: NCBF5 OptoTrak Layout

Table A-12: NCBF5 OptoTrak Location and Description

Marker	Coordinates			Location
	x (in)	y (in)	z (in)	
1	105.9	151.8	3.0	North Beam North Flange
2	111.8	151.9	3.0	North Beam North Flange
3	117.9	151.8	3.0	North Beam North Flange
4	123.9	151.8	3.0	North Beam North Flange
5	130.0	151.9	-0.4	North Beam North Flange
6	136.5	152.3	1.0	North Beam North Flange
7	106.0	136.2	2.9	North Beam South Flange
8	112.0	136.1	2.9	North Beam South Flange
9	118.1	136.1	2.9	North Beam South Flange
10	124.1	136.1	3.0	North Beam South Flange
11	112.0	146.5	-0.4	North Beam Web
12	111.8	142.0	0.7	North Beam Web
13	115.0	146.5	-0.4	North Beam Web
14	115.1	141.5	-0.5	North Beam Web
15	117.8	147.0	0.8	North Beam Web
16	118.2	141.4	-0.5	North Beam Web
17	121.1	146.5	-0.4	North Beam Web
18	121.2	141.5	-0.5	North Beam Web
19	149.8	152.3	7.3	East Column East Flange
20	149.8	135.1	7.3	East Column East Flange
21	149.8	129.0	7.3	East Column East Flange
22	149.8	123.0	7.3	East Column East Flange
23	149.8	117.0	7.3	East Column East Flange
24	149.8	111.0	7.3	East Column East Flange
25	138.2	152.4	7.4	East Column West Flange
26	138.2	135.1	7.4	East Column West Flange
27	138.2	129.1	7.3	East Column West Flange
28	138.7	122.5	6.3	East Column West Flange
29	138.7	116.5	6.3	East Column West Flange

Marker	Coordinates			Location
	x (in)	y (in)	z (in)	
30	138.6	110.4	6.4	East Column West Flange
31	125.2	149.4	-0.4	Gusset Plate
32	129.5	149.4	-0.4	Beam Web
33	130.6	149.8	1.8	Gusset Plate
34	128.2	146.0	-0.4	Beam Web
35	129.4	146.3	1.7	Gusset Plate
36	126.9	142.3	-0.5	Beam Web
37	128.4	142.3	0.5	Gusset Plate
38	125.4	139.3	0.7	Beam Web
39	127.2	138.7	0.4	Gusset Plate
40	130.8	139.3	1.6	Beam Web
41	126.4	134.1	0.0	Gusset Plate
42	131.3	136.3	0.4	Gusset Plate
43	135.9	136.7	1.7	Gusset Plate
44	126.3	131.2	0.4	Gusset Plate
45	136.3	131.3	0.5	Gusset Plate
46	123.0	127.7	0.4	Gusset Plate
47	131.4	126.2	0.6	Gusset Plate
48	128.1	123.0	0.5	Gusset Plate
49	133.5	133.3	2.8	Brace
50	125.0	124.8	2.7	Brace
51	113.5	113.2	2.7	Brace
52	103.7	103.4	2.7	Brace
53	93.2	91.0	2.7	Brace
54	82.7	80.6	2.7	Brace
55	72.1	70.1	2.8	Brace
56	137.3	143.2	8.5	NE Frame Diagonal Mount
57	137.9	144.0	26.1	NE Frame Diagonal Mount
58	129.5	123.7	-16.3	Strong Floor Reference

Highlighted cells indicate that the LED maker may not have been functioning properly during the test.

A.5: NCBF2-R1 Instrumentation Plan

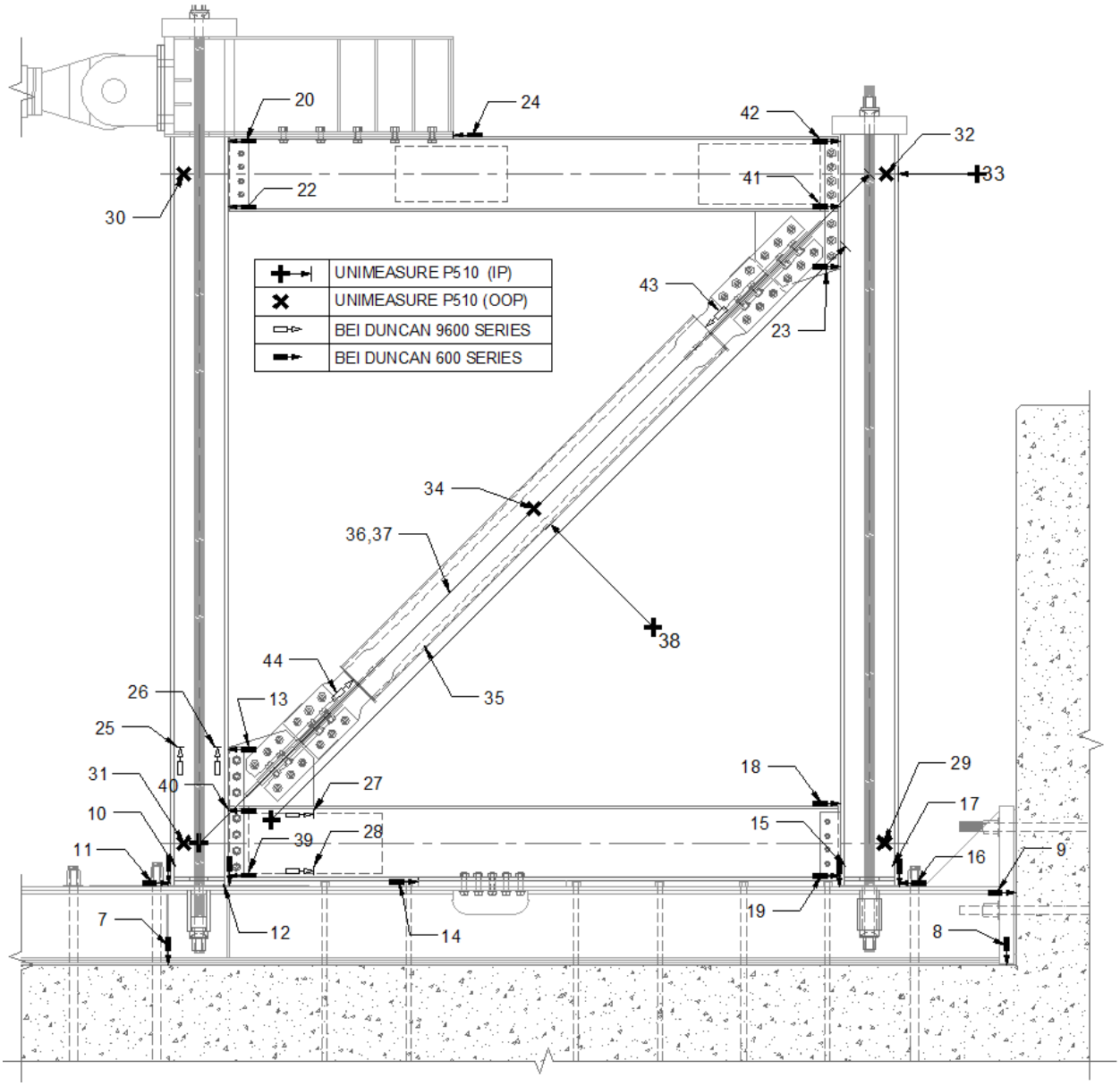

Figure A-13: NCBF2-R1 Potentiometer Layout

Table A-13: NCBF2-R1 Potentiometer Location and Description

Ch. #	Instrument Description	Location			Axis	Length	Instrument Type	Calibration Factor
		x (in)	y (in)	z (in)				
0	Resistor	NA	NA	NA	NA	NA	Resistor	1
1	Actuator Load	NA	NA	NA	NA	NA	Load Cell	50
2	Actuator Displacement	NA	NA	NA	NA	NA	LVDT	1
3	Reaction Block Slip - South	-127.0	105.3	-17.0	X-	0.2	D600	0.04954
4	Actuator Base Slip	-127.0	161.8	14.0	X-	0.2	D600	0.04944
5	Reaction Block Slip - Middle	-127.0	151.3	-17.0	X-	0.2	D600	0.04929
6	Reaction Block Slip - North	-127.0	189.3	-17.0	X-	0.2	D600	0.04974
7	Channel Assembly Uplift - West	-6.8	-26.3	6.4	Y-	0.2	D600	0.05008
8	Channel assembly Uplift - East	174.5	-26.3	8.4	Y-	0.2	D600	0.05009
9	Channel Assembly Slip	175.5	-9.8	8.4	X+	0.7	D600	0.15009
10	West Column West Flange Uplift	-6.4	-9.1	5.0	Y-	0.7	D600	0.1503
11	West Column Slip	-6.2	-8.9	3.0	X+	0.2	D600	0.0491
12	West Column East Flange Uplift	6.5	-9.1	4.0	Y-	0.2	D600	0.04978
13	SW Gusset Plate-To-Beam Gap	6.2	20.5	-0.6	X-	0.7	D600	0.1501
14	Beam Slip at Shear Release	45.0	-8.3	2.4	X+	0.2	D600	0.15081
15	East Column West Flange Uplift	137.6	-9.1	5.0	Y-	0.7	D600	0.15084
16	East Column Slip	150.2	-8.8	2.0	X-	0.7	D600	0.09933
17	East Column East Flange Uplift	150.4	-9.1	5.0	Y-	0.7	D600	0.09862
18	SE Shear Tab Rotation - North	137.9	8.3	1.4	X+	0.7	D600	0.14916
19	SE Shear Tab Rotation - South	137.9	-7.2	1.4	X+	0.7	D600	0.15093
20	NW Shear Tab Rotation - South	6.2	135.7	1.6	X-	0.7	D600	0.14963
21	Resistor	NA	NA	NA	NA	NA	Resistor	NA
22	NW Shear Tab Rotation - North	6.2	151.2	1.6	X-	0.7	D600	0.1522
23	NE Gusset Plate-To-Beam Gap	137.9	123.5	-0.6	X+	0.5	D600	0.10053
24	Load Transfer Beam Slip	54.7	152.3	0.9	X-	0.7	D600	0.14904
25	West Column Plastic Hinge Rotation - West	-3.0	22.6	1.4	Y+	2.0	D9600	0.20271
26	West Column Plastic Hinge Rotation - East	3.0	22.6	1.4	Y+	2.0	D9600	0.2008
27	South Beam Plastic Hinge Rotation - North	24.8	5.0	1.4	X+	2.0	D9600	0.20277
28	South Beam Plastic Hinge Rotation - South	24.8	-5.0	1.4	X+	2.0	D9600	0.2011
29	SE Out-of-Plane Frame Displacement	147.0	0.0	-0.2	Z+	14.7	P510	2.00805
30	NW Out-of-Plane Frame Displacement	-3.0	144.0	-0.2	Z+	14.7	P510	2.00041
31	SW Out-of-Plane Frame Displacement	-3.0	0.0	-0.2	Z+	14.7	P510	2.00102
32	NE Out-of-Plane Frame Displacement	147.0	144.0	-0.2	Z+	14.7	P510	2.01094
33	Frame Lateral Displacement	150.2	144.0	0.0	X-	18.5	P510	1.99215
34	Brace Out-of-Plane Displacement	72.0	72.0	14.9	Z+	11.5	P510	4.01401
35	Brace Elongation	12.3	8.3	-7.0	X+Y+	157.0	P510	3.26321
36	Frame Diagonal Measurement - Bottom	0.0	0.0	23.4	+X+Y	203.6	P510	4.65537
37	Frame Diagonal Measurement - Top	0.0	0.0	28.6	+X+Y	203.6	P510	4.6914
38	Brace In Plane Displacement	75.4	68.5	0.0	X-Y+	26.5	P510	4.36751
39	SW Connection Rotation - South	6.2	-7.2	-3.0	X-	0.5	D600	0.10111
40	SW Connection Rotation - North	6.2	7.2	-3.0	X-	0.5	D600	0.10086
41	NE Connection Rotation -South	137.9	136.8	-3.0	X+	0.75	D600	0.14882
42	NE Connection Rotation - North	137.9	151.2	-3.0	X+	0.75	D600	0.1503
43	BRB Core Plate Elongation NE	33.1	35.2	1.2	X+Y+	4	D9600	0.40101
44	BRB Core Plate Elongation SW	108.8	111.0	1.2	X-Y-	4	D9600	0.42242
45	Terminator	NA	NA	NA	NA	NA	Terminator	NA

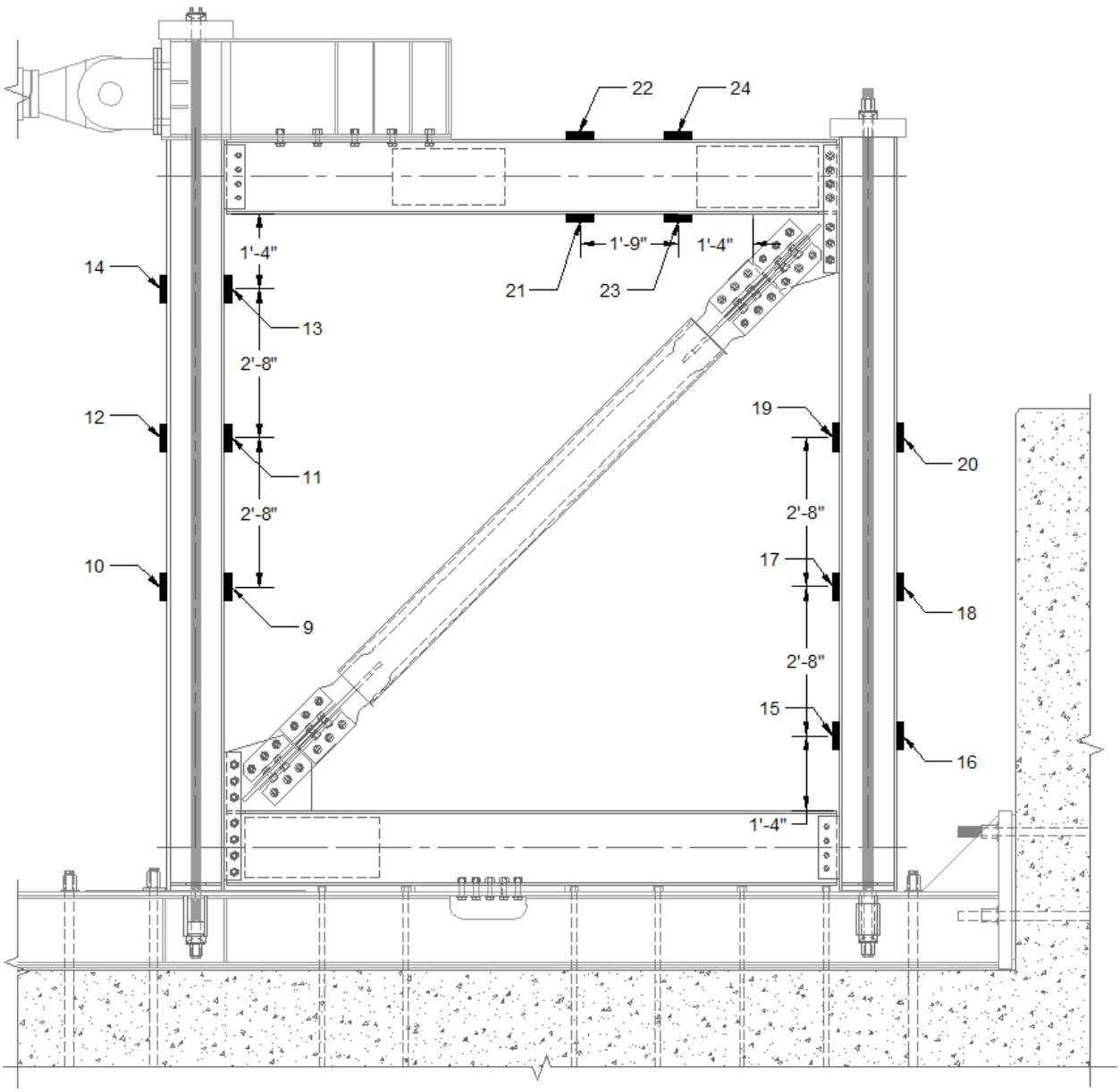

Figure A-14: NCBF2-R1 Strain Gauge Layout

Table A-14: NCBF2-R1 Strain Gauge Location and Description

Ch. #	Instrument Description	Location			Axis	Resistance
		x (in)	y (in)	z (in)		
0	Resistor	NA	NA	NA	NA	NA
1	Resistor	NA	NA	NA	NA	NA
2	Resistor	NA	NA	NA	NA	NA
3	Resistor	NA	NA	NA	NA	NA
4	Resistor	NA	NA	NA	NA	NA
5	Resistor	NA	NA	NA	NA	NA
6	Resistor	NA	NA	NA	NA	NA
7	Resistor	NA	NA	NA	NA	NA
8	Resistor	NA	NA	NA	NA	NA
9	SG9 - West Column SE	6.2	56.0	0.0	+Y	121.3
10	SG10 - West Column SW	-6.2	56.0	0.0	+Y	121.09
11	SG11 - West Column E	6.2	88.0	0.0	+Y	121.03
12	SG12 - West Column W	-6.2	88.0	0.0	+Y	121.25
13	SG13 - West Column NE	6.2	120.0	0.0	+Y	121.18
14	SG14 - West Column NW	-6.2	120.0	0.0	+Y	121.35
15	SG15 - East Column SW	137.9	24.1	0.0	+Y	122.03
16	SG16 - East Column SE	150.2	24.1	0.0	+Y	122.46
17	SG17 - East Column W	137.9	56.1	0.0	+Y	122.66
18	SG18 - East Column E	150.2	56.1	0.0	+Y	122.56
19	SG19 - East Column NW	137.9	88.1	0.0	+Y	121.97
20	SG20 - East Column NE	150.2	88.1	0.0	+Y	122.06
21	SG21 - North Beam SW	82.4	136.0	0.2	+X	122.69
22	SG22 - North Beam NW	82.4	152.0	0.2	+X	122.78
23	SG23 - North Beam SE	103.4	136.0	0.2	+X	122.79
24	SG24 - North Beam NE	103.4	152.0	0.2	+X	122.24
25	Terminator	NA	NA	NA	NA	NA

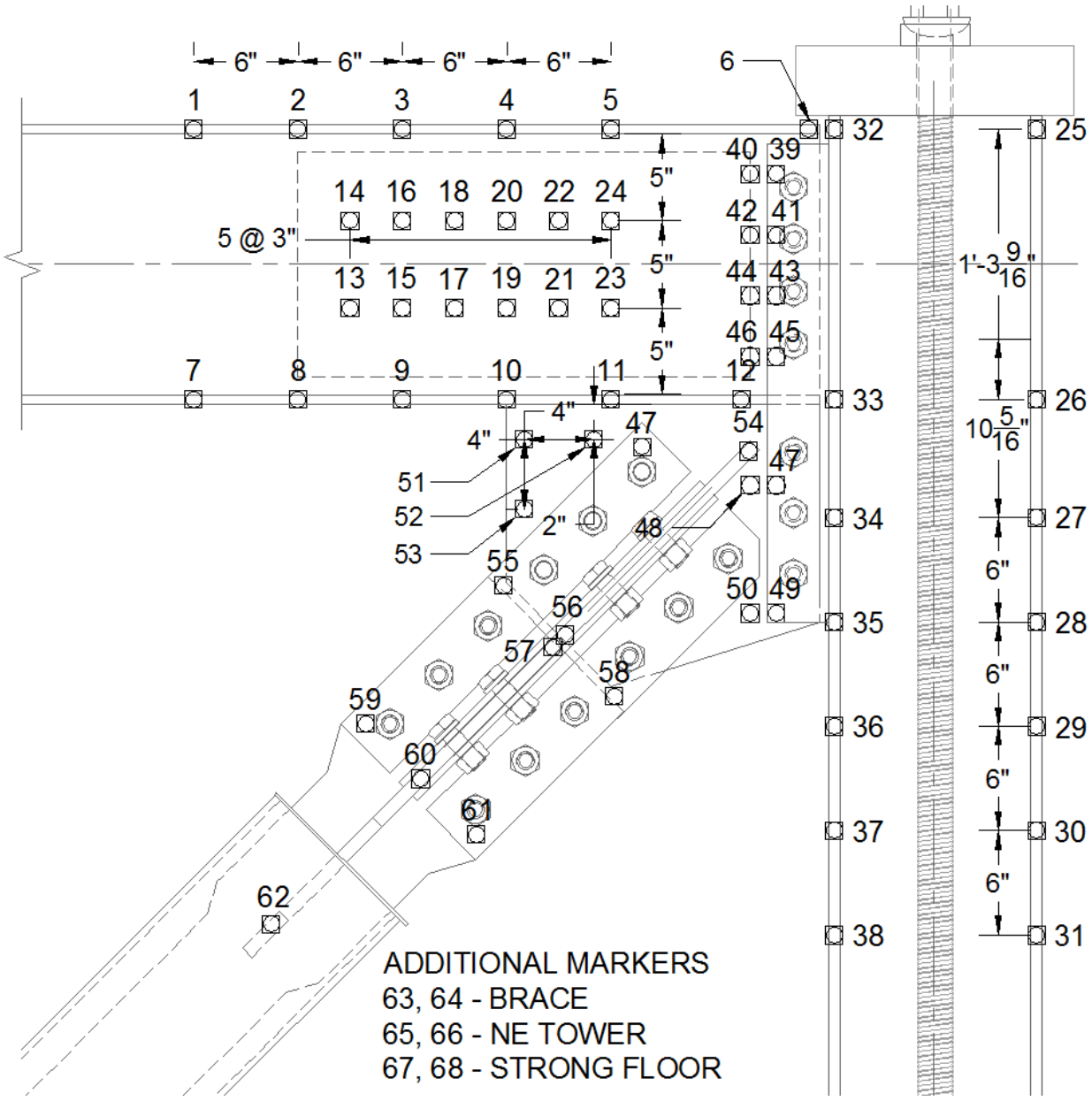

Figure A-15: NCBF2-R1 OptoTrak Layout

Table A-15: NCBF2-R1 OptoTrak Location and Description

Marker	Coordinates			Location
	x (in)	y (in)	z (in)	
1	101.7	151.8	3.9	North Beam North Flange
2	107.7	151.8	3.9	North Beam North Flange
3	113.7	151.9	3.9	North Beam North Flange
4	119.7	151.9	3.9	North Beam North Flange
5	125.7	151.8	3.9	North Beam North Flange
6	137.0	151.8	3.9	North Beam North Flange
7	101.6	136.2	3.6	North Beam South Flange
8	107.7	136.2	3.6	North Beam South Flange
9	113.7	136.2	3.6	North Beam South Flange
10	119.6	136.1	3.6	North Beam South Flange
11	125.6	136.1	3.5	North Beam South Flange
12	133.1	136.1	3.5	North Beam South Flange
13	110.4	141.5	0.4	North Beam Web
14	110.5	146.6	0.5	North Beam Web
15	113.5	141.5	0.4	North Beam Web
16	113.5	146.5	0.4	North Beam Web
17	116.5	141.5	0.4	North Beam Web
18	116.5	146.6	0.4	North Beam Web
19	119.5	141.5	0.3	North Beam Web
20	119.5	146.6	0.4	North Beam Web
21	122.5	141.5	0.3	North Beam Web
22	122.5	146.6	0.4	North Beam Web
23	125.6	141.5	0.3	North Beam Web
24	125.6	146.6	0.4	North Beam Web
25	149.8	151.9	5.7	East Column East Flange
26	149.8	136.3	5.6	East Column East Flange
27	149.9	129.5	5.6	East Column East Flange
28	149.8	123.6	5.6	East Column East Flange
29	149.8	117.5	5.7	East Column East Flange
30	149.8	111.5	5.7	East Column East Flange
31	149.7	105.6	5.7	East Column East Flange
32	138.2	151.9	5.9	East Column West Flange
33	138.2	136.1	5.9	East Column West Flange
34	138.2	129.4	5.9	East Column West Flange

Marker	Coordinates			Location
	x (in)	y (in)	z (in)	
35	138.2	123.5	5.9	East Column West Flange
36	138.2	117.5	5.9	East Column West Flange
37	138.2	111.5	5.9	East Column West Flange
38	138.2	105.6	5.9	East Column West Flange
39	134.4	148.4	1.2	Shear Plate Bolt Group
40	133.3	148.4	0.4	Shear Plate Bolt Group
41	134.5	145.4	1.1	Shear Plate Bolt Group
42	133.2	145.4	0.4	Shear Plate Bolt Group
43	134.5	142.5	1.1	Shear Plate Bolt Group
44	133.2	142.5	0.3	Shear Plate Bolt Group
45	134.4	139.5	1.0	Shear Plate Bolt Group
46	133.2	139.4	0.3	Shear Plate Bolt Group
47	134.4	131.4	0.9	Shear Plate Bolt Group
48	133.3	131.2	0.2	Shear Plate Bolt Group
49	134.4	124.0	0.9	Shear Plate Bolt Group
50	133.3	124.0	0.2	Shear Plate Bolt Group
51	120.5	134.1	0.1	Gusset Plate
52	124.4	134.1	0.2	Gusset Plate
53	120.4	130.0	0.1	Gusset Plate
54	133.2	132.7	5.2	BRB Connection
55	119.0	125.9	0.5	BRB Connection
56	123.0	122.9	5.1	BRB Connection
57	121.9	121.9	5.2	BRB Connection
58	126.0	119.1	0.3	BRB Connection
59	110.7	117.7	0.4	BRB Connection
60	114.0	114.1	5.1	BRB Connection
61	117.6	110.9	0.3	BRB Connection
62	106.0	106.0	4.4	BRB Casing
63	89.0	89.0	4.2	BRB Casing
64	71.9	72.1	4.0	BRB Casing
65	137.5	142.6	23.3	NE Frame Diagonal Mount
66	137.3	142.5	4.0	NE Frame Diagonal Mount
67	128.7	114.1	-17.7	Strong Floor Reference
68	128.3	108.9	-17.7	Strong Floor Reference

Appendix B: Connection Specific DCR Evaluation

This appendix details how the DCR evaluation introduced in Section 2.3.2 was applied to specific connection types identified in the infrastructure review including the bolted end plate (Section B.1), integrated gusset-shear plate (Section B.2), and bolted shear plate connections (Section B.3). Sections B.1 - B.3 include (1) a list of applicable limit states for each connection type (not including limit states directly in the line of the brace)[6], (2) a table detailing individual limit state demands and capacities specific to the connection, (3) a step by step procedure for determine demands at each connection interface, and (4) a figure depicting the distribution of forces on the connection at important steps of the calculation. All of the connections listed above were evaluated using the CVM approach. Assumptions for the CVM are listed in Section 2.3.2.

The welded continuous shear plate connection is not presented in this appendix but follows a similar approach (CVM) to the presented connections. The bolted split shear plate connection and bolted double angle connections were evaluated using the UFM (part 13 AISC 2010). The DCR evaluation presented here was used to determine connection specific DCRs from both the testing program and the infrastructure review.

Note that the capacities of the welds and base metal in each of the connection types listed above were evaluated using two approaches, BR-CVM and GP-CVM (as described in Section 2.3.2), and the computed demands on the weld groups are only applicable to the former method.

[6] Limit states directly in the line of the brace include: brace net section fracture, Whitmore yielding, Whitmore fracture, block shear (brace or gusset plate), and brace-to-gusset splice weld fracture.

B.1 Bolted End Plate

The connection limit states for bolted end plates include shear/tension rupture of the bolts, beam-to-gusset plate weld fracture, gusset plate-to-end plate weld fracture, beam-to-end plate weld fracture, and bolt bearing in the end plate. The DCR evaluation for the limit states related to the bolts in the end plate connection is documented in Table B-1. DCR evaluation of the welds is discussed in Section 2.3.2.

Table B-1: Connection Specific DCR Evaluation for Bolted End Plates

Limit State	Demand	Capacity ($\emptyset \boldsymbol{R_n}$)	(AISC 2014)
Bolt Tension Rupture (Individual Bolt)	$T_i/2$	$\left(1.3F_{nt} - \frac{F_{nt}}{\emptyset F_{nv}} f_{nv} \leq F_{nt}\right) A_{bolt}$	Eq J3-2
Bolt Shear Rupture (Individual Bolt)	$\frac{V_I}{N_{bolts}}$	$\left(1.3F_{nv} - \frac{F_{nv}}{\emptyset F_{nt}} f_{nt} \leq F_{nv}\right) A_{bolt}$	Eq J3-2
End Plate Bearing (Bolt Group)	V_I	$3.0\min\left(t_{ep}F_{uep}, t_{fc}F_{uc}\right) d_{bolt}N_{bolt}$	Eq J3-6-b

Symbol	Name	Equation/Value
V_I, T_i	Connection Demands	Figure B-1
F_{nt}	Nominal Tension Capacity of Bolt	Table J3.2
F_{nv}	Nominal Shear Capacity of Bolt	Table J3.2
f_{nv}	Applied Bolt Shear Stress	$V_I/(N_{bolt}A_{bolt})$
f_{nt}	Applied Bolt Tensile Stress	$T_i/(2A_{bolt})$
A_{bolt}	Cross Sectional Area of the End Plate Bolt	-
d_{bolt}	Diameter of the End Plate Bolts	-
N_{bolts}	Number of Bolts in End Plate	-
t_{ep}	Thickness of the End Plate	-
F_{uep}	Ultimate Tensile Capacity of End Plate	-
t_{fc}	Thickness of the Column Flange	-
F_{ufc}	Ultimate Tensile Capacity of Column	-

Since the end plate bolts are subjected to both shear and tensile force it is necessary to check for the combined capacity of the bolts. It is assumed that the bolt pretension would be overcome and the bolts would begin bearing on the bolt holes for all reference and test connections. The bolt tension rupture and bolt shear rupture limit states consider reduced nominal capacities of the bolts shear and tension strength based on the applied force in the orthogonal direction. The bolt pretension did not factor into the bolt shear or tension capacities.

The forces acting on the bolts and the beam-to-gusset plate weld are determined using the procedure outlined below.

1. Make a cut at the column interface and solve for the overall amount of shear and moment acting on the end plate bolts as shown in Figure B-1a.

2. Distribute the shear and moment force calculated in step one to the end plate and end plate bolts following the procedure outlined in part 7 (pg. 7-10) "Design Considerations for Bolts" of the AISC Steel Manual (AISC 2014) as shown in Figure B-1b.

3. For each set of bolts in tension determine the additional tensile force induced by prying action as detailed in part 9 (pg. 9-10) "Design of Connecting Elements" of the AISC Steel Manual (AISC 2014). The tension forces on the bolts are used in the bolt shear rupture failure mode limit state.

4. Make a cut around the gusset plate and use equilibrium to determine the shear H_b, tension V_b, and moment M_b, acting on the beam-gusset plate weld as shown in Figure B-1c. V_{cgp} is determined assuming each bolt in the end plate carries equal portions of the shear, V_I.

5. The forces on the gusset plate-to-end plate welds, and the beam-to-end plate welds are determined by taking the resultant end plate forces about the centroid of each weld.

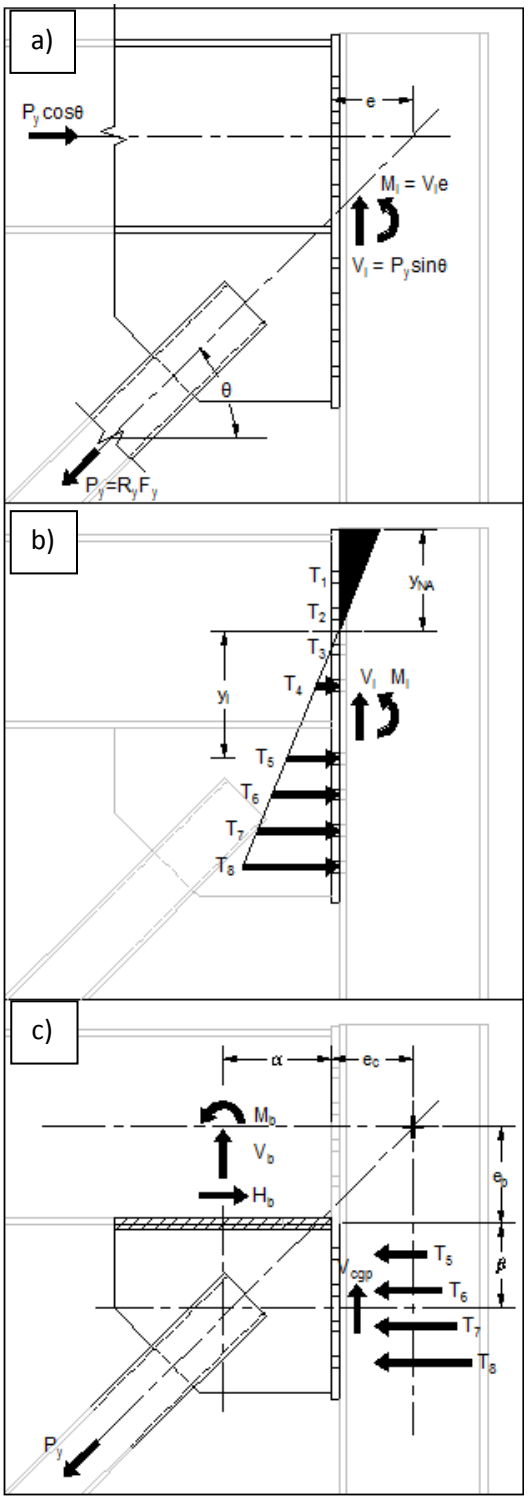

Figure B-1: Distribution of Forces and Free Body Diagrams for Bolted End Plate Connections

B.2 Integrated Gusset-Shear Plate

Connection specific limit states (shown in Table B-2) for the integrated gusset-shear plate connection include bolt shear rupture, bolt bearing, gusset plate base metal yielding at the column interface, and weld fracture of the CJP weld. The DCR evaluation for the limit states related to the bolts connecting the beam and gusset plate is detailed in Table B-2. Weld and base metal limit states for weld are discussed in Section 2.3.2.

Table B-2: Connection Specific DCR Evaluation for Integrated Gusset-Shear Plates

Limit State	Demand	Capacity ($\emptyset R_n$)	(AISC 2014)
Bolt Shear Rupture	$P_y cos\theta$	$\emptyset F_{nv} A_{bolt} N_{bolt}$	Eq J3-2
Bolt Bearing	$P_y cos\theta$	$\emptyset\ 3.0\min(t_{wb}F_{ub}, t_{gp}F_{ugp})\ d_{bolt} N_{bolt}$	Eq J2-4

Symbol	Name	Equation/Value
$A_{bolt}, d_{bolt}, N_{bolt}$	Cross Sectional Area, Diameter, and Number of Bolts	-
t_{wb}	Thickness of the Beam Web	-
F_{ub}	Ultimate Tensile Capacity of the Beam	-
t_{gp}	Thickness of the Gusset Plate	-
F_{ugp}	Ultimate Capacity of the Gusset Plate	-

Figure B-2 shows the assumed force distribution for the integrated gusset shear plate connections. The bolt group shown in Figure B-2 is assumed to transfer the horizontal component of the brace force into the beam, while the vertical component of the brace force and the moment resulting from the eccentricity between the beam and brace lines of action is assumed to go to the column-gusset plate interface. Although the bolt limit states are evaluated only using this horizontal component of the brace force, note that they must also transfer flexural frame forces from the beam into the brace and column.

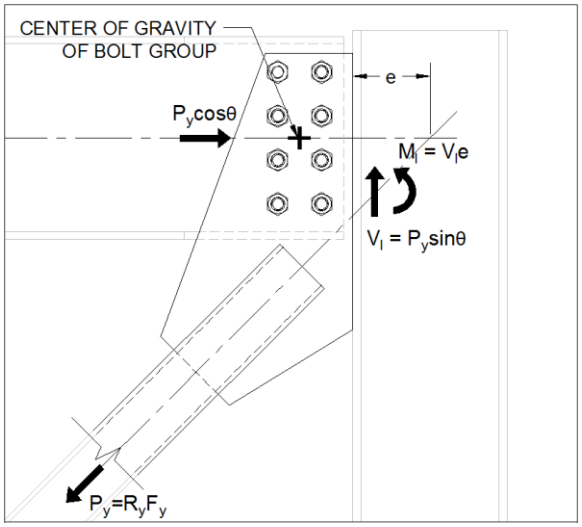

Figure B-2: Distribution of Forces and Free Body Diagrams for Integrated Gusset-Shear Plate Connections

B.3Bolted Continuous Shear Plate

The limit states for bolted continuous shear tabs include bolt shear rupture, shear tab yielding, bolt bearing, beam-to-gusset plate weld fracture, and shear tab weld fracture. The DCR evaluation for the bolt group limit states is detailed in Table B-3 and Figure B-3. The determination of force demands on the bolt group and beam-to-gusset plate weld for this connection are described alongside Figure B-3.

Table B-3: Connection Specific DCR Evaluation for Bolted Continuous Shear Plates

Limit State	**Demand**	**Capacity** $(\emptyset \boldsymbol{R_n})$	**(AISC 2014)**
Bolt Group Shear/ Bearing	$Psin\theta$	$P_{IC}(R_{ult} = \min(R_1, R_2, R_3))$	Part 7

Symbol	**Name**	**Equation/Value**
P_{IC}	Instantaneous Center Load Capacity	Step 2 - Figure B-3
R_{ult}	Ultimate Capacity of Each Bolt in the Bolt Group	-
R_1	Bolt Shear Capacity of Individual Bolt	$\emptyset F_{nv} A_{bolt}$
R_2	Bolt Bearing Capacity of Individual Bolt Part 1	$\emptyset 3.0 \min(t_1 F_{u1}, t_2 F_{u2})\, d_{bolt}$
R_3	Bolt Bearing Capacity of Individual Bolt Part 2	$\emptyset 1.5 l_{clear} \min(t_1 F_{u1}, t_2 F_{u2})$
A_{bolt}	Cross Sectional Area of the End Plate Bolt	-
d_{bolt}	Diameter of the End Plate Bolts	-
F_{nv}	Nominal Shear Capacity of Bolt	Table J3.2
t_1	Thickness of Connection Element 1	-
F_{u1}	Ultimate Tensile Capacity of Connection Element 1	-
t_2	Thickness of Connection Element 2	-
F_{u2}	Ultimate Tensile Capacity of Connection Element 2	-
l_{clear}	Clear distance between Edge of Bolt Hole and Edge of Connecting Element	-

Demands on the bolted continuous shear plate connection elements are determined using the following procedure.

1. Make a cut at the column interface and solve for the shear and moment acting on the weld adjoining the shear plate and column using equilibrium as shown in Figure B-3a.

2. Solve for the instantaneous center and a maximum force the bolt group can develop, P_{IC}, at an eccentricity, e in accordance with part 7 (of the AISC steel design manual 2014) as shown in Figure B-3b.

   Eccentricity for the calculation includes half of the column depth plus the distance between the column flange and the center of gravity of the shear tab bolt group. For each bolt determine the lesser of bolt shear capacity and bolt bearing capacity. The minimum value is used when solving for the instantaneous center, but the assumed maximum displacement (0.34") remains the same for all of the bolts. The clear distance used in the bolt tear out equation must be increased by an amount to account for the angle of the actual resultant load on the bolt.

3. If the maximum force from step 2, P_{IC}, was smaller than the vertical component of the brace force ($P_y \sin\theta$), use the computed bolt forces in step 4. If not, use the center of gravity method and the interface forces calculated in step 1 to determine bolt forces to use in step 4.

4. The forces on the beam-to-gusset plate weld are determined by taking equilibrium about the gusset plate and using the calculated bolt forces from step 3 (V_1, V_2, and V_3) as shown in Figure B-3c.

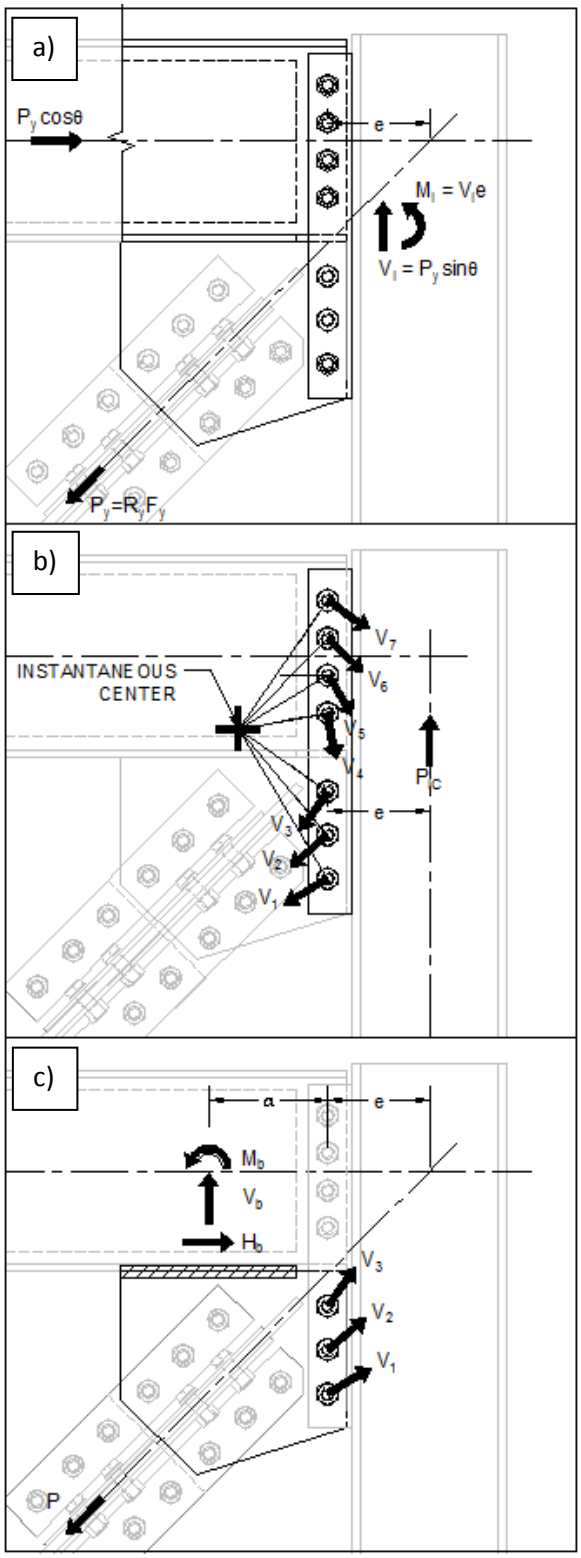

Figure B-3: Distribution of Forces and Free Body Diagrams for Continuous Bolted Shear Plate Connections.

Appendix C: Material Coupon Tests

This appendix contains the tension test results of 28 steel coupons from all of the NCBF tests conducted by Ballard (2015), Sloat (2014), and Johnson (2014). All coupons were tested in accordance with ASTM A370-14. Section C.2 details the experimental setup and discusses the instrumentation, testing procedure, and coupon fabrication. Section C.3 provides a summary of the material strengths for all of the coupons tested and discusses how they were calculated from the test data. Section C.4 contains a table of coupon dimensions and a stress-strain plot for all of the coupons tested.

All of the material presented in this appendix was prepared by Anthony Gasca.

C.1 Coupon Fabrication

Figure C-1 details the dimensions for a standard coupon for the transverse flat tension test defined in ASTM A370-14. The coupons were milled from large sections of steel (blanks) that were removed from the parent material using an acetylene torch. The blanks (~24" x 6") were larger than the final coupon size (18" x 2") to ensure the coupon material properties were not significantly altered by the heat from the torch during cutting. The reduced section of the coupon was finished using a belt sander and produced a smooth finish as shown in Figure C-2.

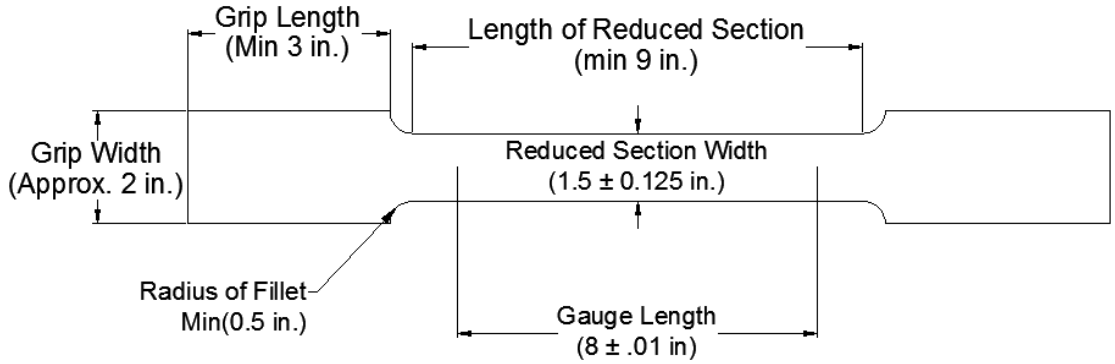

Figure C-1: Standard Coupon Dimensions and Tolerances

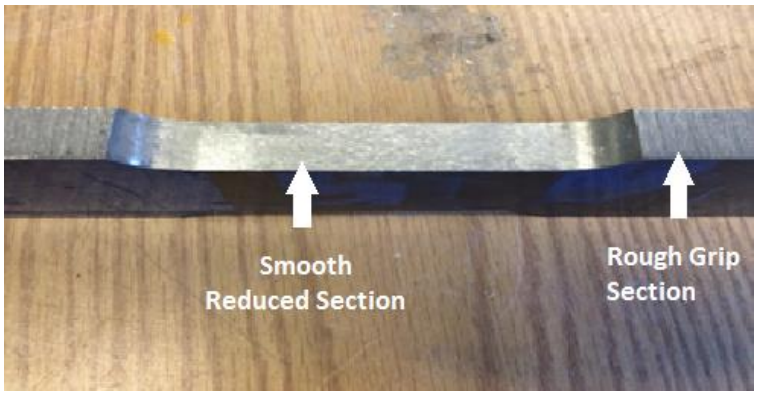

Figure C-2: Example of Coupon Finish (S45)

The dimensions for the coupons can be found in Table C-6. The width of reduced section, gauge length, and thickness were measured using a caliper accurate to 0.001 inch. The coupon grip length, grip width, and length of reduced section of the coupon were measured using a ruler. The value for the thickness of the specimen was taken as the average of the thickness measured at both sides of the reduced section. The value for the width of the reduced section was taken as the average of the width at each end and the middle of the reduced section.

The majority of the coupons have a gauge length of 8 inches. Some of the coupons have a smaller gauge length because the material provided was not a large enough sample to fabricate a coupon with an 8 inch gauge length. The specimens with a reduced length of 2.15 in. were fabricated by an outside source that was not able to complete testing. There did not appear to be a significant difference in the material strength to the coupons with varying gauge lengths.

All of the specimens fabricated had a radius of fillet of 0.5 inch. This is the minimum allowable radius of fillet, but it was used because it was the largest size of cutter that was available for the milling machine at the UW SRL.

C.2 Experimental Setup

The steel coupons were tested using 300-kip capacity Baldwin testing machine as shown in Figure C-3. The machine held the coupons at the grip sections of the coupons. An extensometer was attached to each specimen in order to measure the elongation to the gauge length simultaneously with the load. A string potentiometer was used to measure the crosshead separation of the testing machine. The load on the specimen was recorded at all times during the tests using a load cell attached to the actuator.

Figure C-3: 300 Kip Baldwin testing Machine

The coupons were tested by gradually increasing the tensile load and/or deformation. The rate of stressing was maintained between 10-100 KSI per minute whenever possible throughout the duration of the tests in accordance to section 8.4.1 in ASTM A370-14. This was done until the load began decreasing. At this point, the specimen was considered to be failed, and the extensometer was removed in order to prevent damaging the sensors.

C.3 Experimental Results

A summary of the material strengths for all 14 NCBFs test is shown for the braces, plates, columns, and beams in Table C-1 - Table C-5. Note that some coupons represent multiple specimens and are used to define the material properties for braces and plates in multiple tests. There are limited coupon results for beams and columns used throughout the tests, but the variation of results between individual coupons is small and the use of average material properties for the columns and beams is warranted.

Table C-1: Brace Material Properties

Specimen Name	Brace		Coupon Name	Material Properties (ksi)	
	Type	Shape		Yield	Ultimate
NCBF0	HSS	6x6x1/4	S26	58.7	72.6
NCBF1	HSS	7x7x1/4	S39	64.4	79.0
NCBF1-R1	HSS	5x5x3/8	S03	61.8	66.9
NCBF1-R2	HSS	5x5x3/8	S03	61.8	66.9
NCBF1-R3	HSS	5x5x3/8	S03	61.8	66.9
NCBF1-R4	HSS	6x4x3/8	S24	57.5	66.4
NCBF1-R5	HSS	7x7x1/4	S39	64.4	79.0
NCBF2	HSS	5x5x3/8	S03	61.8	66.9
NCBF2-R1	BRB	$4.8in^2$	NA	46[1]	58[1]
NCBF3-1	HSS	6x6x1/4	S26	58.7	72.6
NCBF3-2	HSS	5x5x3/8	S03	61.8	66.9
NCBF4-R1	HSS	5x5x3/8	R10	62.0	70.1
NCBF4-R2	HSS	6x4x3/8	R13	63.2	70.3
NCBF4-R3	BRB	$4.8in^2$	NA	46[1]	58[1]
NCBF5	HSS	5x5x3/8	R10	62.0	70.1

1- No coupon data for the BRB core plate. Values shown are the nominal capacities

Table C-2: Gusset Plate Material Properties

Specimen Name	Thickness (in)	Coupon Name	Material Properties (ksi)	
			Yield	Ultimate
NCBF0	1/2	NM	NM	NM
NCBF1	3/8	S08	50.1	70.5
NCBF1-R1	3/8	S08	50.1	70.5
NCBF1-R2	3/8	S08	50.1	70.5
NCBF1-R3	3/8	S08	50.1	70.5
NCBF1-R4	3/8	S08	50.1	70.5
NCBF1-R5	3/8	S08	50.1	70.5
NCBF2	3/4	S09	60.3	85.0
NCBF2-R1	3/4	R12	38.5	75.9
NCBF3-1	3/4	S26	58.7	72.6
NCBF3-2	1/2	S45	66.0	88.8
NCBF4-R1	5/8	R14	56.4	77.1
NCBF4-R2	5/8	R14	56.4	77.1
NCBF4-R3	5/8	R15	57.2	83.9
NCBF5	7/8	R08	39.3	69.5

Table C-3: Test Specific Plate Material Properties

Test	Plate Description	Thickness (in)	Coupon Name	Material Strength (ksi)	
				Yield	Ultimate
NCBF1	Shear Plate	3/8	S08	50.1	70.5
NCBF1-R1	Shear Plate	3/8	S08	50.1	70.5
NCBF1-R2	Shear Plate	3/8	S08	50.1	70.5
NCBF1-R3	Shear Plate	3/8	S08	50.1	70.5
	Knife Plate	3/4	S26	58.7	72.6
NCBF1-R4	Shear Plate	3/8	S08	50.1	70.5
	Knife Plate	3/4	S26	58.7	72.6
NCBF-R5	Shear Plate	3/8	S08	50.1	70.5
NCBF2	Shear Plate	3/4	S09	60.3	85.0
NCBF2-R1	Shear Plate	3/4	R12	38.5	75.9
	Rib Plates	3/4	R12	38.5	75.9
NCBF3-1	Shear Plates	3/4	S09	60.3	85.0
NCBF3-2	Shear Plates	3/4	S09	60.3	85.0
NCBF4-R1	End Plate	5/8	R14	56.4	77.1
NCBF4-R2	End Plate	5/8	R14	56.4	77.1
	Knife Plate	3/4	R11	38.3	73.6
	Net Section	3/8	NM	NM	NM
NCBF4-R3	End Plate	5/8	R15	57.2	83.9
	Rib Plates	3/4	R11	38.3	73.6

NM – not measured

Table C-4: Summary of Beam Coupon Results

Test	Sample Location	Coupon Name	Material Strength (ksi)	
			Yield	Ultimate
NCBF2-R1	Column Web	R09	53.5	69.6
NCBF2-R1	Column Flange	R04	52.3	70.6
NCBF3-1	Column Flange	S18	53.2	71.4
NCBF3-2	Column Flange	S10	50.6	71.4
NCBF4-R3	Column Web	R03	50	76.7
NCBF4-R3	Column Flange	R07	51.3	77.8
SCBF1	Column Flange	S22	52.2	70.3
		Mean	**52.2**	**71.4**
		Average	**51.8**	**72.5**
		St. Dev.	**1.3**	**3.3**

Table C-5: Summary of Column Coupon Results

Test	Location	Coupon Name	Material Strength (ksi)	
			Yield	Ultimate
NCBF5	North Beam Web	R2	59.5	74.6
NCBF5	South Beam Web	R5	58.5	74.8
NCBF2-R1	North Beam Web	R1	56.6	71.2
NCBF2-R1	South Beam Web	R6	60.5	78.1
NCBF3-2	Beam web	S32	55.7	70.7
NCBF2	Beam Flange	S13	55.3	76.3
SCBF1	Beam Flange	S27	55.2	74.5
		Mean	**56.6**	**74.6**
		Average	**57.3**	**74.3**
		St. Dev.	**2.2**	**2.6**

Stress strain plots for all of the tested coupons are shown in Figure C-7 - Figure C-11. Stress was found by dividing the measured load with the cross sectional area of the reduced section (Table C-6). The strain for each specimen was determined by dividing the elongation of the extensometer by the gauge length. Note that coupon data for R05 and R09 were lost and stress-strain plots could not be presented.

The yield strength of the coupon was determined using two methods and was based on the shape of the stress profile. In many of the coupons, the stress-strain diagram showed a clear yield plateau (Figure C-4). The yield strength for these coupons was taken as the lowest stress on this plateau. The second method was used for coupons that did not have a clearly defined yield plateau. The yield strength of these coupons was determined using the 2% offset method as described in section 14.2.1 in ASTM A370-14. The ultimate strength of the coupons was the highest stress the coupon endured during the test for both methods.

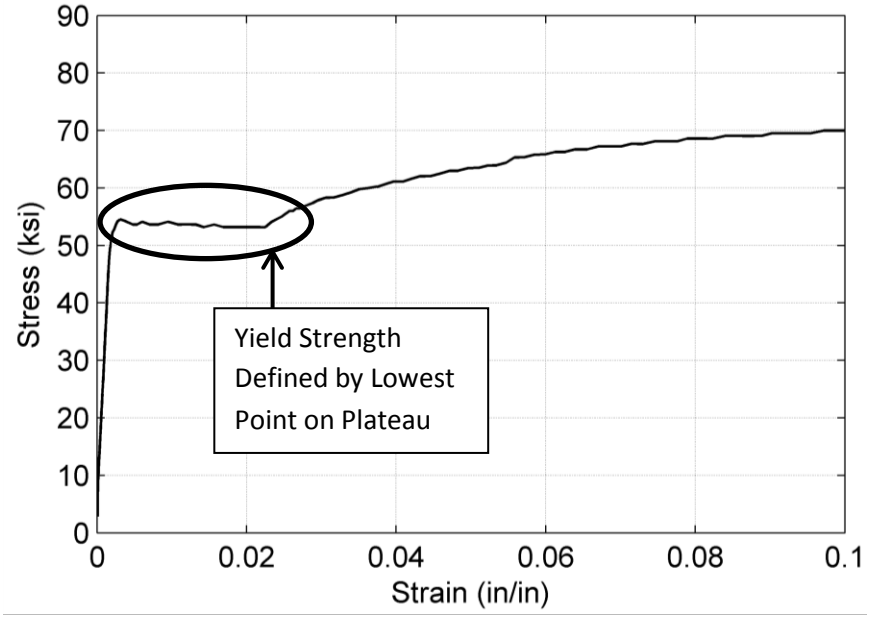

Figure C-4: Yield Strength Determination - Clear Yield Plateau Method (S18)

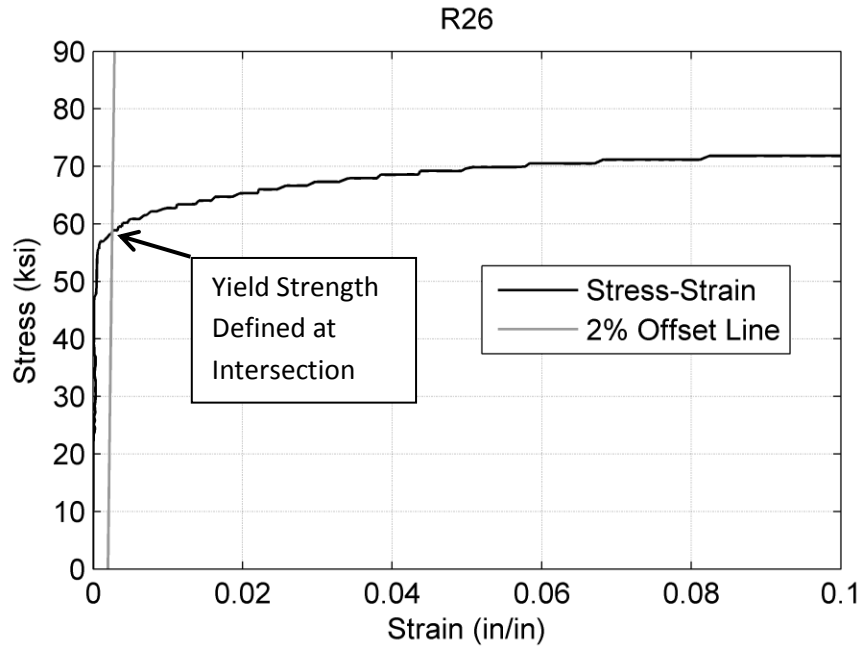

Figure C-5: Yield Strength Determination - 2% Offset (R26)

The data from the several of the initial tests had a significant amount of noise because the data was recorded at a high frequency of 20 HZ. To reduce the amount of noise, a median filter was applied to the data. A median filter works by replacing a value of a data set by the median value of five surrounding data points. Figure C-6 provides an example of how the median filter was used to clean up noisy data. Once the issue was identified, the frequency of data recording for future tests was reduced and the filter was no longer necessary. Test data that a filter was applied to is indicated with an asterisk in Table C-6.

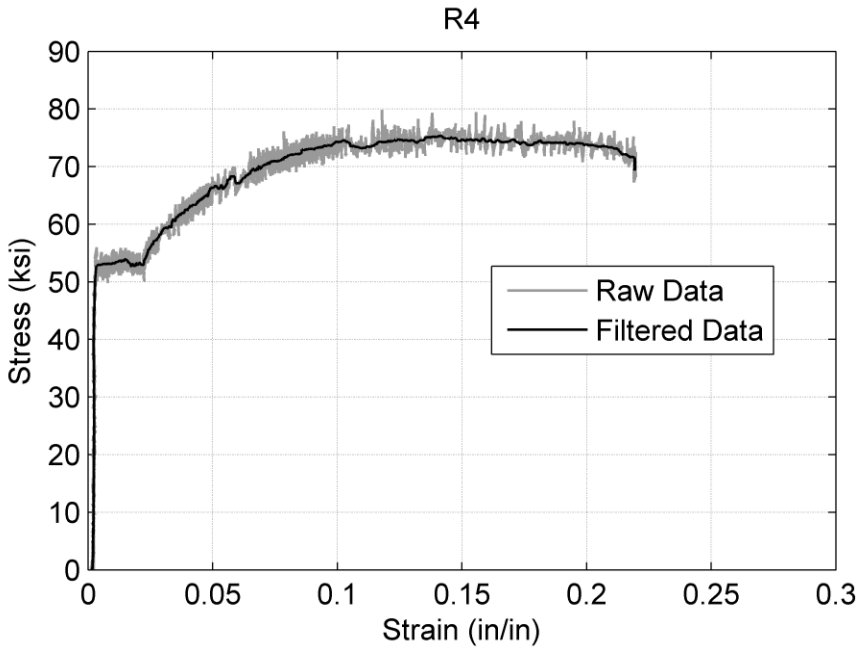

Figure C-6: Example Median Filter Application for Coupon Data

While testing coupon R3, the extensometer was removed before the steel reached its ultimate strength. The plot for this specimen shows a clear yield point, but the ultimate strength is not shown on the plot. The ultimate load on the coupon was recorded, and used to find the ultimate stress.

Table C-6: Coupon Dimensions and Material Properties

Coupon Name	Sampling Information		Grip Width (in)		Reduced Section Dimensions			Gauge Length	Yield Calculation Method	Material Strengths (ksi)	
	Specimen Name	Location	Left	Right	Width	Length	Thick.			Yield	Ultimate
			in.	in.	in.	in.	in.	in.		ksi	ksi
R01	NCBF2-R1	North Beam Web	1.90	1.90	1.483	8.25	0.348	8.00	Plateau*	56.6	71.2
R02	NCBF5	North Beam Web	2.00	1.95	1.495	8.25	0.337	8.00	Plateau*	59.5	74.6
R03	NCBF4-R3	Column Web	1.88	1.90	1.454	8.25	0.433	8.00	Plateau*	50	76.7
R04	NCBF2-R1	Column Flange	1.90	1.95	1.422	8.25	0.665	8.00	Plateau*	52.3	70.6
R05	NCBF5	South Beam Web	2.00	2.05	1.510	8.25	0.334	8.00	Plateau*	58.5	74.8
R06	NCBF2-R1	South Beam Web	2.00	2.00	1.448	8.25	0.317	8.00	Plateau*	60.5	78.1
R07	NCBF4-R3	Column Flange	1.90	1.88	1.495	8.25	0.626	8.00	Plateau*	51.3	77.8
R08	NCBF5	7/8" Plate	2.05	2.05	1.380	8.25	0.875	8.00	Plateau*	39.3	69.5
R09	NCBF2-R1	Column Web	2.00	2.00	1.523	8.25	0.426	8.00	Plateau*	53.5	69.6
R10	NCBF4-R1, NCBF 5	5x5x3/8 HSS	2.13	2.12	1.587	8.25	0.351	8.00	2% Offset	62.0	70.1
R11	NCBF4-R2	3/4" Plate	2.00	2.05	1.547	8.25	0.747	8.00	Plateau*	38.3	73.6
R12	NCBF2-R1	3/4" Plate	1.88	1.90	1.558	8.25	0.740	8.00	Plateau*	38.5	75.9
R13	NCBF4-R2	6x4x3/8 HSS	2.00	2.00	1.602	8.25	0.362	8.00	Plateau	63.2	70.3
R14	NCBF4-R1,R2	5/8" Plate	2.25	2.25	1.530	8.25	0.626	8.00	Plateau	56.4	77.1
R15	NCBF4-R3	5/8" Plate	2.13	2.13	1.422	8.25	0.630	8.00	Plateau	57.2	83.9
S03	NCBF1-R2	5x5x3/8 HSS	2.13	2.10	1.405	8.25	0.365	8.00	Plateau	61.8	66.9
S08	NCBF1 – NCBF1-R5	3/8 in. Plate	2.00	2.00	1.341	2.25	0.369	2.14	Plateau	50.1	70.5
S09	NCBF7	3/4 in. Plate	1.00	1.00	0.489	2.25	0.740	2.12	Plateau	60.3	85.0
S10	NCBF3-2	Column Flange	1.00	1.00	0.506	2.25	0.653	2.12	Plateau	50.6	71.4
S13	NCBF2	Beam Flange	1.00	1.00	0.507	2.25	0.565	2.12	Plateau	55.3	76.3
S18	NCBF3-1	Column Flange	1.00	1.00	0.503	2.25	0.624	2.12	Plateau	53.2	71.4
S22	SCBF1	Column Flange	1.00	1.00	0.509	2.25	0.668	2.12	Plateau	52.2	70.3
S24	NCBF1-R4	6x4x3/8 HSS	2.15	2.13	1.389	8.25	0.364	8.00	2% Offset	57.5	66.4
S26	NCBF0, NCBF3-1	6x6x1/4 HSS	1.50	1.50	0.985	6.13	0.230	6.00	2% Offset	58.7	72.6
S27	SCBF1	Beam Flange	1.10	1.10	0.496	2.25	0.557	2.12	Plateau	55.2	74.5
S32	NCBF3-2	Beam Web	1.00	1.00	0.507	2.25	0.425	2.12	Plateau	55.7	70.7
S39	NCBF1, NCBF1-R5	7x7x1/4 HSS	1.50	1.50	0.943	6.25	0.230	6.00	2% Offset	64.4	79.0
S45	NCBF3-1	1/2 in. Plate	2.00	2.00	1.405	2.25	0.487	2.14	Plateau	66.0	88.8

C.4 Stress-Strain Plots

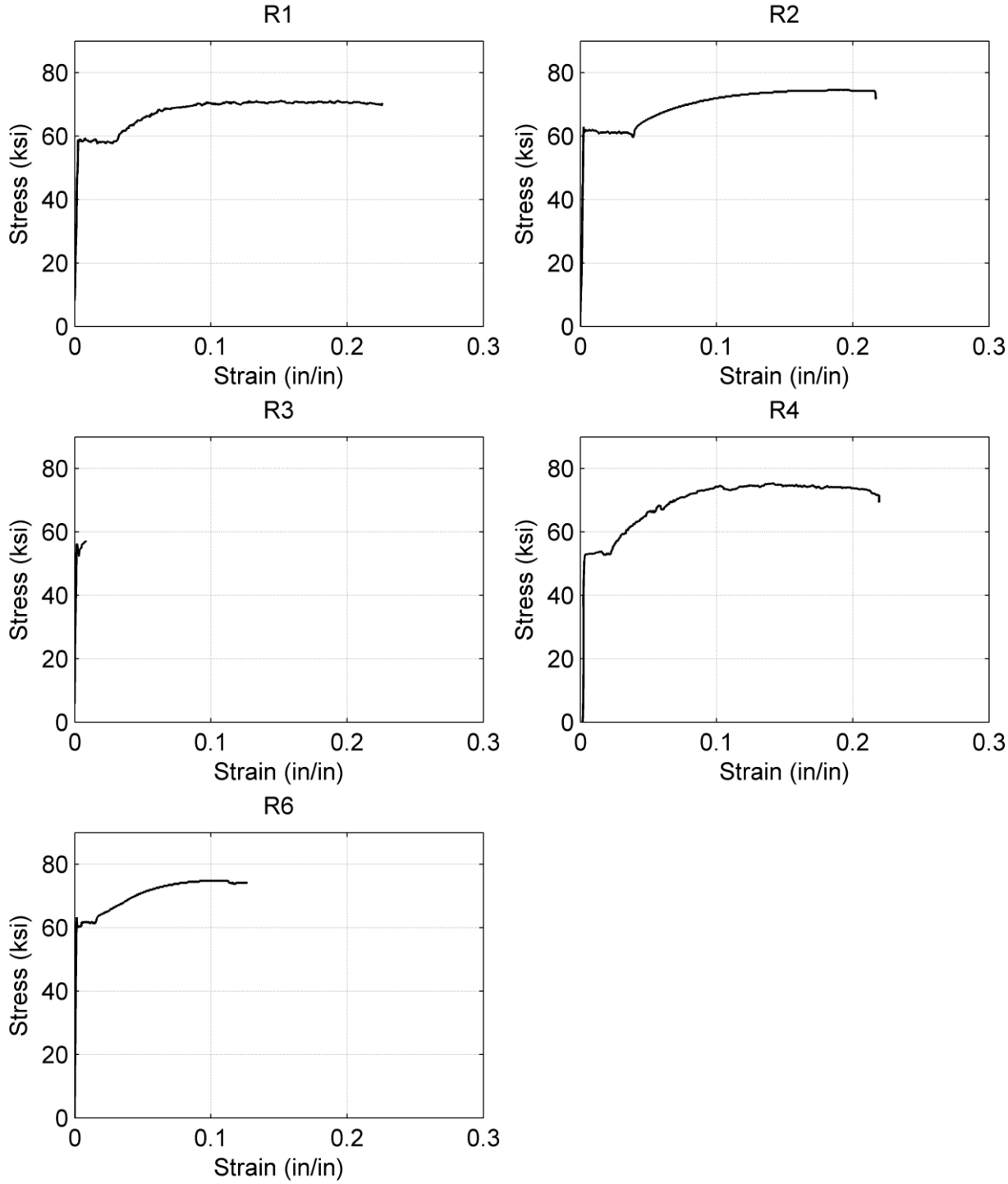

Figure C-7: Stress-Strain Plots for Coupon Tests (1/5)

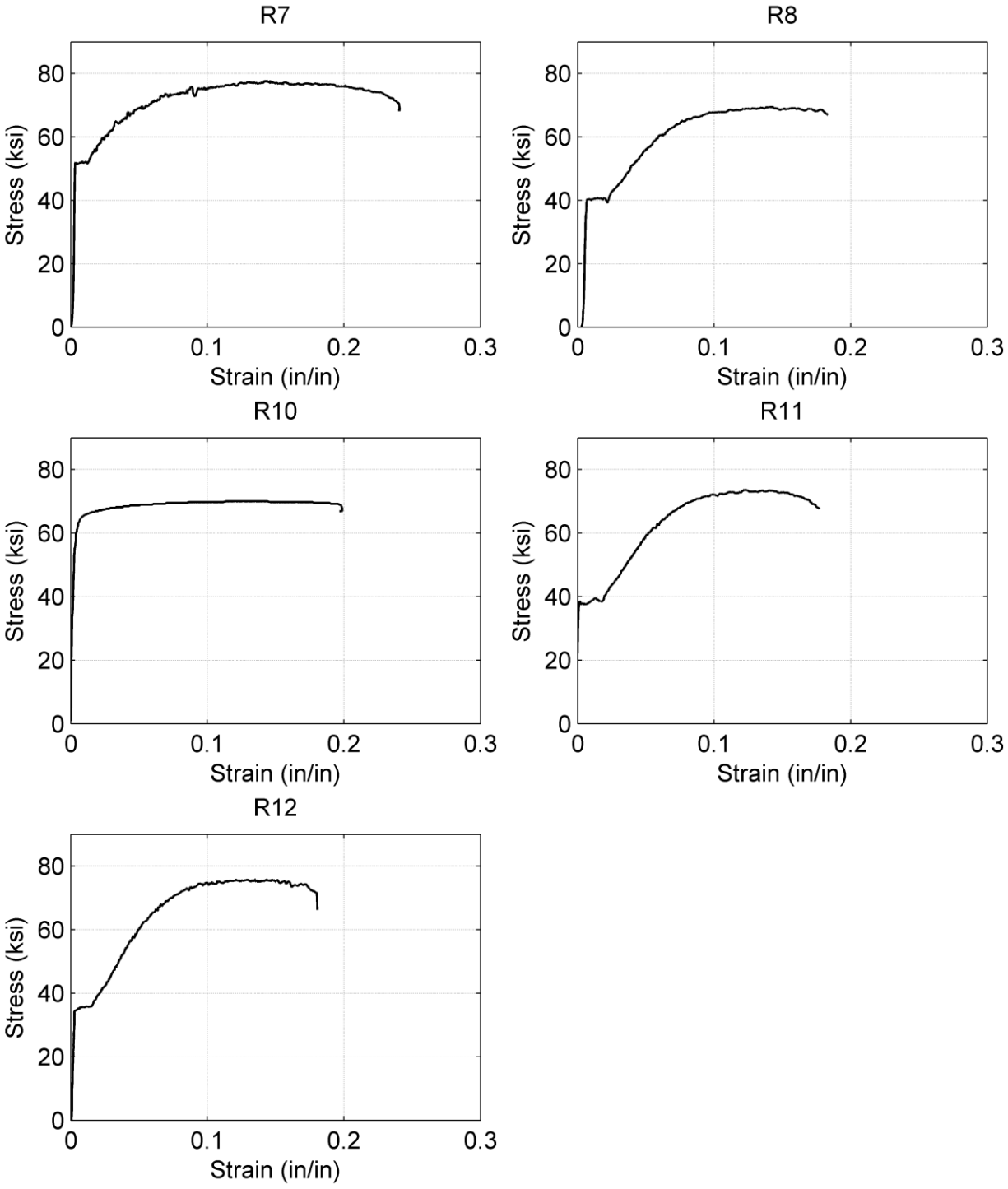

Figure C-8: Stress-Strain Plots for Coupon Tests (2/5)

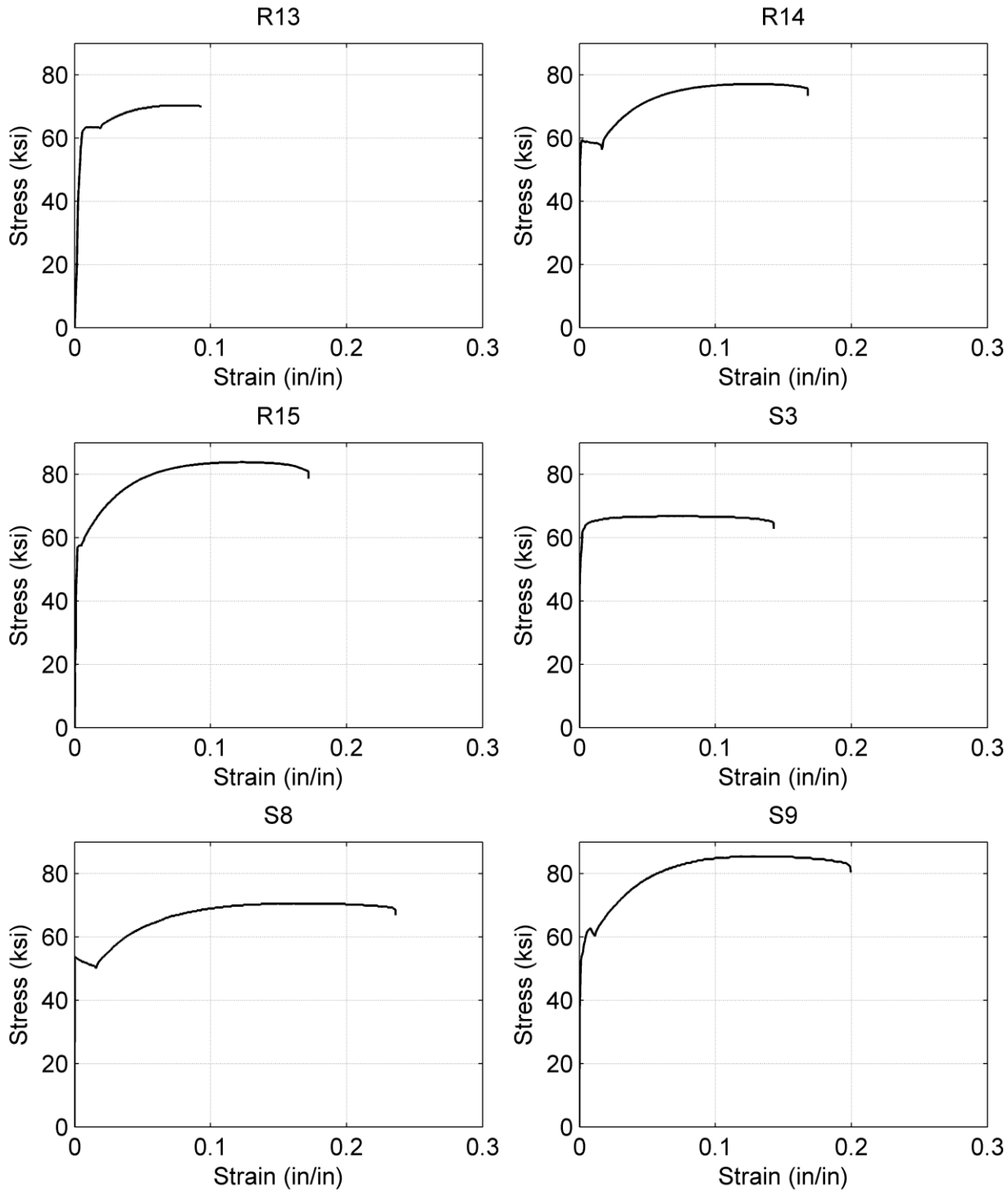

Figure C-9: Stress-Strain Plots for Coupon Tests (3/5)

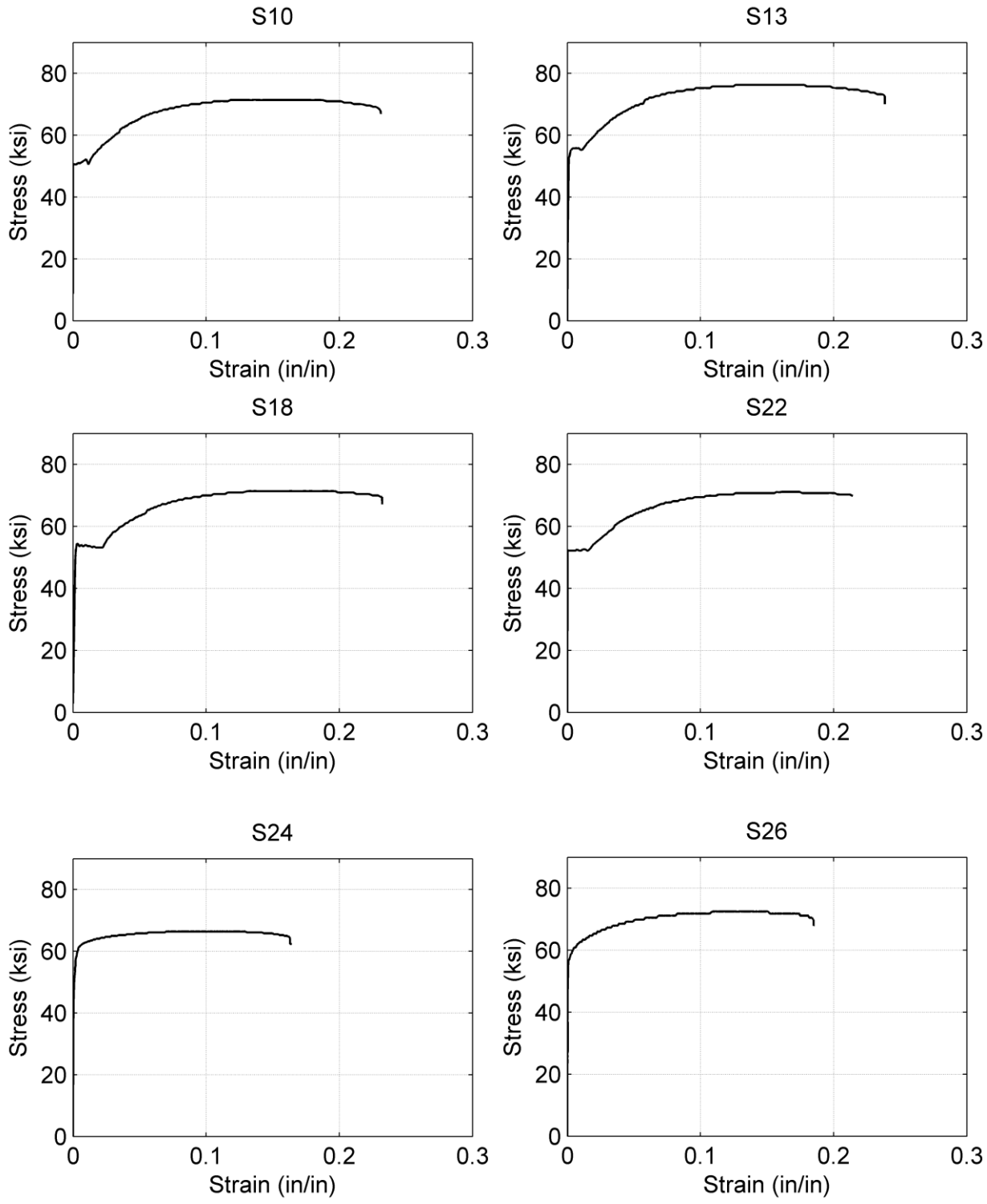

Figure C-10: Stress-Strain Plots for Coupon Tests (4/5)

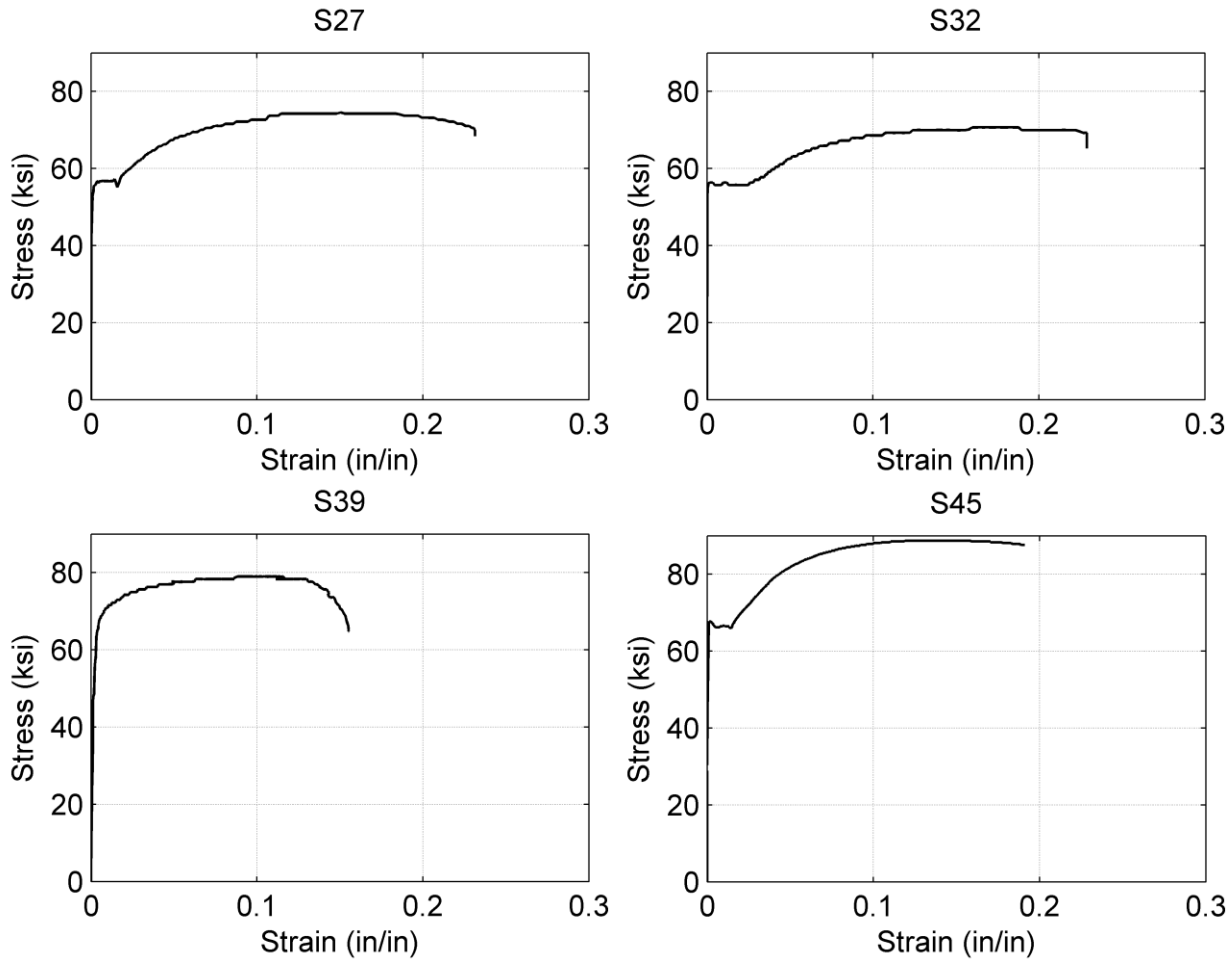

Figure C-11: Stress-Strain Plots for Coupon Tests (5/5)

Appendix D: Supplemental Data Analysis

This appendix contains additional data analysis plots for each of the experiments presented in this thesis including individual member force plots, post tension loss, and connection/ framing member rotations for each of the tested specimens. These plots can be used to better understand the system behavior or each specimen.

D.1 Member Force Plots

Member forces in each specimen were calculated for the east column, the west column, and the north beam in the experimental test setup as described in Section 6.3.2. Moments, shears, and axial forces for each member listed above are plotted against interstory drift for all of the tested specimens in Figure D-1 through Figure D-5. Note that all member forces plotted in these figures represent the change in force from the start of the test and do not include initial forces from post-tensioning the system.

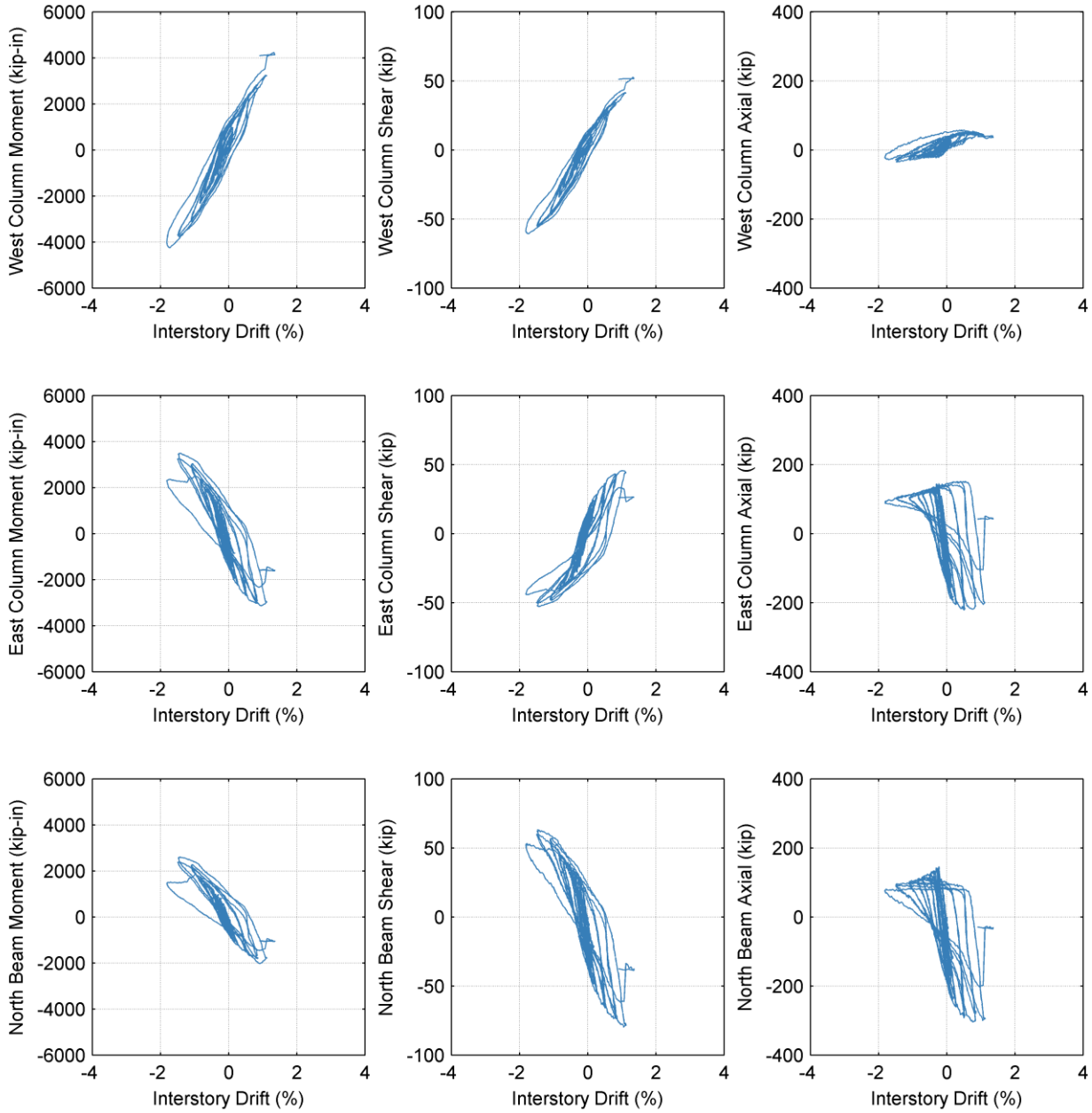

Figure D-1: NCBF4-R1 Frame Forces

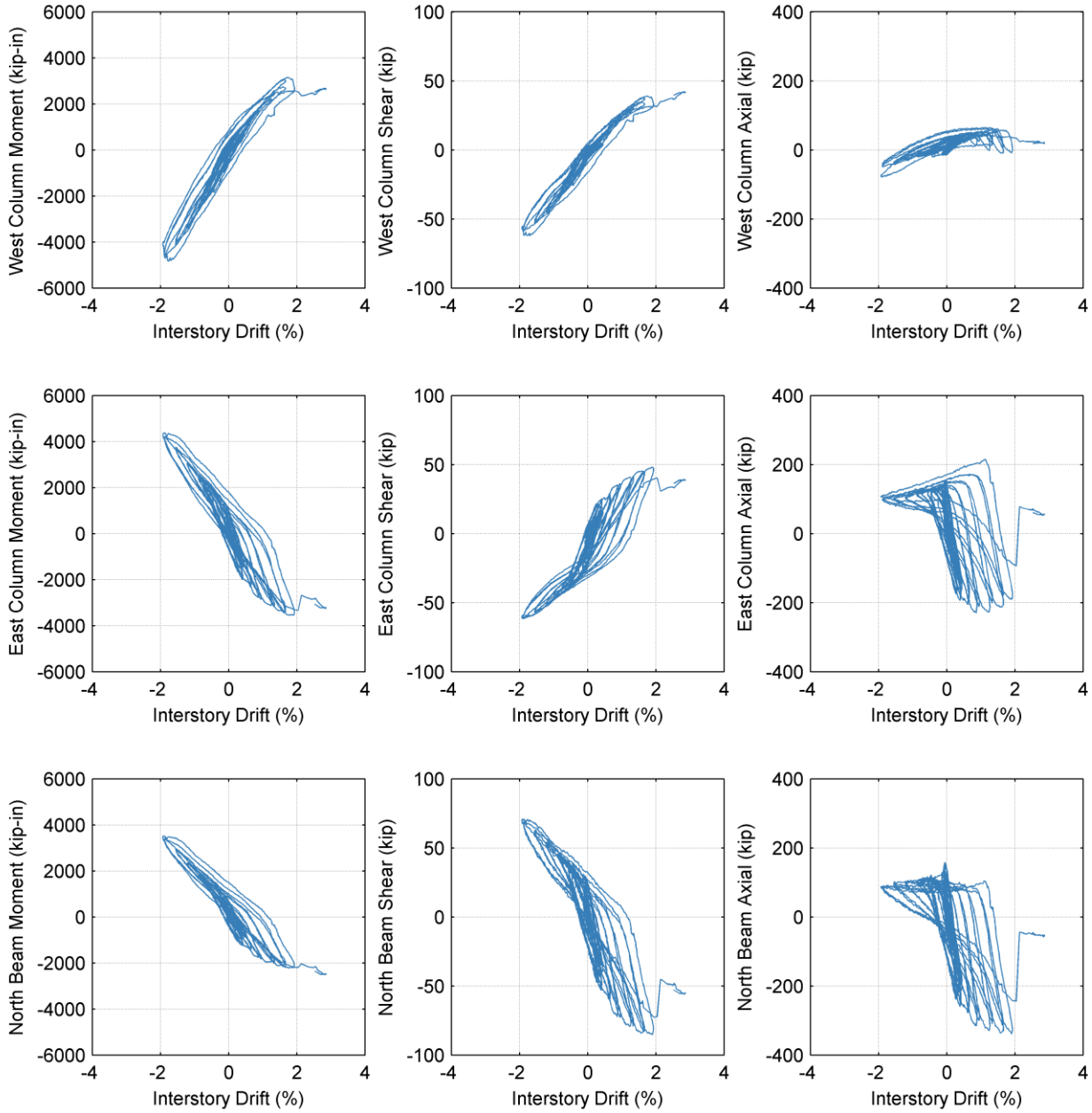

Figure D-2: NCBF4-R2 Frame Forces

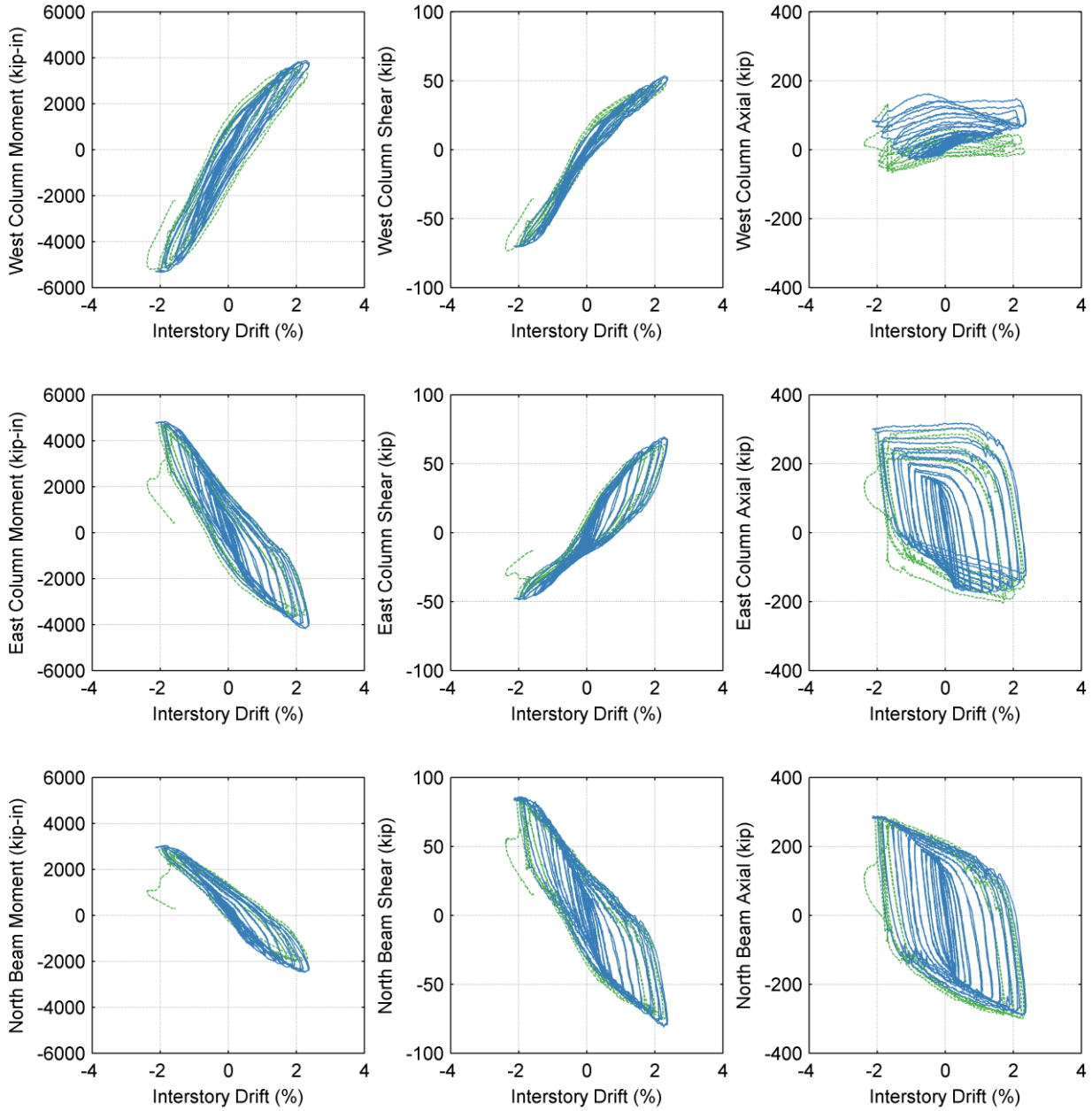

Dashed green line represents system response after re-tensioning of the columns.

Figure D-3: NCBF4-R3 Frame Forces

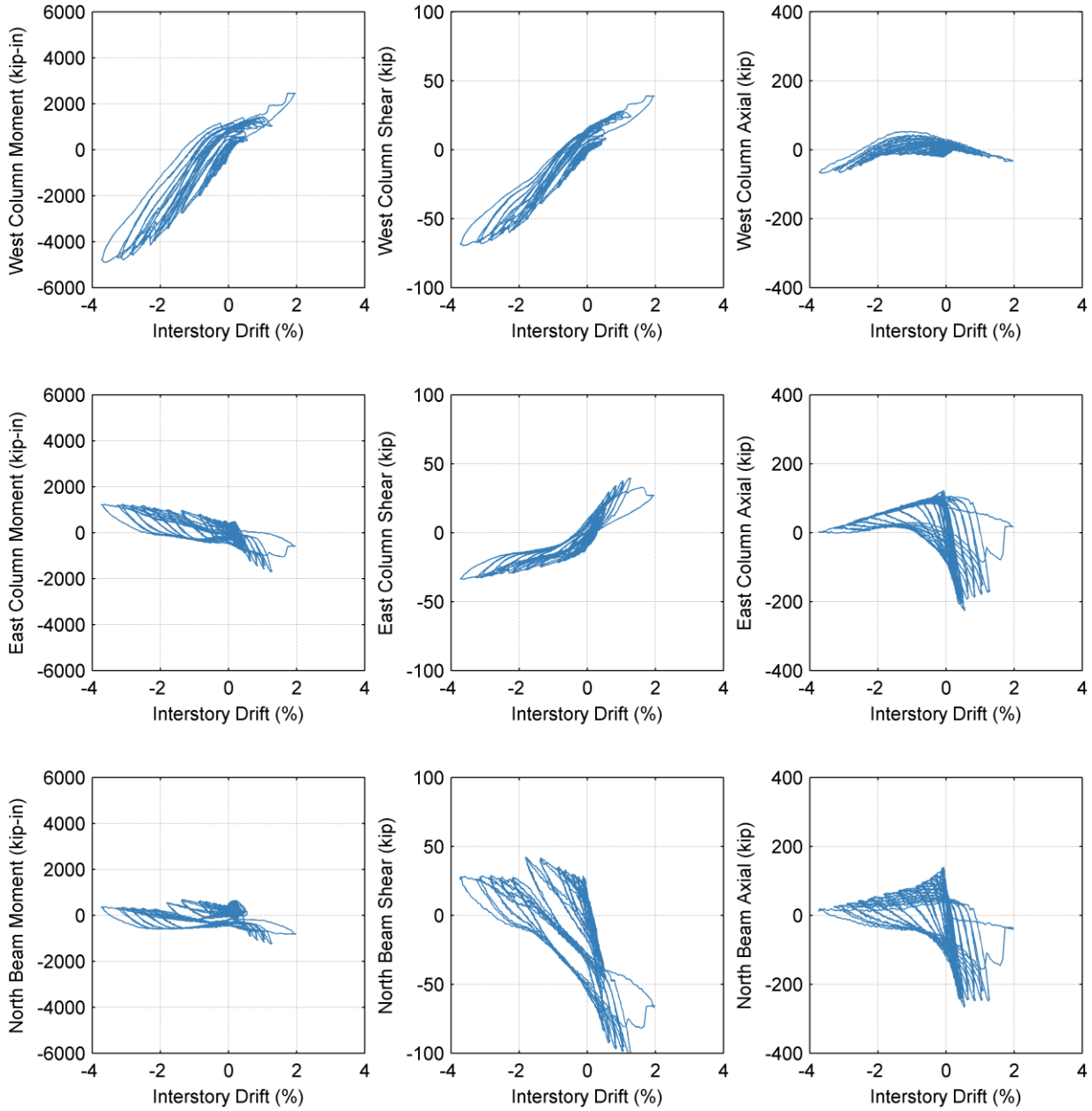

Figure D-4: NCBF5 Frame Forces

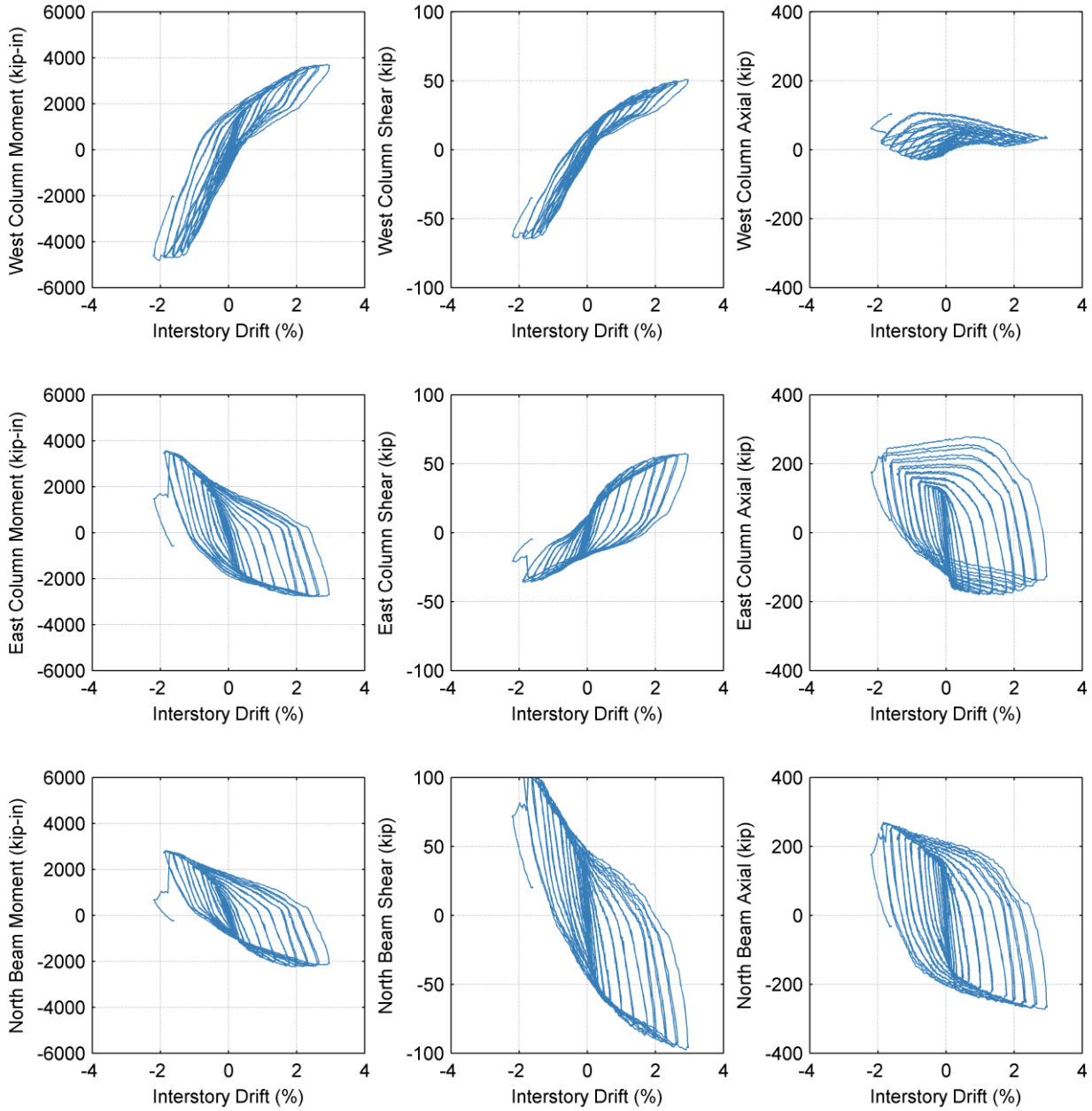

Figure D-5: NCBF2-R1 Frame Forces

D.2 Post Tension Loss in Columns

During each test, both columns were subjected to large compressive forces and moments that lead to local yielding and stable local buckling in the columns at plastic hinge locations (edge of the gusset plate). As the columns deformed at the plastic hinge locations, they became shorter, and some of the initial compressive force provided by the post-tensioning bars in the axial load system was relieved. In some cases, the reduction in post-tension force was significant (~25%) and was enough to allow uplift of both flanges of the west column during testing.

The loss of posttension force in the columns, $Loss_W$ and $Loss_E$, was computed by considering vertical equilibrium of the NE and NW corners (Eq. D-1 and Eq. D-2) of the frame when the actuator load was zero as shown in the free body diagram of Figure D-6. The forces shown in the figure represent the change in member forces from the start of the test as computed in Section 6.3.2. To represent the loss of post-tension force from each cycle, the $Loss_W$ and $Loss_E$ quantities were computed for each loading cycle.

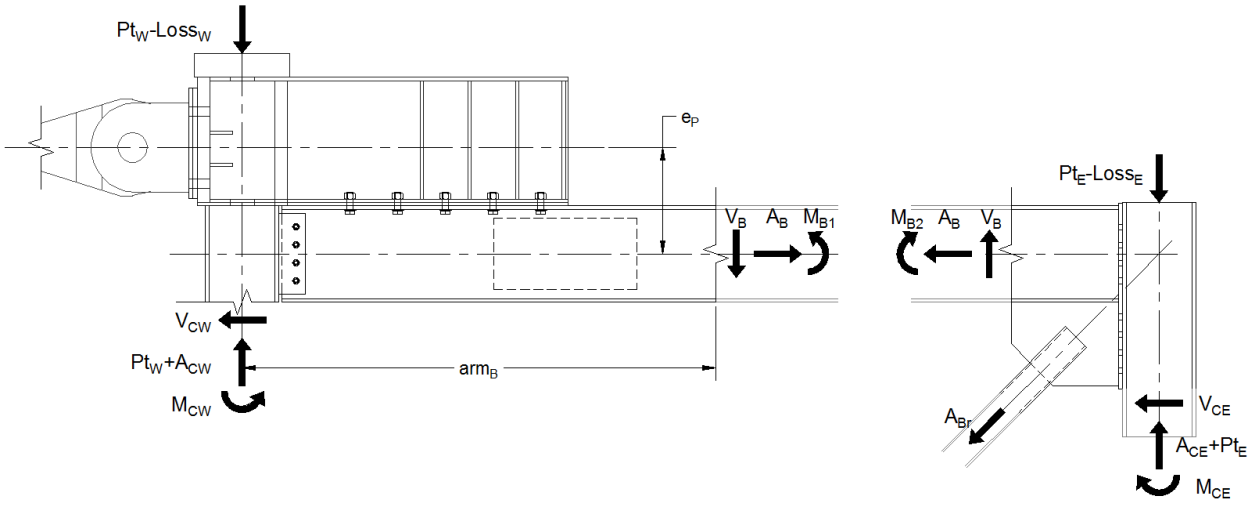

$$Loss_E = V_B - P_{br}\cos(\theta) - A_{CE} \qquad \textbf{Eq. D-1}$$

$$Loss_W = -V_B - A_{CW} \qquad \textbf{Eq. D-2}$$

Figure D-6: Post Tension Loss Calculation Free Body Diagram

Reduction in column post tensioning force vs. drift range for four of the five specimens is shown in Figure D-7while maximum post-tensioning force losses for each column are tabulated in Table D-1. Initial post-tensioning force in each column was 450 kips. Post-tensioning loss for NCBF5 could not be computed with this method because the strain gauge data on the beam was unreliable. This was likely because the beam had extensive yielding and out-of-plane buckling as discussed in 5.6. The decreases in post-tension loss in Figure D-7c for Specimen NCBF4-R3 occur because the columns were re-tensioned during testing (once for the east column and twice for the west column.)

Post-tensioning force losses were significant for all of the tests shown (> 13% of initial post-tension force). For Specimen NCBF4-R1 and NCBF4-R2 the east column post-tensioning force loss was larger than the west column because that east column developed higher compressive forces while the brace was in tension.

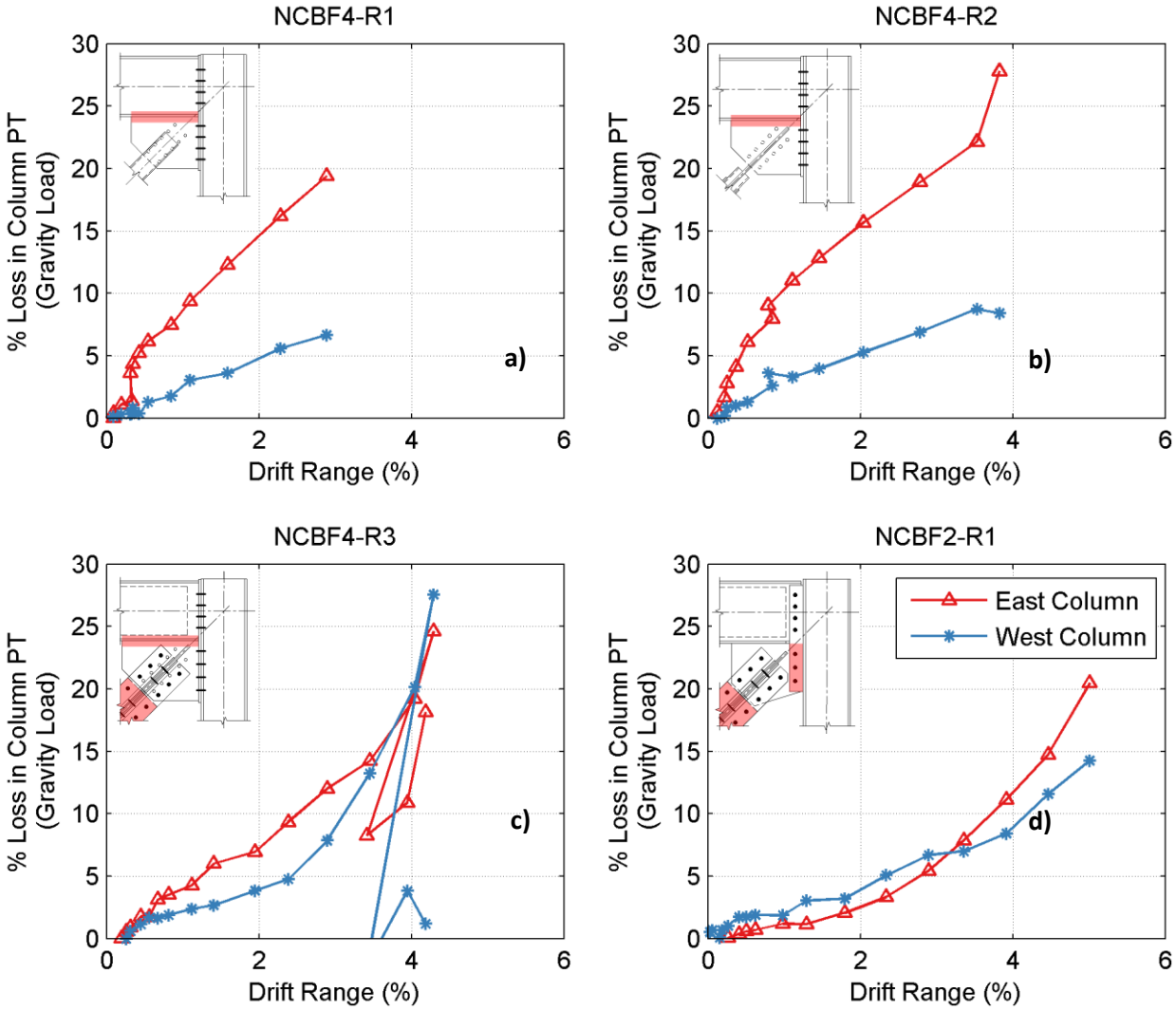

Figure D-7: Reduction of Post Tensioning Force (i.e. Gravity Loads) due to Column Shortening

Table D-1: Reduction of Post Tensioning Force (i.e. Gravity Loads) due to Column Shortening

Specimen Name	Initial PT Force (kip) in Each Column	East Column Losses		West Column Losses		Total Loss	
		kip	%	kip	%	kip	%
NCBF4-R1	450	87	19.3	30	6.7	118	13.0
NCBF4-R2	450	125	27.8	40	8.9	162	18.1
NCBF4-R3	450	111	24.7	124	27.6	235	26.1
NCBF5	450	-	-	-	-	-	-
NCBF2-R1	450	92	20.4	64	14.2	156	17.3

D.3 Connection and Framing Member Rotations

When a frame displaces laterally, the total amount of rotation must be accommodated at each corner of the frame. The rotation can be provided through the combination of beam hinge rotation, column hinge rotation, and connection rotation. Typically the element with the least strength accommodates this rotation. For a simply supported or weak connection, the joint rotation is provided by connection rotation. In a fully restrained or strong connection the beam and column will contribute more to the joint rotation. The quantification of these rotations are of particular interest in the specimens tested because they can provide insight into the yielding hierarchy of the specimen as it undergoes increasing levels of drift/ deformation.

Figure D-8 shows three idealized cases where only one part of the frame contributes to the joint rotation. These three cases serve to illustrate the possible mechanisms for the frame to accommodate rotation equal to the frame drift. For case 1, the beam and gusset plate are assumed to be rigid and all rotation is accommodated by rotation of the column hinge. For case 2, the beam and column are rigid and all of the drift is accommodated by the connection. For case 3, the column and gusset plate connection are assumed to be rigid, and the beam develops all of the rotation. For the connection shown, case 2 is highly unlikely due to the presence of a continuous end plate.

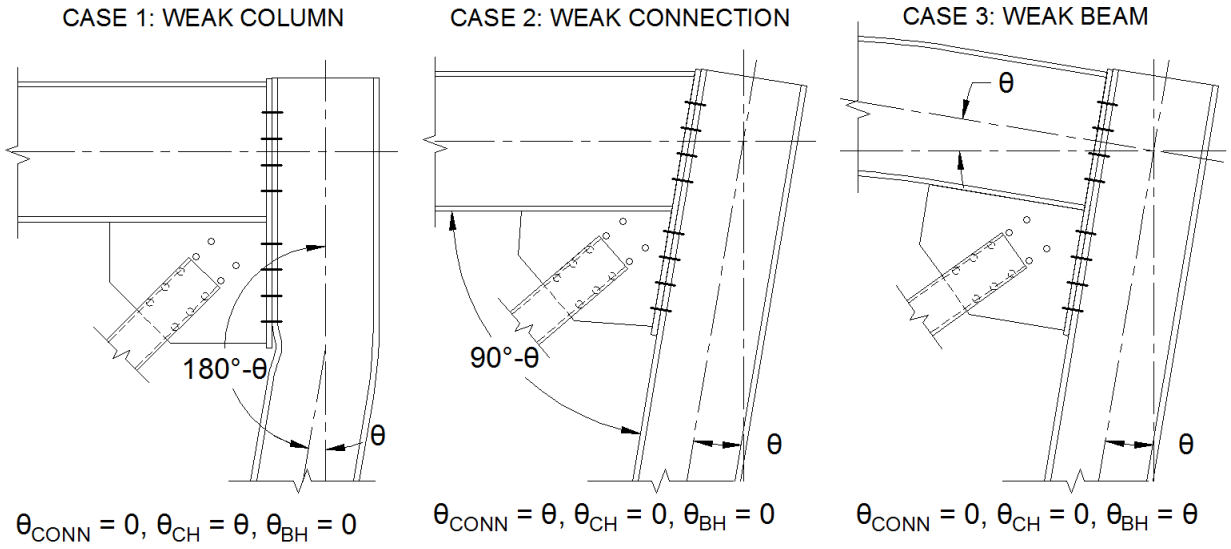

Figure D-8: Idealized Joint Rotation Mechanisms.

In reality, the rotation of each element at a given drift level will be a combination of these three mechanisms. Although the figure may not represent reality, the rotations shown in Figure D-8 can be calculated using the Optotrak markers specified in Figure D-9. Beam rotation is measured by considering the rotation of the beam web inside the gusset plate connection relative to the original beam centerline. Inner column rotation is measured on the outside flange of the column relative to the vertical axis. The outside flange was used since it was less influenced by flange buckling than the inside flange. Connection rotation was measured considering the relative change between the inner beam and

inner column rotation. Column hinge rotation was measured by considering the difference between the inner column rotation and the overall column rotation angle which was nearly equivalent to the drift ratio.

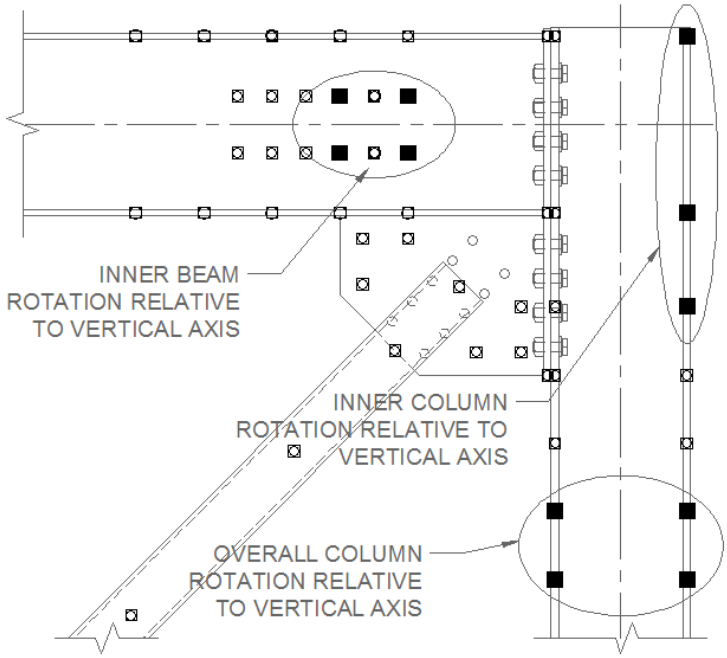

Figure D-9: Optotrak Markers Used to Determine Connection and Framing Member Rotation

Rotational results using this calculation procedure are shown for the NE connection in Figure D-10. Note that the original Optotrak marker locations were not in ideal locations to measure the various rotations, and the results presented in Figure D-10 may have inaccuracies (e.g. at high interstory drifts in specimen NCBF4-R3). For this reason it is difficult to draw conclusions from these plots. However, each plot provides insight into which mechanism was most prevalent for each of the tested specimens. Observations from this calculation are listed below.

- The beam does not contribute much rotation in any of the specimens except for specimen NCBF5. This rotation could have occurred due to the contact of the inner beam flange and the gusset plate while the brace was in tension.

- At negative drift ranges the connection seemed to accommodate a majority of the rotations regardless of the connection type.

- The bolted end plate connections (Specimens NCBF4-R1 – NCBF4-R3) developed significant column rotations especially while the brace is in tension.

- The bolted continuous shear plate connection (NCBF2-R1) originally accommodated most of the rotation at the column interface connection, but at higher positive interstory drifts while was controlled by the column rotation.

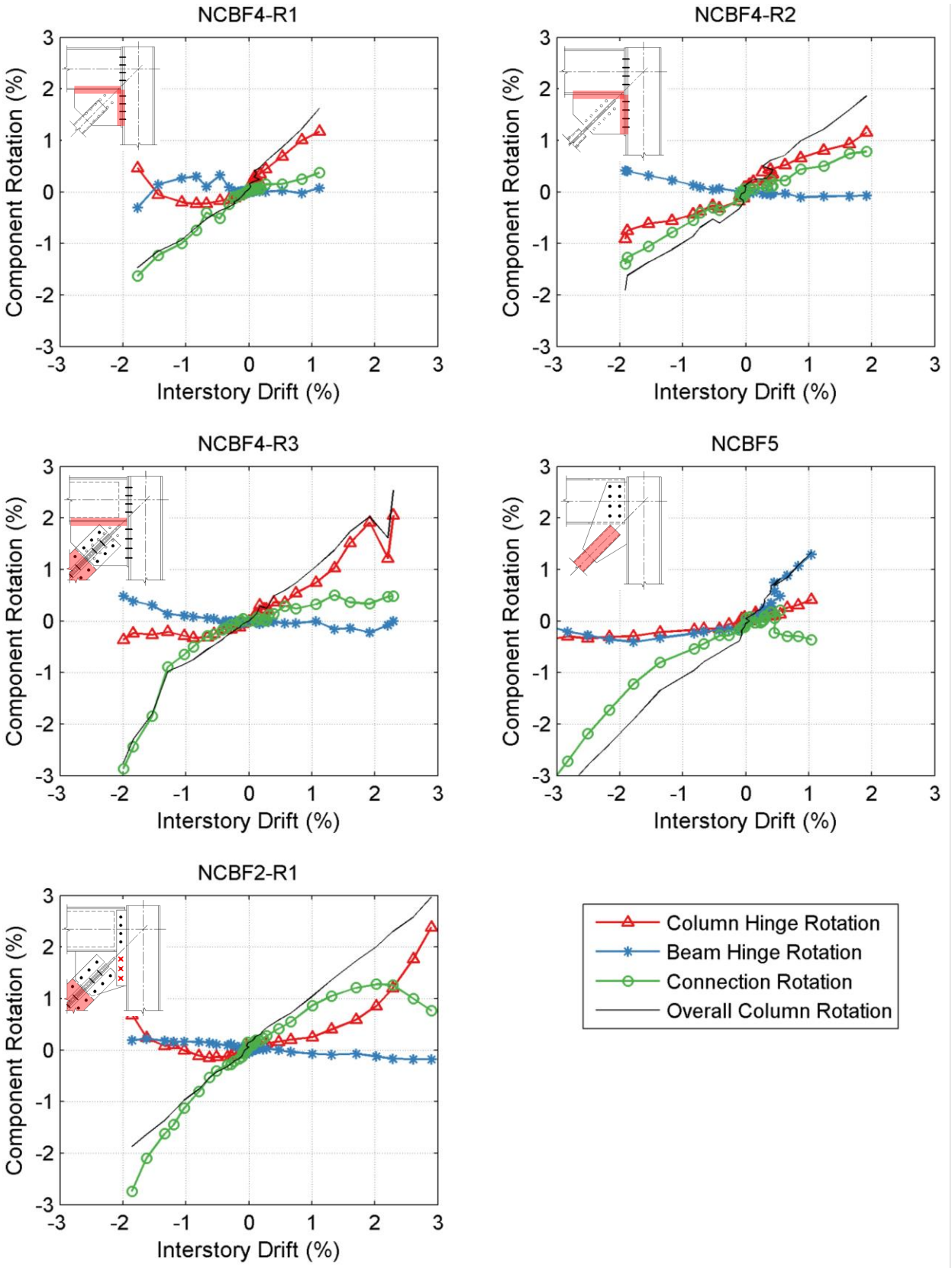

Figure D-10: Contribution of Connection and Framing Member Rotation to Overall Drift

Appendix E: Buckling Restrained Brace

This appendix contains information about the two BRBs tested during the NCBF experimental program. The braces tested were the same braces used in an experimental program conducted by Christopulos (2005) and summarized by Palmer et. all (2011) which is summarized in Section E.1. Section E.2 and Section E.3 show the BRB details and DCR limit state evaluation respectively. More detailed information on the BRBF experimental results, details, design, and material properties can be found in Christopulos (2005).

E.1 Background on BRB Tests at UW

Over the past decade a number of tests have been conducted on buckling restrained braced frame structures (BRBFs). These tests have provided good insight into the performance of BRBFs in the context of modern brace frame design procedure and have generally shown excellent component behavior of individual BRBs.

A paper by Palmer et. all (2011) discussed seven experiments. Six of the experiments were conducted at the UW SRL and utilized a similar experimental setup to the tests presented in Chapter 4. These six experiments were conducted by Christopulos (2005) and also used the same type of BRB used in specimens NCBF4-R3 and NCBF2-R1. The connection detail and experimental test setup for these six tests is shown in Figure E-1. The connection utilized a fully restrained moment connection (welded flanges welded web connection) and used a ¾" gusset plate connected to the BRB with 20 A490 slip critical bolts and 8 ½" rib plates bracketed on either side of a cruciform section. The experimental setup and results for the other test presented in Palmer's (2011) paper will not presented in this appendix.

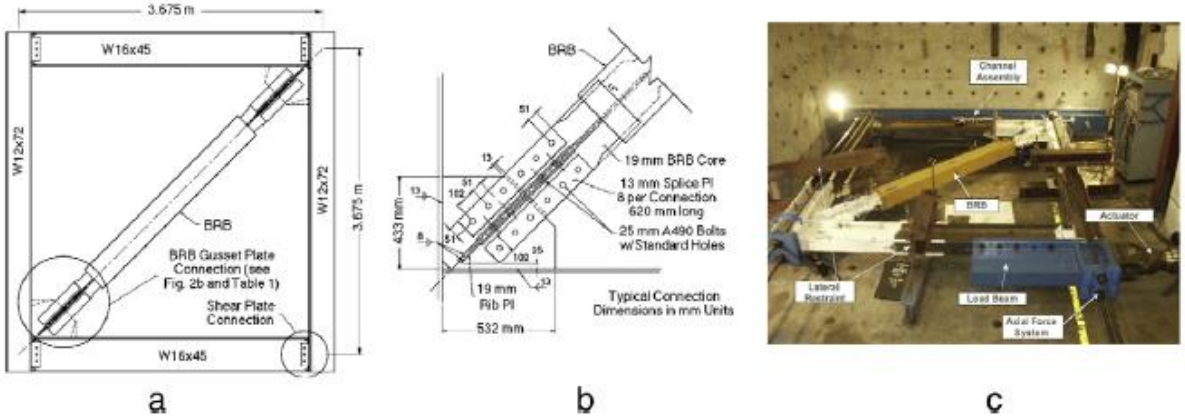

Figure E-1: Experimental Setup for Single Bay BRB tests (Palmer et. all 2011)
a) Frame Geometry, b) Typical BRB connection, and c) photo of test setup.

The experimental results for all of the planar BRBF tests are shown in Table E-1. In general the BRBF frames were able to achieve a drift range of 3.9% to 4.5%. Most of the BRBFs developed severe buckling of the beam flange and web. This introduced an instability that ultimately led the BRB core plate to hinge out-of-plane. In some cases the gusset plate welds fractures and/or the beam flanges tore. Pictures of some of the associated damage are shown in Figure E-2. All of the BRBs had good energy dissipation.

Table E-1: Experimental Results for UW BRBF Specimens Palmer et. all (2011)

Specimen	Gusset	Purpose	Bolts	BRB yield (Tensile) MPa	Beam yield (Tensile) MPa	Column yield (Tensile) MPa	Max. drift % Positive Negative (Cumulative)	Max. resistance kN Positive (Negative)	Failure mode
BRB01	 SQUARE	No internal pin. Parallel core. Near fault cyclic. Slip critical bolts.	10 Slip critical	311 (469)	409 530		3.14 −0.92 (4.06)	1397 −1156	OOP deformation of BRB and beam fracture
BRB02	 15° TAPER	No internal pin. Parallel core. Normal cyclic. Slip critical bolts.	10 Slip critical	311 (469)	398 505	407 468	2.28 −2.17 (4.45)	1476 −1572	OOP deformation of BRB
BRB03	 15° TAPER	No internal pin. Parallel core. Normal cyclic. Fewer bearing bolts.	8 Bearing	311 (469)	379 507		1.89 −1.99 (3.88)	1362 −1541	OOP deformation of BRB
BRB04	 15° TAPER	No internal pin. Rotated perpendicular core. Normal cyclic. Fewer bearing bolts.	8 Bearing	311 (469)	409 530	407 468	2.32 −1.92 (4.24)	1092 −989	OOP deformation of BRB
BRB05 Reference	 SQUARE	No internal pin. Parallel core. Normal cyclic. Slip critical bolts.	10 Slip critical	311 (469)	379 507		2.16 −1.93 (4.09)	1404 −1585	OOP deformation of BRB
BRB06	 SQUARE	With internal pin. Parallel core. Normal cyclic. Slip critical bolts.	10 Slip critical		382* 510*	382* 510*	2.34 −1.83 (4.17)	1615 −1278	Gusset plate weld fracture

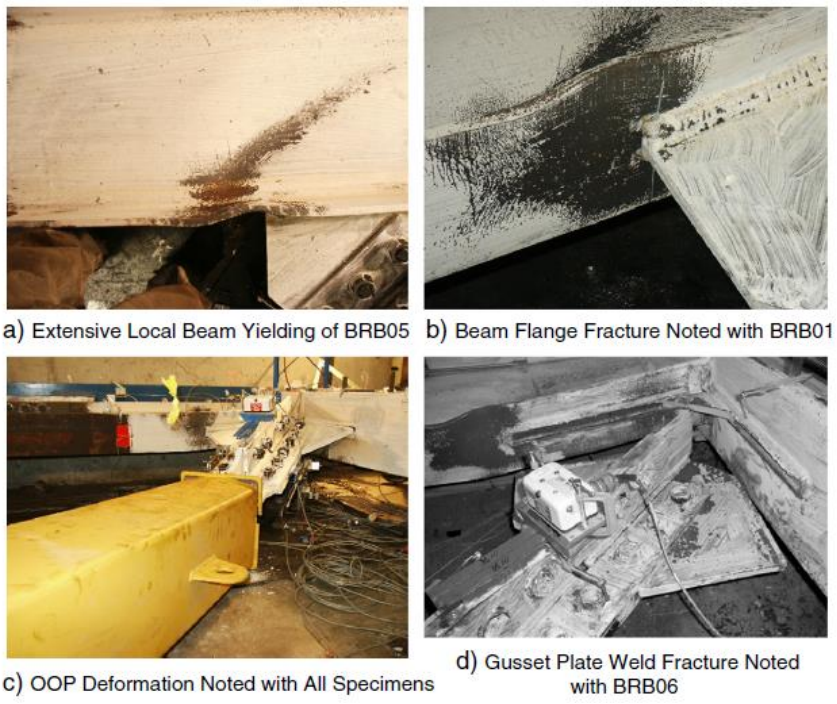

Figure E-2: Photos of Damage During Planer BRBF tests - Palmer et all. (2011)

The research conducted by Palmer et all. (2011) concluded the following:

- BRBFs can achieve higher drift ranges and energy dissipation than required by code
- BRBs deliver large inelastic deformation demands to the connection and the framing member. This can lead to unexpected and/or undesired failure modes if not properly detailed.
- Modest improvements can be made to the drift capacity of a BRB using tapered gusset plates.
- Core plate orientation and bolt pretension did not have a large impact on BRBF performance.

E.2 BRB Detail

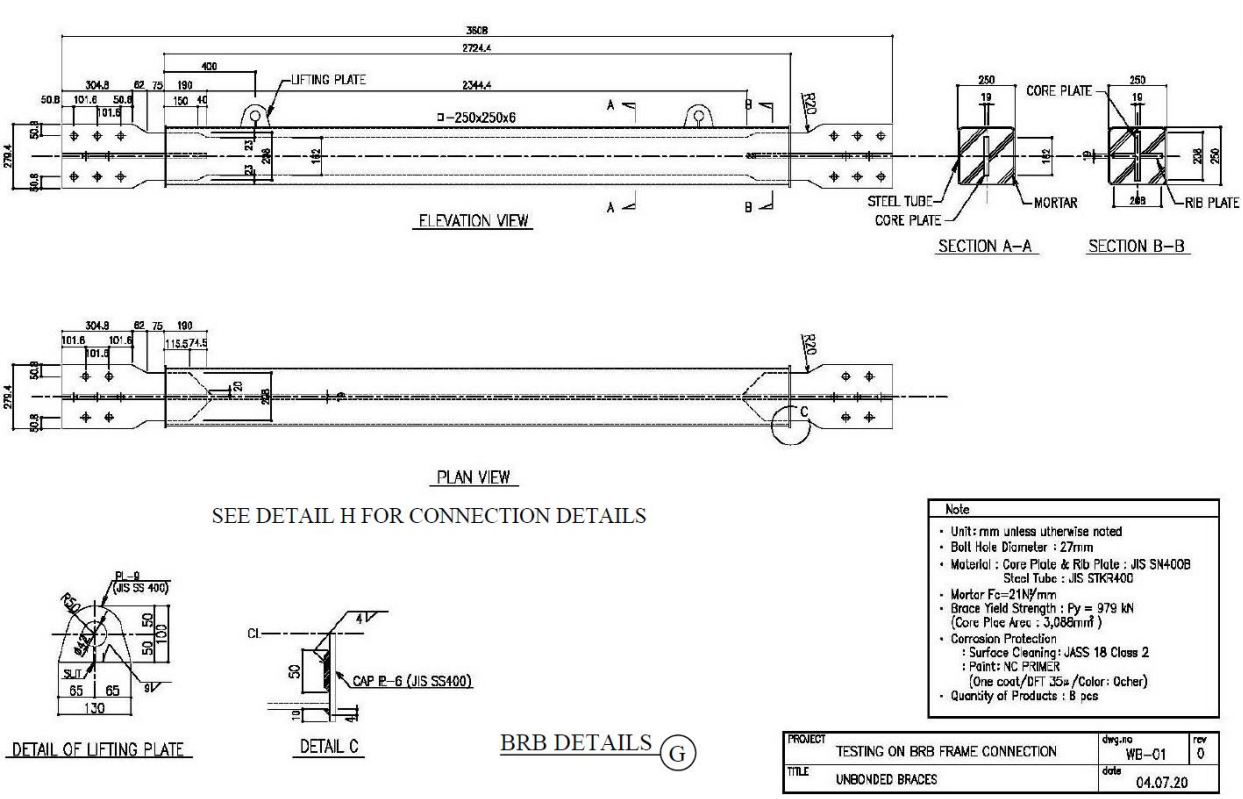

Figure E-3: BRB Detail (Courtesy Nippon Steel)

E.3 BRB Limit State Calculation

The BRB was connected to the gusset plate using ten splice plates bolted on either side of each leg of a cruciform section. Two rib plates were welded to the gusset plate to create a matching cruciform shape. Twenty 1" A490 bolts in each corner transferred the load between the BRB and the gusset plate. The bolts were slip critical and prevented dynamic slip of the BRB during the test. The buckling restrained brace was originally designed to satisfy AISC limit states including the associated resistance factors. Limit states for the buckling restrained brace were originally calculated by Christopulos (2005) and include net section yielding, bolt shear, bolt bearing, bolt slip, and block shear. Splice plates were designed such that yielding would not occur over the net section. The demand and capacities for the BRB limit states are shown in Table E-2. The splice plates are 3/8" thick and 4" wide. Bolt slip and gross tensile yielding of the splice plates controlled the design of the BRB connection.

Table E-2: Limit States for Buckling Restrained Brace

Limit State	Demand	Capacity ($\emptyset \boldsymbol{R_n}$)	(AISC 2014)
Bolt Shear	P_c	$\emptyset F_{nv} A_{bolt} N_{bolt}$	Part 7
Bolt Bearing	P_c	$\emptyset 3.0 \min\left(t_{sp} F_{usp}, t_{gp} F_{gp}\right) d_{bolt}$	-
Bolt Slip	P_c	$\emptyset(\mu D_u h_f T_b n_s) N_{bolt}$	Eq. J3-4
Gross Tensile Yielding	P_y	$\emptyset 8 t_{sp}\left(w_{sp} - d_{hole}\right) F_{ysp}$	-
Block Shear	P_y	$\emptyset(\min\left(0.6 F_{ugp} A_{nv}, 0.6 F_{ygp} A_{gv}\right) + U_{bs} F_{ugp} A_{nt})$	Eq. J4-5

Symbol	Name	Equation/Value
P_y	Expected Brace Capacity in Tension	$\alpha\beta F_y$
P_c	Expected Brace Capacity in Compression	αF_y
F_y	Yield Capacity of Core Plate	46 ksi (Christopulos 2005)
α	Brace Tension Adjustment Factor	1.54 (Christopulos 2005)
β	Brace Compression Adjustment Factor	1.052 (Christopulos 2005)
$N_{bolt}, A_{bolt}, d_{bolt}$	Number, Area, and Diameter of Bolts	10, 0.78in^2, 1.0in
d_{hole}	Diameter of the hole	$d_{bolt} + 1/16"$
t_{sp}, t_{gp}	Thickness of the Splice and Gusset Plate	3/8”, varies
w_{sp}	Width of the Shear Plate	4”
F_{usp}, F_{ugp}	Ultimate Tensile Capacity of Splice and Gusset Plate	varies
μ, D_u, h_f, T_b, n_s	Bolt Slip Capacity Factors	AISC 2010 section J3.8
A_{gv}	Gross Shear Area for Brace Block Shear	$8(10")t_{rp}$
A_{nv}	Net Shear Area for Brace Block Shear	$8(10" - 2.5d_{hole})t_{sp}$
A_{nt}	Net Tension Area for Brace Block Shear	$8(2" - 0.5d_{hole})t_{sp}$